RELATIVE SEA LEVEL CHANGE IN WESTERN ALASKA ESTIMATED FROM SATELLITE ALTIMETRY AND REPEAT GPS MEASUREMENTS

By

Kimberly Grace DeGrandpre

RECOMMENDED:

Dr. Elisabeth Nadin

Dr. Nicole Kinsman

Dr. Jeffrey Freymueller
Advisory Committee Chair

Dr. Paul McCarthy
Chair, Department of Geosciences

APPROVED:

Dr. Paul Layer
Dean, College of Natural Science and Mathematics

Dr. John Eichelberger
Dean of the Graduate School

14 July 2015
Date

RELATIVE SEA LEVEL CHANGE IN WESTERN ALASKA ESTIMATED FROM SATELLITE ALTIMETRY AND REPEAT GPS MEASUREMENTS

A

THESIS

Presented to the Faculty

of the University of Alaska Fairbanks

in Partial Fulfillment of the Requirements

for the Degree of

MASTER OF SCIENCE

By

Kimberly Grace DeGrandpre, B.S.

Fairbanks, Alaska

August 2015

Abstract

Western Alaska is a remote region populated by small coastal communities that are sensitive to variations in local relative sea level (RSL). The focus of this thesis is to address two main questions; what are the RSL trends in Western Alaska and what are the geophysical processes that contribute to the changes observed? Quantification of RSL variation requires measuring vertical velocities for both land surface motion (onshore component) and the ocean surface (offshore component). This study presents a new method for coastal satellite altimetry estimation, the collection of historic water level measurements, analysis of tide gauge measurements from various sources, GPS vertical velocity model for Western Alaska, estimation of an Earth model and glacial isostatic adjustment (GIA) vertical velocities for Northern and Western Alaska, and RSL change model for Western Alaska.

The findings of this study result in a GIA model that predicts measured GPS velocities well. The predicted GIA vertical velocities average -1.06 mm/yr in Western Alaska and are combined with the averaged satellite altimetry cells that exhibit a mean sea level change offshore of Western Alaska of -0.27 mm/yr to produce a RSL change model for Western Alaska that increases approximately +0.79 mm/yr in the region.

Table of Contents

Page

List of Figures

Page

Page

Page

Page

List of Tables

Page

List of Appendices

Acknowledgements

During these past few years in academia I have lost two very important people with whom I wish I could have shared this thesis. Grammie Dona and Uncle Neil always proved that family comes from the heart, not blood, and I miss them dearly. I know you would be proud of this thesis as you both taught me to question everything, follow my heart, push myself, be an active part of this world, and to work hard but to never forget to stop and appreciate the beauty, poetry, and spirit in the nature, culture, and people that surround us.

Thanks goes out to those around me who have helped to support me these past few years, whether they wanted to or not, while I immersed myself in the grants, field work, writing, coding, and associated mood swings. The sanity checks, weekend trips, and enforced nights where thesis work would not be mentioned were essential to my success and happiness. I am lucky to be surrounded by friends and family who love so much.

I also have great appreciation for my committee of Jeff Freymeuller, Nic Kinsman, and Elisabeth Nadine who all contributed differently, but importantly, to my education and development as a young scientist.

This work is funded, in part, with qualified outer continental shelf oil and gas revenues through the Coastal Impact Assistance Program, U.S. Fish and Wildlife Service, U.S. Department of the Interior. The views and conclusions contained in this document are those of the author and should not be interpreted as representing the opinions or policies of the U.S. Government. Mention of trade names or commercial products does not constitute their endorsement by the U.S. Government. This project was also funded, in part, by the U.S. Fish and Wildlife Service on behalf of the Western Alaska Landscape Conservation Cooperative (Project 2013-26). This research was further supported, in part, by a UAF Center for Global Change Student Research Grant with funds from the Cooperative Institute for Alaska Research. The altimeter products were produced by SSALTO/DUACS and distributed by AVISO, with support from CNES (http://www.aviso.altimetry.fr/duacs/).

1 Introduction

Global relative sea level (RSL) change has drawn an increasing amount of attention in the general population and the scientific community due to the geologic, biologic, and ecologic impacts it has on coastal communities and environments. Changes in RSL result from local variations in mean sea level (MSL) and tectonic vertical motion. These can vary widely between areas in close proximity to each other, so a value for RSL is only valid for the particular location. It is important to understand not only what the RSL change is in a region, but also the oceanic and tectonic processes that drive this change. This will allow the best course of action to be taken when planning and mitigating consequences that are associated with changes in RSL. The state of Alaska covers a vast expanse of tectonic and oceanic regimes so it is critical to study different regions individually.

This thesis addresses the topic of RSL change in Western Alaska. Western Alaska is defined here as the western coastline of Alaska from the north shore of the Alaskan Peninsula to the southern half of the Lisburne Peninsula (Figure 1.1) and is one of the more remote areas in Alaska. Because of this, previous to this study there have been very little data available to observe directly or indirectly RSL change. This region is populated by coastal communities that lie on the coasts of the Bering Sea, Norton Sound, Kuskokwim Bay, and Bristol Bay. RSL change affects these coastal communities, but can also affect inland populations that are located on the banks of major rivers such as the Yukon and Kuskokwim rivers. This study of RSL change will aid these populations in making informed decisions when planning the future of their communities, allowing losses and damages to be minimized in the future.

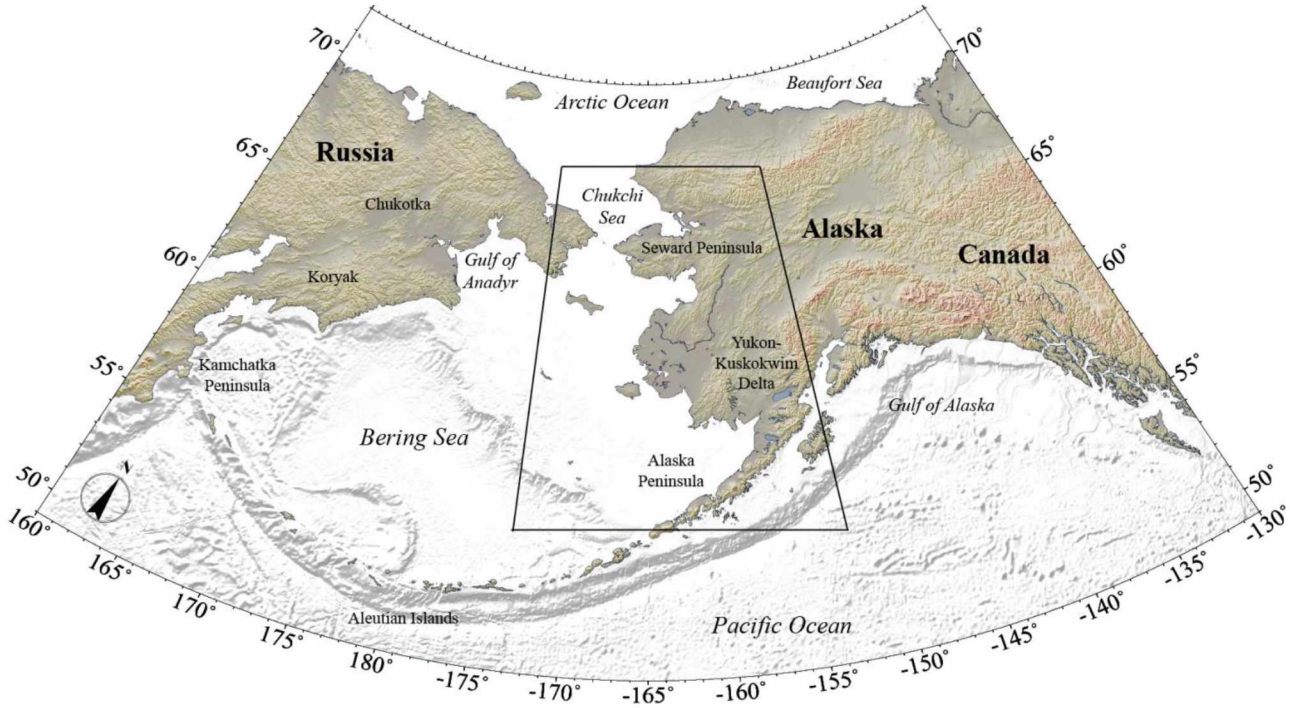

Figure 1.1. Map of the Bering Sea region. The study area, Western Alaska, is outlined in black.

1.1 RSL change

Mean sea level (MSL) is a measure of the height of the ocean surface, described by the National Ocean Service (NOS) as the "arithmetic mean of hourly heights observed over the National Tidal Datum Epoch." (Gill and Schultz, 2001). A tidal datum epoch is used to create a common temporal reference between different spatial regions so that oceanic measurements can be compared. NOS defines the National Tidal Datum Epoch, throughout the United States and associated territories, to have a duration of 19 years, and the most recent epoch spans 1983-2001 (Gill and Schultz, 2001).

RSL is the measurement of local MSL relative to the local ground surface. RSL change is a rate representing the trend that observations of RSL exhibit over time (Gill and Schultz, 2001). This rate can be positive or negative depending upon the relationship between the rate of local sea level change and the vertical velocity of the local ground surface (Figure 1.2). In order to fully quantify rates, directions, and magnitudes of RSL change, it is necessary to have measurements of both MSL change (oceanic component) and vertical velocity of the local ground motion (tectonic component) (Nerem et al., 2014), with both rates of change given in consistent reference systems.

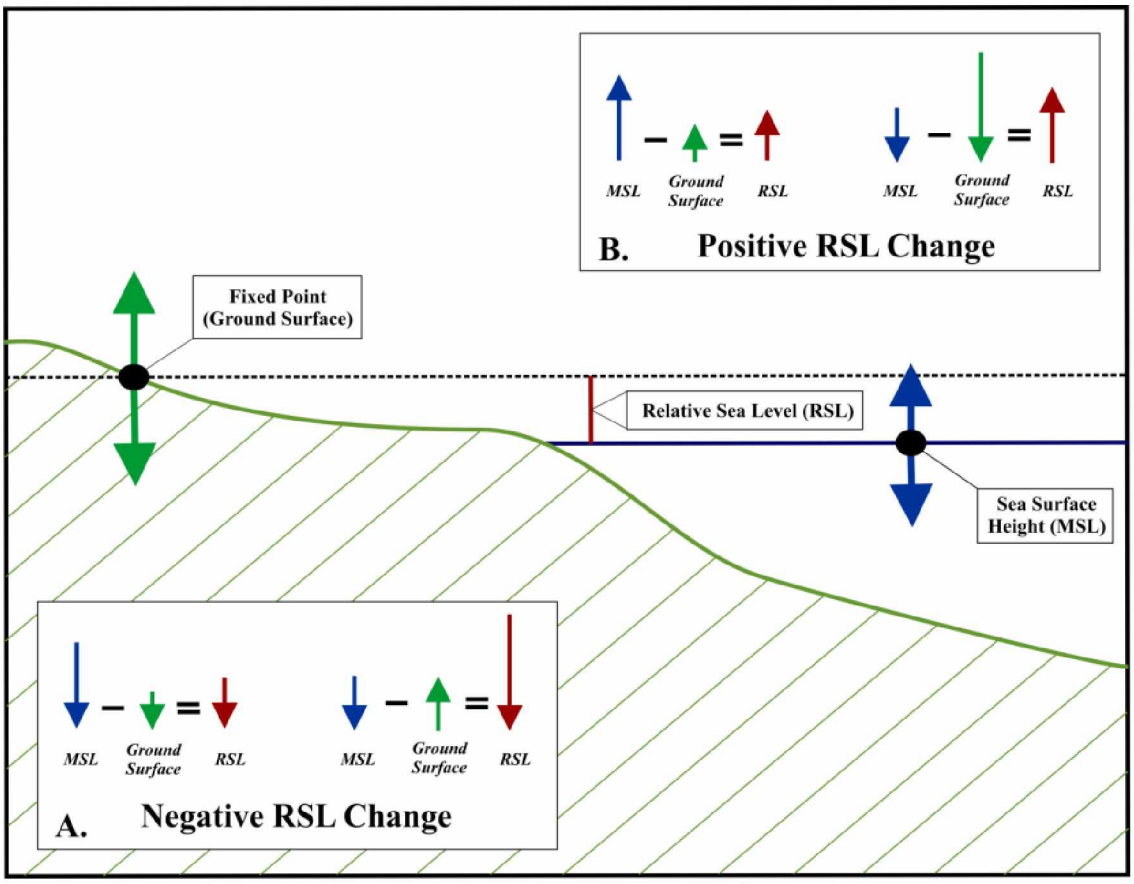

Figure 1.2. Diagram of RSL change. Green arrows represent vertical velocity of the ground surface, blue arrows are MSL change, and red arrows show the combination of green and blue arrows, or the resulting RSL change. Box A shows two possible combinations of movement of the oceanic and tectonic components that result in negative RSL change, which would appear as a decrease in sea level. Box B shows two possible combinations of oceanic and tectonic motion that result in positive RSL change.

Traditional geologic techniques use geomorphology, paleontology, and sedimentology to observe the history and fluctuations of sea level changes through coastal evolution, fossil records, and deposition patterns. Raised beach terraces and wave cut platforms are good indicators of a decrease in RSL, while beach erosion and salt water inundation suggest that RSL is increasing in that location. Some of these processes can be observed over short periods of rapid change that may last only a year, or they can help construct a history of thousands or millions of years of RSL change in a given area. Field observations are a valuable technique for assembling a complete story of local historic RSL change, but they can often be subjective in nature and do not provide quantitative datasets that can be used in models or calculations of contemporary RSL trends.

A tide gauge is the most direct method for observing local RSL. Tide gauges measure water level and are surveyed to a local fixed point of reference on land (Figure 1.3), known as a benchmark, to determine the water level relative to that point. Tide gauge measurements are influenced by both oceanic and tectonic vertical motion, which can differ both spatially and temporally. This means the water-land relationship for the location of the tide gauge must be defined as a function of time. NOAA requires a minimum of 30 years for tide gauge data to publish a RSL trend. The water level trend, measured by the tide gauge over a defined time range, is calculated and represents the RSL change for that location. The RSL measured by a tide gauge is only applicable to its specific location, because the observation of oceanographic processes affecting the water levels combined with the tectonic processes affecting the benchmark are unique to that location and particular tide gauge. Long-term and short-term tide gauges (Figure 1.4) provide valuable quantitative data for tidal and other water land relationships. With a minimum of 30 years of data a tide gauge measures a long term RSL trend. Shorter records can still be used to compute RSL averages separated by long periods of time. With multiple measurements these short-term records can be used to estimate RSL change. For example, the tide gauge in Figure 1.4 was installed for 1month to measure tidal components and provide an estimate of average sea level for the present tidal epoch. The mechanics behind how a tide gauge records data has evolved from a spring and pencil arrangement that was first designed in 1831 by a British civil engineer, J. Mitchell, (Reidy, 2009) to the computerized pneumatic pressure systems that are used to measure water levels today (Gill and Schultz, 2001). The tide gauge, however, only provides data for the location where it is installed and requires maintenance and periodic resurveying.

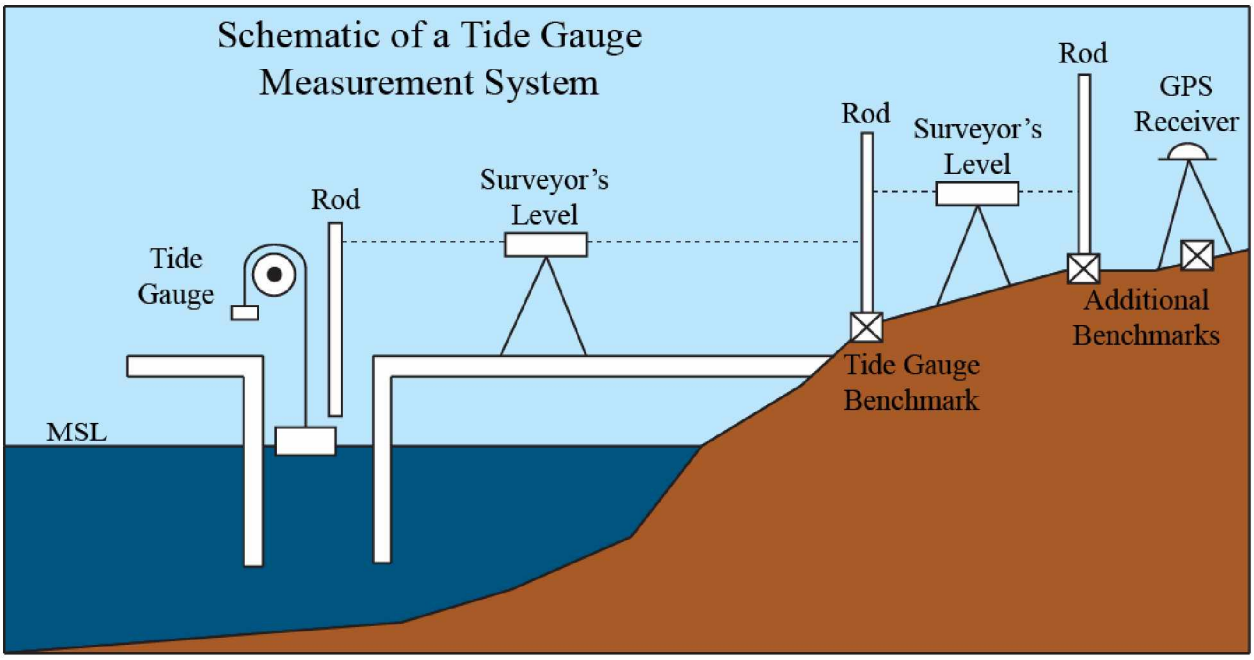

Figure 1.3. Schematic of a tide gauge measurement system. This figure illustrates sea level measurements taken by the tide gauge coupled with the levelling techniques required to survey it to the three tidal benchmarks on land. Modified from Nerem et al., 2014.

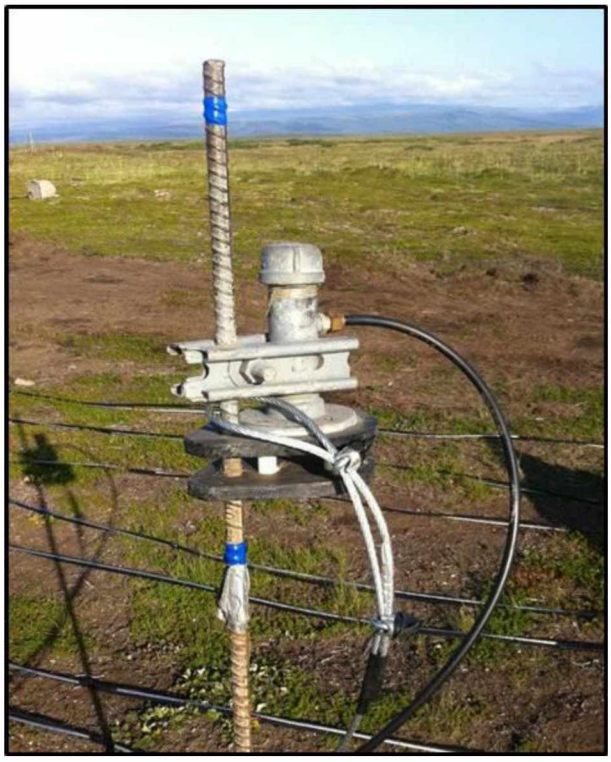

Figure 1.4. Photograph of a modern pneumatic tide gauge mounted to rebar. This tide gauge was used in a temporary installation in Port Heiden on the Alaska Peninsula.

1.2 Oceanographic processes

Global average MSL is currently increasing at an estimated rate of 3.2 +/- 0.4 mm/yr (Nerem et al., 2010; Leuliette and Willis, 2011). This eustatic sea level rise can be attributed to roughly equal contributions from mass balance and thermal expansion (Bindoff et al., 2007; Cazenave et al., 2008; Church et al., 2010). Mass balance involves a shift in water storage from terrestrial (i.e.; ice sheets, glaciers, or permafrost) to oceanic storage (Pfeffer, 2011). Thermal expansion is the change in volume of the oceans in response to increased oceanic temperatures, caused by both the warming of our climate and increased absorption of solar radiation as sea ice becomes less prevalent and reflects lower levels of the sun's energy (Bindoff et al., 2007; Cazenave et al., 2008; Church et al., 2010).

Other, smaller factors can contribute to changes in ocean levels on a regional scale. A byproduct of the two main contributions to sea level rise is an additional effect of decreased density, which can also cause a rise in sea level for a greater water mass. Reduction in density results in expansion of the water body, primarily due to increased water temperatures (Antonov et al., 2005; Domingues et al., 2008). However, on a regional scale, the addition of freshwater is increasing, and the decreased salt content can also cause a reduction in density that contributes a small amount to sea level rise (Johnson and Wijffels, 2011).

Changes in circulation of currents, pressure systems in the atmosphere, winds, and even changes in the gravitational field can cause water to "pile up" in different locations (Proshutinsky and Johnson, 1997; Proshutinsky and Johnson, 2011). These dynamic changes are often more substantial when considering global or large regional sea level changes, rather than smaller localized bodies of water. These changes can be observed in large currents such as the California Current or Gulf Stream and in atmospheric conditions such as El Nino or the Arctic Oscillation (Cazenave and Llovel, 2010). Dynamic changes such as these have a large spatial extent, affecting entire ocean basins, but the time span can range from gradual, for processes relating to the Coriolis effect and a migrating change in gravity, to cyclical events with temporal scales from months to decades (Chelton and Davis, 1982), and to even shorter period variability associated with individual weather systems. Cyclical events, or oscillations, are closely tied to atmospheric conditions and can change the pressure, temperature, and/or the circulation pattern of the affected oceanic system (Chambers et al., 2012). These effects are driven by different factors that involve changes in gravity or atmospheric temperature and pressure, but result in the

same outcome: a mass of water is relocated within or between basins. This is studied by observing the difference between sea surface height and the geoid at a specific point, a relationship known as dynamic topography (Panteleev et al., 2011). When estimating sea level trends, dynamic topography does not affect the global MSL but can produce significant localized differences in trends on shorter time scales. Strong currents like the Kuroshio Current, along the northwest edge of the Pacific basin can produce annual signals of up to +/- 10 cm (Wang and Rapp, 1994) but unless there are permanent changes these dynamics do not influence long-term sea level change.

Tidal harmonics are specific kinds of gravity forced oscillations that are observed globally. The tidal harmonic constituents are results of variation in the alignment of the Sun, Moon, and Earth (Godin, 1991; Pawlowicz et al., 2002). There have been hundreds of tidal constituents identified, but 62 primary ones can provide relatively accurate tidal predictions over extended periods of time (Godin, 1991). These various constituents apply to all coastlines, but vary in their amplitudes, so one constituent may be more influential at a specific location than another. The frequencies of these signals range from hours to decades. The main constituents involved exhibit diurnal and semi-diurnal periods, to a 18.6 year period, resulting from the combination of lunar and ecliptic solar orbits (Gratiot et al., 2008). The tidal constituents must be calculated at locations on an individual basis because of the variations that evolve due to coastal and basin geometry (Pawlowicz et al., 2002). In practice, they are estimated from tide gauge data.

1.3 Oceanographic measurement techniques

Methods for studying sea level change include a wide array of techniques, from geologic measurements of coastal terraces to the use of satellites equipped with various sensors.

Instruments to measure currents, salinity, temperature, and other physical characteristics are often deployed for both short and long-term surveys by taking repeat samples from research cruises, mounting instruments to fixed features, or setting them adrift. These methods can produce very accurate records of factors that influence sea level change, but have limited spatial and temporal coverage. While tide gauges include a land component in their measurement, they are often used for oceanographic purposes to observe local tides and water levels and define the tidal harmonics and oscillations that most impact the area.

Since the first oceanographic satellite, SEASAT (Figure 1.5), was launched by NASA in 1978 (Fu and Holt, 1982; Douglas et al., 2000), a global database of oceanographic information has been developing. Several sensors onboard some of the more recent satellites, such as Jason 2, can perform satellite altimetry and microwave radiometry. These sensors can be used to study sea surface height, wave dynamics, wind speed, atmospheric moisture, and sea surface temperature. Modern satellites achieve spatial coverage of 95% of the ice free oceans approximately every 10 days and have been orbiting longer than their expected lifespans with continuous records extending back to 1992 (Douglas et al., 2000).

Figure 1.5. Black and white photograph of SEASAT over Alaska (Fu and Holt, 1982).

Satellite altimetry is used to measure sea surface height by sending a radar pulse to the Earth's surface and recording the time it takes for that pulse to return to the satellite (Figure 1.6). When many readings are averaged over a long enough time this average, relative to a reference ellipsoid, can be considered an estimate of MSL (AVISO, 2009). These satellites use three

systems to determine their orbits. Radio signals emitted from GPS satellites position the altimetry satellite relative to the ellipsoid, while the French system, Doppler Orbitography and Radiopositioning Integrated by Satellite (DORIS) emits radio signals from stations on land to a receiver on the satellite and uses the Doppler effect to accurately track the altimetry satellite's orbit (AVISO, 2009). The third system, satellite laser ranging (SLR), are land based stations that emit a pulse of light that is reflected from the altimetry satellite by a retroreflector (AVISO, 2009). The total time it takes this pulse of light to return to the station helps to define the altimeter's orbit in addition to the GPS and DORIS systems. As the precise time and location relative to the geocenter are known for these satellites, the round trip time of the radar pulse can be used to calculate elevation of the surface in reference to the geocenter (AVISO, 2009). This measurement can then be used to relate the sea surface height to the geoid, which produces measurements of dynamic topography.

On sloped and irregular surfaces like rivers and land, altimetry is a less practical tool, but for the relatively homogenous ocean surface it is an efficient way to acquire regional and global MSL data (AVISO, 2009). For these reasons, satellite altimetry is not suited for near shore RSL calculations and it is recommended that data within 30-50 km of a shoreline be disregarded because of the inherent noise and inaccuracy from the atmosphere, shallow water dynamics, and coastal features that dominate the signal (AVISO, 2009).

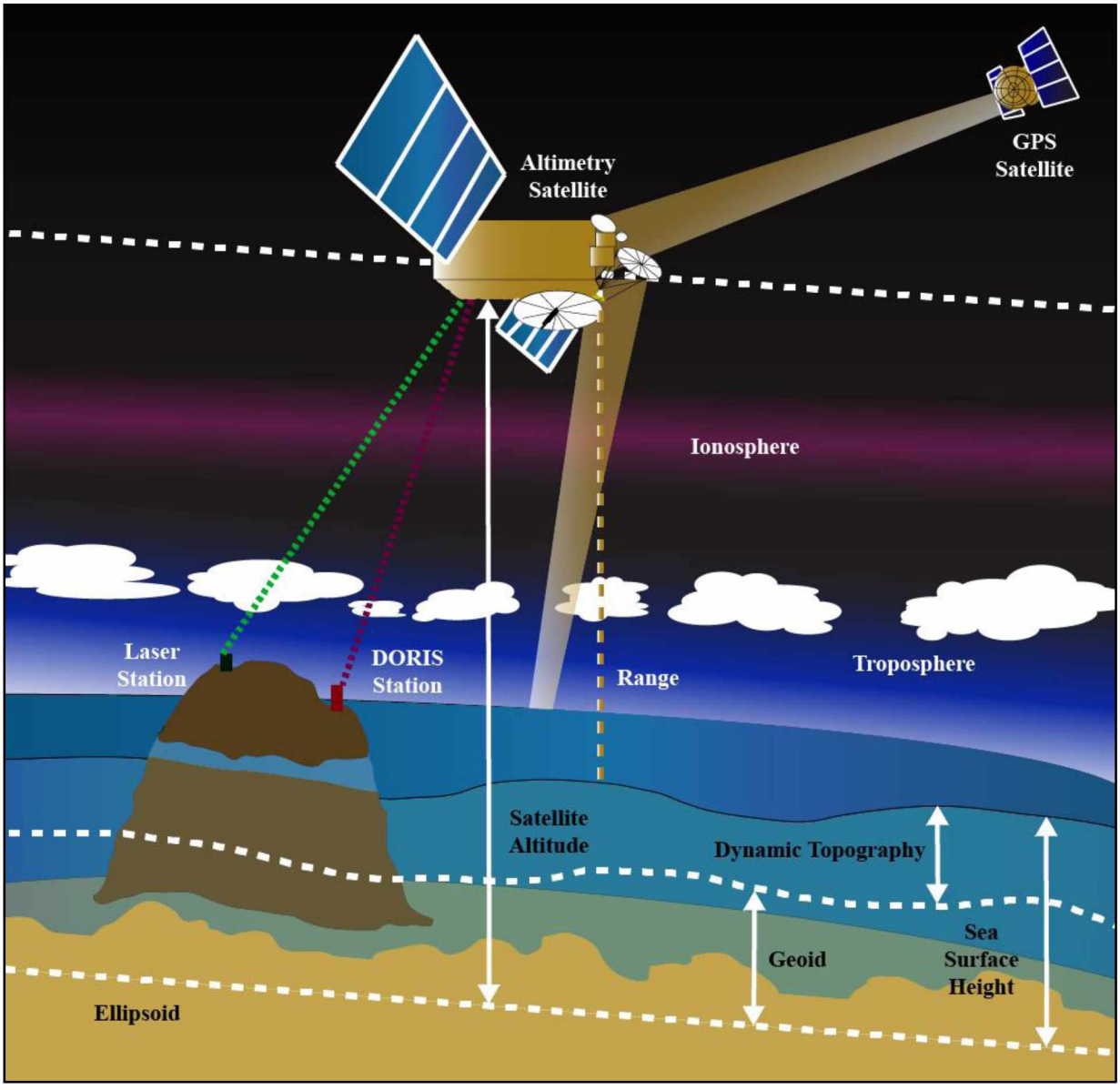

Figure 1.6. Schematic of a satellite altimeter. This figure illustrates how the satellite is referenced to the ellipsoid and makes measurements of sea surface height (i.e., MSL), that are then also referenced to the geoid. The relationship between MSL, dynamic topography, the geoid, and ellipsoid are clearly illustrated here. Modified from AVISO, 2009.

1.4 Tectonic processes

Vertical motion of the land (the tectonic component in RSL) can be caused by many different geophysical processes. Spatially, these processes are generally not considered on a global scale the way oceanic processes are. These changes also have different temporal and spatial scales that range in time from seconds to millions of years, and in space from the size of

small islands or bays to continental coastlines, making the vertical characterization for one location a complicated patchwork of geophysical processes.

The most commonly cited process in Alaska to account for vertical velocity, when addressing the issue of RSL change, is glacial isostatic adjustment (GIA). This is a long-term effect that results from the response of the lithosphere, asthenosphere, and upper mantle to the loading and unloading of mass quantities of ice over hundreds to thousands of years. When an ice sheet forms, it loads the lithosphere beneath it and creates a depression (Figure 1.7A) which displaces the asthenosphere and upper mantle below it. At a certain distance from the ice sheet the lithosphere is flexed upwards, forming a forebulge that is of a much smaller magnitude than the depression under the ice sheet. When deglaciation takes place, the lithosphere that had been depressed returns to its unloaded state (Figure 1.7B), pushed upwards as the displaced asthenosphere and upper mantle re-equilibrate under the conditions of decreased pressure. At the same time, the forebulge collapses.

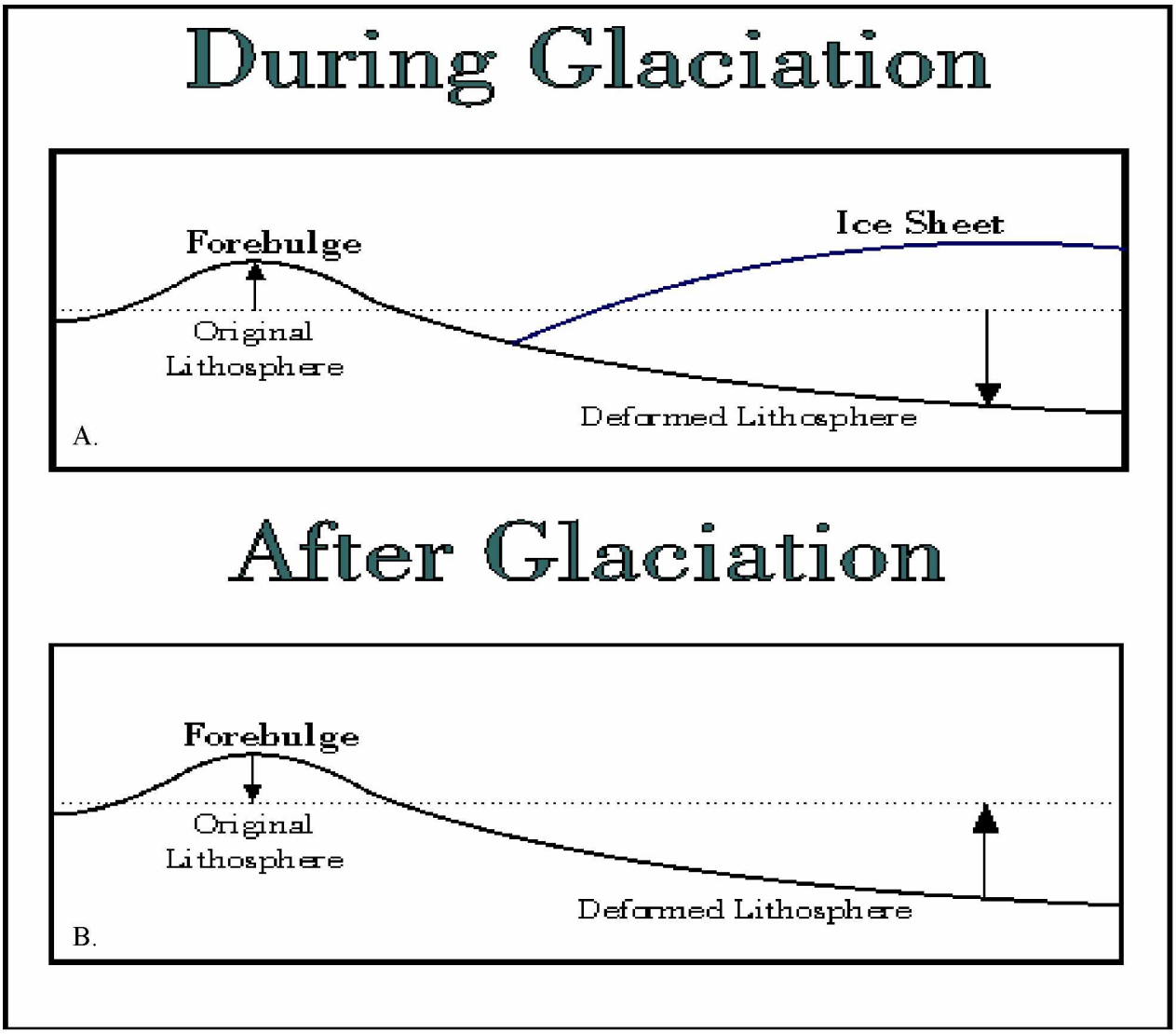

Figure 1.7. Illustration of ice sheet loading (A) and unloading (B) effects on the lithosphere. The direction of vertical displacement of the lithosphere under the ice sheet and of the forebulge are represented with arrows.

The timing and magnitude of the lithospheric response is dependent on the location and thickness of the ice sheet as well as the thickness of the lithosphere, and the thickness and viscosity of the asthenosphere and mantle. Studies of the dynamics of GIA are helping to create more accurate glaciation histories and Earth parameters and models of both the ice loading and of the Earth parameters involved are publically available.

Earthquakes are another process that can account for vertical tectonic motion; the effects can be both immediate and long-term as well as regional and local in nature. Earthquake surface rupture can lead to immediate local vertical displacements with magnitudes ranging from

millimeters to multiple meters per year. Very large earthquakes can also have a regional effect of post-seismic vertical velocity that are on the order of millimeters to centimeters.

A poorly quantified process that potentially has a significant effect on RSL change near large deltas is sediment loading and delta subsidence. This process is hard to constrain because it involves characterization of the physical properties of the sediments being deposited and the rate and history of that sediment deposition. Subsidence results from the constant loading of the delta with river sediments, which are deposited and compacted causing a slow increase in load similar to the formation of an ice sheet during glaciation. Sediment compaction itself may add a significant component of subsidence. Delta subsidence is dependent on the discharge rate and sediment availability of the river and is an effect that is widely observable at large deltas worldwide, which is why it is the most cited RSL land motion component globally, though thousands to millions of years of deposition may be required for a measureable vertical velocity to be calculated. These velocities can be significant at major rivers and deltas such as the Mississippi River Delta in Louisiana where Ivins et al. (2007) found that sediment loading results in 1-8 mm/yr of subsidence.

Processes such as tundra subsidence that result from the melt of permafrost, ground water depletion, and redistribution of large quantities of substrate are also known to cause local land motion. These processes are not well constrained for Western Alaska, so they are not modeled, but could potentially be responsible for components of observed vertical land motion.

Additional processes like volcanism, subduction, and rifting can impact the localized tectonic vertical velocity, but are not important for Western Alaska.

1.5 Tectonic measurement techniques

The tectonic vertical component, like the oceanic component, can be observed using a variety of methods that include geologic observations, modelling, or the use of various types of satellites. Traditional geologic techniques involve observing fault offsets, sediment deposition rates, or erosion and uplift patterns. Mapping changes in vegetation and shorelines can indicate uplift or subsidence, while erosion and deposition patterns can help to constrain the timescale involved. These observational methods can provide quantitative measurements of subsidence or uplift, but may not give clear definition of the processes involved.

Studies in plate tectonic velocities benefit from the use of modelling because of the sizes of plates and the relatively slow velocities typically associated with them. GIA models use parameters of both glacial ice loads and Earth's elastic and viscosity structure to further define parameters used in the model. Models such as ICE-3G (Tushingham and Peltier,1991) and a calculation program like TABOO (Spada et al., 2003; Spada, 2003; Spada et al., 2004) work in conjunction to create values for GIA displacements through time.

The two primary methods for estimating tectonic velocities using satellites are Interferometric Synthetic Aperture Radar (InSAR) and GPS. InSAR is best used for deformation that takes place over a relatively small area, normally less than 100 km^2, and over a geologically short time span of days to years. The deformation is observed through the phase difference between the waves of two radar pulses. For long-term plate motion, InSAR is not ideal, and it is used instead in applications of fault or volcanic deformation that occur on smaller scales both temporally and spatially.

GPS uses a constellation of more than 30 satellites in orbit to obtain position and time measurements for a fixed point on Earth's surface. These measurements can be used to find the precise location of the measured point relative to the geocenter, and repeat measurements can be used to calculate the tectonic velocity at that point. Unlike satellite altimetry or InSAR, GPS requires an antenna and receiver set up on the surface in order to record the time it takes for the signal from each satellite to reach that point. Depending on the receiver, additional constellations such as Galileo and GLONASS can be used as well for better satellite coverage. This equipment is temporarily or permanently installed over a fixed point on the surface known as a benchmark (Figure 1.8). The ideal benchmark is fixed to the crust and its motion therefore reflects the tectonic motion at that point. GPS can measure displacements larger than ~1 mm in horizontal directions and ~3-5 mm for the, vertical motion. The spatial extent is only limited by the benchmark and equipment installation locations.

Temporary installations of GPS equipment are commonly referred to as campaign surveys (Figure 1.9), where a receiver and antenna are set up for a few days on a benchmark before being moved. Horizontal measurements have much better accuracy due to the distribution of the satellites, so a measurement can be estimated in as little as eight hours while a minimum of three days' occupation is required in order to achieve vertical velocities with sub-centimeter accuracy. These campaign measurements may be repeated at a particular benchmark every year

or so, depending on the temporal resolution required, to determine a tectonic velocity for that specific location. Continuous GPS data are obtained when equipment is permanently installed on a fixed monument. These data are collected continuously and can lead to insights about seasonal variations in tectonic velocity as well as a better constrained trend than the campaign survey would provide. Numbers of continuous sites are limited, however, as they are generally costly to install and maintain.

Figure 1.8. Photographs of two types of benchmarks used for GPS campaign surveys. (A) a standard brass disk benchmark in Kalskag that is installed directly into bedrock. (B) a steel rod type benchmark in Emmonak that is driven into sediment refusal in locations where no outcropping bedrock is present.

Figure 1.9. Photograph of a GPS campaign site in Council, Alaska. This site shows the temporary installation of a GPS receiver and antenna in the summer of 2013 as part of this study.

1.6 Overview

Chapter 2 will cover the motivation behind this study and previous work in the area, as well as further describe the oceanic and tectonic settings and processes relevant to Western Alaska. In Chapter 3 the data collected and used during this study are explained and Chapter 4 highlights the results of the GIA and RSL change models that were produced from this data. Chapter 5 is a discussion of the implications these results have on the communities in Western Alaska and an interpretation of what the GIA and RSL trends imply in these locations. Chapter 6 concludes this study with an evaluation of the techniques used and a culmination of the results, interpretations, and projections previously discussed. This thesis finishes with suggestions for continuing and future work concerning RSL change in Western Alaska.

2.Background

2.1 Motivation

The communities of Western Alaska represent 6.9% of the overall population of the state, totaling 50,930 people (Bureau, U.S.C., 2013), with village populations ranging from a few hundred people, to larger towns (e.g. Nome) of up to a few thousand. Most of these communities are built in low lying coastal environments, which are sensitive to changes in RSL. Effects resulting from RSL change can vary temporally, from increasing the severity and frequency of short-term effects such as storm surges, flooding, and erosion, to threatening ecosystems, populations, and coastline composition through coastal evolution or inundation over longer time periods of decades to centuries. The shorter time scale effects of RSL change often cause the majority of damage, due to a lack of preparation time available to coastal residents. These changes are manifested most significantly through flooding and erosion (Figure 2.1 and Figure 2.2), which have eroded land near homes and coastlines, disrupted water and sewage lines, and caused millions of dollars in damage (Forbes, 2011). The frequency of such events have anecdotally increased over the past decade and during a series of storms in the fall of 2013, five communities were declared federal disaster areas. For coastal communities, erosion and coastal evolution can take decades of small changes to pose a significant threat. Many villages are built on coastal features such as dunes, sand spits, or barrier islands and after many years of coastal evolution, these environments can leave villages vulnerable to damage from short-term events or even slowly destroy them through long-term changes. If communities recognize these threats, they can take precautions to protect life and property by planning accordingly.

As communities repair and some face relocation, there is now a demonstrated need for improvements in Local Hazard Mitigation Plans that would greatly benefit from having a RSL change model for Western Alaska (Forbes, 2011).

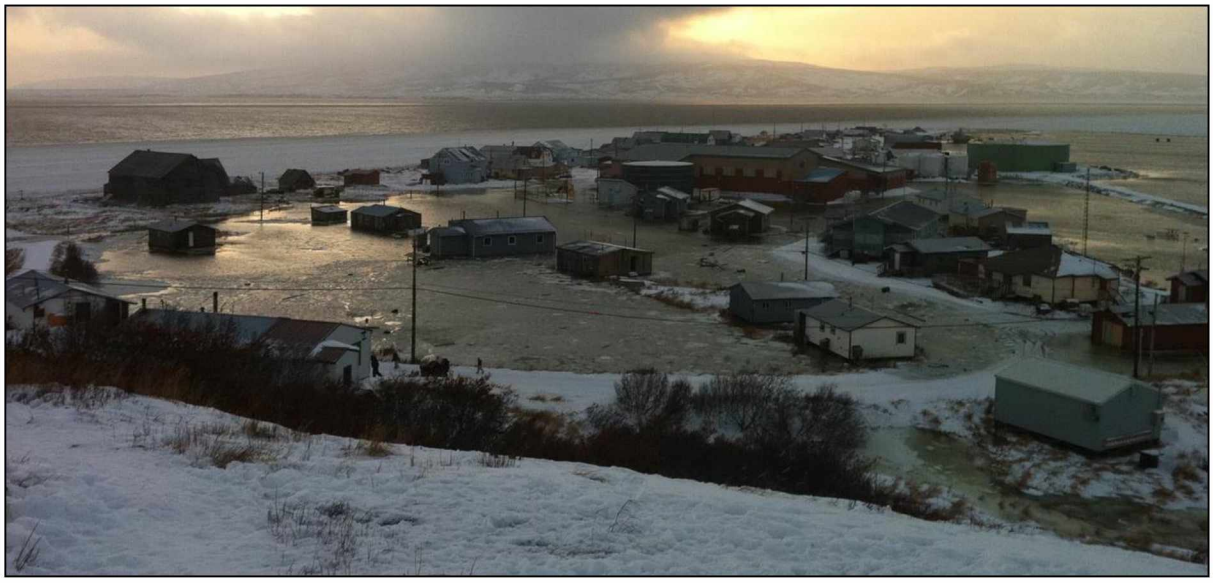

Figure 2.1. An example of the 2011 flooding in Western Alaska. This is the community of Golovin on the southern coast of the Seward Peninsula. The November storm surge flooded the entire village located on the lower sand spit shown here. The village has since begun plans and preparations to migrate to the higher elevation ground. Photograph courtesy of John Peterson.

Figure 2.2. An example of coastal erosion occurring on the southern side of the Bering Sea. This photograph was taken in the fall of 2013 as part of this study. This site is on the Alaska Peninsula, where the village of Meshik was forced to relocate and abandon buildings.

Humans are not, however, the only species affected by RSL change in Western Alaska. A slow increase in RSL change can result in salt water inundation of terrestrial fresh water sources, which changes the nature of the land and water resources. This forces an evolution or migration of the organisms that are dependent on these resources, throughout the entire food chain. Western Alaska is biologically and ecologically important for the summer migration of many species of birds, the fall run of salmon, moose, caribou, wolf and musk ox habitat, and as an ever evolving landscape which alternates between deltaic movements and permafrost fluctuations arising from a changing climate in Alaska.

This thesis provides the required foundation for future work that consider the changes and risks that coastal environments and communities of Western Alaska may face in both the near and far future.

2.2 RSL trends

The effects of RSL change are individual to the specific location it is defined for, as RSL change can be a negative or a positive value based on the relationship between the oceanic and tectonic components. These effects can be drastically different in areas located near each other depending on the geophysical effects controlling these dynamics.

RSL trends have been studied in southeast Alaska where positive vertical velocities, or uplift rates, of the local ground motion from glacial melt far exceed the contemporary rates of MSL rise, resulting in an effective negative trend in RSL (Larsen et al., 2005). There have been no such studies in Western Alaska, where the processes controlling tectonic vertical velocities are significantly different from those in southeast Alaska.

The importance of RSL change has been recognized and there are measured rates available along most of the shoreline of the United States and the southern coasts of Alaska (Figure 2.3), but challenges arise when attempting to study RSL change in Western Alaska because of the remote locations and lack of instrumentation involved.

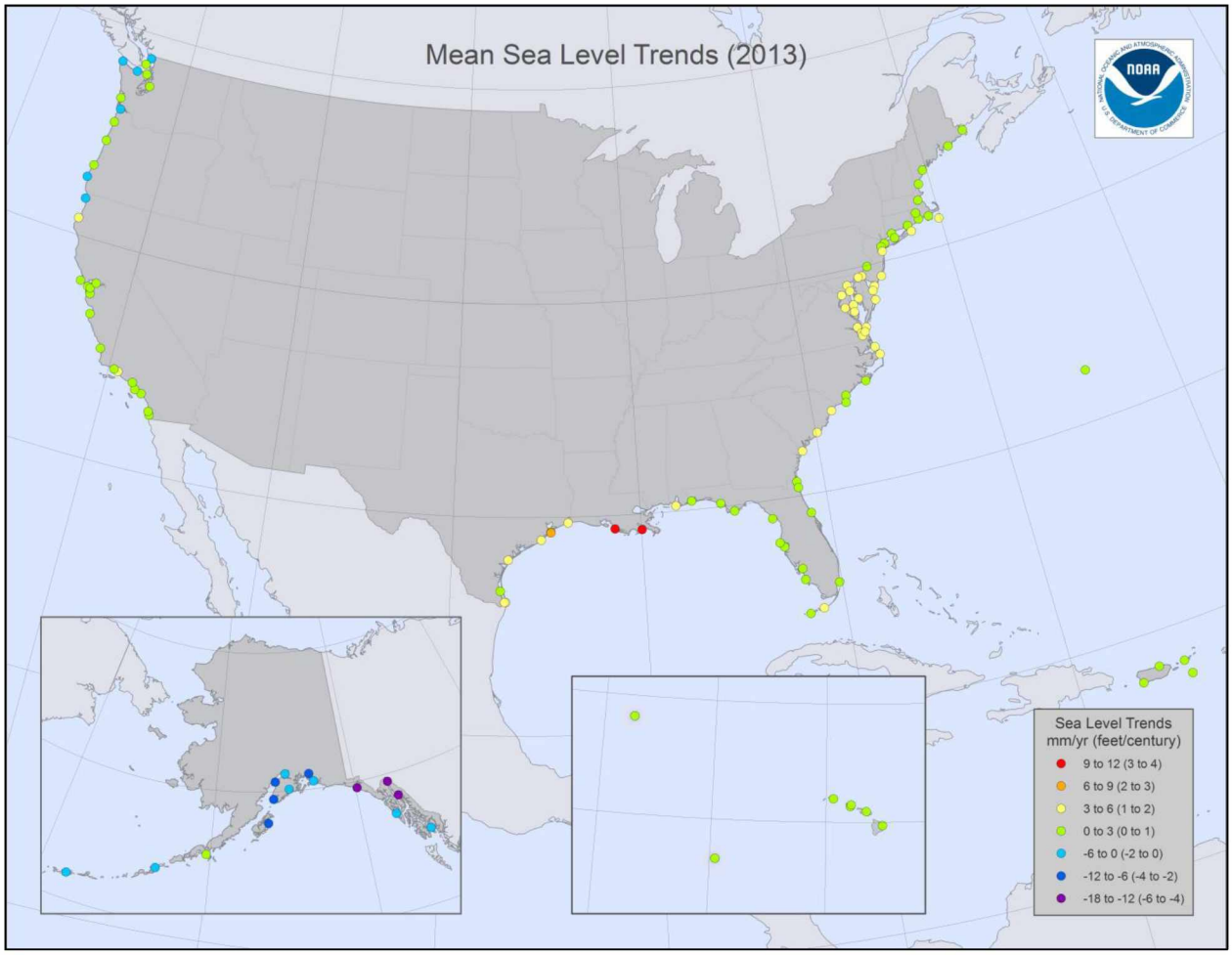

Figure 2.3. Locations in the US where published RSL trends are available; note no data available for Western or Northern Alaska. This figure illustrates the RSL trends published by NOAA from various tide gauges and is available at http://tidesandcurrents.noaa.gov/sltrends/slrmap.htm.

A network of tide gauges in Western Alaska could provide accurate observations of RSL changes, but there is only one long-term tide gauge available. This tide gauge is in Nome, Alaska, and data from 1992 to present can be obtained from various online sources (ie: NOAA, PSMSL, or UHSLC/SOEST). There is an additional tide gauge installed in Kotzebue Sound, at the Red Dog mine dock, but this record is just over one decade long, and is not used in this study due to the short duration record. A RSL trend for Nome has not yet been published by NOAA, as the time span of data collection is not long enough to remove significant oceanic signals and is less than the required minimum of 30 years. However, an approximate calculation of the least squares linear RSL trend with seasonal and interannual signals removed gives an estimated rate of -0.48 +/- 4.24 mm/yr (C.E. Zervas, personal communication, January 30, 2015). The

significant associated error reflects the uncertainty in the time series because of the data's limited time span (C.E. Zervas, personal communication, January 30, 2015). Because of the large uncertainty, the Nome tide gauge is not yet useful for predicting future RSL change.

There are historic water level measurements available throughout Western Alaska dating from the 1950's to 2011, with extensive spatial coverage, but they pose many challenges relating to accuracy, continuity, and precision. These measurements are obtained from methods similar to those used by a long-term tide gauge, relating water level back to a fixed point on land, but instead of a permanent installation they are repeated short-term installations that measure the water level using either a tide gauge or staff for instantaneous readings. Unfortunately, when the RSL trends were calculated from these data there are significant differences in both magnitude and sign between stations located near each other (Appendix 1). These historic water levels are considered to have too much error, and are not used in this study, but are reported in the appendix for potential future use.

The data coverage in Western Alaska for constraining RSL rates, oceanic processes, and tectonic processes are sparse and it has not yet been possible to accurately predict RSL change. In the course of this study, new data were acquired making it feasible to address the issue of RSL change in Western Alaska using satellite altimetry and repeat GPS measurements. The tide gauges in Sand Point and Seldovia (Figure 2.4) are used to assess the error in these RSL change estimates as the tide gauge RSL rate should be equal to the vertical velocity of the GPS measurements added to the change observed from satellite altimetry (Equation 2.1 and Figure 1.2).

$$\textit{RSL change (tide gauge)} = \textit{MSL rate (satellite altimetry)} - \textit{tectonic vertical velocity (GPS)} \quad (2.1)$$

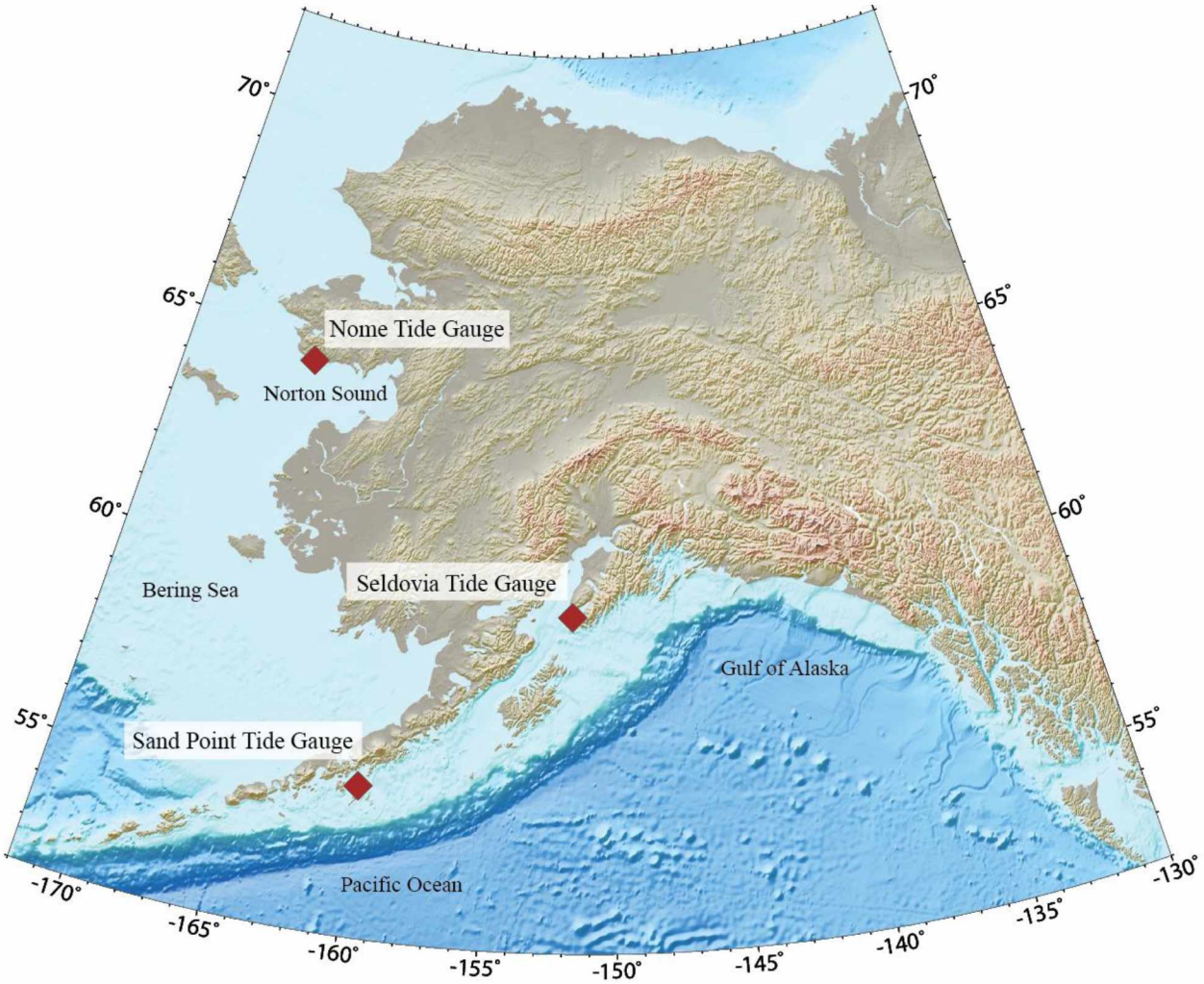

Figure 2.4. Location map of Nome, Sand Point, and Seldovia tide gauges. Note the variety in oceanic setting. Nome is in the shallow Norton Sound, Sand Point is on the steep subduction zone that is exposed to the open Pacific Ocean, and Seldovia is surrounded by complicated bathymetry of the islands and peninsulas that make up the coastline in Cook Inlet.

2.3 Oceanic Setting

The offshore component of this study involves the MSL change in the Bering Sea, which is bordered on the north by the Chukchi Sea and on the south by the Pacific Ocean. The Bering Sea is characterized by an extensive shallow continental shelf environment on the eastern half of the basin along the coast of Western Alaska. Therefore, the geometry and dynamics of smaller bodies of water, such as Norton Sound, Kuskokwim Bay, and Bristol Bay, play significant roles in local sea level trend dynamics. Fourteen main channels through the Aleutian Islands transport

water from the North Pacific Ocean into the Bering Sea (Stabeno et al., 1999). Once in the Bering Sea, water is either moved counter clockwise in an ocean gyre over the deeper, western half in the Bering Slope Current, or travels east on the north side of the Aleutians, as part of the Aleutian North Slope Current (Stabeno et al., 1999; Panteleev et al., 2011). This current continues east to the coast of Western Alaska, where it turns north and passes through the Bering Strait, where the distance between Russia and Alaska is the most narrow, to the Chukchi Sea on its way to the Arctic Ocean (Stabeno et al., 1999; Panteleev et al., 2011).

Sea level change is controlled by factors such as the inverse barometer effect, mass balance of water between terrestrial and oceanic storage, thermosteric expansion, variations in density / salinity, and circulation changes (Bindoff et al., 2007; Cazenave et al., 2008; Church et al., 2010). There have been no studies on the coastal margin of Western Alaska to quantify which of these forcing mechanisms contribute most to overall local sea level change, but there do exist preliminary studies of Bering Sea that explore the dynamic nature of these properties.

Driving forces of MSL change in the Bering Sea involve interactions between ocean, ice, and atmosphere, all of which are sensitive to local and global atmospheric pressure systems. The Aleutian low is responsible for the cyclical nature of both ocean and wind currents on temporal scales that range from weeks to years (Stabeno et al., 1999). An increase in daylight and high insolation in the summer weakens the Aleutian Low, while the Siberian High dominates Asia in the winter, leading to increased intensity of the Aleutian Low, resulting in strong, cold winds from the northeast (Stabeno et al., 1999).

Sea surface and atmospheric temperature in the Bering Sea have also been correlated to longer, annual or decadal atmospheric pressure oscillations. The Aleutian Low controls most of the dynamic processes in the Bering Sea, shifting the bulge of the eastern Bering Sea gyre and warming and cooling the atmosphere and sea surface temperature as its strength and location vary. However, it has been shown the Aleutian Low is controlled, in part, by the Southern Oscillation (SO) (Bjerknes, 1972; Stabeno et al., 1999).

The SO is characterized by decadal to annual periods of basin scale fluctuations in sea level pressure over the western and central portion of the Pacific in tropical latitudes. This oscillation is defined as a weakening of the normal equatorial east winds, referred to as an El Niño event, which alternates to a strengthening of this sea level pressure gradient and produces enhanced easterlies, known as a La Niña event (Stabeno et al., 1999). These stronger easterly

surface winds along the equator during La Niña events result in an increase in sea surface temperature (Figure 2.5) and MSL, with a decrease in the thermocline in the Western Pacific, and vice versa for El Niño events (Stabeno et al., 1999). While this oscillation takes place at the equator, there are also effects in the upper troposphere that interact with mid latitude westerlies, which can, in turn, affect weather systems as far north as the Aleutian Low (Stabeno et al., 1999). Stabeno et al. (1999) found significant correlations between the SO and sea surface and atmospheric temperature in the Bering Sea, with lag ranges of 0-12 months. The SO El Niño winters result in cyclonic systems that force a net flux of warm air in the Bering Sea northwards towards the Arctic, with a weakened Aleutian Low moved to slightly southeast of its normal position (Stabeno et al., 1999), resulting in an increase in temperature and MSL. The SO La Niña winters exhibit the opposite effects and favor anticyclones that have higher central pressure and move cold air southward, displacing the Aleutian Low westward of its regular position (Stabeno et al., 1999). This decreases temperature and MSL as well as shifting the location of the Bering Sea gyre to the west. These trends affect the current systems and thermosteric balance in the Bering Sea along the coasts of Western Alaska as the transport of water to the Arctic fluctuates with these oscillations.

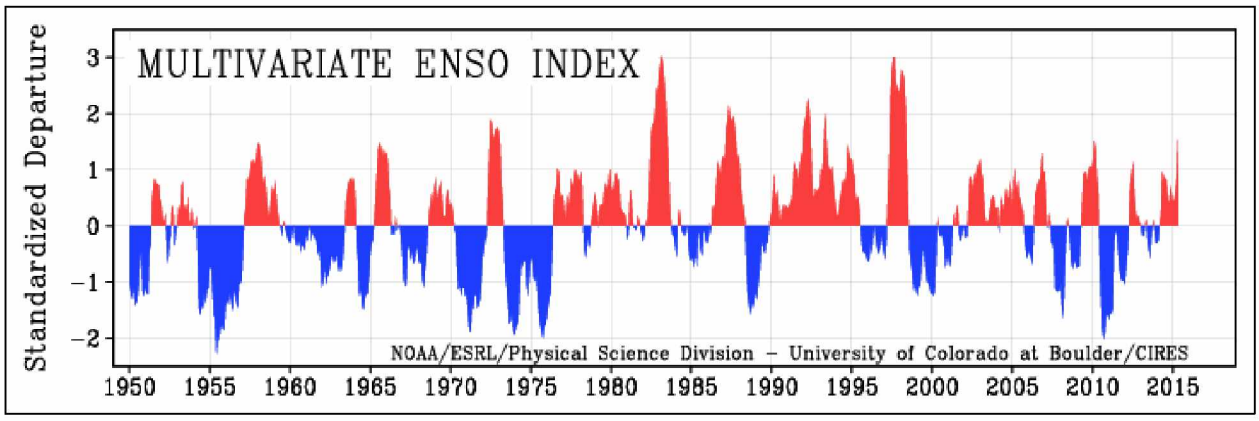

Figure 2.5. Multivariate El Niño Southern Oscillation (ENSO) index. This time series shows the oscillations from warm La Niña (red) events in the Western Pacific to the cooler El Niño (blue) events. Figure modified from Wolter and Timlin (1993 and 1998).

The shallow nature of the Bering Sea shelf (an average of <100 m) (Stabeno et al., 1999) means that deep water currents and density effects have less influence on sea level along the Western Coast of Alaska. Also, large scale gravity induced sea level changes are restricted to the

deeper, western half of the Bering Sea, where the counterclockwise gyre is predominant (Panteleev et al., 2011). Tidal currents become a greater influence in these shallow shelf regions, mixing the surface water and contributing to the flux of salt and heat (Stabeno et al., 1999), which control the depth of the thermocline and halocline layers formed by density and temperature stratification in the water column. These tidal harmonics are important along the coast of Western Alaska, but play a more significant role south of 60°N latitude (Stabeno et al., 1999). Additional studies of mass balance and long-term trends in thermosteric expansion, and current / density variations are needed to further interpret any MSL deviations in the Bering Sea, as it has proven to be a dynamic body of water with complicated processes due to bathymetry, latitude, and basin geometry.

Tidal oscillations are often well defined for coastal communities, but in Western Alaska, due to a lack of tide gauge coverage, tide predictions for locations hundreds of miles away are often assimilated with local knowledge to construct a simplistic time table for local tidal prediction points. Tide gauges are most commonly used to directly observe modern RSL change because they measure the change in sea level relative to a local ground surface, producing a tidal datum that is an elevation reference defined by a particular phase in the tidal cycle (e.g., mean lower low water (MLLW)) (NOAA, 2013). Tide gauges can also be used to evaluate tidal harmonics for the location. Very limited tidal data that span shorter periods of one to six months exist for a few select locations, but are stored by a variety of private, public, and government organizations that don't necessarily make the data readily available for public use.

The limitations in available oceanographic data necessitate that less optimal instruments are required to evaluate coastal MSL trends in Western Alaska. Satellite altimetry records provide excellent spatial coverage and a continuous record back to 1992 is available, but from Figure 2.5 we see that these data span an uneven distribution of El Niño and La Niña oscillations (ENSO).Since 1992 there have been 7 significant "warm" ENSO periods and 6 significant, but smaller "cold" ENSO periods. This biases the MSL trends in the satellite altimetry record towards rates measured during times of "warm" oscillations, which results in longer periods of cooler sea surface temperatures in the Bering Sea and a decrease in MSL rates. A longer dataset is required to better resolve this atmospheric oscillation bias, but the MSL trend can be assumed to increase in the future as the ENSO index fluctuates and has a continued influence on MSL rates in the Bering Sea.

An additional issue when using satellite altimetry is that the measurements are considered to be unreliable within 30-50 km of the shoreline (AVISO, 2009). Even taking these data restrictions into account satellite altimetry is the only available data that provides both spatial and temporal coverage in Western Alaska.

Satellite altimetry data from seven satellites (ERS-1, TOPEX/Poseidon, ERS-2, ENVISAT, Jason-1, Jason-2, SARAL) are publically available as a continuous dataset from 1992 to present for the Bering Sea. Using available satellite altimetry data from the TOPEX and Jason series satellites, the Colorado University Sea Level Research group has produced a regional MSL trend for the Bering Sea, exhibiting approximately +2.6 mm/yr from 1992 to the present (Figure 2.6) (Nerem et al., 2014), only slightly less than the global average of 3.2 +/- 0.4 mm/yr (Nerem et al., 2010; Leuliette and Willis, 2011). This model calculates a regional average for the Bering Sea rather than producing a set of rates as gridded data points.

In Figure 2.6 the annual, high frequency signal of high and low values with differences that range between 100 mm/yr and 200 mm/yr is easily seen repeatedly throughout the model. A long-term decadal oscillation is seen to be high in the 1990s, with a peak amplitude in late 1997 and a low in the beginning of 2001, but it does not appear to repeat itself into the later 2000s. Instead a much longer-term, very low frequency signal is potentially dominating the model as gradual increases in amplitude peak in late 2009-2011. This low frequency signal could be the main component in the trend calculation as it is not clear whether or not it concludes one full cycle.

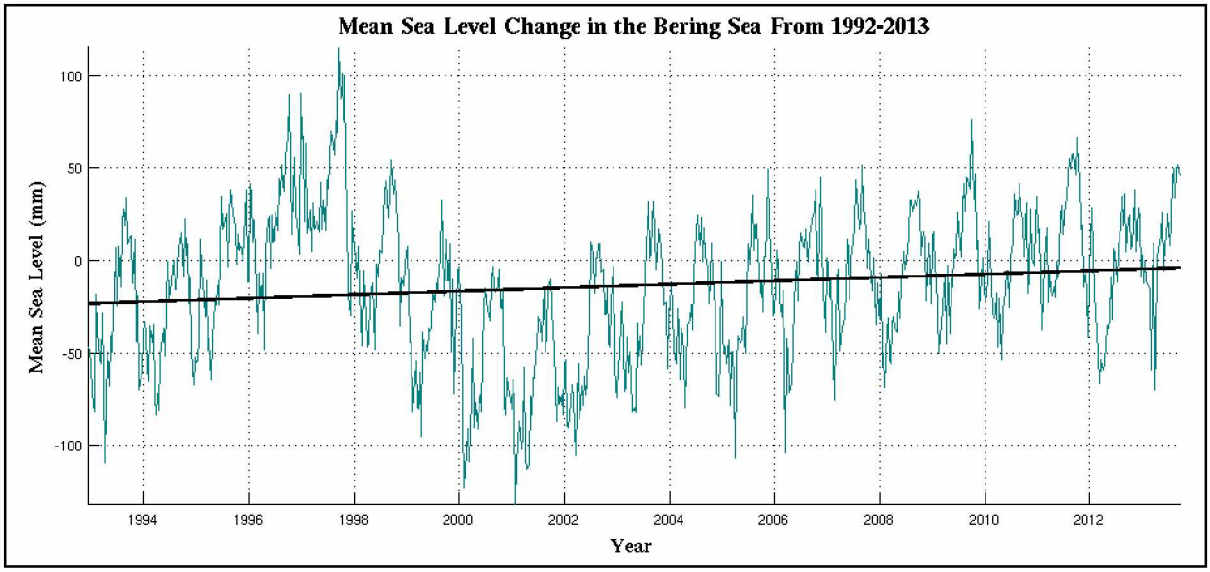

Figure 2.6. Bering Sea regional average MSL and linear trend. The trend here was calculated from a series of satellite altimetry data obtained from the Colorado University Sea Level Research Group website at Colorado State University (Nerem et al., 2014).

Satellite altimetry is not the best suited technique for studying RSL change, or even coastal MSL change (Ablain et al., 2015), but data limitations leave this as the only method presently available in Western Alaska. While it is established that noise from shallow water dynamics, atmosphere, and land restrict accuracy of satellite altimetry to between 30km and 50 km offshore (AVISO, 2009), a study by Deng et al. (2002) along the coast of Australia found that depending on the coastal environment, potentially this limit in accuracy could be reduced to distances of 8-22 km. Due to the shallow shelf and complicated geometry of the coastline along Western Alaska, this study assumes inherent error at the established conservative estimate of 50 km (AVISO, 2009) and provides a preliminary approximation of direction and relative magnitude with the objective of assembling the ground work for future more accurate observations of MSL trends in Western Alaska when new datasets are available.

2.4 Tectonic setting

The tectonic environment of Western Alaska is widely accepted to be underlain by the Bering Plate / North American Plate boundary (Lander et al., 1996; Mackey et al., 1997; Fujita et al., 2002; Cross and Freymueller, 2008; Cross, 2007). In 2005, a GPS campaign was conducted to occupy geodetic benchmarks in Western Alaska and the Aleutians, in order to quantify the horizontal motions of the Bering plate and to define the plate boundary (Figure 2.7). Cross

(2007) and Cross and Freymueller (2008) proposed clockwise rotation of a plate defined by a southern boundary with the Pacific plate along the Aleutian islands; Eastern Russia and the Kamchatka Peninsula represent the western boundary with the Eurasian plate; while the Seward Peninsula down to the Alaska Peninsula compose the eastern contact of the Bering plate with the North American plate. The Bering plate boundaries with the Eurasian and North American plates are not well understood and available GPS data of horizontal and vertical velocities are limited in the region of study (Cross and Freymueller, 2008).

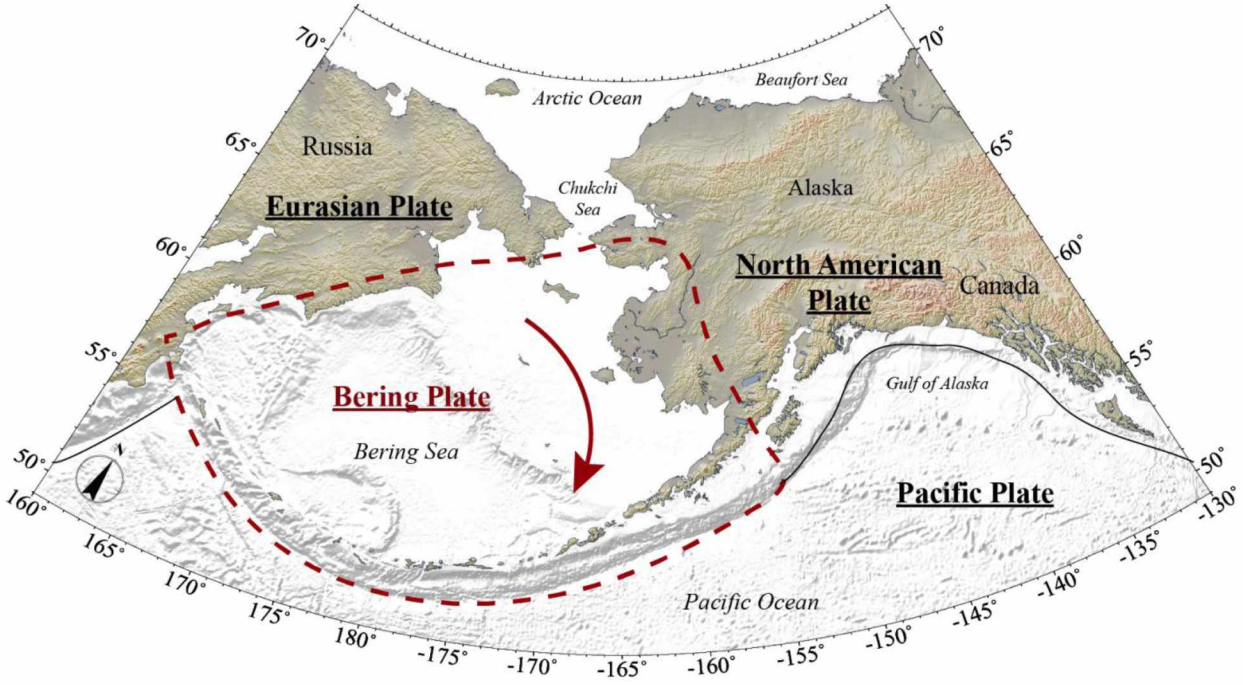

Figure 2.7. Proposed Bering plate boundaries and rotation. The Southern boundary with the Pacific plate is well defined by the Aleutian subduction trench, but the west, north, and east boundaries are harder to define and require improved GPS coverage to further constrain these boundary locations (Cross and Freymueller, 2008).

Tectonic vertical velocities in Western Alaska are believed to be controlled by a combination of glacial isostatic adjustment (GIA) and subsidence of the Yukon-Kuskokwim Delta as a result of sediment and water loading. Smaller signals from post seismic deformation may contribute to the vertical motion in limited areas, but are small enough over most of Western Alaska that they do not need to be considered.

GIA vertical velocities result from the loading and unloading of ice sheets. In Western Alaska the relevant ice sheets are the Pleistocene Laurentide and Cordilleran ice sheets. As these

ice sheets grew over most of the northern North American continent 95,000 – 25,000 years ago, their weight deformed the lithosphere causing a depression with related mantle displacement. As the lithosphere was depressed under the ice sheet, a forebulge formed due to the flexural properties of the lithosphere and was located in the vicinity of Alaska.

Modeling of GIA is done using a post glacial rebound calculator, consisting of ice loading models such as ICE-3G (Tushingham and Peltier, 1991) in conjunction with an Earth model, such as the three layer model for North America by James and Morgan (1990). The displacements predicted by these models are dependent upon the thickness of the lithosphere, asthenosphere, and upper mantle along with the viscosity structure of these layers.

These Earth structure parameters are not well defined in Alaska, so there are a few acceptable possibilities for model results (Figure 2.8). These results are based on varying the lithospheric thickness parameter from a continental shield-type lithosphere of 100 km, to a Southern Alaska-type based model with a thickness of 50 km. One of the effects of these different lithospheric thicknesses is the location of the forebulge. In the continental shield-type model the forebulge is located over the center of the state of Alaska, while in the Southern Alaska-type model it is shifted west, to the Seward Peninsula coast.

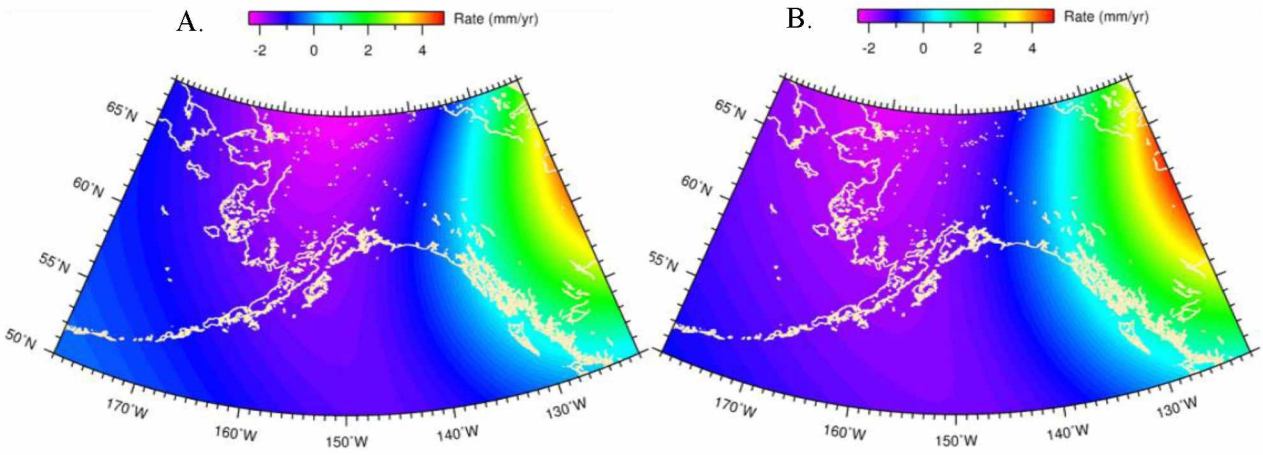

Figure 2.8. Comparison of GIA models based on ICE-3G. Continental shield-type (A) and Alaska-type (B) Earth models are presented. The difference in location of the forebulge can be observed as the highest values of subsidence (purple) are located over the center of the state in the continental shield-type model, but are shifted to the western coast in the Alaska-type model. Figure courtesy of Dr. Jeffrey Freymueller.

Recent updates to GIA models in Southeast Alaska by Hu and Freymueller (2015) (in preparation) find that the best fit parameters for the region affected by the post-Little Ice Age deglaciation consist of an Earth model with a lithospheric thickness of 50km, asthenospheric thickness of 240 km, asthenospheric viscosity of $3x10^{19}$ Pa s, upper mantle viscosity of $2.4x10^{21}$ Pa s, and lower mantle viscosity of $5.01x10^{21}$Pa s. These are models best fit for Southeast Alaska, and it is not clear if they can be extrapolated over the rest of the state to Northern and Western Alaska. This study includes an updated best fit GIA model for Northern and Western Alaska, resulting in better defined Earth structure and viscosity profiles fit specifically for these regions.

Delta subsidence is expected to be responsible for additional tectonic vertical motion on the Yukon-Kuskokwim (Y-K) Delta because of the magnitude of sedimentation associated with these rivers. The Yukon River (Figure 2.9) is the third longest river in North America and has one of the largest drainage basins, estimated at approximately 830,000 km^2, about one quarter of the Mississippi River drainage basin (Milliman and Farnsworth, 2011). Measured mean annual discharge of the Yukon River at the village of Kaltag, was estimated at approximately 6,220 m^3 s^{-1} (Roden, 1967). The Yukon River Delta alone (Figure 2.10) is larger than the state of Oregon, with a total load of $60x10^6$ tons of sediment per year (Milliman and Syvitski, 1992) being deposited into the Bering Sea off the west coast of Alaska.

The Kuskokwim river is smaller, but still a large river with many meanders over a large area of deltaic environments that cover the majority of Western Alaska (Figure 2.11). The estimated drainage basin for the Kuskokwim River is an area of 80,550 km^2, with a measured mean annual discharge rate of 950 m^3 s^{-1} at Crooked Creek (Roden, 1967). Milliman and Syvitski (1992) estimate the total load of the Kuskokwim River to be between $5x10^6$ and $10x10^6$ tons/year (Figure 2.12).

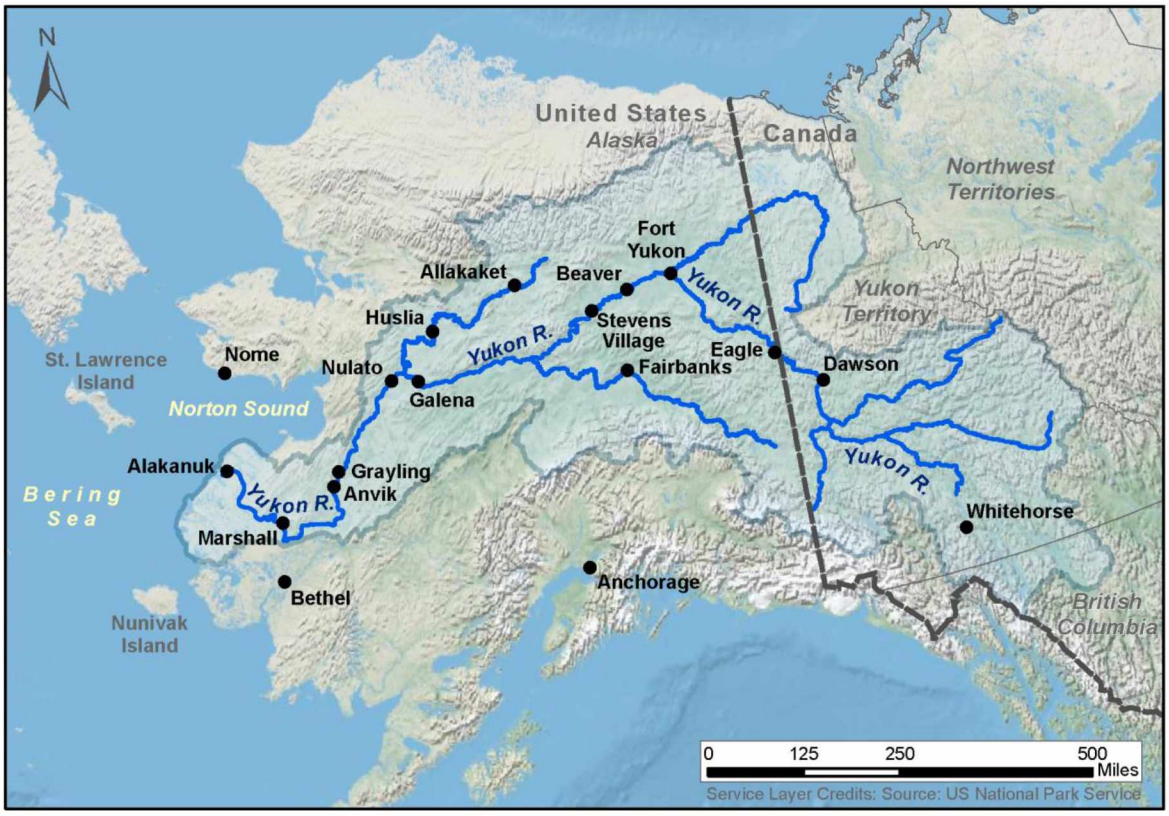

Figure 2.9. Map of the Yukon River and associated tributaries. The Yukon River flows west to the outlet in the Bering Sea, just south of Norton Sound. The Kuskokwim River and associated delta and drainage basin borders the Yukon River drainage basin to the south and goes through the community of Bethel. The extent of the drainage basin is highlighted in light blue. Copyright Alaska Department of Fish and Game. Used with permission (Schabert et al., 2015b).

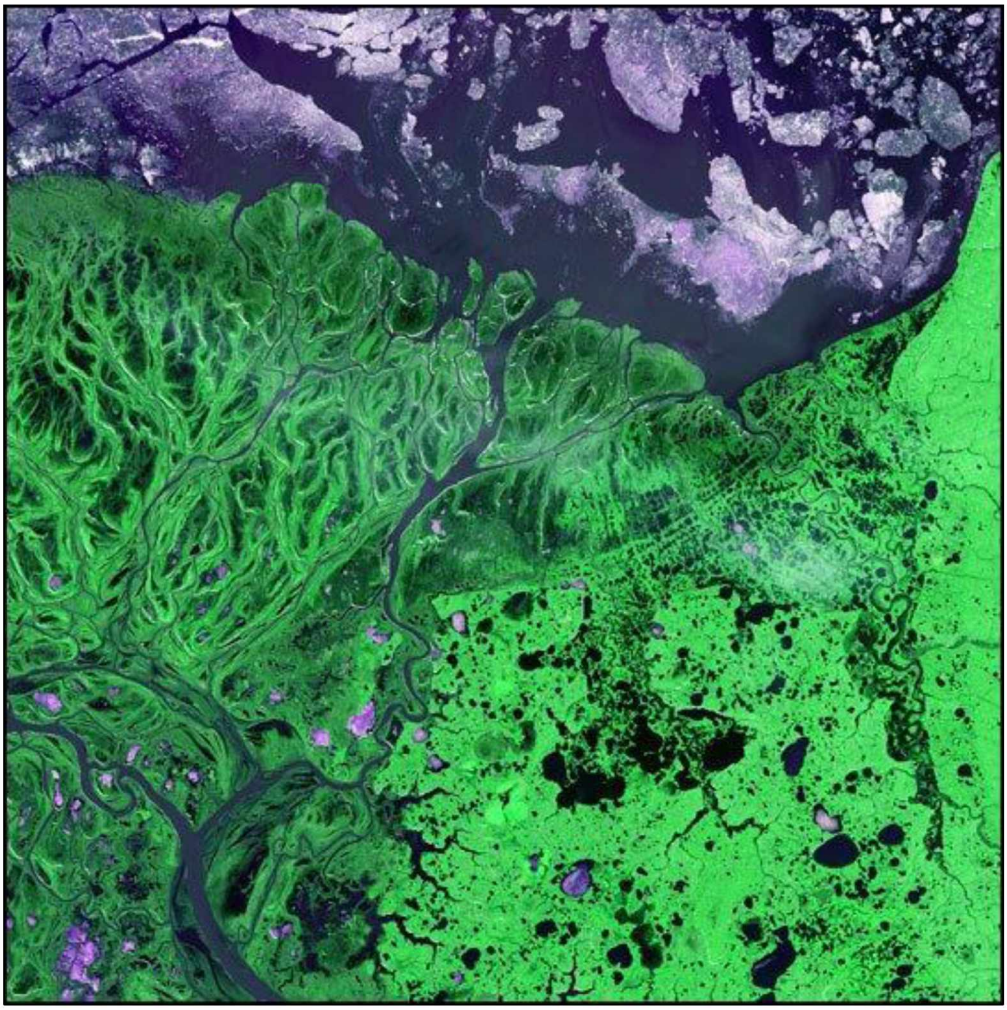

Figure 2.10. Advanced Spaceborne Thermal Emission and Reflection Radiometer (ASTER) image. This was taken from NASA's Terra satellite of the Yukon River and the Yukon Delta acquired on May 26, 2002. The many meanders of the river appear in birdfeet patterns that branch across the delta on the left side of the image. On the right, the saturated lands rife with melt ponds show the flat and low elevation of this deltaic environment. Image provided by the USGS EROS Data Center Satellite Systems Branch as part of the Earth as Art II image series.

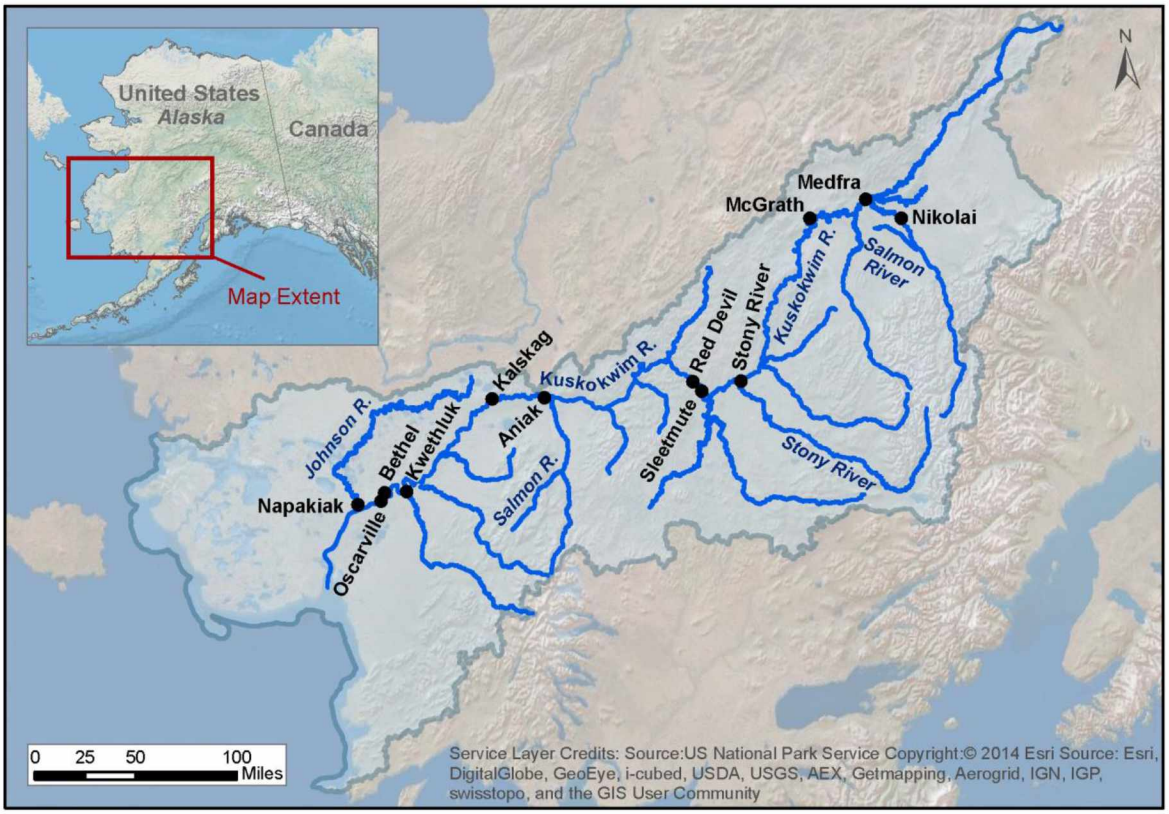

Figure 2.11. Map of the Kuskokwim River and associated tributaries. The Kuskokwim River flows southwest to the outlet in Kuskokwim Bay. The Yukon River and Yukon River Delta can be seen just north of the Kuskokwim. The extent of the drainage basin is highlighted in light blue in the main map. Copyright Alaska Department of Fish and Game. Used with permission (Schabert et al., 2015a).

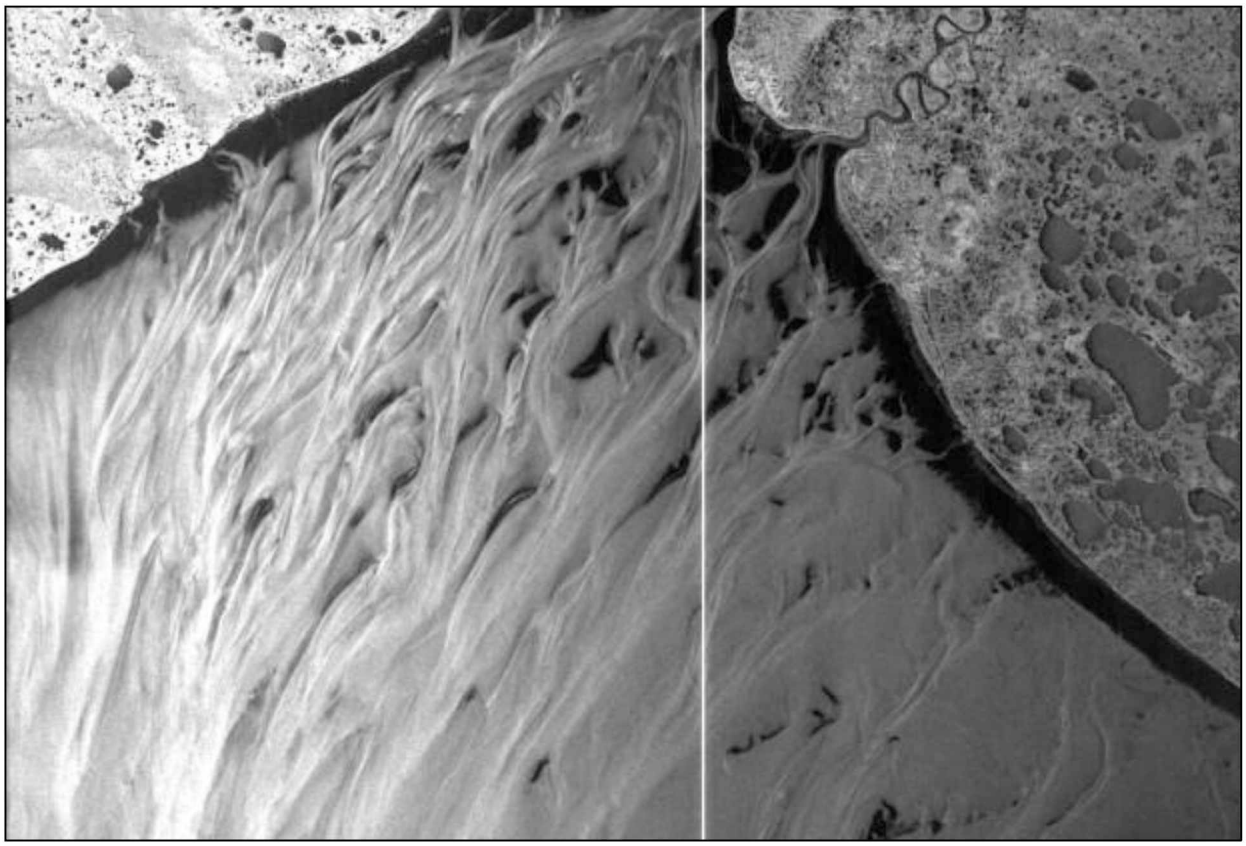

Figure 2.12. Photographs of Kuskokwim Bay taken from SEASAT. The active transport of sediment transported offshore from the Kuskokwim river and its distributaries is readily seen from space. The amount of water that covers the land of the Y-K Delta is visible as dark circles and ovals. There are many permafrost melt ponds and abandoned river meanders that dominate this deltaic environment. Photograph courtesy of the Alaska Satellite Facility.

Models of delta subsidence due to sediment loading as a function of drainage and discharge areas and rates have yet to be standardized or made publically available, and a specific model that could provide an estimate of the vertical motion associated with the delta subsidence of the Y-K Delta has not yet been created. While no specific model exists for the Y-K Delta, the magnitude of these rivers implies the sediment deposition is large enough to produce loading deformation in the region comparable to approximately one quarter of the Mississippi River Delta, or 0.25 – 2 mm/yr. This study does not attempt to model or collect data related to the creation of a delta subsidence model for the Y-K Delta, but our data will be evaluated to determine if it is an important factor in the tectonic motion of Western Alaska.

2.5 Field campaigns

This thesis work addresses the limitation in remote and sparsely populated Western Alaska, where GPS data are lacking both temporally and spatially. Field work for this study involved the occupation of 44 benchmarks in 16 communities across Western Alaska during the summers of 2013 and 2014 (Figure 2.13) using Trimble 5700 GPS receivers with Zephyr Geodetic antennae (Figure 2.14), set up for static occupations of three to ten days. Some of these measurements were the first or second occupation of the site, which means these data will not be used in this study, but can be used with more occupations at a later date; sites with two surveys often can be used for studies of horizontal motions, but are usually not reliable enough for studies of vertical motions. The data obtained during these surveys are stored in the University of Alaska Fairbanks (UAF), Geophysical Institute (GI) databases, the UNAVCO data archive, and were made publically available as OPUS solutions through the National Geodetic Survey (NGS) shared database.

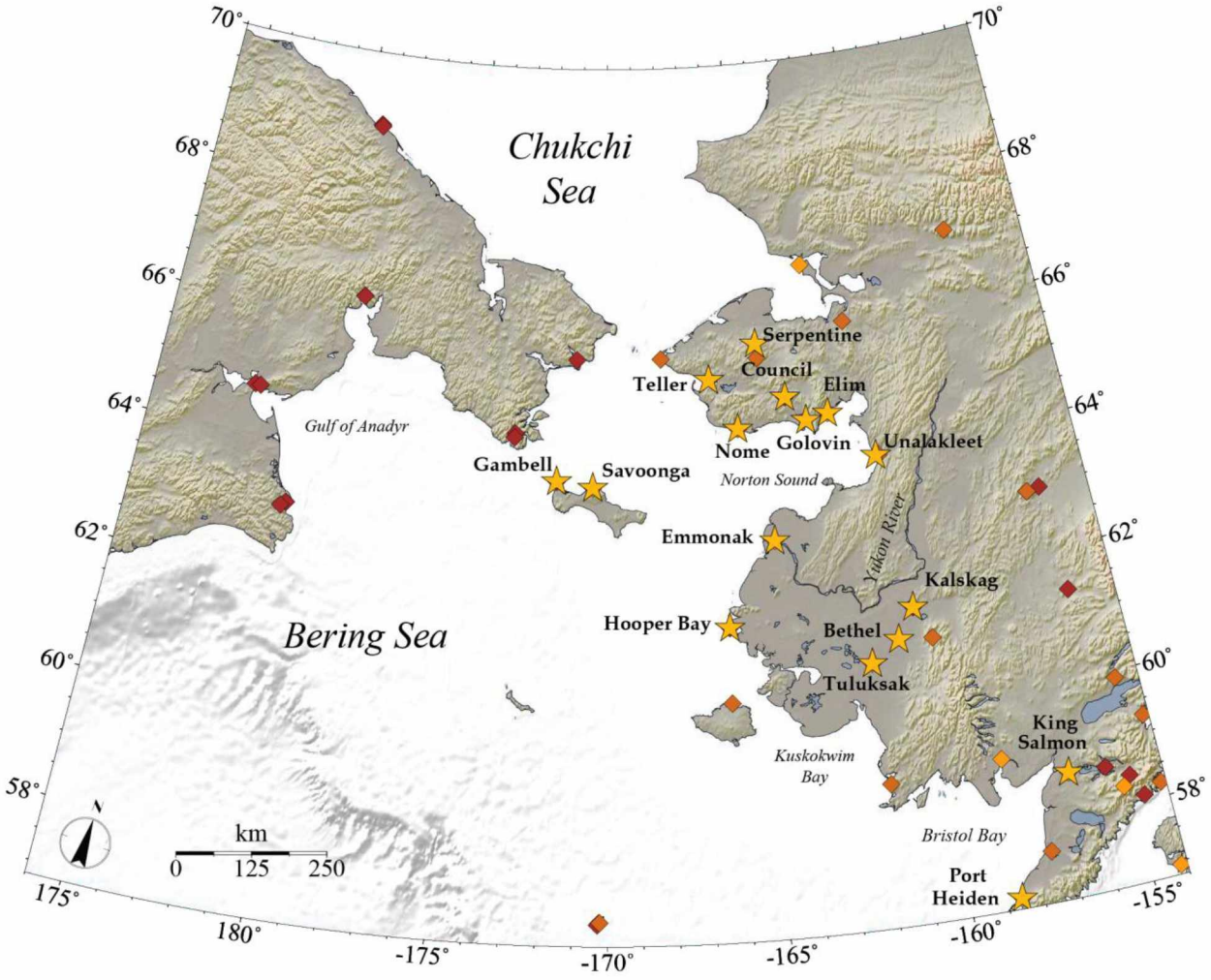

Figure 2.13. Locations of GPS sites in Western Alaska. Orange diamonds represent sites of continuously operating GPS. Red diamonds represent campaign sites where repeat static observations exist. Yellow stars with community labels are campaign locations visited in the summers of 2013 and 2014 as part of this study.

Figure 2.14. Campaign site 3651 in Golovin, Alaska. This photograph shows the site occupied with a tripod setup of a Trimble 5700 receiver and Zephyr Geodetic antenna in the summer of 2013 as part of this study.

Campaign site occupations are only beneficial after repeat measurements of these sites have been conducted, so they can be used to create a position time series, and thus an estimate of the rate of motion (velocity). Most GPS sites in Western Alaska had only one or two occupations before this study, but by adding a third occupation to the time series of GPS positions, a more accurate velocity trend can be reported (Figure 2.15). Campaign sites visited during field work were selected based upon cost-effectiveness and accessibility, as well as the length of data already available for a site. Sites with two data points within the past two decades were given highest priority, but opportunistic collection of sites with only one point or older data were also undertaken when possible.

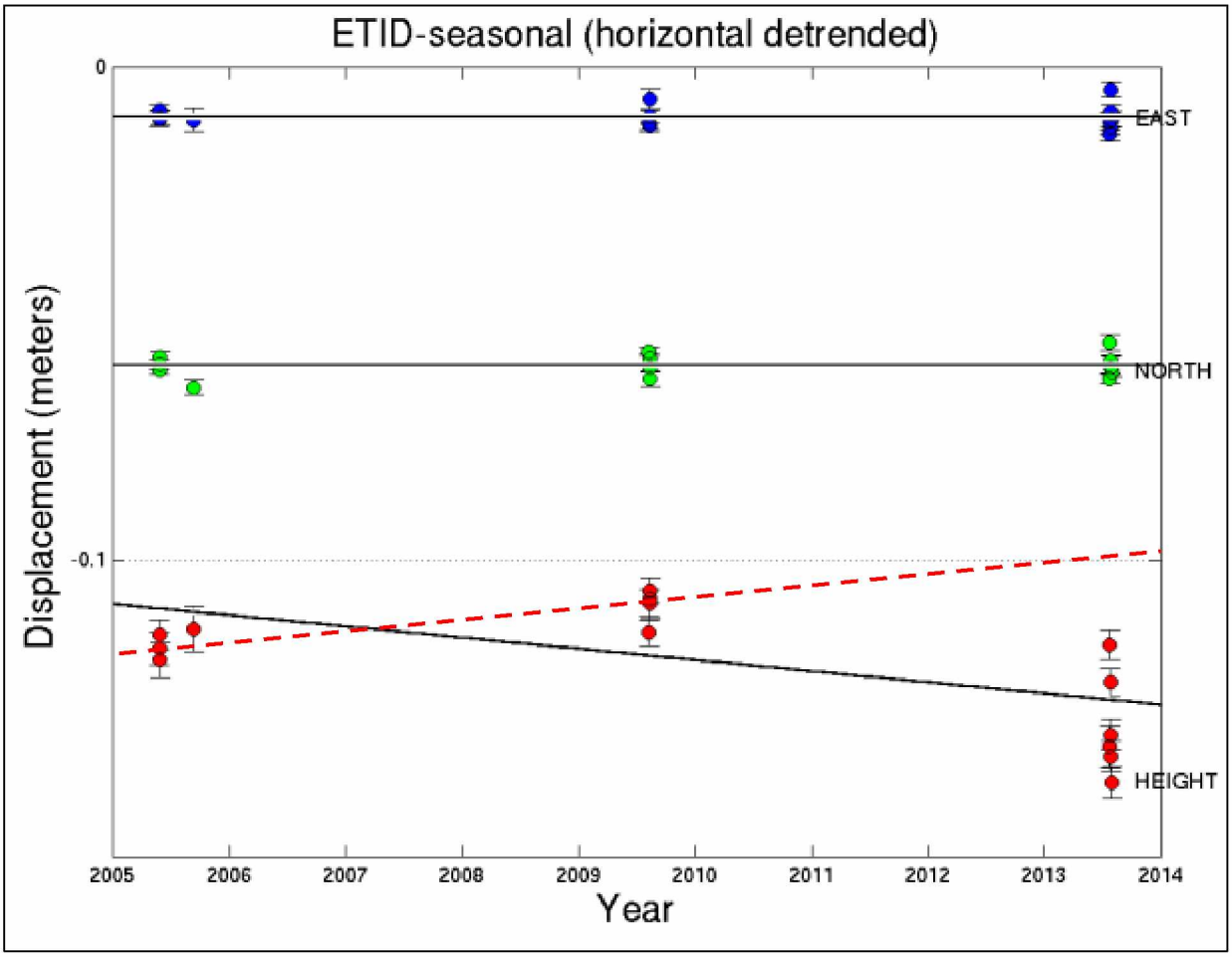

Figure 2.15. GPS position time series by directional component for the station ETID in Elim, AK. The top line is east velocity, middle line is north velocity and bottom line is vertical velocity. Each dot indicates one day of observations. At ETID there are three occupations, including one from this study in 2013. The trend shows an apparent negative vertical velocity (1.45 mm/yr), or subsidence, in this area. The significance of including a third time-step is apparent, as the trend of the first two data points (red dashed line) appears to be slightly positive (indicating uplift).

There are also several continuously operating GPS sites, the majority of which have been installed by UNAVCO as part of the Plate Boundary Observatory project, which comprises the geodetic component of EarthScope. Most of the continuous sites in Western Alaska were installed between 2006 and 2008, and data have been recorded continuously since their installation. These data are publically available online in the UNAVCO archive.

3 Data

3.1 Tide gauge data and analysis

The data from tide gauges were obtained by the NOS/ NOAA and are available in a variety of formats, depending on the amount of processing that NOAA has performed on the data, and the reference datum the water levels are associated with. Tide gauge data are measured relative to an arbitrary zero mark that was determined upon installation. NOAA uses a tabulation process to convert this arbitrary datum to one with a physical meaning in oceanography. In this study, data that have been tabulated to be relative to local MSL are used. The preliminary processing that NOAA performs on water level data includes filling in data gaps of up to 3 or 4 hours using a least-squares fit of the six minute data, making relevant comparisons with backup sensors, tide staffs, nearby stations, or predicted tides, and visually verifying data continuity. Tidal harmonics for the location of the tide gauge are estimated with periods that range from just over 3 hours to 1 year. NOAA provides these data for all tide stations. When a long enough time series has been collected, these tidal harmonics, seasonal, and interannual signals are removed and a least squares linear trend is estimated and published online, with associated error as a MSL trend. No trend has been published for Nome, due to the short length of the data, but trends are available for Sand Point and Seldovia.

In order to assess which data would be most accurate for use in this study, a comparison of the various datasets is completed for the tide gauge in Nome, as well as similar tide gauges with longer, more complete records in Sand Point and Seldovia (Appendix 2). Based on these comparisons, I use mean monthly water level data relative to MSL with no additional processing done by NOAA to remove tidal, seasonal, or interannual signals.

The comparisons in Appendix 2 also indicate that the Nome tide gauge data are more consistent when the time series is truncated at both ends to exclude data from the first and last 11 months, so that only data between November 1992 and November 2014 are used.The mean is then removed from the data and a trend is calculated using the "detrend" function of MATLAB to remove the best fit straight line linear trend from the data. The same method is used in the comparison at the Sand Point and Seldovia tide gauges as well, and produces trends consistent with those calculated by NOAA. An additional MSL trend calculation and error estimate for the Nome tide gauge data is provided by Zervas (personal communication, January 30, 2015). NOAA has not published these values because the magnitude of the uncertainty associated with

the MSL trend calculation is almost ten times that of the trend itself. These values are used in this study to assess the error contributed to RSL change calculations from tide gauge data.

3.2 Satellite altimetry data and analysis

The offshore component of RSL change (MSL change) in this study is approximated from satellite altimetry data. These data are available freely through several websites, including Archiving, Validation, and Interpretation of Satellite Oceanographic Data (AVISO), the Colorado University Sea Level Group, and the NOAA/NESDIS/STAR Laboratory for Satellite Altimetry. Satellite altimetry MSL trend data from AVISO were used here because processed data from 1992 to present are readily available and widely used in the scientific community.

The data available through AVISO includes products of the French space agency, Centre National d'Etudes Spatiales (CNES), NASA, NOAA, and the European Space Agency (ESA). Various datasets are available, including single and multi-mission products, along track data and gridded datasets. Both delayed and near real time products are available. Data come from the total collection of altimetry satellites, including GEOSAT, ERS-1 and ERS-2, TOPEX/Poseidon, GFO, Jason-1 and Jason-2, Envisat, CryoSat-2, SARAL, and HY-2A. All data and products are available publically online with the creation of a free account through AVISO.

Satellite altimetry data undergo a series of processing steps that involve applying the most recent recommended corrections, models, and reference frames. This processing addresses the instrument error, including corrections to the orbit and clock of the satellite through radiometer drift corrections, alternative retracking, and better ultra-stable oscillator corrections (AVISO, 2009). Geophysical corrections are also made to account for the ionosphere and atmosphere, as well as processes such as Earth, ocean, and polar tides (AVISO, 2009). The most current reference surfaces are also applied, such as mean sea surface and ice, land, and ocean masks. These tasks are split up between agencies depending on which satellite the data originated from and the type of product being produced (AVISO, 2009).

The error associated with satellite altimetry data is difficult to establish, as it consists of the uncertainty inherent in the various models and corrections that are applied (AVISO, 2009). This becomes increasingly difficult with the addition of satellites to construct a multi-mission dataset, but has been estimated between 0.4 – 0.6 mm/year (Ablain et al., 2009). Ablain et al. (2015) further define this error to be 0.6 mm/yr for the global MSL trend, but maybe as high as

1-2 mm/yr for regional sea level trends, and are currently working on a new algorithm to better define these uncertainties.

The product used in this study is a multi-mission, delayed time, global, gridded dataset of sea level rate from 1992 to 2014. This product uses all available data from all available satellites to calculate rates of sea level change on 0.25° by 0.25° grid cells (AVISO, 2009). The error estimate of Ablain et al. (2009) will be applied to the averaged satellite altimetry cells used in this study until further definition of uncertainties with these measurements can be produced.

3.3 GPS data and analysis

During the summers of 2013 and 2014, I conducted campaign GPS surveys in Western Alaska in an effort to expand the geodetic database compiled at the University of Alaska Fairbanks – Geophysical Institute (UAF-GI) (Appendix 3). The data obtained from these campaign occupations were processed at the UAF-GI, using scripts created by Dr. Jeffrey Freymueller. Additionally, continuous data are automatically downloaded and processed nightly. Position solutions using absolute phase center models for the antennas and receivers are then estimated for all campaign and continuous data in Alaska, available as part of the UAF-GI database using the GIPSY/OASIS II software goa-5.0, developed by the Jet Propulsion Laboratory (JPL) in Pasadena, California. The orbit and clock products are provided by JPL and are used with the GMF tropospheric mapping function, Global Pressure and Temperature model, and the ocean tide model TPXO 7.0 to remain consistent with the orbits and clock products and avoid systematic errors. Site positions are transformed into the International Terrestrial Reference Frame (ITRF) 2008 and a time series is extracted with daily solutions weighted by the inverse of their covariance matrices that are produced by the GIPSY analysis. Further details of the GPS processing and parameter estimation methods can be found in Fu et al., (2012). Displacements and velocities are then estimated from these time series.

To estimate displacements and velocities, 604 time series from continuous stations and 260 time series from campaign sites are used to fit a vertical velocity model (Equation 3.1) of Alaska, using MATLAB scripts created by Dr. Jeffrey Freymueller, with adaptations by Daniel Landskron of Vienna University of Technology. The position model used in this fit is as follows:

$$x(t) = a + bt + c_1\sin(2\pi t) + c_2\cos(2\pi t) + c_3\sin(4\pi t) + c_4\cos(4\pi t) + c_5 H(t - t_d) + c_6 H(t - t_v)t \quad (3.1)$$

Where x is position at time 0, t is time, a is the intercept, b is the slope, $c_1 - c_4$ are seasonal coefficients, c_5 is the magnitude of displacement, c_6 is the magnitude of velocity change, H is the Heaviside function, t_d is the time of displacement, and t_v is the time of a change in velocity. Not all of the terms included in Equation 3.1 are required for every site. In practice the reference time is defined around the midpoint of the data.

Non-linear terms or corrections are needed for a variety of reasons. Seasonal corrections are made where evidence of cyclical loading effects due to local water and snow loading cause variations in height. This seasonal signal creates sharp low amplitudes in the winter (Figure 3.1) as snow begins to accumulate and broader high amplitudes in the summer as the snow melts and significant runoff occurs (Freymueller et al., 2008; Fu and Freymueller, 2012). These variations can have displacements with peak-to-peak amplitudes of up to ~20 mm in a matter of a few months, but do not result in permanent deformation. For most continuous sites, a seasonal model is estimated as part of the fit. If a seasonal model cannot be estimated from the time series, as is the case for campaign sites and a few continuous sites with persistent seasonal data gaps, a seasonal model based on satellite gravity data from the Gravity Recovery and Climate Experiment (GRACE) satellites is applied (Fu and Freymueller, 2012).

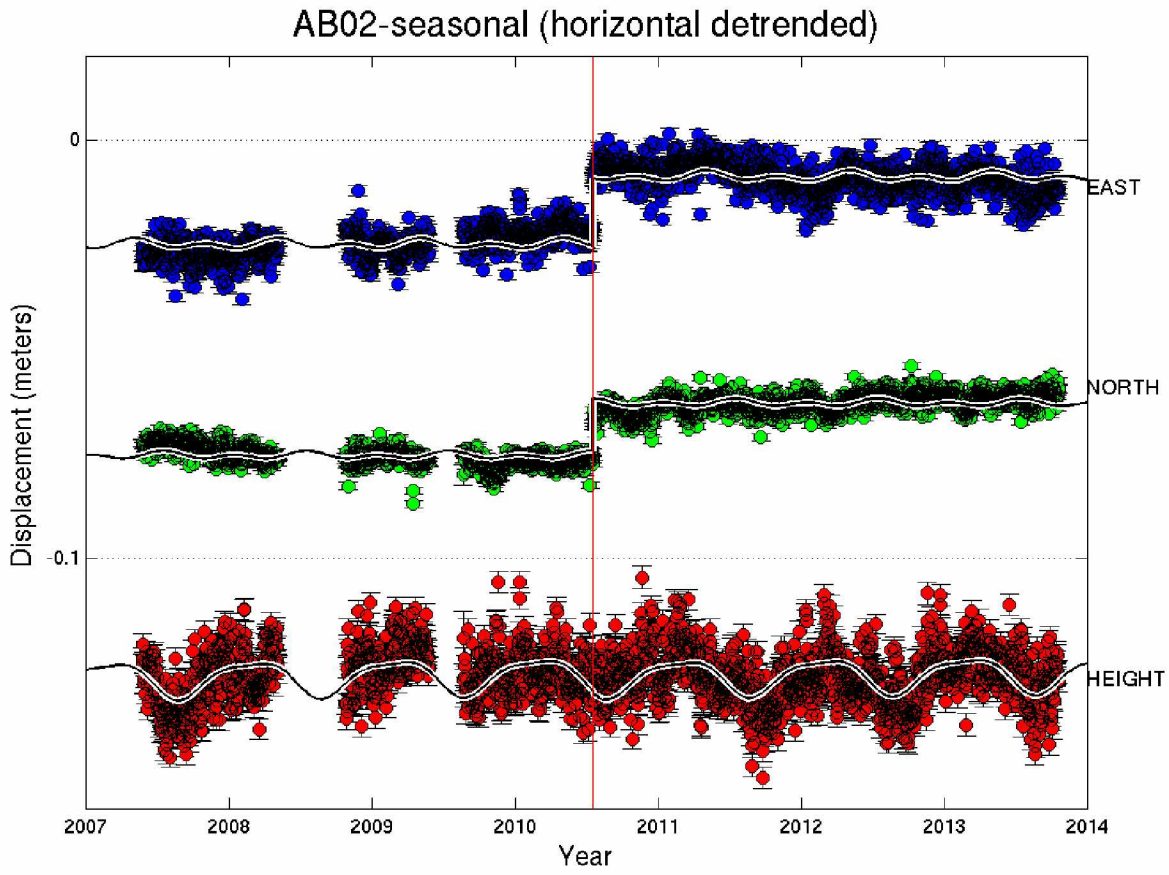

Figure 3.1. Vertical and detrended horizontal position time series of GPS site AB02. This site is located in the Aleutian Islands. The blue data (top) are East positions, the green (middle) are North positions, and the red (bottom) are vertical position. This is an obvious example of the seasonal signal caused by snow and water loading with amplitudes of ~20 mm. The seasonal models for each time series are overlaid on top of the data. The narrow low position troughs of the winter contrast with the broad high positions of the summer in the vertical time series over a somewhat regular annual cycle. The horizontal positions in the East and North directions have much smaller seasonal amplitudes on what appears to be a biennial cycle. A 6.7 earthquake in the Aleutian Fox Islands on July 18, 2010, indicated by the vertical red line, created significant permanent offset at this GPS station of approximately 20 mm to the East and 10 mm to the North.

Permanent displacements in GPS data can result from measurement errors and short-term tectonic events. The replacement of equipment at continuous stations or an incorrect setup or antenna height measurement at a campaign station can result in the instantaneous offset in both vertical and horizontal directions, though usually on the order of millimeters. Tectonically, offsets can be produced by earthquakes and can range from millimeters to multi-meter displacements. When time series do not include a really large earthquake, the trend is calculated

using the full extent of the data and sites with simple step-like offsets modeled by including a step function (Heaviside function) in the model, if needed. When a large earthquake produces significant post-seismic deformation so that the trends pre- and post-event are dissimilar, the time series are segmented and only pre-event data is used in trend calculations.

Gross outliers are stripped from the data and an additional error of 3 mm/T, where T is the length of the time series in years, is added in quadrature to each vertical velocity uncertainty. This additive error is based upon the analysis performed by Santamaría Gomez et al. (2011), and empirically compensates for time-correlated errors in the data that are ignored in the least squares fit. Velocities are calculated in ITRF 2008 (ITRF) and then converted to velocities relative to the North American (NOAM) plate using the model GEODVEL by Argus et al. (2010). Argus et al. (2010) also estimated a frame origin bias in ITRF, mainly in the z direction. This correction is applied to the GPS data used in this study along with the removal of the NOAM plate motion. In this thesis I modeled these velocities relative to the NOAM plate, and corrected for geocenter bias. For vertical velocities in Alaska the geocenter correction results in a subtraction of approximately 0.9 mm/yr from the ITRF vertical velocity (Argus et al., 2010).

The resulting velocity model produces north, east, and vertical site velocities for 864 GPS sites in Alaska (Figure 3.2 and Appendix 4). When there are multiple sites at a given location in Western Alaska, a linear least squares method (weighted by the uncertainty of each measurement) was used to obtain an average velocity and uncertainty for that location, and the stability of the sites was assessed based on the consistency of these measurements.

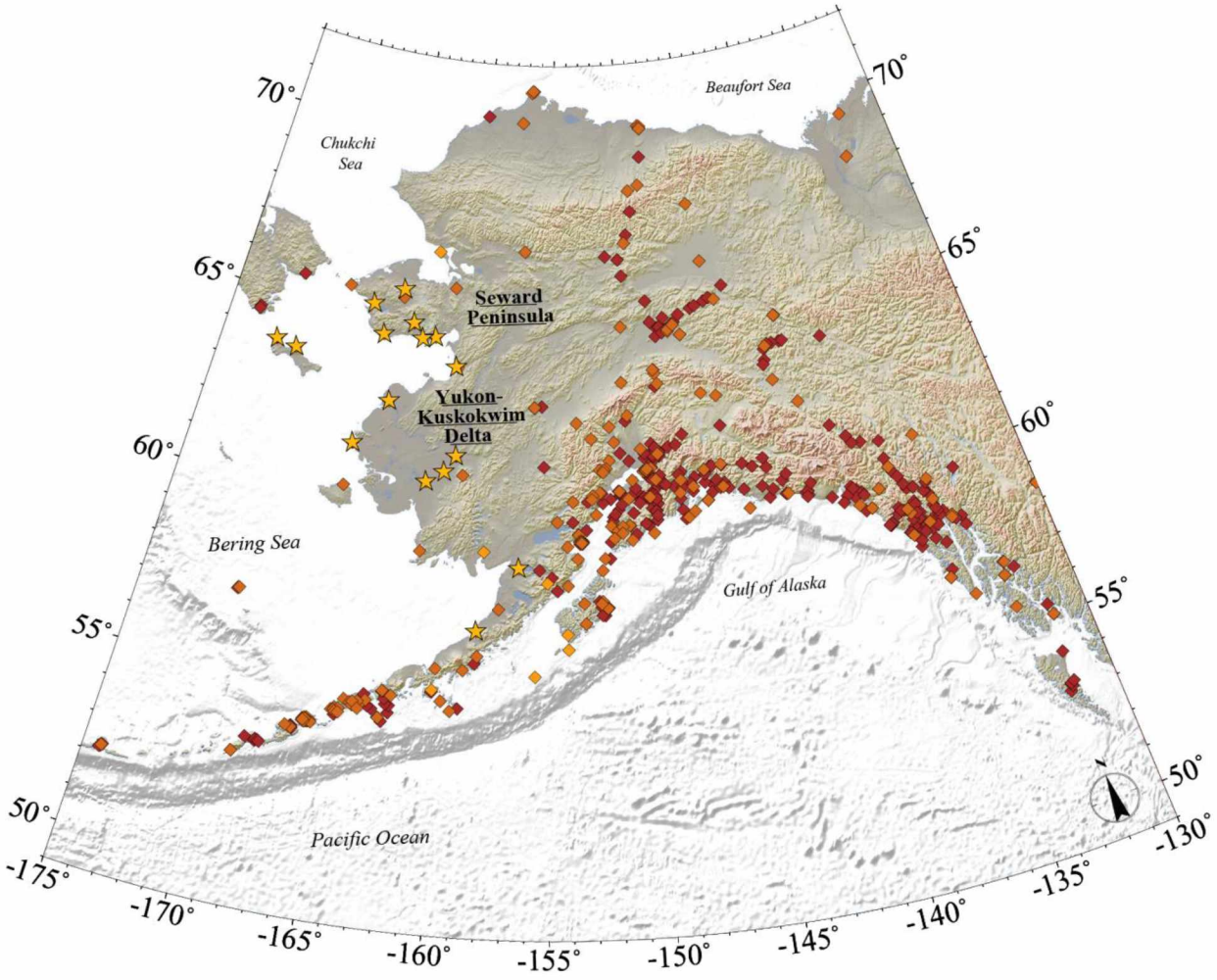

Figure 3.2. Locations of GPS receivers used in the Alaska tectonic velocity model. Orange diamonds are sites of continuously operating GPS. Red diamonds are campaign sites where repeat static observations are made. Yellow stars are campaign locations that were visited in 2013 and 2014 as part of this study.

4 Results

4.1 Tide gauge relative sea level trend

The Nome tide gauge mean monthly water level data relative to local MSL, obtained online through NOAA from November 1992 – January 2014, was used in a linear least squares analysis to produce a trend of +0.50 mm/yr (Figure 4.1) . There is no calculated or provided error with this rate (estimation of uncertainty requires an in-depth assessment of the time-correlated errors in the data), but the uncertainty of +/- 4.24 mm/yr calculated by Zervas (personal communication, January 30, 2015) for a NOAA estimate of rate from mean monthly water level values relative to MSL is adopted. The rate calculated by Zervas (personal communication, January 30, 2015) had an opposite trend of -0.48 mm/yr, but both values are well within the range of error. For other tide gauges, the approach I used for Nome gave a very close agreement with the trends published by NOAA (Appendix 2). As the water level values are tied to the primary tidal benchmark, they represent RSL change in Nome, Alaska.

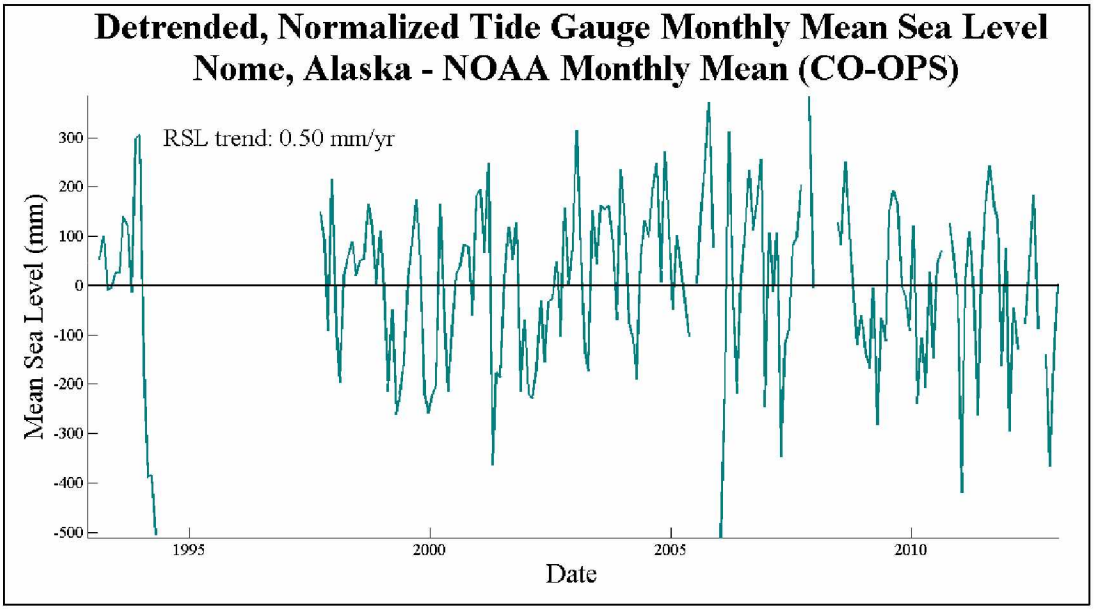

Figure 4.1. Plot of monthly mean water level values relative to MSL. These values were obtained from NOAA and exhibit a RSL trend of +0.50 mm/yr. Data extends from November 1992 to January 2014.

4.2 Satellite altimetry mean sea level trends

A gridded dataset of MSL trends from 1992 – 2014 observed from satellite altimetry was obtained from AVISO (Figure 4.2). Offshore of Western Alaska the MSL trend is visually

assessed to have rates between -1 and 1 mm/yr. Nerem et al. (2014) calculate a regional average of 2.6 mm/yr for the Bering Sea that is much higher than the trends visually observed for Western Alaska, but appears to be an accurate approximation of the central to western Bering Sea regions. Their trend includes and is dominated by the Western Bering gyre with elevated rates of MSL trend due to longer wavelength atmospheric oscillations such as the ENSO. This gradient is located in the western half of the Bering Sea, but is not permanently located there and subject to relocation under changing atmospheric conditions (Bjerknes, 1972; Stabeno et al., 1999).

Due to the sensitivity of satellite altimetry in near shore settings, an effort to resolve any influence the coast may have on the data was undertaken through a test of cell averaging and standard deviation comparison. Coastal environments can vary greatly within a small region, so this test was performed at three locations with different coastal settings .

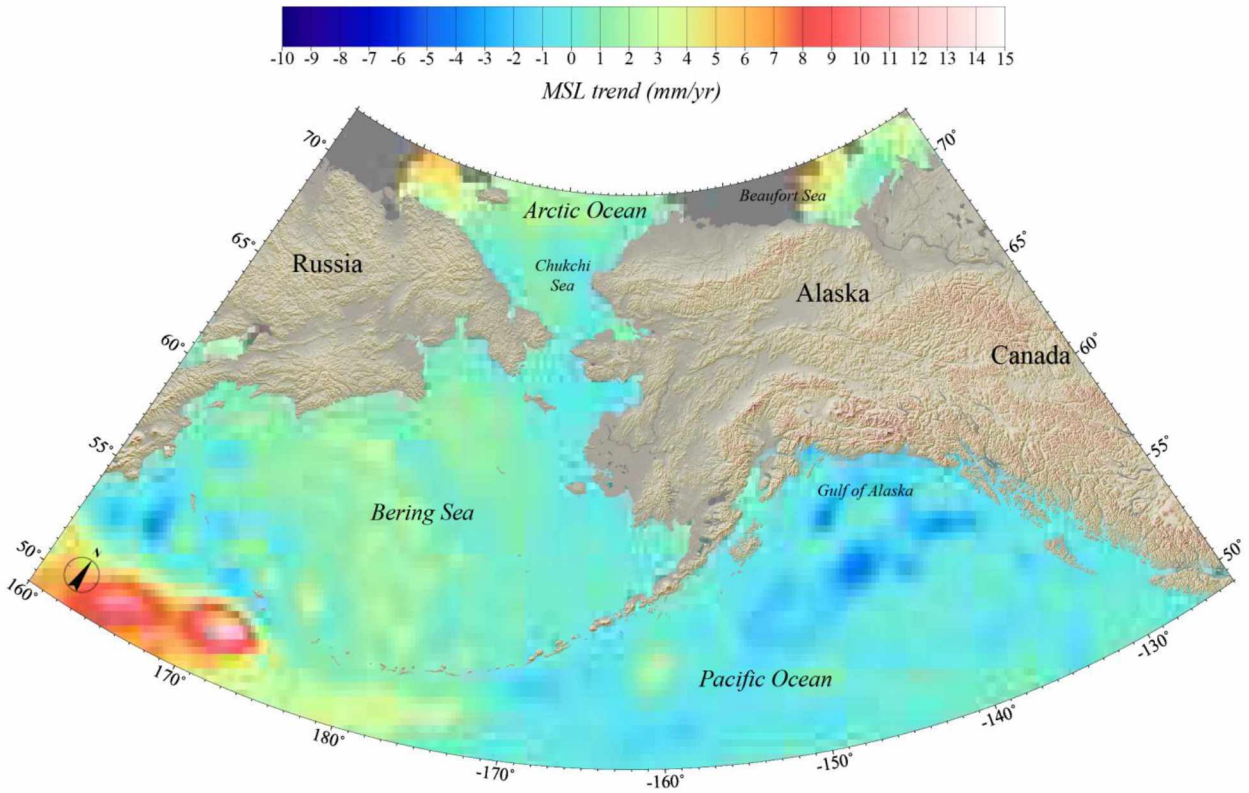

Figure 4.2. Map of satellite altimetry with 0.25° x 0.25° gridded MSL trend. This product was provided by AVISO, using a merged dataset acquired by satellites from 1992 to 2014 for the Bering Sea region.

Nome, Alaska has a shallow sloping shelf offshore that is part of the protected basin of Norton Sound. This location was used because of its similarity to offshore environments surrounding other coastal communities of Western Alaska. To verify that the performance of spatial averaging performed in this coastal environment was not a product of the shallow shelf or basin, two environmentally diverse locations, Sand Point and Seldovia, Alaska, also were selected for comparison.The coast along Sand Point, Alaska on Popof Island, on the south side of the Aluetian Islands, is considered the least complicated shoreline, and should have the least amount of interference from coastal effects. While the coastal effects are less at Sand Point, there is a higher liklihood of oceanic processes dominating the nearshore estimates as the bathymetry drops off steeply into the open Pacific Ocean. Seldovia, Alaska represents a more complicated coastal environment of relatively steep bathymetry into Kachemak Bay on the Kenai Peninsula, leading to Cook Inlet. There is no open water and coastlines of the neighboring islands, peninsulas, and mainland of Alaska dominate the region offshore of Seldovia.

Gridded data cells provided by AVISO are 0.25° x 0.25° and a standard area of 2.00° x 2.00° was defined for use offshore of these three areas. The standard AVISO cells were averaged into larger cells of 0.50° and 1.00° sizes within the 2.00° x 2.00° region (Figure 4.3). The rates and standard deviations of each cell in the variously split 2.00° x 2.00° region were then calculated and compared for each location in a series of histograms (Figure 4.4, Figure 4.5, and Appendix 5). The coastal cells are noted in each of these plots, in an effort to observe the influence these cells have on regionally averaged calculations. In Nome and Sand Point these coastal cells, on average, have larger MSL trends than the offshore cells; while in Seldovia, they have consistently lower MSL trends. There is no clear correlation between coastal cells and standard deviation. These methods are used in order to determine the size of offshore cells that, when averaged, provide the most accurate estimate of MSL rate without undue coastal or oceanic influences. Cells that are too small could potentially be dominated by noise, while cells that are too large begin to incorporate longer wavelength signal variations and might not represent the local MSL trend. The standard deviations between the cells used will help to isolate the size of cell that has the least variation within it. The standard deviations from each location show consistant minimization when using cells that are 0.50° x 0.50° (Table 4.1). Applying this method to cells offshore of coastal communities in Western Alaska, we find an average of + 0.16 mm/yr change in MSL in the Eastern Bering Sea, with an average of + 0.16 mm/yr for locations

offshore of the Seward Peninsula, and a higher rate of + 0.41 mm/yr off the coast of the YK Delta (Figure 4.6). Some communities are located very close to each other, so when this cell averaging method is applied they may potentially have identical trends calculated. This is most notable in Norton Sound and Bristol Bay where these small basins result in communities sharing the same cells to be averaged in the 0.50° x 0.50° grid area. For each case communities are approached as individual locations and a MSL rate is estimated for each, using the described method, regardless of their proximity to other communities.

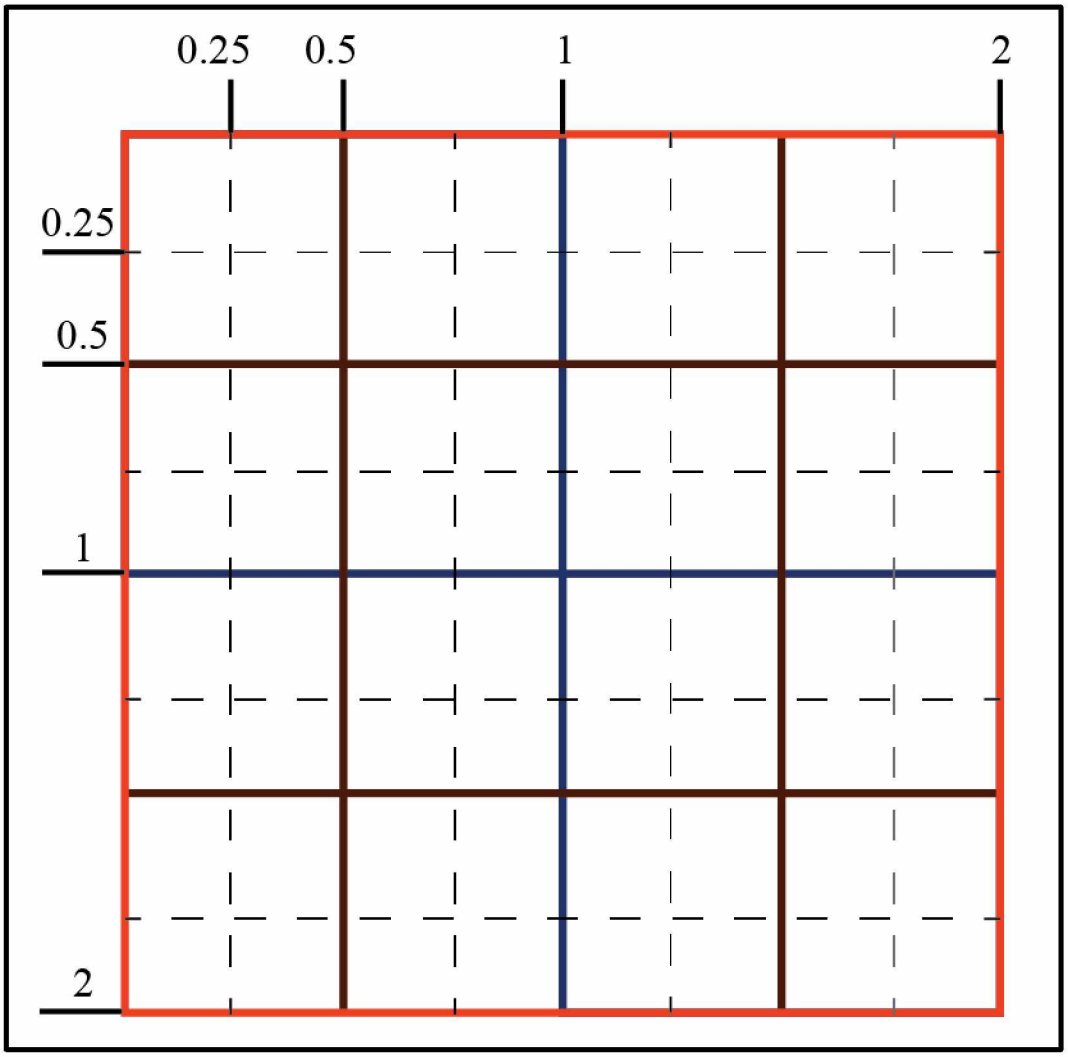

Figure 4.3. Illustration of how satellite altimetry cell average method is performed. The dashed lines represent the provided satellite altimetry data cells that are 0.25° x 0.25°. The brown lines show the 0.50° x 0.50° merged cells that were found to be optimal in noise reduction. The blue lines show the 1° x 1° regions and the orange box represents the 2° x 2° sample area. Degree marks are indicated along the outside of the sample area.

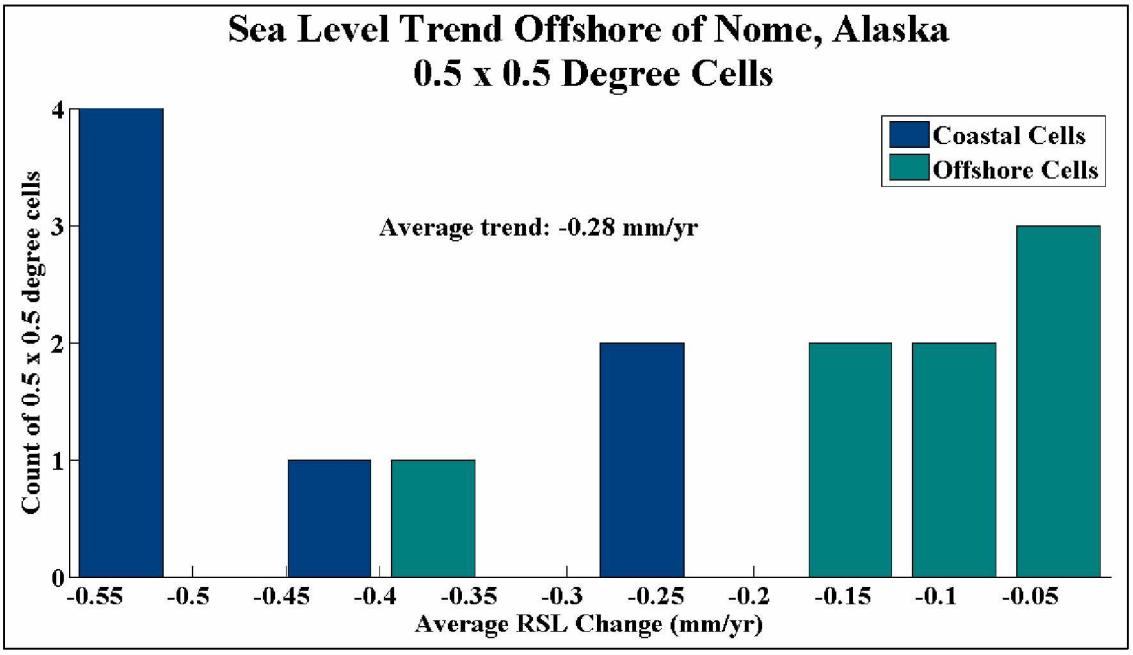

Figure 4.4. Histogram of MSL trends calculated from averaged satellite altimetry cells. For this plot the cells were averaged to 0.50° x 0.50° in a 2.00° x 2.00° region offshore of Nome, Alaska. Coastal cells are in dark blue, and cells that are not along the coast are green. One of the coastal cells is covered by the offshore cell that has an average MSL trend of -0.35 mm/yr.

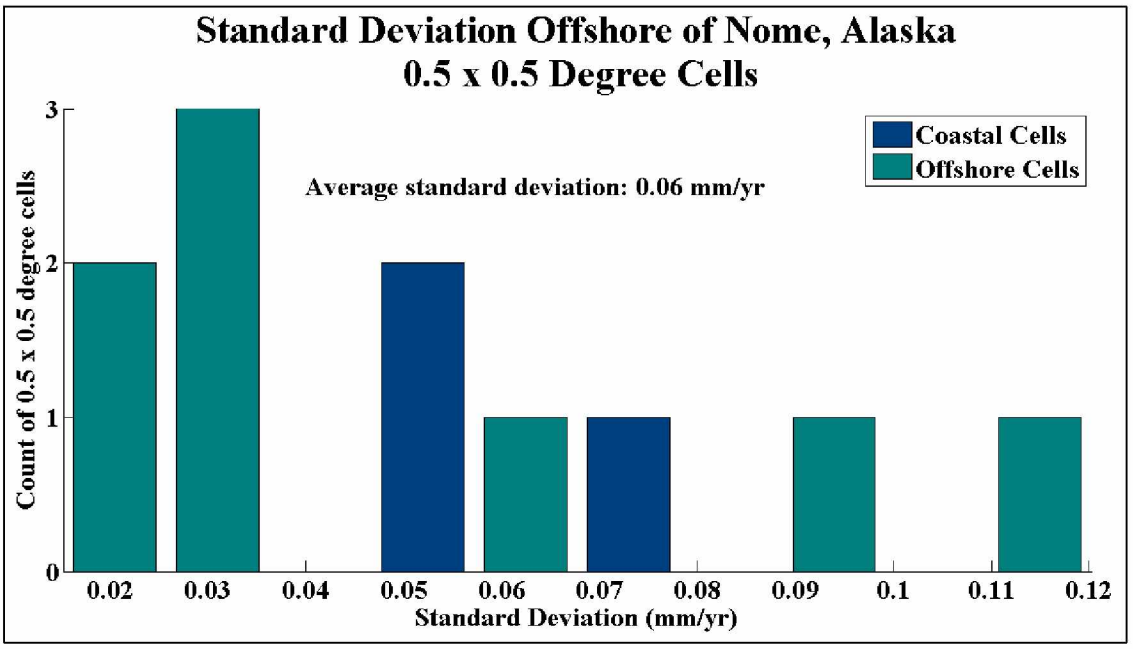

Figure 4.5. Histogram of the standard deviations between averaged satellite altimetry cells. For this plot these cells averaged were to 0.50° x 0.50° in a 2.00° x 2.00° region offshore of Nome, Alaska. Coastal cells are in dark blue, and cells that are not along the coast are green. The offshore cells have plotted over the five coastal cells not shown here. The standard deviations of these cells are 0.05, 0.05, 0.06, 0.07, and 0.09 mm/yr.

Table 4.1. Average MSL rates and standard deviations for three different satellite altimetry cell sizes are compared between three locations; Nome, Sand Point, and Seldovia, Alaska. While all of the averaged MSL rates for each location are relatively similar, differences in the standard deviations of these various averaged cell sizes are observed, with the minimum value at all three locations being when 0.50° x 0.50° cells are used.

Size of Averaged Cell Squares	**Nome**		**Sand Point**		**Seldovia**	
	Average MSL Rate (mm/yr)	*Average Standard Deviation (mm/yr)*	*Average MSL Rate (mm/yr)*	*Average Standard Deviation (mm/yr)*	*Average MSL Rate (mm/yr)*	*Average Standard Deviation (mm/yr)*
0.25° x 0.25° cells	-0.2811	0.2054	1.1400	0.8747	0.1850	0.5609
0.50° x 0.50° cells		0.0554		0.2529		0.2254
1.00° x 1.00° cells		0.1077		0.4196		0.3556

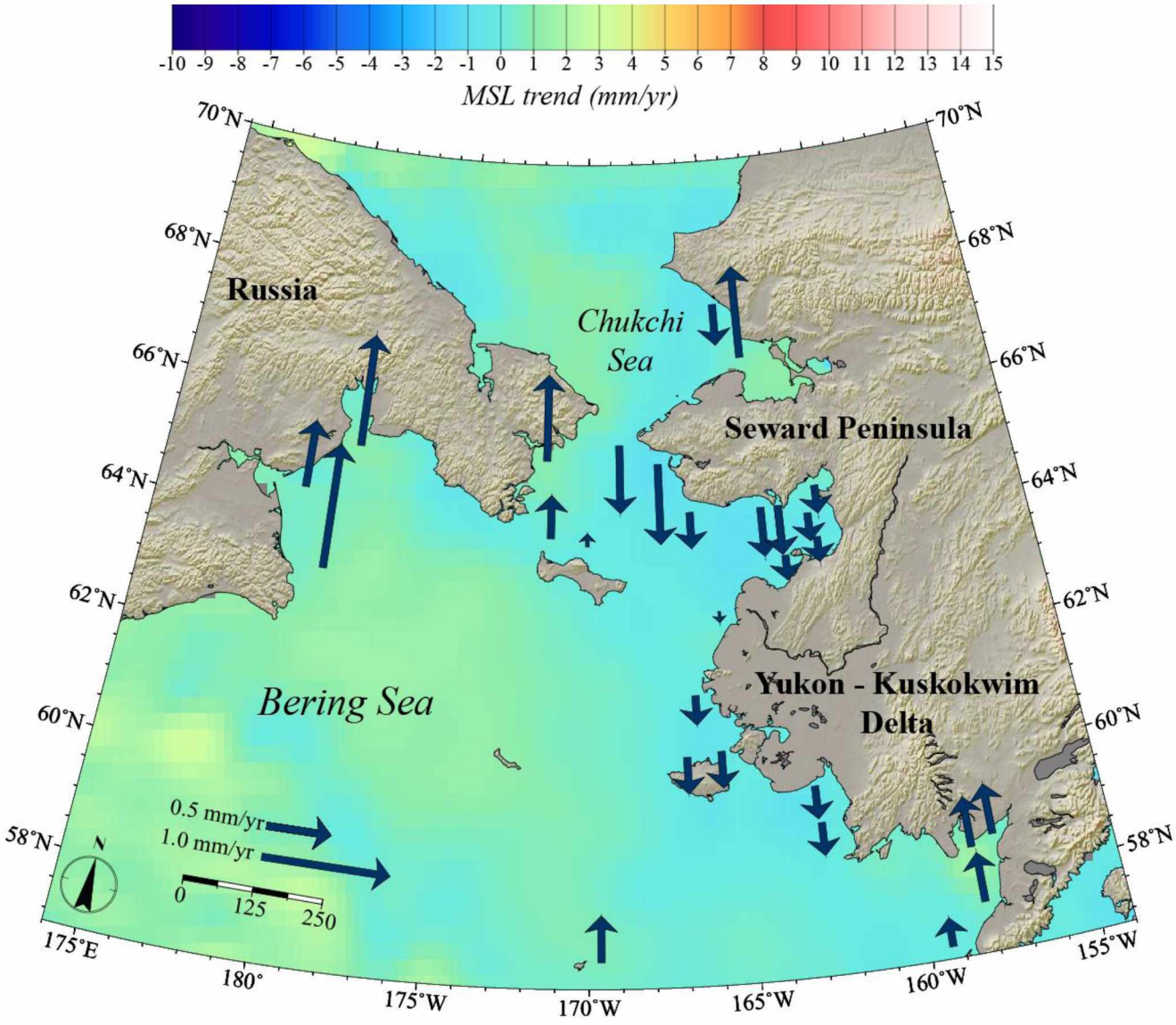

Figure 4.6. Map of satellite altimetry and averaged rates. The 0.25° x 0.25° gridded MSL trend dataset is provided by AVISO, using a merged dataset acquired by satellites from 1992 to 2014 for the region offshore of Western Alaska. Blue arrows represent the average MSL trend in a 2.00° x 2.00° region offshore of communities in Western Alaska, using cells that have been combined to 0.50° x 0.50°.

4.3 GPS vertical velocities

GPS vertical velocities relative to North America are produced from both campaign and continuous sites across Alaska and the Bering Sea region (Figure 4.7). The horizontal velocities are also calculated (Appendix 6), but they are not used in RSL change calculations.

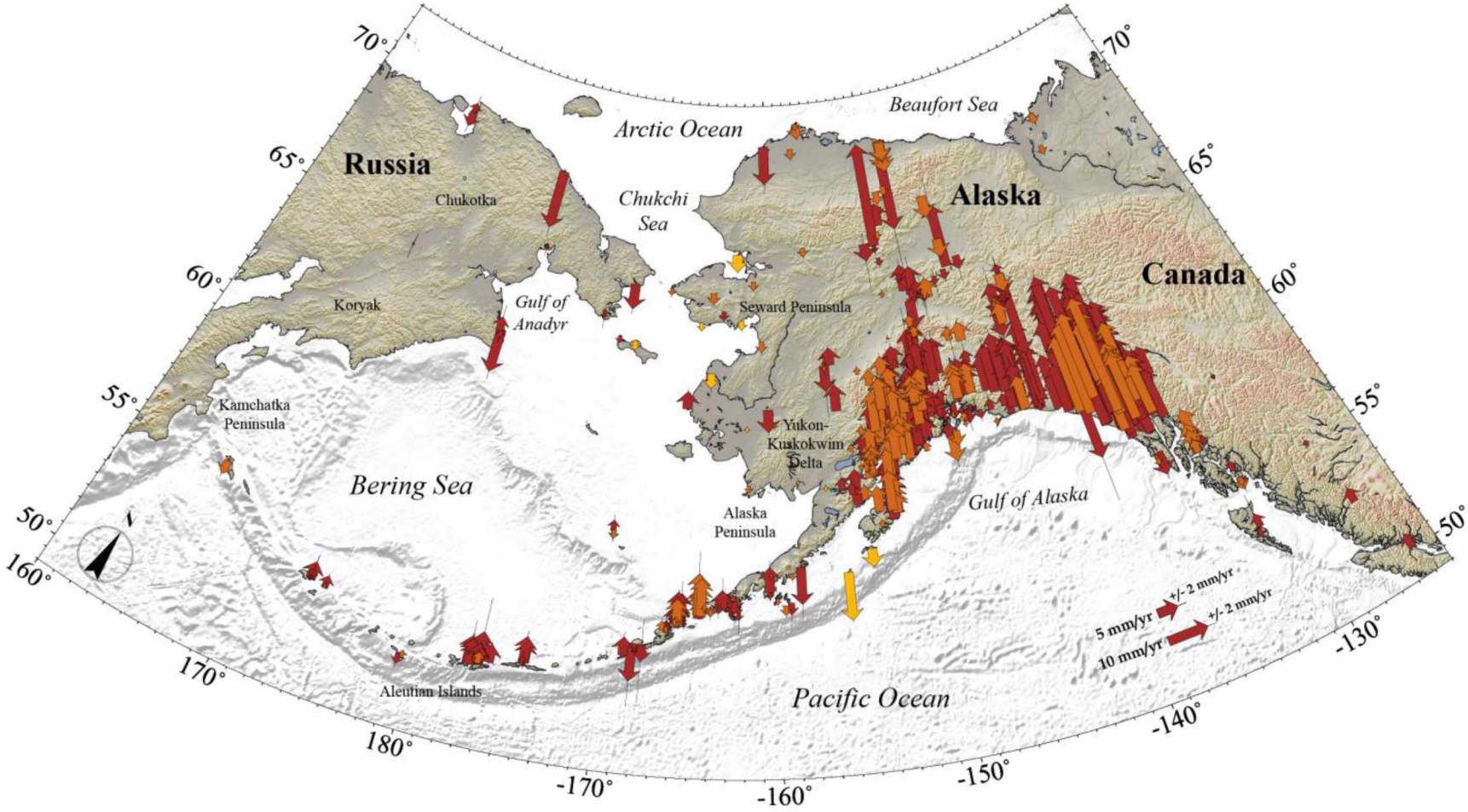

Figure 4.7. Vertical velocity model for Alaska relative to the North American plate. Arrow bases show the locations of the GPS sites. Error is expressed as a vertical bar off the end of the arrow. Arrows pointing up signify uplift, while arrows pointing down indicate subsidence. Orange arrows are velocities calculated from continuous GPS stations, red arrows represent velocities calculated at campaign GPS sites, and yellow arrows are velocities where a weighted mean was calculated between various combinations of campaign and continuous stations. Here, the uplift due to the subducting Pacific Plate is evident in south-central Alaska. South-east Alaska uplift is due to subduction that is compounded by isostatic rebound from glacial ice loss. In contrast northern and western Alaska are dominated by negative velocities showing regional subsidence.

Many locations in Alaska have multiple measurements from nearby survey points. To combine these into a single estimate for modeling, multiple measurements were individually weighted by their associated error through a least squares inversion and the mean used as the vertical velocity for that location (Table 4.2). No sites were removed from a location even if some might appear to be outliers. Differences between nearby sites, when they are significant relative to measurement errors, will be addressed later in this thesis.

Table 4.2. Table of locations and velocities that were averaged. These velocities are relative to NOAM and are used in the GPS plots presented in this study. Locations that are in bold italics are also used in RSL change calculations, while communities indicated with an * are used to evaluate the GIA model. All stations are campaign stations unless noted with an * following the station ID, in which case they are continuous.

Community	Station ID	Vertical Velocity (mm/yr)	Uncertainty (mm/yr)	Weighted Mean (mm/yr)	Mean Uncertainty (mm/yr)
*Bethel	BET1*	-2.54040	0.48778	1.212	0.272
	BETB	6.67192	0.69710		
	BETC	0.61761	0.44980		
	CABN	4.39117	0.65219		
Chirikof Island	AC13*	-11.75032	0.51535	-11.397	0.469
	CHIR	-9.67423	1.13765		
Dillingham	***AB14****	***-0.84575***	***0.41964***	***-0.822***	***0.571***
	DILL	***6.15333***	***2.11446***		
Elim	***AC31****	***-1.88416***	***0.41385***	***-2.223***	***0.378***
	ELIB	***-3.58233***	***0.94335***		
	ETID	***-1.44928***	***5.20837***		
Emmonak	***EMNA***	***-3.02379***	***0.96156***	***-3.591***	***0.863***
	EMNB	***-8.39915***	***2.43451***		
	EMNC	***-1.41290***	***3.31349***		
King Salmon	***AC24****	***0.37104***	***0.40378***	***1.142***	***0.306***
	AKNA	***0.66271***	***0.71849***		
	AKNB	***3.72798***	***0.63025***		
	ESKI	***-12.11823***	***3.95321***		
Kotzebue	***AB18****	***-4.16423***	***0.43657***	***-4.031***	***0.326***
	OTZ1*	***-3.86174***	***0.49116***		
Nome	***2BAD***	***-1.39255***	***0.55804***	***-1.751***	***0.225***
	8756	***-1.52597***	***0.78419***		
	875G	***-0.24783***	***2.66101***		
	AB11*	***-1.76748***	***0.41614***		
	NOME	***-2.92380***	***0.58661***		
	OMEA	***-1.08776***	***0.57998***		
	OMEB	***-1.81566***	***0.57966***		
Port Heiden	***AC40****	***0.90337***	***0.62027***	***-0.650***	***0.277***
	HEID	***-1.00243***	***0.34519***		
	JIMM	***-1.17704***	***0.69830***		
Sand Point	AB07*	-1.79540	0.35631	-1.119	0.296
	SDP1	0.08920	1.18894		
	SNDP	0.46367	0.59445		
Savoonga	***AB04****	***-2.28690***	***0.59488***	***-2.268***	***0.558***
	SVAC	***-2.12807***	***1.61850***		
Sitkinak Island	AC45*	-4.84558	0.40451	-4.031	0.386
	SITK	0.50409	1.30511		
Ugolnaya	***ANAD***	***-1.16722***	***0.68513***	***-1.532***	***0.621***
	UGOL	***-3.21466***	***1.47053***		

4.4 GIA model

The GPS data in Western Alaska and along the coastline in particular are sparse. To test whether GIA can explain the observed motions well enough that a GIA model could provide the necessary interpolation between points, 50 GPS vertical velocities referenced to the NOAM were compared to vertical velocities of the same points produced by GIA modelling (Appendix 7). A suite of over 50,000 models were tested by varying the thickness and viscosity of the Earth structure in Alaska. To model these dynamics, the post glacial rebound calculator TABOO (Spada et al., 2003; Spada, 2003; Spada et al., 2004) was used, which uses an incompressible, self gravitating, non-rotating, Maxwell viscoelastic spherically symmetric Earth model. Axial-symmetric disks are used to describe the surface load, in this case representing the Laurentide and Cordilleran ice sheets. The surface load geometry and history used in the models presented here is defined by the ICE-3G global late Pleistocene model (Tushingham and Peltier, 1991).

A four layer Earth model (Figure 4.8) developed by Hu and Freymueller (2015) (in preparation), was used to vary the lithospheric thickness, asthenospheric thickness and viscosity, and upper mantle thickness and viscosity. The viscosity of the lower mantle was held constant at 3.00×10^{21} Pa s. The upper mantle thickness varied depending on the lithosphere and asthenosphere thickness so that the upper boundary of the lower mantle would consistently remain at 670 km. The ranges over which the remaining parameters were varied are as follows; lithosphere thickness, 25 – 120 km, asthenosphere thickness and viscosity, 40 – 300 km and $5 \times 10^{18} – 2 \times 10^{21}$ Pa s, and upper mantle viscosity $1 \times 10^{20} – 2 \times 10^{21}$ Pa s. The reference model by James and Morgan (1990), as well a similar three layer fixed model by the GIA benchmark group (Kaufmann and Johnston, 1997; Kaufmann and Lambeck, 2000), were also tested as control models. The models predicted velocities at the location of GPS measurements, so the weighted root sum of squares (WRSS) between the model and GPS velocities could be used to calculate the normalized weighted root mean square (RMSN) (Equation 4.1), allowing for direct comparison between models.

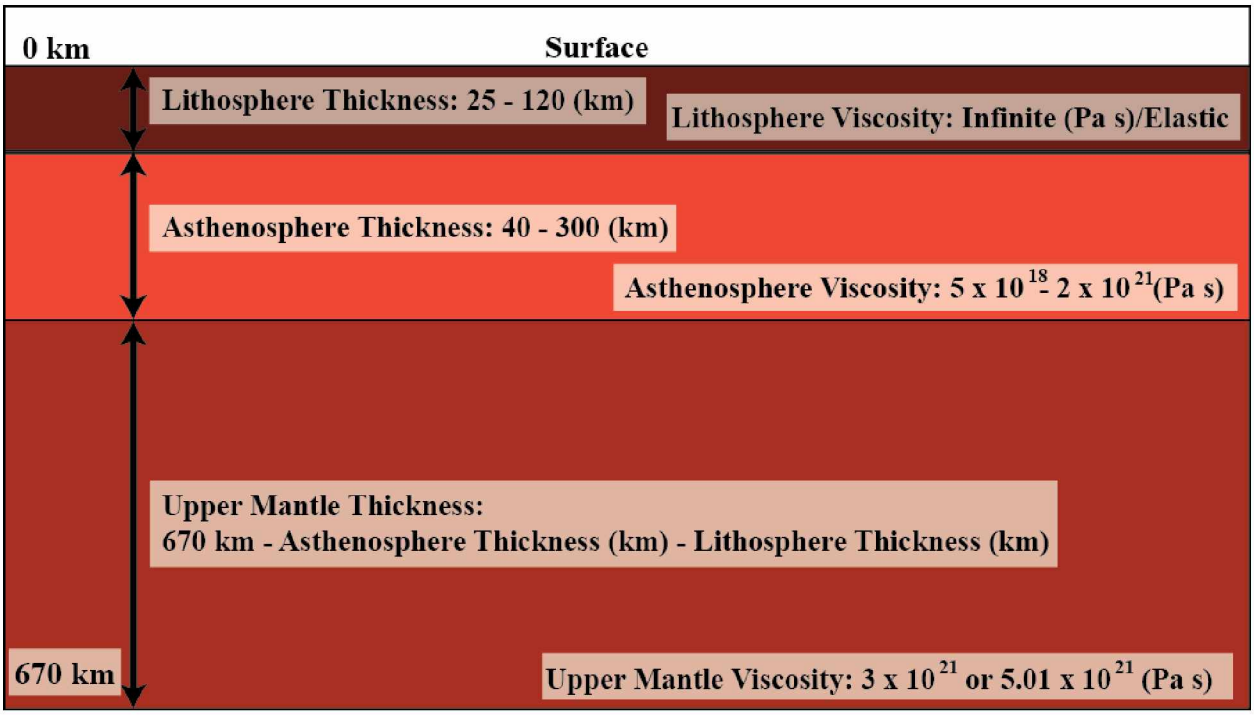

Figure 4.8. Diagram of the top three layers in the four layer GIA model used in this study. Each layer is labeled with the ranges parameters were varied over. Lithosphere viscosity was held constant and the over all depth of these layers is fixed at 670. The upper mantle is bounded below by the lower mantle.

The best fit model is evaluated by comparing the RMSN for each model, weighting the model misfit and normalizing the variance with the inverse square of the uncertainty associated with each GPS measurement. The WRSS is the numerator of the RMSN.

$$RMSN = \sqrt{\frac{\sum_{i=1}^{n} w(i)(v(i)_{gps} - v\,(i)_{gia})}{\sum_{i=1}^{n} w(i)}}, \qquad w(i) = \frac{1}{\sigma(i)^2} \tag{4.1.}$$

where n is the number of data, i is the ith data point representing specific locations where GPS is measured and GIA is modeled, w is the weighting factor defined by the inverse of the squared GPS uncertainty (σ),and v_{gps} and v_{gia} are the vertical velocities of the calculated from GPS measurements and modeled GIA estimates.

The best fit Earth model parameters found in this study based on vertical velocities (Figure 4.9) of Western and Northern Alaska, resulting from GIA of the Laurentide and Cordilleran ice sheets are defined as follows: 120 km lithosphere over a 100 km asthenosphere with a viscosity of 2.5 x 10^{19} Pa s, overlying a 450 km thick upper mantle with a viscosity of 1.5

x 10^{21} Pa s (Figure 4.10). These values are for a fixed lower mantle viscosity of 3 x 10^{21} Pa s. An additional model was tested using a lower mantle viscosity of 5 x 10^{21} Pa s. This model was best fit when thickness and viscosity parameters were a 120 km lithosphere over a 70 km asthenosphere with a viscosity of 1 x 10^{20} Pa s, overlying a 480 km thick upper mantle with a viscosity of 5 x 10^{20} Pa s. This model did not fit the data as well as the low viscosity model with a minimum WRSS of 675.36 as opposed to the minimum WRSS of 422.65 for the lower viscosity lower mantle presented here. This does show the effect an increase in lower mantle viscosity has on the Earth model: the estimated lithosphere thickness is unaffected, but the asthenosphere gets thinner and the viscosity of the asthenosphere and uppermantle converge to a more homogenous viscosity on the order of 10^{20} Pa s.

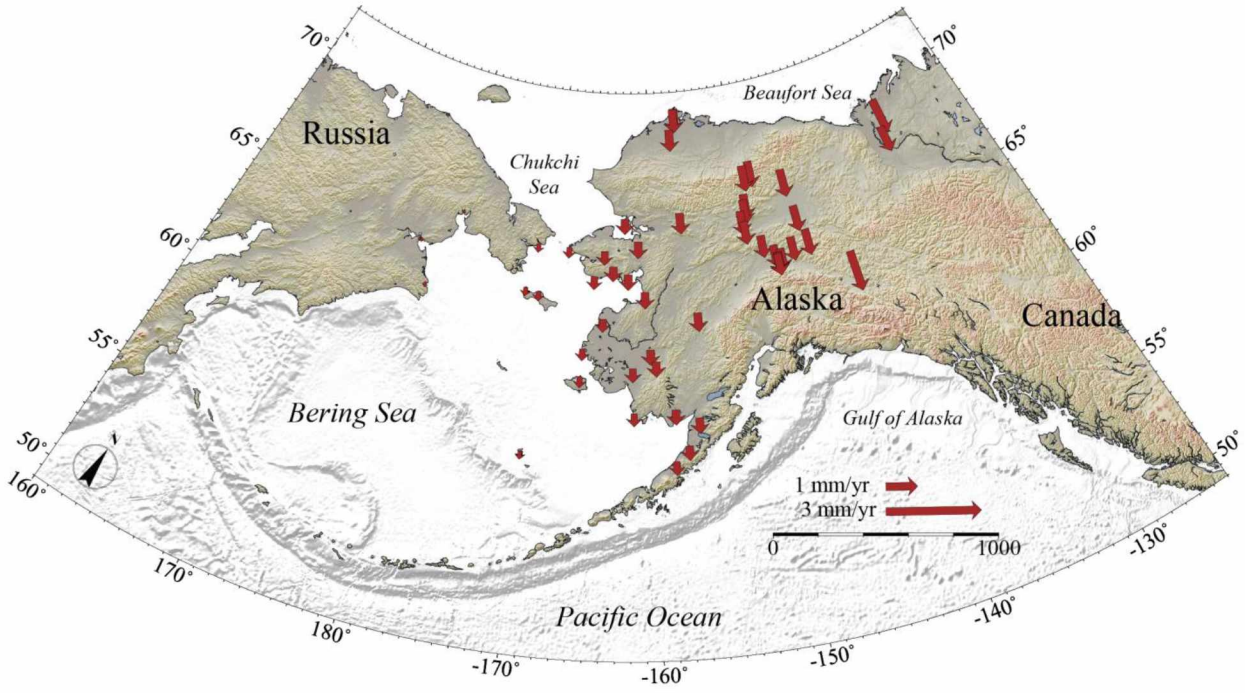

Figure 4.9. Map of vertical velocities produced by the best fit GIA model. The best fit parameters for this model are a 120 km lithosphere over a 100 km asthenosphere with a viscosity of 2.5 x 10^{19} Pa s, overlying a 450 km thick upper mantle with a viscosity of 1.5 x 10^{21} Pa s.

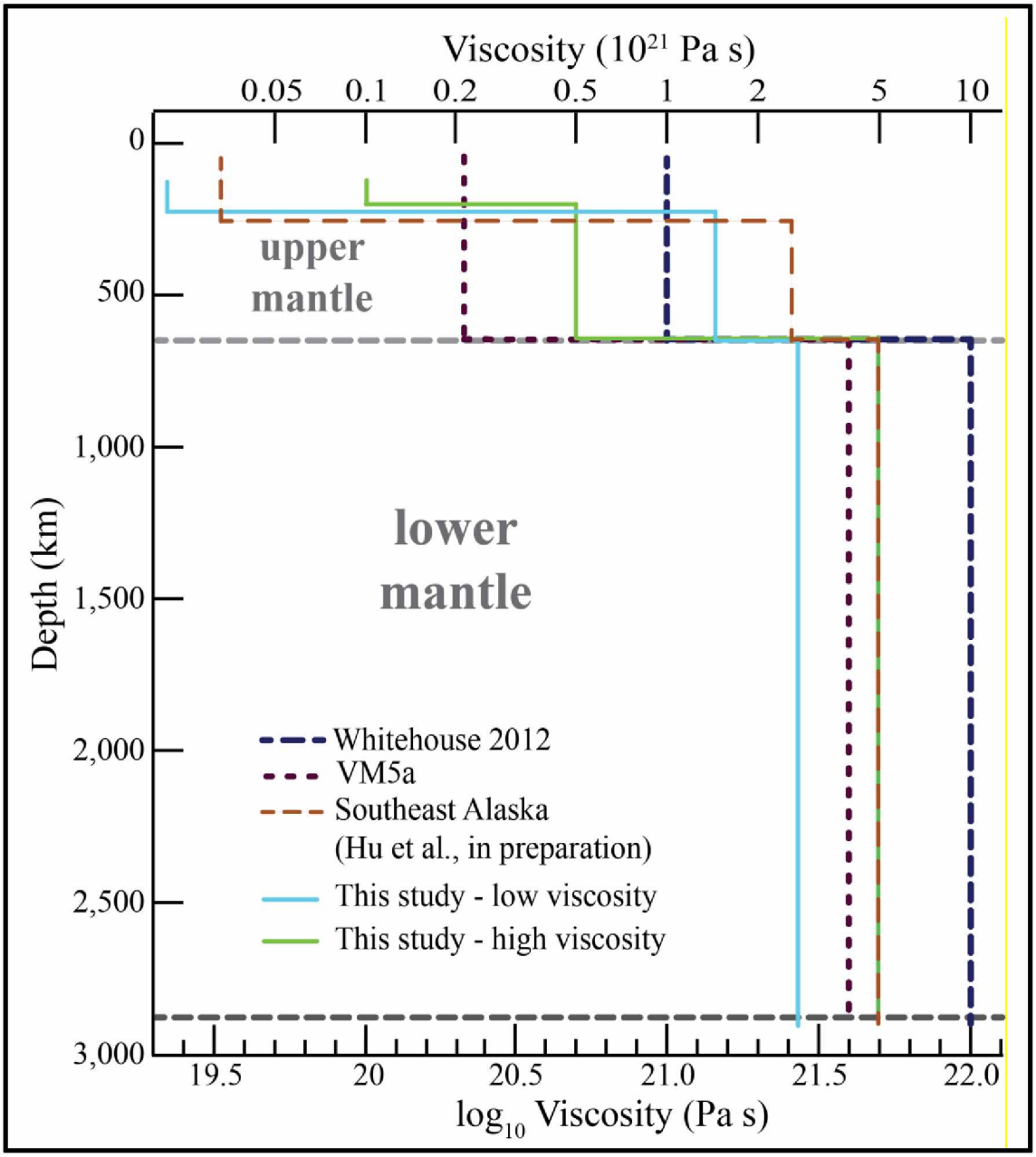

Figure 4.10. Viscosity profile with depth from the surface (top) to the core/mantle boundary (bottom). Four published models are included with the best fit profile observed during this study using GIA modelling of Western and Northern Alaska.

The geoid is the shape the surface of the oceans would assume, if the only processes effecting them were the Earth's graviation and rotation. This shape has the same potential gravity at every point, so as the Earth's gravity field changes, so too does the shape of the geoid. This change in the geoid over time is the geoid rate, and is accounted for and estimated in the GIA model using TABOO (Spada et al., 2003; Spada, 2003; Spada et al., 2004). To ensure that the

estimated velocities estimated effects of GIA and are not due to a gravity gradient across the Bering Sea, the geoid rates for Western Alaska were compared to the geoid rate at a point in the middle of the Bering Sea (180° E, 55° N). The geoid rate in the Bering Sea is – 0.05 mm/yr and values in Western Alaska were estimated to be between - 0.02 mm/yr and - 0.05 mm/yr. These rates are small relative to the velocities observed in Western Alaska, and there is not any significant gradient from west to east across the Bering Sea.

To test if the difference between the corrected geocenter of ITRF 2008 used for the GPS velocities and the geocenter used in the TABOO model biased the misfit, analysis of the residuals from the best fit GIA model relative to the sine of their latitude was performed (Figure 4.10) and found to show no significant latitudinal variation in the residuals. A latitude dependence would be expected if the z-axis component of the geocenter frame correction was wrong, and would produce a residual proportional to the sine of latitude. Figure 4.10 indicates no evidence for any remaining frame bias.

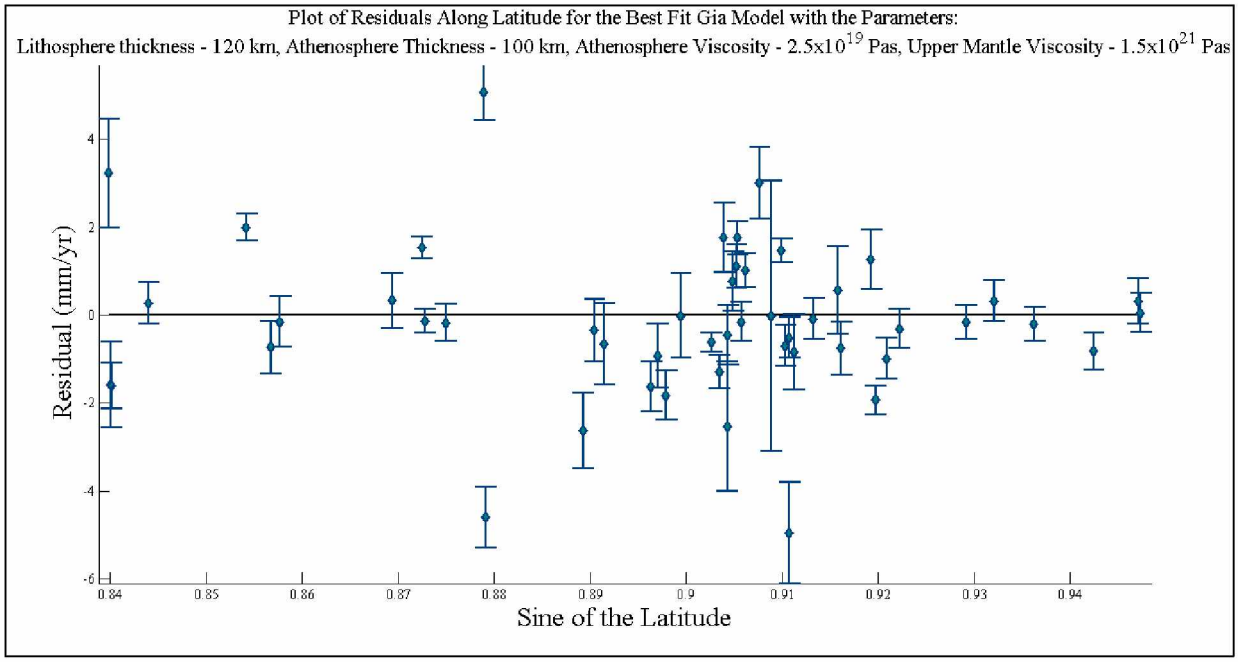

Figure 4.11. Plot of the best fit GIA model residuals. These residuals the difference of the observed GPS measurements that are relative to the corrected ITRF 2008 reference frame and the best fit predictions from a GIA model that is referenced to an estimated center of mass for a radially symmetric Earth. The residuals are plotted against the sine of the latitude of their calculation, to test for any bias in the difference between these reference frames. The error bars are the uncertainty associated with each GPS measurement. The plot shows that the residuals do not exhibit a latitudinal trend that would imply reference errors between the GIA model and the GPS data.

Figure 4.10 also helps to visualize the locations in Alaska that are better fit by the model. The smaller residual values on the right side of the plot where sine of the latitude is 0.94 are for latitudes around 70° N and the values on the left side of the plot where the sine of the latitude is 0.84 are latitudes around 57° N. This figure shows that the model is better fit to Northern Alaska, which is what is expected of the GIA model used here; the long wavelength signal remaining from displacement of the Laurentide and Cordilleran ice sheets is small enough that it is overshadowed by larger tectonic events that occur in the southern regions of Alaska. The range of the residuals increases as the latitude decreases and additional processes such as plate convergence, earthquakes, GIA signals resulting from the Little Ice Age deglaciation, and localized motion begin to dominate the GPS signal. The residuals appear to increase for latitudes less than 62.25° (which has a sine of 0.885). These lower latitude sites are all located on the YK Delta and Alaska Peninsula, as only sites above 63° in the central and eastern region of the state were used in the GIA model. This pattern of residuals suggests that either the GPS data on the YK Delta are less reliable or that other tectonic or local processes dominate the vertical velocity of the YK Delta. We suspect a combination of the two factors are contributing to both the larger model residual and the larger error in the GPS observed by the error bars on the residual plot for lower latitude calculations and measurements.

To test the parameters and better understand which variable in Earth structure has the most effect on our model, plots of each parameter against their WRSS values were created (Figure 4.11). For each plot in Figure 4.11 the best fit values for three parameters were fixed so that the variation in the remaining parameter could be observed. The lithospheric thickness appears to almost undulate, with minimum WRSS values occuring at both the 65 and 120 km points. This could indicate that a GPS site with a very large residual is dominating what could be a true best fit model, or that the region studied has a variable lithospheric thickness. The asthenospheric thickness, however, indicates the minimization of the WRSS at 100 km with a gradual decrease in WRSS as the asthenosphere gets thicker approaching 100 km, but as it continues to thicken past 100 km the WRSS increases much more rapidly. This indicates that this model favors a thinner asthenosphere. This same pattern occurs on a much smaller scale for the asthenosphere viscosity, with lower viscosity asthenospheric WRSS being lower in general than the higher viscosity asthenosphere. The opposite is true for upper mantle viscosity with a clear

minimization of the WRSS as the viscosity approaches 1 x 10^{21} Pa s, and only slight increases to the WRSS as the viscosity continues to increase.

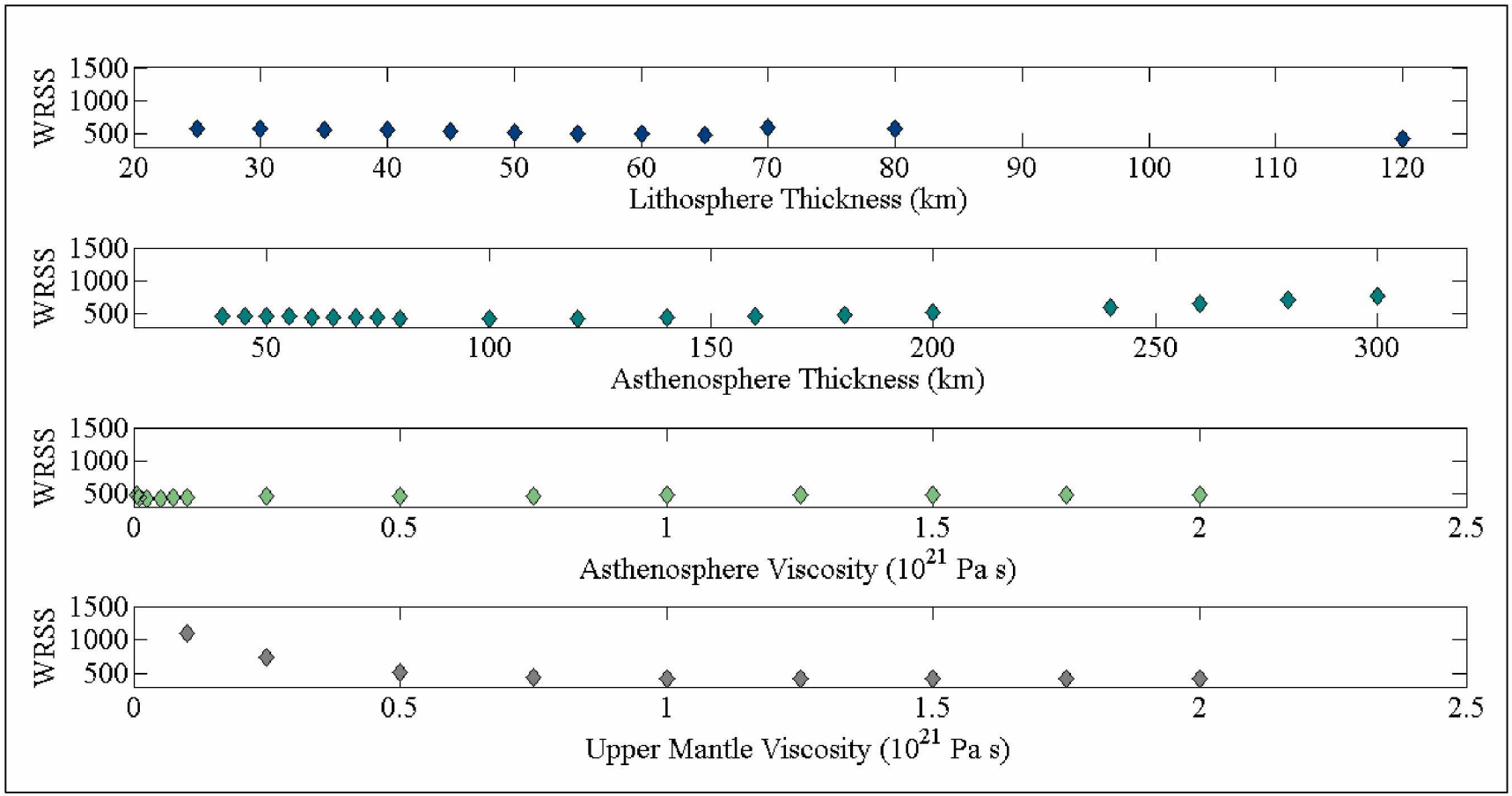

Figure 4.12. Plots for each GIA model parameter against their WRSS. In each case the three parameters not being plotted were fixed to the best fit values, so that only variation in parameter at a time is observed.

5 Discussion

5.1 Interpretation of the Earth model

No prevailing Earth model for Western Alaska had been presented before this study, so the results from the GIA modelling performed here are a significant contribution to the definition of this model, even though the parameters do not appear to be tightly constrained given this dataset (Figure 4.11). The best fit GIA model resulting from this study, to be used later in RSL change estimations, is a 120 km thick lithosphere over a 100 km thick asthenosphere with a viscosity of 2.5×10^{19} Pa s, overlying a 420 km thick upper mantle with a viscosity of 1.5×10^{21} Pa s (Figure 5.1 and Table 5.1). These results are from a model with a lower mantle viscosity of 3×10^{21} Pa s. To compare this model with the one for Southeast Alaska (Hu and Freymueller, 2015, in preparation) an additional model with an increased lower mantle viscosity of 5.01×10^{21} Pa s was tested (Appendix 8). This higher viscosity lower mantle model did not fit the GPS data as well as our lower viscosity lower mantle model and so is not included in the main section of this discussion or used in RSL change calculations.

In Figure 5.1 the best fit modeled velocities result in a pattern of greater subsidence to the north that decreases to the south and west. The red lines indicate uplift and the green are subsidence, which seems to indicate that the subsiding forebulge was popped up on both sides as uplift in northeastern Canada and off the north shore of Russia bound two sides of the elliptical subsidence. These results suggest the location of a forebulge formed by the Laurentide and Cordilleran ice sheets was focused over the northern coast of Alaska in the Beaufort Sea and sloped to the south across the extent of central Alaska. This former forebulge is now subsiding at velocities of approximately 1-2.5 mm/yr across much of Alaska. Effects of this forebulge are seen throughout Western Alaska with the very edge of the forebulge going through the Bering Strait and St. Lawrence Island. For comparison, the rate of subsidence along the Atlantic coast from the same mechanism is up to a factor or two larger (Snay et al., 2007).

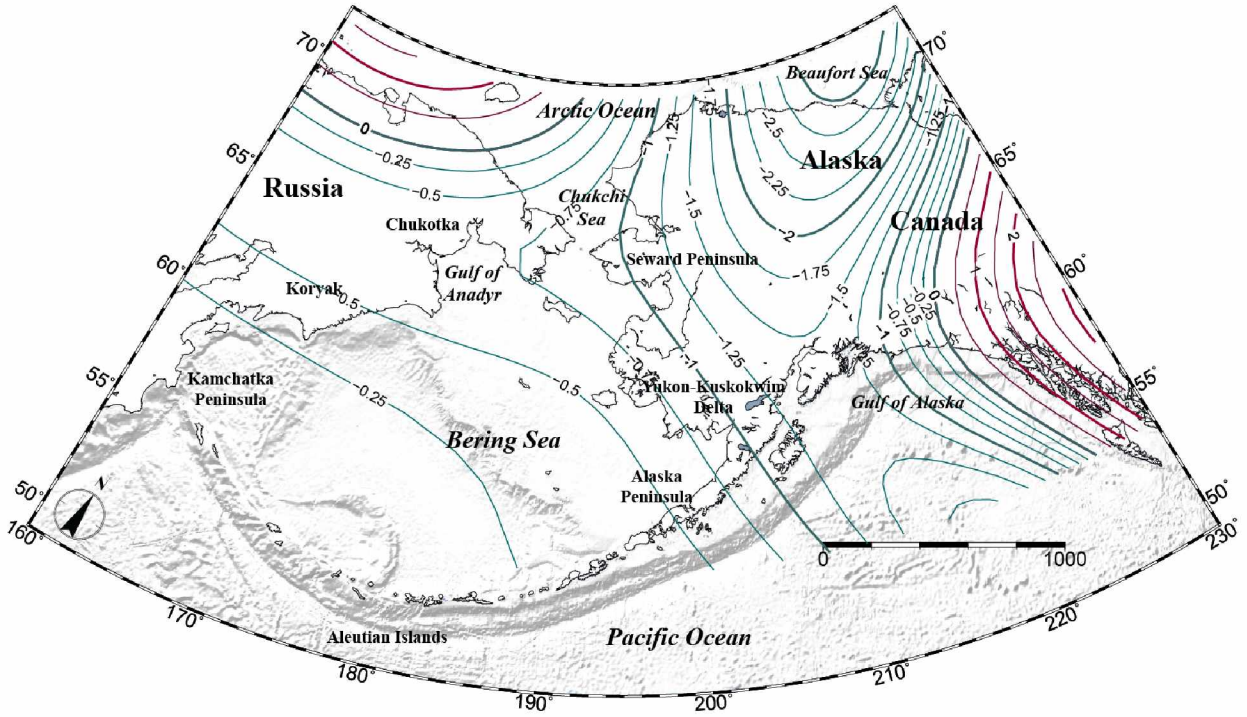

Figure 5.1. Best fit GIA vertical velocity model contour map for Alaska. Contours are every 0.25 mm/yr with 0, 1, and 2 in bold, negative values are in green and positive values are red.

Table 5.1. Best fit GIA tectonic vertical velocity model, indicated as "All", with the minimum and maximum range of parameters within one standard deviation of the mean. The best fit models for the different regions outlined in Figure 5.2. are also provided with weighted RMSN for comparison purposes.

Best fit parameters	Region Model is Fit to				
	All	North	West	Seward	Delta
Lithosphere Thickness (km)	120	120	80	30	120
Asthenosphere Thickness (km)	100	120	280	80	300
Asthenosphere Viscosity (10^21 Pa s)	0.025	0.025	0.1	0.005	1
Upper Mantle Viscosity (10 ^21 Pa s)	1.5	2	2	2	1
RMSN	0.1365	0.13121	0.17825	0.34995	0.18141

These best fit parameters have a lithospheric thickness similar to values seen for continental shields, as opposed to the thin lithosphere of Southern Alaska. This suggests that the lithospheric thickness varies significantly across Alaska and is defined by the subduction boundaries. The lithospheric thickness was found to have a minimized WRSS when a continental root of 120 km was applied, but there were also indications (Figure 4.11) of a second minima at ~65 km. The second smallest misfit is for a lithospheric thickness of 65 km, which is much more

of an intermediate type, and only slightly thicker than the 55 km thick lithosphere estimated in Southern Alaska. This ambiguity in thickness over such a large range prompted testing of sub-regions within the modeled Northern and Western area used in this study. The testing of these sub-regions indicates where potential GPS errors or large residuals may have a greater impact on the model.Tests for model fit to different regions defined as Northern Alaska, Western Alaska, Seward Peninsula, and YK Delta (Figure 5.2) were performed by comparing only select sites in those specific regions in an effort to identify lithospheric thickness variation and reduce model dependence on extreme outliers (Table 5.1).

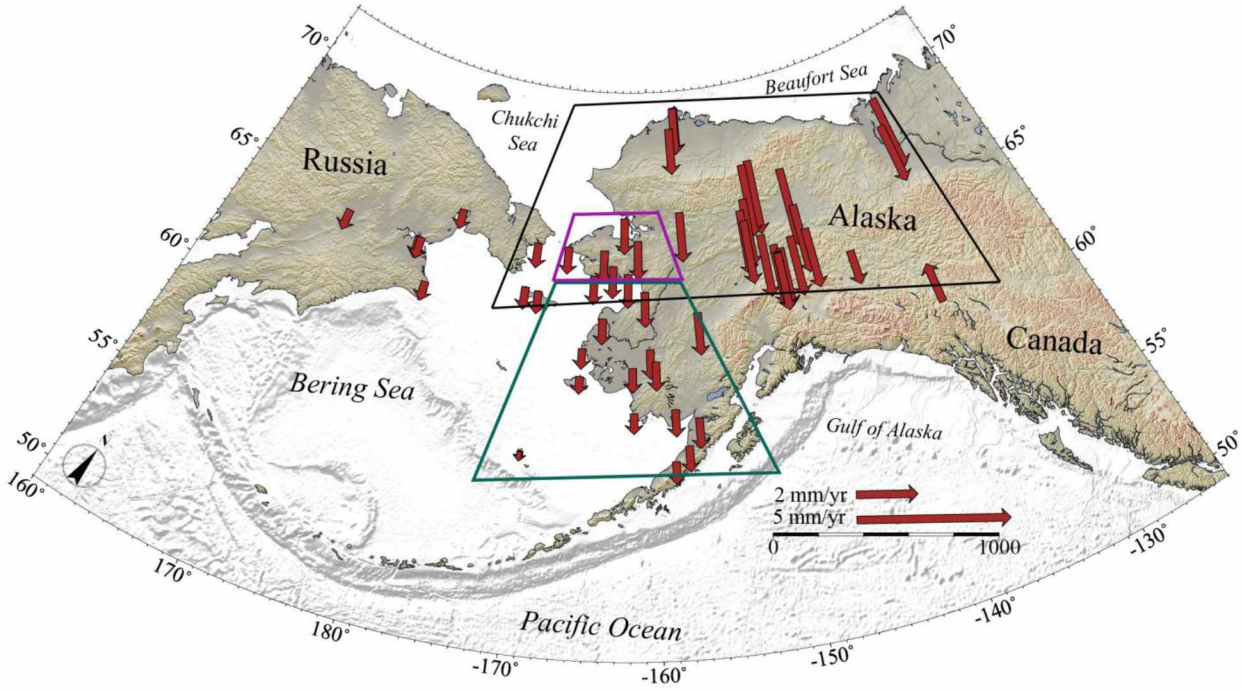

Figure 5.2. Map of best fit GIA model vertical velocities. Boxes are drawn to show the separate sub-regions that were tested. The black box bounds the velocities that were fit to a model for the Northern region. The purple box bounds the region referred to as the Seward Peninsula, the green box encloses the velocities used to test the crustal thickness in the YK Delta region, and the West region is defined as the combination of the Seward Peninsula and the YK Delta boxes.

The thickness and viscosity of the asthenosphere and upper mantle are even more poorly understood in Alaska than the lithospheric thickness. The best fit model has a relatively low viscosity asthenosphere, more like Southern Alaska than a continental shield. The geometry and viscosity of the asthenosphere and upper mantle beneath Alaska are influenced by the subduction zone setting of Southern Alaska. Studies using GPS, seismic velocity, gravity and GIA

modelling show that upper mantle and asthenosphere viscosity of cool and dry continental shield areas is between $10^{20} - 10^{21}$ Pa s (Mitrovica and Forte, 1997; Kaufmann and Lambeck, 2002; Milne et al., 2001). Tectonically active regions have a lower viscosity that can be as low as 10^{18} - 10^{19} Pa s (Dixon et al., 2004). This lower viscosity is primarily attributed to increased temperature (Dixon et al., 2004), but seismic tomography also suggests that large volumes of the mantle wedge above subduction zones are anomalously wet (Nolet and Zielhuis, 1994) from the dehydration of the subducting slab. This region of hot, wet mantle with lower viscosities can extend far from the subduction trench, and along the west coast of the U.S. it is found to extend to depths of 110km as far away from the coast as the Colorado Plateau (Dixon et al., 2004). The long-lived subduction zone along the coasts of Southern Alaska is capable of introducing the flux of heat and water necessary to lower viscosities at distances that could extend towards north-central and Western Alaska. An extension of the North American continental shield would result in higher viscosities of colder, dry mantle. The transition zone from the continental root of North America to the active subduction on the southern coast of Alaska is not well understood, and a large range in predicted viscosity and thickness parameters is expected.

The estimated thicknesses that are best fit to Northern and Western Alaska are for an asthenosphere of 120 km and an upper mantle thickness of 100 km. This results in a three layer profile with two thirds being made up of a higher viscosity (1.5×10^{21} Pa s) upper mantle with a much lower viscosity (2.5×10^{19} Pa s) asthenosphere and thick elastic lithosphere composing the remaining one third of the structure. The best fit results for Southern Alaska estimated by Hu and Freymueller (2015) (in preparation) are for a 55 km lithosphere and 230 km asthenosphere with a viscosity of 3×10^{19} Pa s. The viscosity of the upper mantle was not tested in that model and was kept at a constant value of 2.4×10^{21} Pa s. The smaller load in that case was not sensitive to the viscosity below about 300 km depth. The thickness of the lithsphere in the model by Hu and Freymueller (2015) (in preparation) is significantly thinner than the 120 km thickness estimated in this study and the asthenospheric thickness is double what was best fit here. This indicates a separation of Earth structure along the Alaska Range and the Denali Fault. The thin lithosphere with a thick asthenosphere beneath it subducts beneath the continental root in Northern and Western Alaska.

The viscosity profiles of the asthenosphere and upper mantle are essentially identical between the best fit model found in this study and in the Southern Alaska model (Hu and

Freymueller, 2015, in preparation). The lower asthenospheric viscosity is expected, as Southern Alaska is a tectonically active region with ongoing subduction introducing heat and water into the asthenosphere, but the continuation of this viscosity into Northern and Western Alaska indicates the potential for a hot, wet mantle wedge extending far from the subduction trench, as is found on the west coast of the U.S. The thickness and viscosities estimated in this study agree with an Earth model made up of a thick continental root with thinner, potentially warmer, and wetter asthenosphere beneath, influenced by the Southern Alaska subduction zone and perhaps by residual effects of the ~100 million year old Brooks Range orogeny. The Southern Alaska model of Hu and Freymueller (2015) (in preparation) and the model defined in this study are complementary for an Earth model that involves a transition from active subduction to more stable continental interior.

The best fit GIA model used in this study explains much of the vertical velocity that is measured using GPS in Northern and Northwestern Alaska, with clear evidence of forebulge subsidence. The location and magnitude of this forebulge subsidence is now better defined using the model presented here. The GIA model presented here provides similar subsidence rate predictions over a wide range of model parameters. It does not appear to explain all of the vertical velocities seen in the GPS measurements, but it explains the main signal in the tectonically quiet northern part of the state. This model also provides consistent, smoothly varying, vertical velocities that extend across Western Alaska and provide better spatial coverage than GPS measurements. These modeled velocities will be used to augment as a proxy for a robust, continuous GPS network, providing the onshore tectonic vertical velocity measurement needed in this study of RSL change in Western Alaska.

5.2 Evaluation of the GIA model in Western Alaska

The GIA model of Western Alaska fits the majority of the data in Western Alaska with a few exceptions. These large residuals may result from a real, local tectonic motion that is not explained by glacial rebound or they could be related to error in the measurement. In an effort to utilize the most accurate tectonic vertical velocity estimates in the RSL change model, the sites with large residuals are evaluated here. This analysis attempts to determine which velocities result from local tectonic or other factors that should be represented using the measured GPS velocities, and which velocities are likely an artifact of measurement error and are better

estimated from the GIA modelling. The residuals outside of Western Alaska are not analyzed, as they will not be used in any further calculations for RSL change. For sites where the model fits the data well, we use the model values.

In Figure 5.3 the residuals of the best fit GIA model are plotted, with the locations of anamolous residuals in Western Alaska labeled for further discussion here.

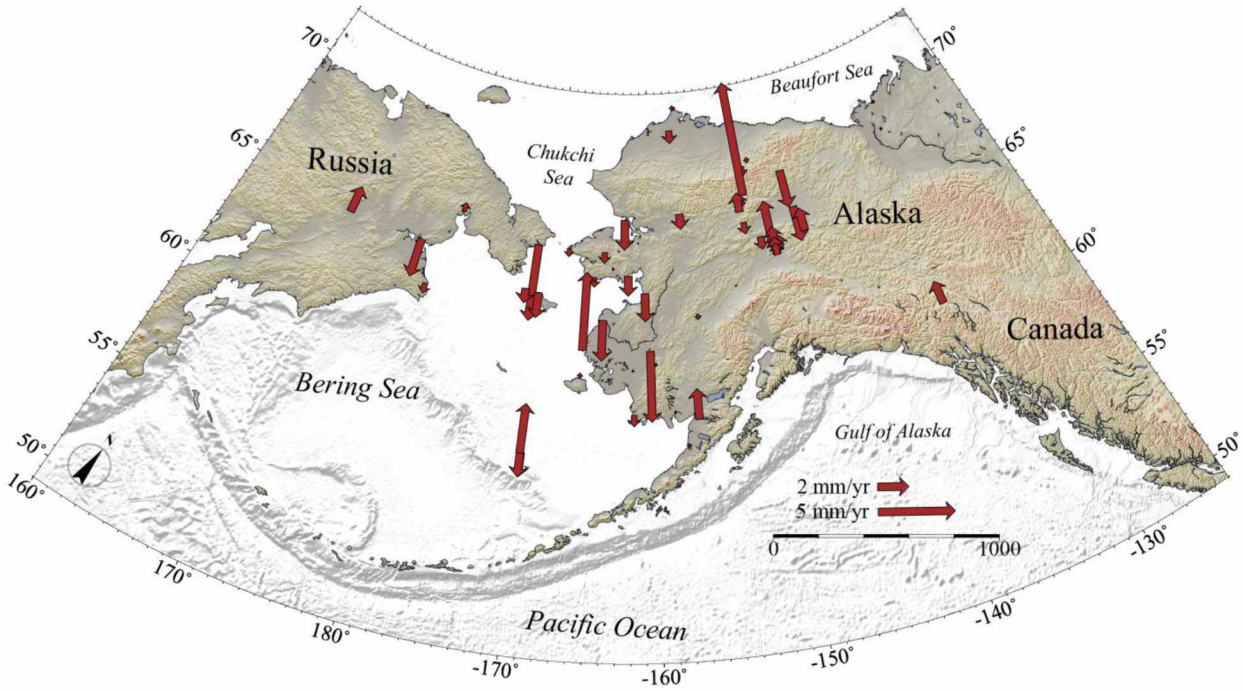

Figure 5.3. Plot of the residuals from the best fit GIA model estimates of vertical velocity.

The Seward Peninsula has consistent residuals, showing that the GIA model underestimates the measured GPS velocities by slightly less than 1 mm/yr, except for the velocity at Kotzebue, where the residual is approximately 3 mm/yr. Kotzebue is a weighted average vertical velocity from two continuous stations (Table 4.2) that are located within 3.5 km from each other on a sand spit in Kotzebue Sound. These stations exhibit similar velocities of - 4.164 and -3.862 mm/yr, and do not appear to be fixed to unstable structures, yet the estimation from the best fit GIA model predicts only -2.104 mm/yr of subsidence. These stations also have no significant offsets from earthquake events or equipment changes that would explain a difference in rate of this magnitude. The GPS measurements for Kotzebue are therefore assessed as reliable and accelerated local subsidence of the sand spit in Kotzebue Sound probably accounts for the resulting model residual.

The YK Delta has many locations with anamolous residuals, the most egregious being at Hooper Bay and Bethel, where the residuals indicate not only a difference in magnitude, but in sign of the vertical velocity, measuring uplift where the model has predicted subsidence. Emmonak and Kalskag also have considerable residuals, however at least both are over estimations of the subsidence predicted by the model rather than significant uplift where subsidence is modeled.

Hooper Bay measurements come from one campaign station, HOOP (Appendix 4). The benchmark is a steel rod driven to refusal into sand dunes along the runway of the Hooper Bay airport in 1991. HOOP has been occupied four times, the first three occupations in 1991, 2001, and 2006 were short-term occupations of less than two full days. It was not until 2014 that a long measurement over four days was collected. Uncertainties are large for the shorter measurements in 1991 and 2001. The vertical velocity measured for this site is 4.111 mm/yr +/- 0.627 mm/yr. The estimated velocity produced by the GIA model is -0.717 mm/yr. The benchmark could be unstable due to its installation into a highly mobile sand dune, and half of the measurements are from decades when GPS data and processing was less precise. The GPS data at this location is further considered unreliable as there are only a few short duration occupations, and the GIA modeled velocities will be used in this location.

The velocity at Bethel is a weighted average of one continuous station and three campaign sites (Table 4.2). These four sites are very inconsistent and have velocities that range from -2.540 +/- 0.488 mm/yr to 6.672 +/- 0.697mm/yr. There are no earthquake or obvious offsets that could account for this range in data, but Bethel is situated on the bank of the Kuskokwim River. The villages in this river setting are built on unconsolidated river sands and gravels covered in saturated tundra and marsh vegetation that commonly result in benckmark instability. The campaign site BETB (6.672 mm/yr) has only two occupations, a short two day record in 2001 and a three day record in 2014. The other two campaign sites BETC (0.618 mm/yr) and CABN (4.391 mm/yr) have three occupations in 2001, 2006, and 2014 (BETC) and 1991, 2006, and 2014 (CABN). BETB and BETC are steel rods with greased sleeves driven to refusal in the gravel of the aprons of Bethel airport runways. CABN is a steel rod driven to refusal in the tundra less than 1 km from the airport. There is some ambiguity in the station documentation surrounding this station and its destruction and reinstallation. These campaign sites are considered unreliable and inconsistent, due to probable benchmark instabilitities,

measurement or processing errors, or a combination of both of these factors. The continuous site at Bethel, BET1 (-2.540 mm/yr) has been running with minimal data gaps since 2008 and exhibits no offset in the East, North, or vertical directions. The GIA model for this location predicts a rate of -0.853 mm/yr, resulting in a misfit of 1.687 mm/yr. The continuous station exhibits no obvious reason for error, but the environment of Bethel suggests that the estimate of average expected tectonic velocity may differ from the local ground motion.

Upriver from Bethel, the village of Kalskag also exhibits a significant model residual. Kalskag is also built on the banks of the Kuskokwim river on unconsolidated river sands and gravels, but it is drier and there is much less tundra in the area. Unlike Bethel, Kalskag is built at the foot of the Kuskokwim Mountains, and bedrock is visable from town. There is only one campaign site, KALS (Appendix 4), with three measurments in 1991, 2006, and 2014. The measured vertical velocity at KALS is -4.294 +/- 0.660 mm/yr and the predicted GIA model velocity is -0.957 mm/yr. While the benchmark at KALS may be more stable than those in Bethel, this site is considered to be unreliable as it has only two precise occupations and the GIA model is determined to be a better suited portrayal of vertical velocity.

The final large residual in the YK Delta is in Emmonak where three campaign stations, EMNA, EMNB, and EMNC, have measurements of -3.024 +/- 0.962 mm/yr, -8.399 +/- 2.435 mm/yr, and -1.413 +/- 3.313 mm/yr, respectively (Table 4.2). The measurements here have very high associated error and ENMB is not consistent with the other two measurements. These three marks are steel rods driven to refusal all within a few hundred meters of each other. These benchmarks are in the aprons of the Emmonak airport, on the banks of the Yukon River in unconsolidated river sands and gravels. These benchmarks are of questionable stability due to their wide range in measured values and large associated errors. The estimated vertical velocity from the GIA model of -0.834 mm/yr will be applied at this location.

There is one station is Eastern Russia that also exhibits a large resdidual, but we have no data sheets for this station, LAV1, in Lavrentiya, as it was surveyed by a Russian group. This campaign site is the only velocity measurement available at this location. There are three measurements in 2005, 2007, and 2009 that result in the vertical velocity of -5.838 +/- 1.147. No other information for this station was found, although it is located outside of town, so groundwater pumping is not a likely cause of localized subsidence. Given the large uncertainty

of this measurement, the GIA model prediction will be used as the estimate for tectonic vertical velocity at this location.

Of these six locations evaluated the GIA model was selected for use in the tectonic vertical velocity model at five locations, with only the site in Kotzebue expected to have accurate measurements of local vertical motion occuring. Four of these locations, Kotzebue, Hooper Bay, Emmonak, and Lavrentiya will be used in creating the RSL change model for Western Alaska, so it is important to establish which data is more appropriate for use in these communities where large model residuals were calculated.

5.3 Evaluation of RSL change prediction methods at Sand Point and Seldovia tide gauges

Tide gauge data provide measurements of water levels relative to a fixed point on land, recording observations of RSL through time, and is the most direct way to measure RSL change. Continuous tide station data to observe RSL trends in Western Alaska is limited to the Nome tide gauge, but this dataset has a limited time span (1992 – present), includes many measurement gaps, and has a very high estimated error (4.24 mm/yr) (C.E. Zervas, personal communication, January 30, 2015). This tide gauge data will also only provide an estimate of RSL change at Nome.

I create a model of RSL change for the coast of Western Alaska by averaging satellite altimetry MSL trend coastal cells as a measurement of the oceanic component of RSL change, and combining it with tectonic vertical velocities observed using GPS or predicted using the GIA model. A minimum check of the error involved with this approach is performed using Equation 2.1 for the the tide gauge data from Sand Point and Seldovia, Alaska. The results from these comparisons will help us to understand the accuracy of the RSL change model being applied to Western Alaska, and estimate any additional error that may not be accounted for in the satellite altimetry and GPS uncertainties.

These locations were chosen for this analysis because they have long-term records with minimal data gaps for both the tide gauge and GPS time series. A full analysis of the tide gauge records available at these locations is included in Appendix 2. The values used in this discussion are trends I calculated in Appendix 2 from monthly mean water level measurements relative to the MSL datum. These locations have published trends available online through NOAA, but the same method that is used to analyze the Nome data is used here for the purpose of consistency.

Table 5.2 shows the trends used and the calculations made for the evaluation of our RSL change model estimates. The method employed in this study to predict RSL change at locations in Western Alaska produces RSL trends of +2.81 mm/yr at Sand Point and -7.26 mm/yr at Seldovia. These values are compared to the measured trends of 0.84 mm/yr and -9.35 mm/yr from the Sand Point and Seldovia tide gauges, respectively. Sand Point has a RSL change model misfit of 1.97 mm/yr, which is evaluated using Equation 5.1 and Equation 5.2 . Equation 5.1 calculates the root sum of squares (RSS) for the uncertainties associated with the MSL (satellite altimetry), tectonic velocity (GPS), and RSL change (tide gauge) measurements and Equation 5.2 compares this cumulative measurement uncertainty with the model misfit. If the uncertainty in the measurements explains the model misfit then the RSS will equal the misfit. Equation 5.2 takes the root difference of squares to calculate the error of the calculated RSL trend misclosure with the model. This calculation shows a consistent uncertainty that is not accounted for in the measurement uncertainties of 1.59 mm/yr at Sand Point and 1.80 mm/yr for Seldovia.

Table 5.2 RSL change model calculations for Sand Point and Seldovia compared to the observed RSL trend from their corresponding tide gauges. The RSS (Equation 5.1) of the uncertainties for the tide gauge, satellite altimetry, and GPS measurements is used to evaluate the model misfit.

	Sand Point		**Seldovia**	
	Velocity (mm/yr)	*Uncertainty (+/- mm/yr)*	*Velocity (mm/yr)*	*Uncertainty (+/- mm/yr)*
MSL (satellite altimetry)	1.69	0.60	0.21	0.60
Tectonic velocity (GPS)	-1.12	0.30	7.47	0.30
RSL change calculated (MSL - tectonic velocity)	2.81	0.90	-7.26	0.89
RSL change observed (tide gauge)	0.84	0.95	-9.35	0.82
RSL change misfit (observed - calculated)	-1.97		-2.09	
RSS of uncertainties (Equation 5.1)	1.16		1.06	
Additive error of misfit and RSS of uncertainties (Equation 5.2)	1.59		1.80	

$$RSS = \sqrt{\sigma_{tg}^2 + \sigma_{sa}^2 + \sigma_{gps}^2} \quad (5.1)$$

where σ_{tg} is the tide gauge uncertainty, σ_{sa} is the uncertainty associated with satellite altimetry measurements, and σ_{gps} is the GPS error.

$$E = \sqrt{m^2 - R^2} \quad (5.2)$$

where E is the additive error unacounted for in the data uncertainties, m is the model misfit, and R is the RSS of the data uncertainties.

The method applied in this thesis fails to estimate the RSL change observed from tide gauge data within the established error bounds. It is interesting to note, however, that while Sand Point and Seldovia have very different vertical processes influencing the tide gauge measurements (Appendix 2.), the misfit for both locations is almost the same (approximately 1.6 – 1.8 mm/yr). Another interesting observation is that the misfit for both places is negative, which suggests that the RSL change model applied in this thesis is underestimating the RSL change observed at tide gauges by approximately 2 mm/yr. This pattern of similarity between two locations with very different oceanic and tectonic settings suggests a systematic bias in the tide gauge, satellite altimetry and/or GPS measurements of an average 1.7 mm/yr.

The measurement of misfit error for these RSL change estimations involves uncertainties from all three components (tide gauge, satellite altimetry, and GPS), so the error that is found to be unaccounted for cannot be attributed to a specific measurement. It is worth noting, however, that this value is consistent with the 1-2 mm/yr bias estimation by Ablain et al. (2015) of error in regional satellite altimetry calculations. Ablain et al. (2015) estimate that these regional averages are underestimating the averaged rates of satellite altimetry, which is what we find here, both estimates indicating that MSL is rising at a faster rate than the averaging of satellite altimetry indicates. The error associated with the GPS measurements is not expected to get this large, so it is likely that the RSL change model using satellite altimetry is understimating the actual RSL trend by 1-2 mm/yr due to errors associated with the satellite altimetry measurements. This additional uncertainty will be considered in the similar calculations for Nome RSL change

(Table 5.3) because the error associated with the tide gauge (4.24 mm/yr) is much larger than any of the measurements.

Table 5.3. Velocities for satellite altimetry, GPS, and tide gauges are recorded, with RSL change calculated from the satellite altimetry and GPS values for comparison. The RSL change misfit and RSS are used to estimate if the methods applied in this study are within the uncertainty bounds of the data used.

	Nome - Using GPS		**Nome - Using best fit GIA model**	
	Velocity (mm/yr)	*Uncertainty (+/- mm/yr)*	*Velocity (mm/yr)*	*Uncertainty (+/- mm/yr)*
MSL (satellite altimetry)	-0.28	0.60	-0.28	0.60
Tectonic velocity (GPS)	-1.75	0.22	-1.13	
RSL change calculated (MSL - tectonic velocity)	1.47	0.82	0.85	0.60
RSL change observed (tide gauge)	0.50	4.24	0.50	4.24
RSL change misfit (observed - calculated)	-0.97		-0.35	
RSS of uncertainties (Equation 5.1)	4.29		4.28	
Additive error of misfit and RSS of uncertainties (Equation 5.2)	4.18		4.27	

The calculations for Nome show very small misfits of -0.97 mm/yr and -0.35 mm/yr when calculating RSL change using GPS and GIA respectively. These misfits to the tide gauge data are well within the calculated RSS of 4.29 mm/yr for the GPS RSL change estimate and 4.28 mm/yr for the GIA RSL change estimate. The tide gauge uncertainty dominates these calculations, so the average additive error (1.7 mm/yr) found to be in the Sand Point and Seldovia estimates is applied here. This results in a misfit of -0.97 mm/yr +/- 1.7 mm/yr for RSL change calculations using GPS data and a misfit of -0.35 mm/yr +/- 1.7 mm/yr when using the best fit GIA model to calculate RSL change in Nome.

The lack of tide gauge measurements anywhere else in Western Alaska make supplementary tide gauge comparisons such as the ones performed here not possible at this time. Until additional tide gauge data is obtained in Western Alaska the method applied in this study of using average cells of coastal MSL trends from satellite altimetry and vertical velocities estimated from the GIA model that is best fit to GPS data in Alaska is reasonably validated by the only available comparison to tide gauge water level measurements in Nome.

5.4 RSL change model for Western Alaska

This study combines the compilation of the offshore component, or MSL trend from satellite altimetry and the onshore component of GPS or best fit GIA vertical velocities, to construct an RSL change model for Western Alaska (Figure 5.4, Figure 5.5, Figure 5.6, Figure 5.7, and Table 5.4).

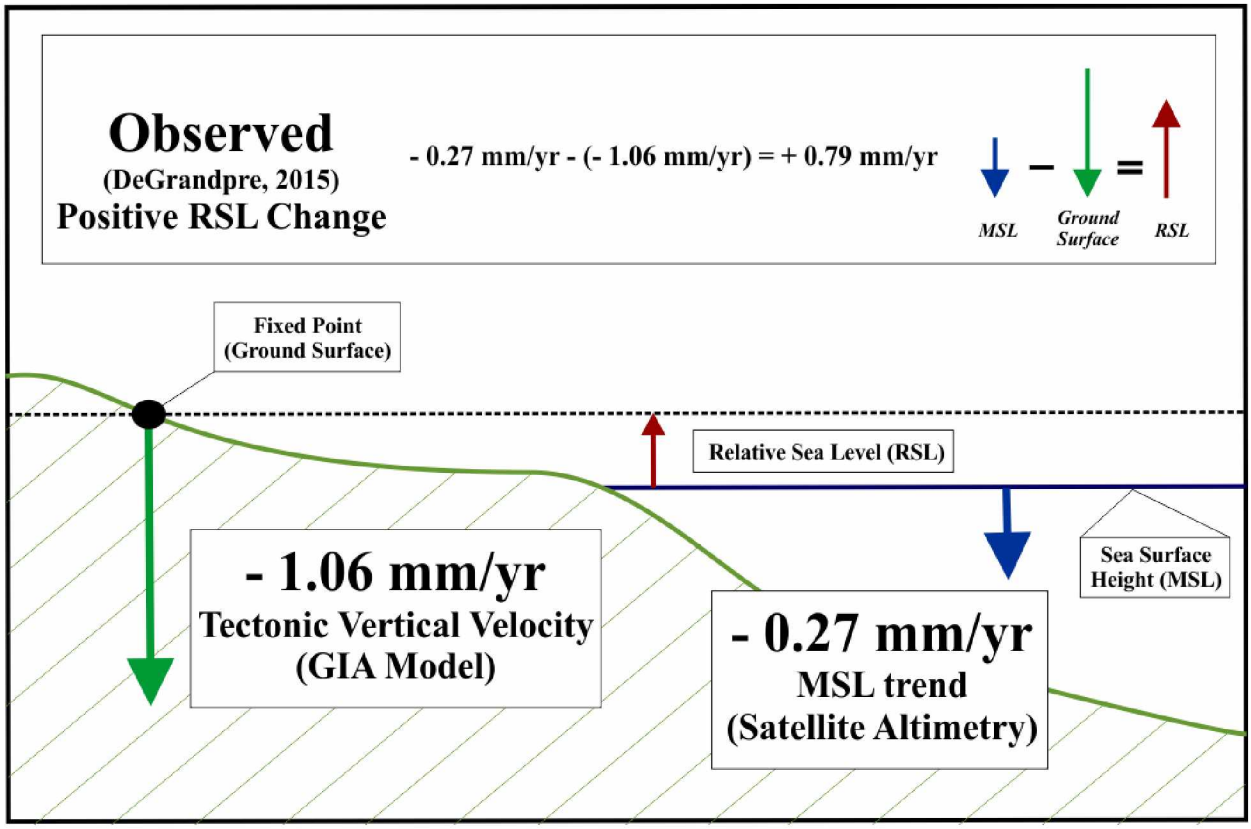

Figure 5.4. Diagram of the average tectonic vertical velocity, average MSL trend, and average RSL change calculation for Western Alaska.

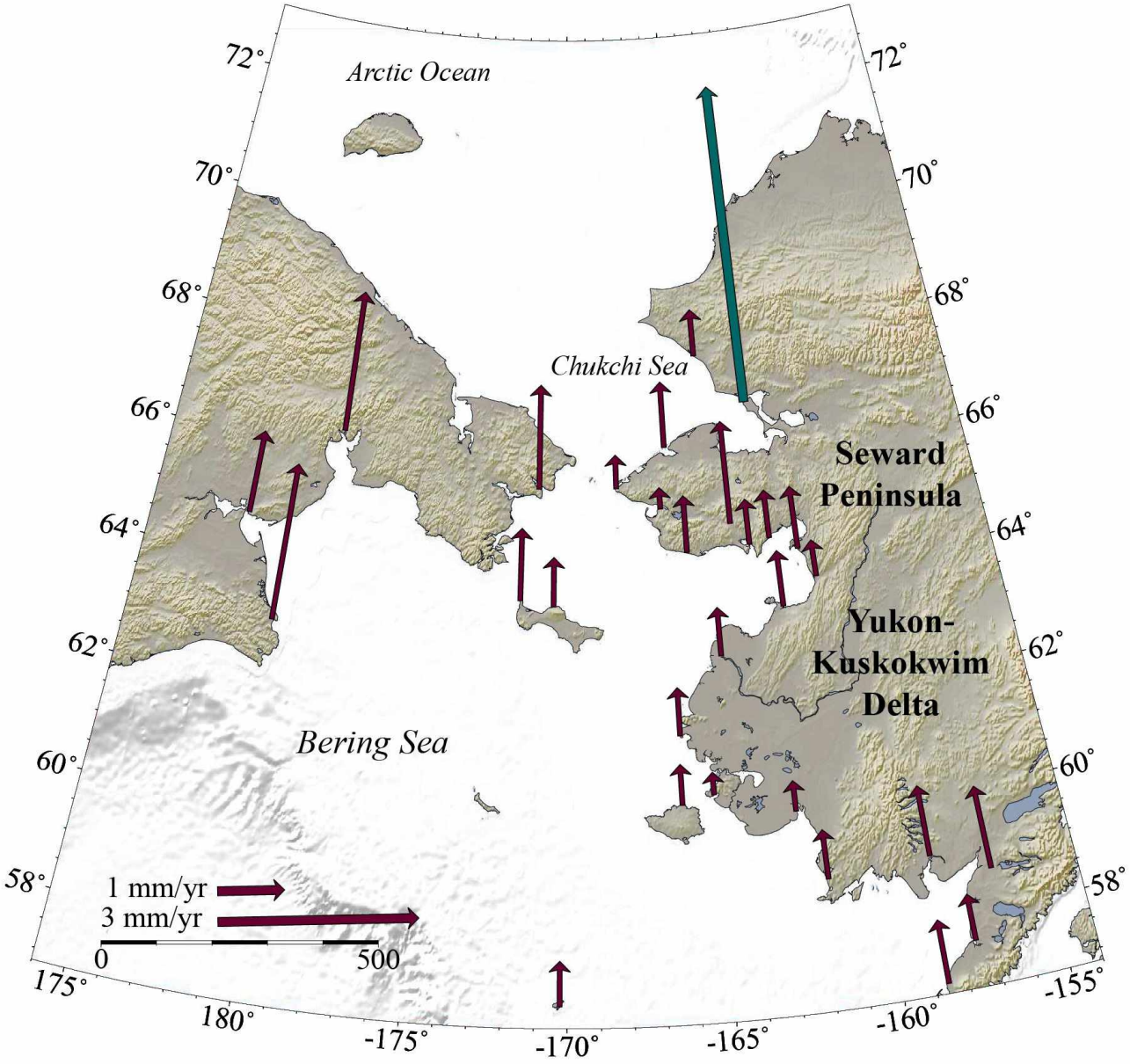

Figure 5.5. RSL change model for Western Alaska. This model is produced using satellite altimetry and the best fit GIA vertical velocity estimates (purple arrows) with the exception of Kotzebue (green arrow) where the GPS measured velocities are used in place of the GIA model. The model underestimates the measured GPS values, but is considered to be a better approximation in Western Alaska except in Kotzebue where the model did not fit the apparent local tectonic effects.

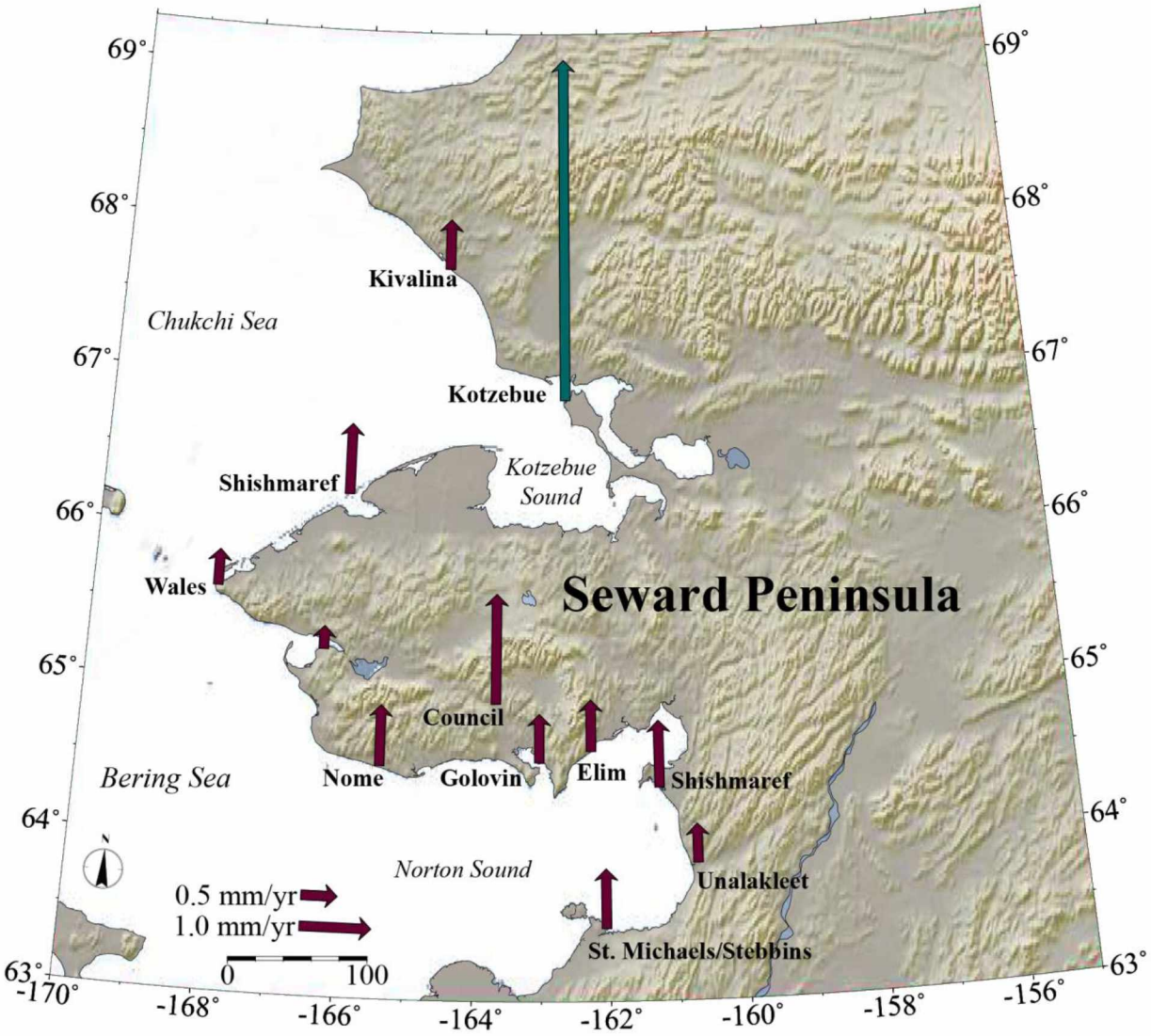

Figure 5.6. RSL change model for the Seward Peninsula. This model is the same as the model presented in Figure 5.5 and is produced by combining satellite altimetry with the tectonic vertical velocity estimates from the best fit GIA model. At Kotzebue, the GPS velocity is used instead of the model (Section 5.2). The rates on the Seward Peninsula show increasing RSL of 0.5 – 1 mm/yr with the exception of Kotzebue, the furthest north estimate of approximately 3 mm/yr.

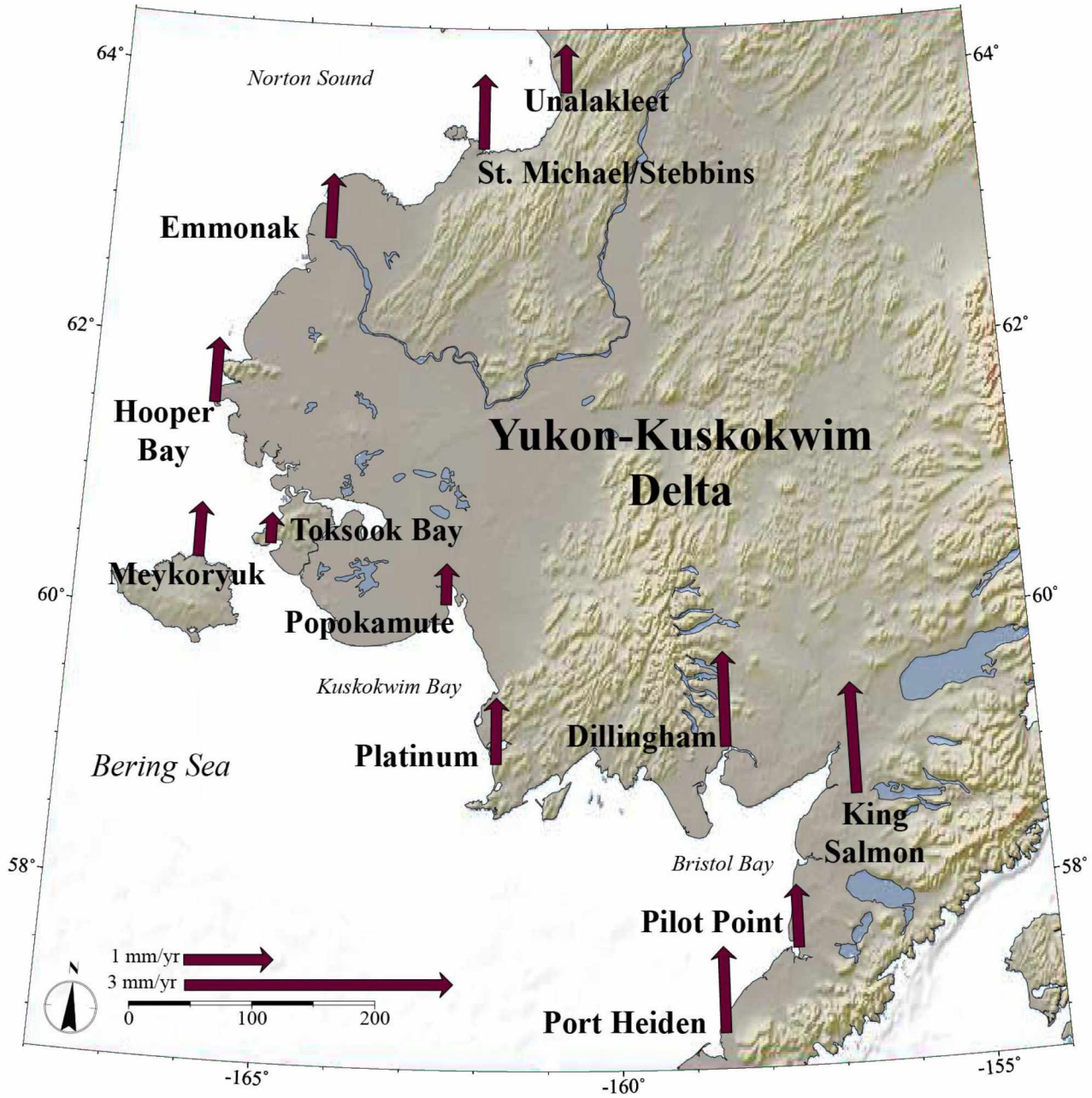

Figure 5.7. RSL change model for the YK Delta. This model is the same as the model in Figure 5.5 and is produced by combining satellite altimetry and tectonic vertical velocities from the best fit GIA model. Rates for the YK Delta range from 0.5 – 2 mm/yr of RSL change with an increase over all of the locations.

Table 5.4. Satellite altimetry MSL trend calculated using the 0.5° x 0.5° grid averaging offshore of each location and tectonic velocities estimated using GPS observations and the best fit GIA model are used to calculate two potential velocities for RSL change. The locations listed are all locations in Western Alaska where GPS velocities are available so that satellite altimetry and GIA estimates can be compared.

Community	**MSL Trend (mm/yr)**		**Tectonic Vertical Velocity (mm/yr)**			**RSL (mm/yr)**	
	Satellite Altimetry	*Satellite Altimetry Standard Deviation*	*GPS*	*GPS Uncertainty*	*Best Fit GIA Model*	*Satellite Altimetry and GPS*	*Satellite Altimetry and GIA*
BERINGOVO	0.9631	0.0710	-2.046	0.927	-1.38240	3.01	2.35
COUNCIL	-0.3773	0.1497	-2.057	0.436	-1.90660	1.68	1.53
DILLINGHAM	0.3907	0.1028	-0.822	0.571	-0.67358	1.21	1.06
ELIM	-0.2184	0.1810	-2.230	0.378	-0.93611	2.01	0.72
EMMONAK	-0.0886	0.1024	-3.591	0.863	-0.96073	3.50	0.87
EVGENIKOT	0.8547	0.1358	-0.667	0.993	-1.23160	1.52	2.09
GAMBELL	0.3332	0.0865	-1.675	0.718	-0.74487	2.01	1.08
GOLOVIN	-0.3773	0.1497	NA	NA	-1.05260	NA	0.68
HOOPER BAY	-0.2281	0.0649	4.111	0.627	-0.94857	-4.34	0.72
KING SALMON	0.3907	0.1028	1.142	0.306	-0.85296	-0.75	1.24
KIVALINA	-0.3146	0.0782	NA	NA	-1.00310	NA	0.69
KOTZEBUE	0.7029	0.0811	-4.031	0.326	-2.10410	4.73	2.81
LAVRENTIYA	0.6633	0.0848	-5.838	1.147	-0.88705	6.50	1.55
MEYKORYUK	-0.2842	0.0831	-0.562	0.621	-0.89243	0.28	0.61
NOME	-0.2811	0.0554	-1.751	0.225	-1.13090	1.47	0.85
PILOT POINT	0.3825	0.1284	-0.049	0.473	-0.31869	0.43	0.70
PLATINUM	-0.2546	0.0820	-1.731	0.608	-0.99707	1.48	0.74
POPOKAMUTE	-0.2546	0.0820	NA	NA	-0.71326	NA	0.46
PORT HEIDEN	0.2234	0.0895	-0.650	0.277	-0.74024	0.87	0.96
SAVOONGA	0.1025	0.0584	-2.268	0.558	-0.63585	2.37	0.74
SHISHMAREF	0.0111	0.0950	NA	NA	-0.96608	NA	0.98
SHAKTOOLIK	-0.2184	0.1810	NA	NA	-1.14660	NA	0.93
ST. MICHAEL/ STEBBINS	-0.1938	0.1714	NA	NA	-1.02460	NA	0.83
ST. PAUL ISLAND	0.3600	0.0627	-1.988	0.504	-0.31813	2.35	0.68
TELLER	-0.6181	0.1086	NA	NA	-0.93722	NA	0.32
TOKSOOK BAY	-0.2842	0.0831	NA	NA	-0.62001	NA	0.34
UGOLNAYA	0.5157	0.0774	-1.532	0.621	-0.71090	2.05	1.23
UNALAKLEET	-0.1938	0.1714	-2.560	0.557	-0.73465	2.37	0.54
WALES	-0.5229	0.1074	-1.577	0.451	-1.02580	1.05	0.50

The average RSL change on the Seward Peninsula is 1.78 mm/yr when using GPS values for the onshore component and 1.12 mm/yr when using the GIA model values (Table 5.5 and Figure 5.6). In the YK Delta average RSL change is found to range from 0.51 mm/yr (GPS model) to 0.45 mm/yr (GIA model) (Figure 5.7). If both of the GPS RSL velocities for the Seward Peninsula and the YK Delta are used, an average rate of RSL change for Western Alaska of 1.14 mm/yr is calculated. When this same calculation is done for the best fit GIA RSL velocities an average rate of RSL change of 0.79 mm/yr is estimated for Western Alaska.

Table 5.5. Average rates for satellite altimetry, GPS, GIA, and RSL calculated using GPS and the GIA model are given for the Seward Peninsula and the YK Delta. The values listed for Western Alaska are the averages of the values for the Seward Peninsula and the YK Delta.

Location	Average Velocity (mm/yr)				
	Satellite Altimetry	GPS	Best Fit GIA	GPS RSL	GIA RSL
Seward Peninsula	-0.1272	-1.9036	-1.2499	1.78	1.12
YK Delta	-0.4125	-0.9185	-0.8629	0.51	0.45
Western Alaska	-0.2698	-1.4111	-1.0564	1.14	0.79

These vertical tectonic velocities are compared so that a more general trend can be expressed for Western Alaska. Previous sections have determined that the best fit GIA model is appropriate to apply everywhere in Western Alaska, except for Kotzebue, where local tectonic motion is suspected of producing the significant subsidence measured with GPS.

Satellite altimetry is the second component to this model and contains its own sources of error. The method used in this study of coastal averaging of satellite altimetry has not previously been used in MSL or RSL change applications. There are associated uncertainties (Appendix 5) with these averaging calculations, but they are related to the magnitude of the MSL trends in the defined region that the satellite altimetry is averaged over. They were found to be minimized for cells that are averaged to 0.5°x0.5° cells. This size of 0.5° equates to approximately 50 km, which happens to also be the estimated distance from shore that satellite altimetry begins to be more reliable. In the estimates of RSL change modeled here, the cells that are closest to shore are used in the averaging to obtain a MSL trend for the location. In Western Alaska this averaging method does not make a significant difference as the MSL trend for the region does not vary widely (Figure 4.6).

To assess the error involved with the overall estimate of RSL change, Equation 5.2 is used to approximate the difference between methods used here and the RSL trend calculated from tide gauge data in Nome Alaska (Table 5.3).

The trends in Table 5.3 show excellent agreement between the Nome tide gauge and the RSL change estimate using satellite altimetry and modeled GIA velocities. These results suggest that the method employed in this study to average satellite altimetry data over 0.5°x0.5° cells and compare that value to the best fit GIA model estimates of tectonic vertical velocities provide a suitable first-order model for RSL change.

The larger RSL changes estimated in Western Alaska occur in the small bays and sounds, which are unfortunately where many communities are located. The Eastern ends of Kotzebue Sound, Norton Sound, and Bristol Bay show a slightly greater estimate for RSL trend than locations that are on the coast of the Bering or Chukchi Seas. The Gulf of Anadyr also shows this trend, though it applies to values on the western side of the basin. This phenomenon is visible in the satellite altimetry data (Figure 4.6) as slightly higher bulges in these semi-enclosed bodies of water. The reason for this could include factors such as locations of warmer, freshwater input where thermal expansion and density stratification have influenced the MSL rate, or it could be gravity or atmospherically driven as water gets piled up in these shallow bays due to winds or the rotation of the Earth. The causes for the trends and spatial patterns modeled here are unclear and leave a lot of room for speculation until further studies of oceanographic and geophysical processes can better define the magnitudes of the processes involved.

The average MSL trend estimated for Western Alaska (~ -0.27 mm/yr) is much lower than the average regional trend for the Bering Sea (~ +2.6 mm/yr) (Nerem et al., 2014) and the global average (~ +3.2 mm/yr) (Nerem et al., 2010; Leuliette and Willis, 2011). It is worth noting that the Bering Sea regional trend is dominated by the bulge formed by the Bering Sea gyre in the western half of the basin. This bulge is a result from a combination of long wavelength signals of cyclical atmospheric processes and the effects of gravity. Satellite altimetry dates back to 1992, which means that any cyclical signal longer than 30 years has potentially not yet been observed in the satellite altimetry record. This means that atmospheric effects such as the steep gradient that has formed in the western half of the Bering Sea have not yet been observed to move. It is expected that this dynamic topography will change with time because the gradient created by the gyre cannot grow indefinitely. If this gyre migrates east, or

the gyre disintegrates and the mass of water that formed it is redistributed throughout the rest of the Bering Sea, the RSL change in Western Alaska could rapidly increase by a few mm/yr because of increases in the rate of MSL rise to the rates currently observed in the western half of the Bering Sea.

The RSL change model presented here is a best first-order estimate available, even though there are potentially large errors in these values. It can be discerned from these calculations, however, that in Western Alaska, RSL is rising. The magnitudes of these rates are difficult to constrain at this time, but average to +0.79 mm/yr for the locations included in this model. The minimum RSL change of +0.32 mm/yr is calculated at Teller and the maximum rate of RSL change is +4.73 mm/yr in the community of Kotzebue using the vertical velocity from measured GPS rather than the GIA model. The tectonic vertical velocities produced by the best fit GIA model support the hypothesis that the subsidence of a forebulge from the Laurentide and Cordilleran ice sheets could be influencing the increase in RSL change in Western Alaska, contrary to RSL rates in other regions of the state, like Southeast Alaska where rapid uplift from the post-Little Ice Age deglaciation is causing a decrease in RSL. The estimates presented here for RSL change in Western Alaska are the first of their kind, but require future updates to monitor the evolution of these trends with time as oceanographic and geophysical processes continue to develop and measurements become more temporally and spatially available, and accurate. If MSL in Western Alaska starts to rise at rates equal to or exceeding the Bering Sea average rate, then the coastal subsidence would result in more rapid rates of RSL rise.

5.5 Implication of RSL change model for communities

The estimates of RSL change in Western Alaska using satellite altimetry and the best fit GIA model are all positive (increasing RSL). This increase in RSL is not very large (~ +0.79 mm/yr), but in an environment as flat as Western Alaska small changes in RSL can have large effects on the environment as the sea level propagates farther inland than it would on steeper coasts. The implications of increasing RSL in Western Alaska are greater risks to communities and potentially significant effects on local ecosystems.

RSL estimates presented here are not applicable in future years. The tectonic velocities are considered stable, as the response to the GIA unloading and processes like delta loading are long wavelength signals that do not have shorter decadal variations. As we have seen in section

2.3, the satellite altimetry record is short and does not span a comprehensive range of oceanic and atmospheric conditions for the region, as seen in the ENSO indices. This means that the MSL rates measured with satellite altimetry may be subject to change with the ratio of El Niño to La Niña events in the satellite altimetry record, or relative to another index such as the Pacific Decadal Oscillation. The MSL trend has the potential of increasing from the current Western Alaska estimate of – 0.27 mm/yr to the higher regional estimate of + 2.6 mm/yr by Nerem et al., (2014) or even the global average of + 3.2 mm/yr (Nerem et al., 2010; Leuliette and Willis, 2011). An increase in MSL rates in Western Alaska of these magnitudes could result in an increase in regional RSL to values between + 3.5 and + 4.5 mm/yr. The current estimated MSL rate for Western Alaska presented in this thesis is significantly smaller than the regional and global averages at this time.

As the RSL in a community increases, storm surges, wave height, flooding, and erosion progress farther inland, near to homes and engineered and community structures. These natural hazards are exacerbated by the increase in RSL and mitigation plans will need to account for the inland progression of these threats. Where communities presently experience annual damage to infrastructure, plans need to be made that incorporate RSL estimates so that when actions are taken to assuage the effects of these natural hazards they are not merely negated in the near future as the increase in RSL continues to present the same hazards farther inland. Presently when addressing community hazards that are effected by RSL change the US Army Corp of Engineers (USACE) include "low", "intermediate", and "high" estimates in site analysis reports (U.S. Army Corps of Engineers (USACE) Alaska District, 2014). In high risk communities like Golovin, the USACE needs a value for RSL change, but because there is no tide gauge these estimates are made using the National Resource Council (NRC) linear equations involving eustatic sea level change over time which is then added to the local rate of vertical land movement. This study provides at the minimum, a better approximation of local vertical land motion using the GIA model that can then be coupled with the NRC equations used by the USACE. The RSL change model presented here could also be considered the "low" approximation because of the expected underestimation of MSL trend from satellite altimetry and poor definition of ocean circulation changes, sediment loading, and permafrost subsidence.

Many of the communities in Western Alaska are supported by subsistence hunting and gathering that could also be greatly impacted as RSL rises. The inundation of saltwater quickly

transforms the water bodies and vegetation in these flat coastal environments, which propagates upwards to change the assemblage of organisms that populate and utilize this new habitat. Mammals, birds, and fish that a community once survived on might migrate to other locations and plants such as roots and berries might find the new environment inhospitable and be unable to continue growing in the area.

The long-term effects of RSL change on an ecosystem can be quite drastic and further investigation into the specific results this increase of RSL will have in Western Alaska are needed so that adequate preparation can be made. This RSL change model is the first tool needed in order to proceed with these future studies and it provides a foundation for predicting side effects from this RSL change that have a more direct impact on communities and ecosystems.

6 Conclusions

6.1 Summation of methods and products

This study produced a collection of data, new methodologies, and never before estimated models for a variety of oceanographic and geophysical processes in Western Alaska that are valuable products for scientific investigations, engineering projects, and communities in this region.

Assembling historic water level, tide gauge, GPS, and satellite altimetry data in one location will aid in future estimates of RSL change in Western Alaska. These products are all publically available, but at different locations, some of which are not obvious. The comparison of tide gauge data available for Nome, Sand Point, and Seldovia provides awareness about these datasets that was not previously considered. Often these products are downloaded and used with the assumption that they are equal to datasets at other sources that are presented as identical. Appendix 2 shows that this is not the case and a variety of processing, updating, and content differences exist between the same products available at two widely used sources (PSMSL and NOAA websites).

The use of coastal altimetry is not optimal, but this study has provided an averaging method that attempts to reduce the near coast noise and estimate coastal MSL in the absence of other data. This method showed consistency between locations of different coastal environments at Nome, Sand Point, and Seldovia and provides an alternative option for coastal MSL trend estimates in data sparse regions. The results of this methodology are MSL rates for the coast of Western Alaska with an average of - 0.27 mm/yr and specific measurements for remote locations across Alaska and Russia that range from - 0.62 mm/yr in Teller, Alaska to + 0.96 mm/yr in Beringovo, Russia.

GIA modelling has been done for the more tectonically active regions in Southeast Alaska, but it is not until this study that a model for the Northern and Western areas of Alaska has been estimated. Previous to the modelling done in this thesis, these Southern Alaska models were extrapolated across the rest of Alaska where tectonic processes and settings are drastically different. The results of the model presented here show the subsidence of a forebulge resulting from the deglaciation of the Laurentide and Cordilleran Ice sheets that is centered over central northern Alaska and extending to the Bering Sea. The best fit parameters resulting from this model define a thicker lithosphere (120 km) than estimations in Southeast Alaska have predicted

(55 km). The asthenospheric thickness between these two models does not vary significantly and the asthenosphere is estimated to only thicken slightly (approximately 30 km) to the north and west in Alaska. The viscosity of the asthenosphere is also essentially identical, indicating an extension of the hot, wet mantle that results from active subduction. The upper mantle viscosity was not estimated in the Southeastern Alaska model, but is found here to be similarly high (1.5×10^{21} Pa s), supporting the conclusion of a higher viscosity, stable upper mantle in Northern and Western Alaska that is consistent with the upper mantle in Southeastern Alaska. This model provides a basis for future modelling and eliminates the possibility of a continuously thin lithosphere across Alaska, and suggests that Alaska lithosphere varies across the state. These modeled viscosities are continuous, suggesting that the heat and water flux in the mantle due to subduction propagates farther north and west in the lithosphere than the active tectonic region.

The main focus of this study was to estimate an RSL change model in Western Alaska, and due to the lack of traditional RSL measurements from tide gauges a model was constructed using the method of averaging satellite altimetry data developed here and creating a GIA model of tectonic vertical velocity that is best fit to the available GPS data. This RSL change model is relevant for community planning and the study of ecosystems in Western Alaska and will be valuable in these applications. RSL change was estimated to be increasing everywhere in Western Alaska and found to have an average + 0.79 mm/yr with a minimum rate of + 0.32 mm/yr in Teller and a maximum rate in Kotzebue of + 4.73 mm/yr using the tectonic vertical velocity measured with GPS. These RSL rates of change in Western Alaska are hypothesized to become larger in the future as atmospheric oscillations that have not yet been observed within the existing satellite altimetry record introduce more rapid MSL rise to the area. Estimates of RSL change modeled in this thesis indicate that communities in Western Alaska should incorporate this trend into community planning as an increase in RSL can exacerbate natural hazards such as flooding, erosion, and storm surges that already pose serious threats to some populations.

The methods and products that resulted from this thesis are the first-order estimates of oceanographic and geophysical processes and trends effecting Western Alaska. The models presented here are still crude and rudimentary, but they provide a framework on which future work can be based.

6.2 Future work

More accurate models of RSL change in Western Alaska will be needed as the climate and processes affecting these measurements evolve. The best way to measure this directly would be the installation of a tide gauge network, although a few decades of measurements will be needed. Tide gauges cover much of the U.S. coast, but the whole coast of Western Alaska (as defined in this work) has only one record in Nome. As the importance of RSL change becomes more understood, additional tide gauges will hopefully be installed so that models such as the ones performed here can be verified against direct measurements and oceanographic and geophysical processes can be better understood and predicted. Present plans for future expansion of the tide gauge network in Western Alaska are limited to a 2016 installation in Unalakleet as part of the National Water Level Observation Network (NWLON).

Barring direct measurements of RSL change, general data collection of sea level and tectonic velocities would significantly help to augment the models presented here and provide a more robust dataset for future modelling. A report of prioritized GPS benchmarks for future occupation in Western Alaska is included in Appendix 9. These additional measurements will help to better define the Earth model in Northern and Western Alaska with use in comparison to continued GIA modelling of the area. A more robust GPS network is essential for the purposes of estimating the tectonic motion and defining the poorly understood Bering plate.

Continued use of satellite altimetry will provide more accurate estimates of MSL trends in Western Alaska and further developments in coastal altimetry processing and application will reduce the associated and suspected errors inherent in this data. This study found a discrepancy in measurement error on the order of 1-2 mm/yr, which agrees with estimates of regional uncertainties estimated for satellite altimetry (Ablain et al., 2015). This same study by Ablain et al. (2015) proposes future reductions in satellite altimetry error to 0.3 and 0.5 mm/yr for global and regional estimates. They state that algorithms are being developed that aim to reduce and better define errors associated with satellite altimetry and suggest that these algorithms will become available in October of 2015 (Ablain et al., 2015). The continued update and modelling of these improved satellite altimetry estimates is essential to understanding and modelling MSL and RSL trends in Western Alaska and the Bering Sea region.

A delta subsidence model for the YK Delta would be a valuable asset to evaluate RSL change in Western Alaska. The model itself could be created using the Earth and loading models

combined in the program TABOO to produce the GIA model. The model would be identical with the exception of adjustments to the loading model that reflect the specific geometry, rate, and density of the sediment deposition at the Yukon River delta and the Kuskokwim River delta. The most beneficial measurements needed for these delta subsidence model parameters are the sediment load (sediment suspended in the water column) and discharge (rate of flow for the volume of water) for each river.

As the oceanographic and geophysical processes change and evolve the measurements of MSL, tectonic vertical velocity, and RSL change used in this study will need to be updated, so that they remain applicable and useful to the people of Western Alaska.

References

Ablain, M., Cazenave, A., Larnicol, G., Balmaseda, M., Cipollini, P., Faugère, Y., Fernandes, M.J., Henry, O., Johannessen, J.A. and Knudsen, P., 2015. Improved sea level record over the satellite altimetry era (1993–2010) from the Climate Change Initiative Project. Ocean Science Discussions, 11(4): 2029-2071.

Ablain, M., Cazenave, A., Valladeau, G. and Guinehut, S., 2009. A new assessment of global mean sea level from altimeters highlights a reduction of global trend from 2005 to 2008. Ocean Science Discussions, 6: 31-56.

Antonov, J.I., Levitus, S. and Boyer, T.P., 2005. Thermosteric sea level rise, 1955–2003. Geophysical Research Letters, 32(12).

Argus, D.F., Gordon, R.G., Heflin, M.B., Ma, C., Eanes, R.J., Willis, P., Peltier, W.R. and Owen, S.E., 2010. The angular velocities of the plates and the velocity of Earth's centre from space geodesy. Geophysical Journal International, 180(3): 913-960.

AVISO, 2009. SSALTO/DUACS user handbook:(M) SLA and (M) ADT near-real time and delayed time products. SALP-MU-P-EA-21065-CLS, Centre National d'Etudes Spatiales, Toulouse, France.

Bindoff, N.L., Willebrand, J., Artale, V., Cazenave, A., Gregory, J.M., Gulev, S., Hanawa, K., Le Quéré, C., Levitus, S., Nojiri, Y., Shum, C.K., Talley, L.D. and Unnikrishnan, A.S., 2007. Observations: Oceanic climate change and sea level, Climate Change 2007: The Physical Science Basis. Cambridge University Press, pp. 385-432.

Bjerknes, J., 1972. Large-scale atmospheric response to the 1964-65 Pacific equatorial warming. Journal of Physical Oceanography, 2(3): 212-217.

Bureau, U.S.C., 2013. State and County QuickFacts. United States Census Bureau.

Cazenave, A. and Llovel, W., 2010. Contemporary Sea Level Rise. Annual Review of Marine Science, 2(1): 145-173.

Cazenave, A., Lombard, A. and Llovel, W., 2008. Present-day sea level rise: A synthesis. Comptes Rendus Geoscience, 340(11): 761-770.

Chambers, D.P., Merrifield, M.A. and Nerem, R.S., 2012. Is there a 60-year oscillation in global mean sea level? Geophysical Research Letters, 39(18).

Church, J.A., Woodworth, P.L., Aarup, T. and Wilson, W.S., 2010. Understanding sea-level rise and variability. John Wiley & Sons.

Chelton, D.B. and Davis, R.E., 1982. Monthly Mean Sea-Level Variability Along the West Coast of North America. Journal of Physical Oceanography, 12(8): 757-784.

Cross, R.S., 2007. GPS based tectonic analysis of the Aleutian arc and Bering plate, University of Alaska Fairbanks, Fairbanks, AK, 100 pp.

Cross, R.S. and Freymueller, J.T., 2008. Evidence for and implications of a Bering plate based on geodetic measurements from the Aleutians and western Alaska. Journal of Geophysical Research: Solid Earth, 113(B7): n/a-n/a.

Deng, X., Featherstone, W.E., Hwang, C. and Berry, P.A.M., 2002. Estimation of contamination of ERS-2 and POSEIDON satellite radar altimetry close to the coasts of Australia. Marine Geodesy, 25(4): 249-271.

Dixon, J.E., Dixon, T.H., Bell, D.R. and Malservisi, R., 2004. Lateral variation in upper mantle viscosity: role of water. Earth and Planetary Science Letters, 222(2): 451-467.

Domingues, C.M., Church, J.A., White, N.J., Gleckler, P.J., Wijffels, S.E., Barker, P.M. and Dunn, J.R., 2008. Improved estimates of upper-ocean warming and multi-decadal sea-level rise. Nature, 453(7198): 1090-1093.

Douglas, B., Kearney, M.T. and Leatherman, S.P., 2000. Sea level rise: History and Consequences. Academic Press, San Diego, CA, 232 pp.

Forbes, D.L., 2011. State of the Arctic coast 2010: Scientific review and outlook. Land-Ocean Interactions in the Coastal Zone, Institute of Coastal Research, 178 pp.

Fournier, T.J. and Freymueller, J.T., 2007. Transition from locked to creeping subduction in the Shumagin region, Alaska. Geophysical Research Letters, 34(6).

Freymueller, J.T., Cohen, S.C. and Fletcher, H.J., 2000. Spatial variations in present-day deformation, Kenai Peninsula, Alaska, and their implications. Journal of Geophysical Research: Solid Earth (1978–2012), 105(B4): 8079-8101.

Freymueller, J.T., Woodard, H., Cohen, S.C., Cross, R., Elliott, J., Larsen, C.F., Hreinsdottir, S. and Zweck, C., 2008. Active deformation processes in Alaska, based on 15 years of GPS measurements. In: J.T. Freymueller, P.J. Haeussler, R.L. Wesson and G. Ekström (Editors), Active tectonics and seismic potential of Alaska. American Geophysical Union, Washington, DC, pp. 1-42.

Fu, L. L. and Holt, B., 1982. SEASAT views oceans and sea ice with synthetic aperture radar. NASA-CR-168919, JPL-PUB-81-120, NAS 1.26:168919, Jet Propulsion Laboratory, California Institute of Technology, Pasadena, CA.

Fu, Y. and Freymueller, J.T., 2012. Seasonal and long-term vertical deformation in the Nepal Himalaya constrained by GPS and GRACE measurements. Journal of Geophysical Research: Solid Earth (1978–2012), 117(B3).

Fujita, K., Mackey, K.G., McCaleb, R.C., Gunbina, L.V., Kovalev, V.N., Imaev, V.S. and Smirnov, V.N., 2002. Seismicity of Chukotka, northeastern Russia. Geological Society of America Special Paper Series, 360: 259-272.

Gill, S.K. and Schultz, J.R., 2001. Tidal datums and their applications, National Oceanic and Atmospheric Administration, Silver Spring, MD.

Godin, G., 1991. The analysis of tides and currents (Review). In: B.B. Parker (Editor), Tidal hydrodynamics. John Wiley & Sons, New York, pp. 675-709.

Gratiot, N., Anthony, E.J., Gardel, A., Gaucherel, C., Proisy, C. and Wells, J.T., 2008. Significant contribution of the 18.6 year tidal cycle to regional coastal changes. Nature Geoscience, 1(3): 169-172.

Holgate, S.J., Matthews, A., Woodworth, P.L., Rickards, L.J., Tamisiea, M.E., Bradshaw, E., Foden, P.R., Gordon, K.M., Jevrejeva, S. and Pugh, J., 2012. New data systems and products at the permanent service for mean sea level. Journal of Coastal Research, 29(3): 493-504.

Hu, Y. and Freymueller, J.T., 2015. In Preparation.

Ivins, E.R., Dokka, R.K. and Blom, R.G., 2007. Post-glacial sediment load and subsidence in coastal Louisiana. Geophysical Research Letters, 34(16).

James, T.S. and Morgan, W.J., 1990. Horizontal motions due to post-glacial rebound. Geophysical Research Letters, 17(7): 957-960.

Johnson, G.C. and Wijffels, S.E., 2011. Ocean density change contributions to sea level rise. Oceanography, 24(2): 112-121.

Kaufmann, G. and Johnston, P., 1997. Benchmark comparisons for models of glacial isostatic adjustment. Australian National University, Canberra, Australia.

Kaufmann, G. and Lambeck, K., 2000. Mantle dynamics, postglacial rebound and the radial viscosity profile. Physics of the Earth and Planetary Interiors, 121(3): 301-324.

Kaufmann, G. and Lambeck, K., 2002. Glacial isostatic adjustment and the radial viscosity profile from inverse modeling. Journal of Geophysical Research: Solid Earth (1978–2012), 107(B11): ETG 5-1-ETG 5-15.

Lander, A.V., Bukchin, B.G., Droznin, D.V. and Kiryushin, A.V., 1996. The tectonic environment and source parameters of the Khailino, Koryakiya earthquake of March 8, 1991: Does a Beringia plate exist? Computational Seismology and Geodynamics, 3: 80-96.

Larsen, C.F., Motyka, R.J., Freymueller, J.T., Echelmeyer, K.A. and Ivins, E.R., 2005. Rapid viscoelastic uplift in southeast Alaska caused by post-Little Ice Age glacial retreat. Earth and Planetary Science Letters, 237(3–4): 548-560.

Leuliette, E.W. and Willis, J.K., 2011. Balancing the sea level budget. Oceanography, 24(2): 122-129.

Mackey, K.G., Fujita, K., Gunbina, L.V., Kovalev, V.N., Imaev, V.S., Koz'min, B.M. and Imaeva, L.P., 1997. Seismicity of the Bering Strait region: Evidence for a Bering block. Geology, 25(11): 979-982.

Milliman, J.D. and Farnsworth, K.L., 2011. River discharge to the coastal ocean: a global synthesis. Cambridge University Press, Cambridge, UK.

Milliman, J.D. and Syvitski, J.P.M., 1992. Geomorphic/tectonic control of sediment discharge to the ocean: the importance of small mountainous rivers. The Journal of Geology, 100(5): 525-544.

Milne, G.A., Davis, J.L., Mitrovica, J.X., Scherneck, H.-G., Johansson, J.M., Vermeer, M. and Koivula, H., 2001. Space-geodetic constraints on glacial isostatic adjustment in Fennoscandia. Science, 291(5512): 2381-2385.

Mitrovica, J.X. and Forte, A.M., 1997. Radial profile of mantle viscosity: results from the joint inversion of convection and postglacial rebound observables. Journal of Geophysical Research: Solid Earth (1978–2012), 102(B2): 2751-2769.

Nerem, R.S., Chambers, D.P., Choe, C. and Mitchum, G.T., 2010. Estimating Mean Sea Level Change from the TOPEX and Jason Altimeter Missions. Marine Geodesy, 33(sup1): 435-446.

Nerem, R.S., Choe, J., Masters, D., Mitchum, G.T. and Chambers, D.P., 2014. Regional Sea Level Time Series. CU Sea Level Research Group, University of Colorado, Boulder, CO.

NOAA, 2013. Water Levels. National Ocean Service.

NOAA/NOS, 2003. Computational Techniques for Tidal Datums Handbook. U.S. Department of Commerce, National Oceanic and Atmospheric Administration, NOAA Special Publication NOS CO-OPS 2, Silver Spring, MD.

Nolet, G. and Zielhuis, A., 1994. Low S velocities under the Tornquist-Teisseyre zone: Evidence for water injection into the transition zone by subduction. Journal of Geophysical Research: Solid Earth (1978–2012), 99(B8): 15813-15820.

Panteleev, G., Yaremchuk, M., Stabeno, P. J., Luchin, V., Nechaev, D. A., & Kikuchi, T., 2011. Dynamic topography of the Bering Sea. Journal of Geophysical Research: Oceans (1978–2012), 116(C5).

Pfeffer, W.T., 2011. Land ice and sea level rise: A thirty-year perspective. Oceanography 24(2):94–111, http://dx.doi.org/10.5670/oceanog.2011.30.

Pawlowicz, R., Beardsley, B. and Lentz, S., 2002. Classical tidal harmonic analysis including error estimates in MATLAB using T_TIDE. Computers & Geosciences, 28(8): 929-937.

Permanent Service for Mean Sea Level (PSMSL), 2015. "Tide Gauge Data", Retrieved 15 Jan 2015 from http://www.psmsl.org/data/obtaining/.

Proshutinsky, A.Y. and Johnson, M.A., 2011. Arctic Ocean Oscillation Index (AOO): interannual and decadal changes of the Arctic climate, Geophys. Research Abstracts.

Proshutinsky, A.Y. and Johnson, M.A., 1997. Two circulation regimes of the wind-driven Arctic Ocean. Journal of Geophysical Research, 102(C6): 12,493-412,514.

Reidy, M.S., 2009. Tides of history: ocean science and Her Majesty's Navy. University of Chicago Press, Chicago.

Roden, G.I., 1967. On river discharge into the northeastern Pacific Ocean and the Bering Sea. Journal of Geophysical Research, 72(22): 5613-5629.

Santamaría-Gómez, A., Bouin, M.-N., Collilieux, X. and Wöppelmann, G., 2011. Correlated errors in GPS position time series: Implications for velocity estimates. Journal of Geophysical Research: Solid Earth, 116(B1).

Schabert, K.L., Runfola, D.M. and Ikuta, H., 2015a. Kuskokwim River, Chinook News.

Schabert, K.L., Runfola, D.M. and Ikuta, H., 2015b. Yukon River, Chinook News.

Snay, R., Cline, M., Dillinger, W., Foote, R., Hilla, S., Kass, W., Ray, J., Rohde, J., Sella, G. and Soler, T., 2007. Using global positioning system-derived crustal velocities to estimate rates of absolute sea level change from North American tide gauge records. Journal of Geophysical Research: Solid Earth (1978–2012), 112(B4).

Spada, G., 2003. The theory behind TABOO. Samizdat Press, Golden-White River Junction, CO.

Spada, G., Antonioli, A., Boschi, L., Brandi, V., Cianetti, S., Galvani, G., Giunchi, C., Perniola, B., Agostinetti, N.P. and Piersanti, A., 2003. TABOO, User Guide. Samizdat Press, Golden-White River Junction, CO.

Spada, G., Antonioli, A., Boschi, L., Brandi, V., Cianetti, S., Galvani, G., Giunchi, C., Perniola, B., Agostinetti, N.P. and Piersanti, A., 2004. Modeling Earth's post-glacial rebound. Eos, Transactions American Geophysical Union, 85(6): 62-64.

Stabeno, P.J., Schumacher, J.D. and Ohtani, K., 1999. The physical oceanography of the Bering Sea. Dynamics of the Bering Sea: 1-28.

Suito, H. and Freymueller, J.T., 2009. A viscoelastic and afterslip postseismic deformation model for the 1964 Alaska earthquake. Journal of Geophysical Research: Solid Earth (1978–2012), 114(B11).

Tushingham, A.M. and Peltier, W.R., 1991. Ice-3G: A new global model of Late Pleistocene deglaciation based upon geophysical predictions of post-glacial relative sea level change. Journal of Geophysical Research: Solid Earth, 96(B3): 4497-4523.

U.S. Army Corps of Engineers (USACE) Alaska District. 2014. “Section 103 Coastal Storm Damage Reduction Feasibility Study - Appendix A. Hydraulic Design Golovin, Alaska".

Wang, Y.M. and Rapp, R.H., 1994. Estimation of sea surface dynamic topography, ocean tides, and secular changes from Topex altimeter data. 430, Department of Geodetic Science and Surveying, The Ohio State University.

Wolter, K., and Timlin, M.S., 1993. Monitoring ENSO in COADS with a seasonally adjusted principal component index. Proc. of the 17th Climate Diagnostics Workshop, Norman, OK, NOAA/NMC/CAC, NSSL, Oklahoma Clim. Survey, CIMMS and the School of Meteor., Univ. of Oklahoma, 52-57.

Wolter, K., and Timlin, M.S., 1998. Measuring the strength of ENSO events - how does 1997/98 rank? Weather, 53, 315-324.

Zervas, C., Gill, S. and Sweet, W., 2013. Estimating vertical land motion from long-term tide gauge records, National Ocean Service Center for Operational Oceanographics Products and Services.

Appendix 1
Historic Water Level Analysis

Historic water level measurements, much like campaign GPS measurements were used to calculate relative sea level (RSL) trends in communities along the coast of the Bering Sea (Figure A.1.1). These temporary water level observations range over 60 years from 1951 to 2011 at various sites, but most sites have only two measurements. These values are instantaneous water levels, so they record the water level relative to a local benchmark. Each value is then adjusted to be relative to a tidal datum; these records are referenced to mean lower low water (MLLW), mean high water (MHW), and/or mean higher high water (MHHW). All locations have only two measurements with the exception of St. Paul Island where one benchmark (NO 4 (1946)) has three measurements.

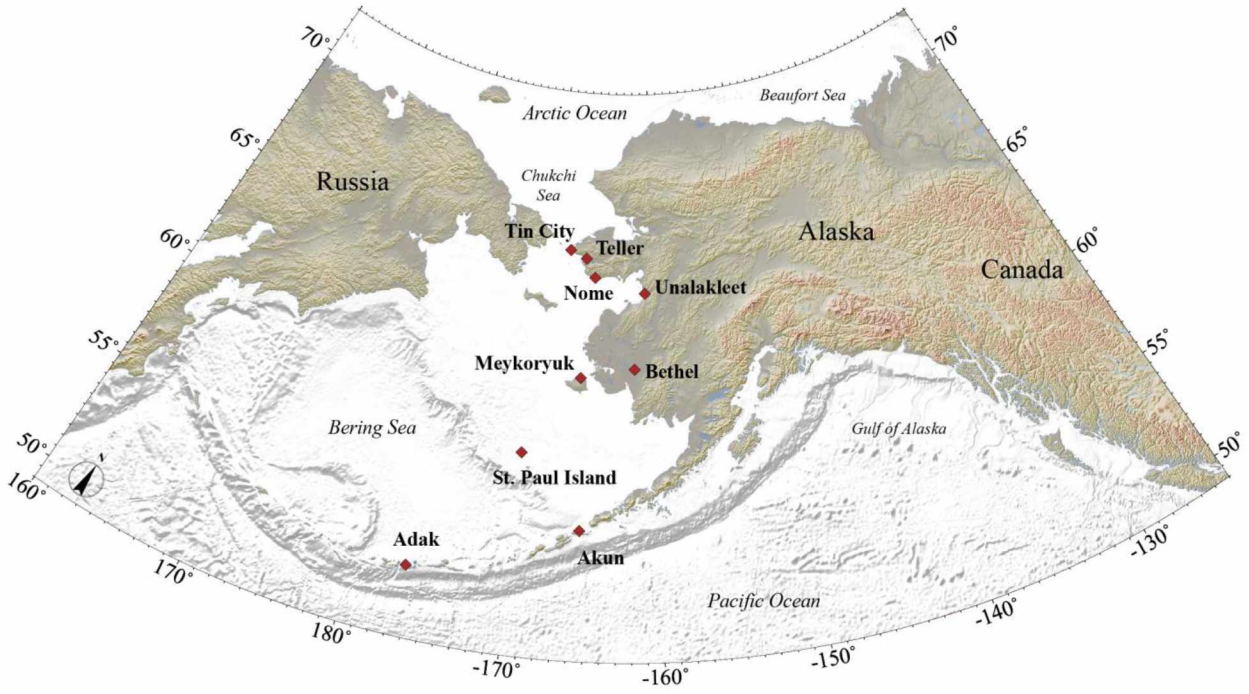

Figure A1.1. Map of the Bering Sea region and the locations where historic water level data has been obtained.

RSL trends vary between each community (Table A.1.1), but also between benchmarks in the same community, indicating relatively large amounts of error associated with this type of approach. Adak, Akun, and Teller exhibit consistent trends between the benchmarks in the

community, and even share similar trends of -1.5 to -4.2 mm/yr. At St. Paul Island each time span shows consistent trends, but the trends between these two time spans are very dissimilar and exhibit both increasing and decreasing RSL trends. This is not completely impossible as one time span is around three times as long as the other. The rest of the communities' RSL change estimates can vary between benchmarks at rates of up to 113.1 mm/yr.

Information sheets for each location are included at the end of this summary that detail the available information and the RSL change calculations. The dates between listed time spans and headings on data tables are often not the same. The dates listed as the time span represent the actual time span of the data, while the dates listed at the top of data tables refer to the publishing date of the water level records, so that those records can be later referenced if needed. When available, notes on the data collection period and method as well as benchmark condition are given at the bottom of the information sheet.

Unfortunately the lack of consistency between communities and sometimes between benchmarks in one community signifies that there are potentially large uncertainties associated with these measurements, and there are no quantifications of error provided. While some of the rates seem reasonable and are consistent at a location it would be a biased selection of data to decide to use some of these measurements rather than others. These measurements were not used in the creation of a RSL trend map of Western Alaska, but could be considered in comparisons with the RSL trend values constructed using satellite altimetry and GPS measurements.

Table A1.1. Summary of relative sea level trends at locations in the Bering Sea region. Rates are calculated from water level records that date from the early 1900s to present.

Benchmark ID	Community	Measurement Range	Velocity (mm/yr)
NO 18 (1957)	ADAK	1969 – 2003	-4.0
BM 23 (1968)	ADAK	34 years	-4.2
BM 1 (1937)	AKUN		-3.1
BM 2 (1937)	AKUN	1951 – 2010	-3.2
BM 3 (1937)	AKUN	59 years	-3.1
BM 4 (1938)	AKUN		-3.1
BM 6 (1970)	BETHEL	1970 – 2010	-0.9
BM 7 (1970)	BETHEL	40 years	1.0
TIDE (1951)	MEKORYUK	1951 – 2010	3.6
MEKORYUK (1951)	MEKORYUK	59 years	16.2
BM 3 (1969)	NOME	1969 – 2002 32 years	-5.9
BM 7 (1969)	NOME	1969 – 1977	-152.0
TGBM 1 USE (1944)	NOME	7 years	-41.3
TGBM 2 USE (1944)	NOME		-265.1
NO 4 (1946)	ST. PAUL ISLAND	1989 – 2011 22 years	6.3
NO 3 (1946)	ST. PAUL ISLAND	2004 – 2011 7 years	-4.0
4212 L (1976)	ST. PAUL ISLAND	1989 – 2004 15 years	6.2
4212 N (2002)	ST. PAUL ISLAND		-3.2
4212 P (2002)	ST. PAUL ISLAND	2004 – 2011	-3.7
SP - 3 USACE (2001)	ST. PAUL ISLAND	7 years	-3.1
RBD 1 (1994)	ST. PAUL ISLAND		-3.3
NO 1 (1950)	TELLER	1950 – 2010	-1.5
NO 2 (1950)	TELLER	60 years	-1.5
NO 3 (1950)	TELLER		-1.6
TIN CITY NO 2 (1960)	TIN CITY	1960-2007 47 years	24.1
BM A (1977)	UNALAKLEET	1977 – 2001 34 years	1.1

--------- ADAK ISLAND – Sweeper Cove, Kuluk Bay

Time Span: 1969 – 2003 (34 years)

Difference between datums:
2003 MHHW 1.131 m higher than MLLW.
1969 MHHW 1.128 m higher than MLLW.

Change in the difference between datums from 1969 to 2003: 0.003 m

AVAILABLE DATA

BM ID	June 10, 1969		April 21, 2003	
	MLLW (ft)	MHHW (ft)	MLLW (m)	MHHW (m)
NO 18 (1957)	18.57	14.87	5.797	4.666
BM 23 (1968)	18.44	14.74	5.764	4.633

RSL CHANGE CALCULATIONS

NO 18 (1957)

	June 10, 1969	April 21, 2003	RSL Change (m)	RSL Change (mm/yr)
MLLW (m)	5.660	5.797	-0.137	-4.0
MHHW (m)	4.532	4.666	-0.134	-3.9

BM 23 (1968)

	June 10, 1969	April 21, 2003	RSL Change (m)	RSL Change (mm/yr)
MLLW (m)	5.621	5.764	-0.143	-4.2
MHHW (m)	4.493	4.633	-0.140	-4.1

NOTES

- June 10 1969 data - MLLW is based on 3 years of records 1958-1960, reduced to mean values. No MHW observed. *Note: the tides at this locality are largely diurnal.
- April 21 2003 data - TIME PERIOD: January 1983-December 2001, TIDAL EPOCH: 1983-2001.

--------- AKUN ISLAND – Akun Cove

Time Span: 1951 – 2010 (59 years)

Difference between datums:
2010 MHW 0.880 m higher than MLLW.
1951 MHW 0.823 m higher than MLLW.

Change in the difference between datums from 1951 to 2010: 0.057 m

AVAILABLE DATA

BM ID	November 30 1951		June 7 2010	
	MLLW (ft)	MHW (ft)	MLLW (m)	MHW (m)
BM 1 (1937)	5.77	3.07	1.943	1.063
BM 2 (1937)	7.98	5.28	2.62	1.740
BM 3 (1937)	7.96	5.26	2.609	1.729
BM 4 (1938)	8.48	5.78	2.766	1.886

RSL CHANGE CALCULATIONS

BM 1 (1937)

	November 30, 1951	June 7, 2010	RSL Change (m)	RSL Change (mm/yr)
MLLW (m)	1.759	1.943	-0.184	-3.1
MHW (m)	0.936	1.063	-0.127	-2.2

BM 2 (1937)

	November 30, 1951	June 7, 2010	RSL Change (m)	RSL Change (mm/yr)
MLLW (m)	2.432	2.62	-0.188	-3.2
MHW (m)	1.609	1.740	-0.131	-2.2

BM 3 (1937)

	November 30, 1951	June 7, 2010	RSL Change (m)	RSL Change (mm/yr)
MLLW (m)	2.426	2.609	-0.183	-3.1
MHW (m)	1.603	1.729	-0.126	-2.1

BM 4 (1938)

	November 30, 1951	June 7, 2010	RSL Change (m)	RSL Change (mm/yr)
MLLW (m)	2.585	2.766	-0.181	-3.1
MHW (m)	1.762	1.886	-0.124	-2.1

NOTES

- November 30 1951 data - MLLW based on 19HW/18LW, August 12-23 1937; 18HW/18LW, June 29-July 8 1938; and 16HW/17LW, August 22-31, 1938.
- April 21 2003 data - TIME PERIOD: May 2009 - August 2009, TIDAL EPOCH: 1983 - 2001.

--------- BETHEL – Kuskokwim River

Time Span: 1970 – 2010 (40 years)

Difference between datums:
2010 MHW 0.843 m higher than MLLW.
1970 MHW 0.823 m higher than MLLW.

Change in the difference between datums from 1970 to 2010: 0.020 m

AVAILABLE DATA

BM ID	January 22, 1971		January 14, 2011	
	MLLW (ft)	MHW (ft)	MLLW (m)	MHW (m)
BM 6 (1970)	21.30	18.60	6.528	5.685
BM 7 (1970)	27.12	24.42	8.225	7.382

RSL CHANGE CALCULATIONS

BM 6 (1970)

	January 22, 1971	January 14, 2011	RSL Change (m)	RSL Change (mm/yr)
MLLW (m)	6.492	6.528	-0.036	-0.9
MHW (m)	5.669	5.685	-0.016	-0.4

BM 7 (1970)

	January 22, 1971	January 14, 2011	RSL Change (m)	RSL Change (mm/yr)
MLLW (m)	8.266	8.225	0.041	1.0
MHW (m)	7.443	7.382	0.061	1.5

NOTES

- January 22, 1971 data - MLLW based on 3 months of records from July-September 1970, reduced to mean values.
- January 14, 2011 data - TIME PERIOD: June 210-September 2010, TIDAL EPOCH: 1983-2001

--------- MEKORYUK – Mekoryuk River Entrance, Nunivak Island

Time Span: 1951 – 2010 (59 years)

Difference between datums:
2010 MHW 2.149 m higher than MLLW.
1951 MHW 2.469 m higher than MLLW.

Change in the difference between datums from 1951 to 2010: -0.320 m

AVAILABLE DATA

BM ID	February 12 1952		January 14 2011	
	MLLW (ft)	MHW (ft)	MLLW (m)	MHW (m)
TIDE (1951)	12.67	4.57	3.649	1.500
MEKORYUK (1951)	44.94	36.84	12.743	10.594

RSL CHANGE CALCULATIONS

TIDE (1951)

	February 12, 1952	January 14, 2011	RSL Change (m)	RSL Trend (mm/yr)
MLLW (m)	3.862	3.649	0.213	3.6
MHW (m)	1.393	1.500	-0.107	-1.8

MEKORYUK (1951)

	February 12, 1952	January 14, 2011	RSL Change (m)	RSL Trend (mm/yr)
MLLW (m)	13.698	12.743	0.955	16.2
MHW (m)	11.229	10.594	0.635	10.8

NOTES

- November 30, 1951 data - MLLW based on 5 high water and 4 low water levels.
- June 24-26, 1951 reduced to mean values.
- TIME PERIOD: July 2010-September 2010, TIDAL EPOCH: 1983 – 2001.
- Benchmark TIDE (1951) is set in a rock outcrop but MEKORYUK (1951) is set in a concrete block on a 13 m bluff or near the bluff (2010). In 1951 it was described as on "top of sand dune".

--------- NOME – Nome Harbor, Seward Peninsula

Time Span: 1969 – 1977 (7 years)

Time Span: 1976 – 1977 (1 year)

Time Span: 1969 – 2002 (32 years)

Difference between datums:
Only MLLW is provided for 1976 and 1977
1969 MHHW 0.488 m higher than MLLW.
2002 MHHW 0.468 m higher than MLLW.

Change in the difference between datums from 1969 to 2002: 0.020 m

AVAILABLE DATA

BM ID	January 12, 1971		June 24, 1976	June 28, 1977	February 9, 2009	
	MLLW (ft)	MHHW (ft)	MLLW (ft) (assumed)	MLLW (ft) assumed	MLLW (m)	MHHW (m)
BM 3 (1969)	16.11	14.51			5.098	4.630
BM 7 (1969)	17.18		20.103	20.171		
TGBM 1 USE (1944)	8.39		9.129	9.203		
TGBM 2 USE (1944)	6.18		11.314	11.398		

RSL CHANGE CALCULATIONS

BM 3 (1969)

	January 12, 1971	February 9, 2009	RSL Change (m)	RSL Trend (mm/yr)
MLLW (m)	4.910	5.098	-0.188	-5.9
MHHW (m)	4.423	4.630	-0.207	-6.5

BM 7 (1969)

	January 12, 1971	June 24, 1976	June 28, 1977
MLLW (m)	5.236	6.127	6.148

	RSL Change (m)	RSL Trend (mm/yr)
1969 - 1976	-0.891	-178.2
1976 - 1977	-0.021	-20.7

1969 - 1977	-0.912	-152.0

TGBM 1 USE (1944)

	January 12, 1971	June 24, 1976	June 28, 1977
MLLW (m)	2.557	2.783	2.805

	RSL Change (m)	RSL Trend (mm/yr)
1969 - 1976	-0.225	-45.1
1976 - 1977	-0.023	-22.6
1969 - 1977	-0.248	-41.3

TGBM 2 USE (1944)

	January 12, 1971	June 24, 1976	June 28, 1977
MLLW (m)	1.884	3.449	3.474

	RSL Change (m)	RSL Trend (mm/yr)
1969 - 1976	-1.565	-313.0
1976 - 1977	-0.026	-25.6
1969 - 1977	-1.590	-265.1

NOTES

- January 12 1971 data - MLLW based on July-August 1969 and July 19-September 17, 1970 reduced to mean values.
- April 21 2003 data - TIME PERIOD: August 1997-July 2002, TIDAL EPOCH: 1983 - 2001.
- Note: The tides at this locality are chiefly diurnal.
- Note: No values other than the assumed MLLW are given in the 76/77 records.
- Note: The 76/77 values appear to be false, or show that there is some sinking of the tide gauge or raising of the height stick (see record) because of the approximate 20 mm/yr change between 76/77. The measurements are made in decimal feet and this value is suspiciously close to 1 inch, which could indicate operator error when recording or measuring the water level.

--------- ST. PAUL ISLAND – Village Cove

Time Span: 1977 – 2002 (25 years)

Time Span: 1977 – 2011 (34 years)

Time Span: 2002 – 2011 (9 years)

Difference between datums:
1977 MHW 0.893 m higher than MLLW.
2002 MHW 0.887 m lower than MLLW. .
2011 MHW 0.938 m higher than MLLW.

Change in the difference between datums from 1977 to 2002: -0.006 m
Change in the difference between datums from 1977 to 2011: 0.045 m
Change in the difference between datums from 2002 to 2011: 0.051 m

AVAILABLE DATA

BM ID	December 13, 1989		June 28, 2004		December 12, 2011	
	MLLW (ft)	MHW (ft)	MLLW (m)	MHW (m)	MLLW (m)	MHW (m)
NO 4 (1946)	32.91	29.98	9.867	8.980	9.896	8.958
NO 3 (1946)			4.681	3.794	4.717	3.779
4212 L (1976)	26.47	23.54	7.912	7.025		
4212 N (2002)			3.261	2.374	3.29	2.352
4212 P (2002)			3.762	2.875	3.795	2.857
SP - 3 USACE (2001)			4.664	3.777	4.692	3.754
RBD 1 (1994)			8.660	7.773	8.69	7.752

RSL CHANGE CALCULATIONS

NO 4 (1946)

	December 13, 1989	June 28, 2004	December 12, 2011
MLLW (m)	10.031	9.867	9.896
MHW (m)	9.138	8.980	8.958

MLLW	RSL Change (m)	RSL Trend (mm/yr)	MHW	RSL Change (m)	RSL Trend (mm/yr)
1977 - 2002	0.164	6.6	1977 - 2002	0.158	6.3
2002 - 2011	-0.029	-3.2	2002 - 2011	0.022	2.4
1977 - 2011	0.135	4.0	1977 - 2011	0.180	5.3

NO 3 (1946)

	June 28, 2004	December 12, 2011	RSL Change (m)	RSL Trend (mm/yr)
MLLW (m)	4.681	4.717	-0.036	-4.0
MHW (m)	3.794	3.779	0.015	1.7

4212 L (1976)

	December 13, 1989	June 28, 2004	RSL Change (m)	RSL Trend (mm/yr)
MLLW (m)	8.068	7.912	0.156	6.2
MHW (m)	7.175	7.025	0.150	6.0

4212 N (2002)

	June 28, 2004	December 12, 2011	RSL Change (m)	RSL Trend (mm/yr)
MLLW (m)	3.261	3.29	-0.029	-3.2
MHW (m)	2.374	2.352	0.022	2.4

4212 P (2002)

	June 28, 2004	December 12, 2011	RSL Change (m)	RSL Trend (mm/yr)
MLLW (m)	3.762	3.795	-0.033	-3.7
MHW (m)	2.875	2.857	0.018	2.0

SP - 3 USACE (2001)

	June 28, 2004	December 12, 2011	RSL Change (m)	RSL Trend (mm/yr)
MLLW (m)	4.664	4.692	-0.028	-3.1
MHW (m)	3.777	3.754	0.023	2.6

RBD 1 (1994)

	June 28, 2004	December 12, 2011	RSL Change (m)	RSL Trend (mm/yr)
MLLW (m)	8.660	8.69	-0.030	-3.3
MHW (m)	7.773	7.752	0.021	2.3

NOTES

- TIME PERIOD: November 1977 (1 month), TIDAL EPOCH: 1960-1978.
- TIME PERIOD:May 2002 (1 month), TIDAL EPOCH: 1983 - 2001.
- TIME PERIOD: March 2007 - February 2010 and October 2010 - September 2011,
- TIDAL EPOCH: 1983 - 2001.

--------- TELLER – Point Spencer, Port Clarence

Time span: 1950 - 2010 (60 years)

Difference between datums:
1950 MHW 0.366 m higher than MLLW.
2010 MHW 0.362 m higher than MLLW.

Change in the difference between datums from 1950 to 2010: 0.004 m

AVAILABLE DATA

BM ID	1950		November 16, 2010	
	MLLW (ft)	MHW (ft)	MLLW (m)	MHW (m)
NO 1 (1950)	9.46	8.26	2.976	2.614
NO 2 (1950)	9.55	8.35	3.000	2.638
NO 3 (1950)	9.39	8.19	2.957	2.595

RSL CHANGE CALCULATIONS

NO 1 (1950)

	1950	November 16, 2010	RSL Change (m)	RSL Trend (mm/yr)
MLLW (m)	2.883	2.976	-0.093	-1.5
MHW (m)	2.518	2.614	-0.096	-1.6

NO 2 (1950)

	1950	November 16, 2010	RSL Change (m)	RSL Trend (mm/yr)
MLLW (m)	2.911	3.000	-0.089	-1.5
MHW (m)	2.545	2.638	-0.093	-1.5

NO 3 (1950)

	1950	November 16, 2010	RSL Change (m)	RSL Trend (mm/yr)
MLLW (m)	2.862	2.957	-0.095	-1.6
MHW (m)	2.496	2.595	-0.099	-1.6

NOTES

- 1950 data - MLLW based on 1 month of automatic gage records, August 1950, reduced to mean values.
- November 16, 2010 data - TIME PERIOD: July 20 - September 1, 2010, TIDAL EPOCH: 1983 - 2001.

--------- TIN CITY – Bering Strait

Time span: 1960 - 2007 (47 years)

AVAILABLE DATA

BM ID	December 29, 1960 MLLW (ft)	March 19, 2009 MLLW (m)
Tin City NO 2 (1960)	11.601	2.405

RSL CHANGE CALCULATIONS

Tin City NO 2 (1960)

	December 29, 1960	March 19, 2009	RSL Change (m)	RSL Trend (mm/yr)
MLLW (m)	3.536	2.405	1.131	24.1

NOTES

- December 29 1960 data - TIME PERIOD: 17 August 1960 - 28 August 1960.
- March 19 2009 data - TIME PERIOD: September 2007 - September 2007 (1 month), TIDAL EPOCH: 1983 - 2001.
- Note: 1960 data is elevation above staff "zero" assumed here to be MLLW, but could be anything?

--------- UNALAKLEET – Norton Sound

Time span: 1977 - 2011 (34 years)

AVAILABLE DATA

	October 9, 1977	November 29, 2011
BM ID	MLLW (ft)	MLLW (m)
BM A (1977)	16.529	5.002

RSL CHANGE CALCULATIONS

BM A (1977)

	October 9, 1977	November 29, 2011	RSL Change (m)	RSL Trend (mm/yr)
MLLW (m)	5.038	5.002	1.131	24.1

NOTES

- October 9 1977 data - TIME PERIOD: 1 July 1977 - 9 October 1977.
- November 29 2011 data - TIME PERIOD: July 2011 - August 2011, TIDAL EPOCH: 1983 - 2001.
- Note: 1977 data is elevation above staff "zero" assumed here to be MLLW, but could be anything?

Appendix 2

Data Comparison of Tide Gauges in Nome, Sand Point, and Seldovia, Alaska

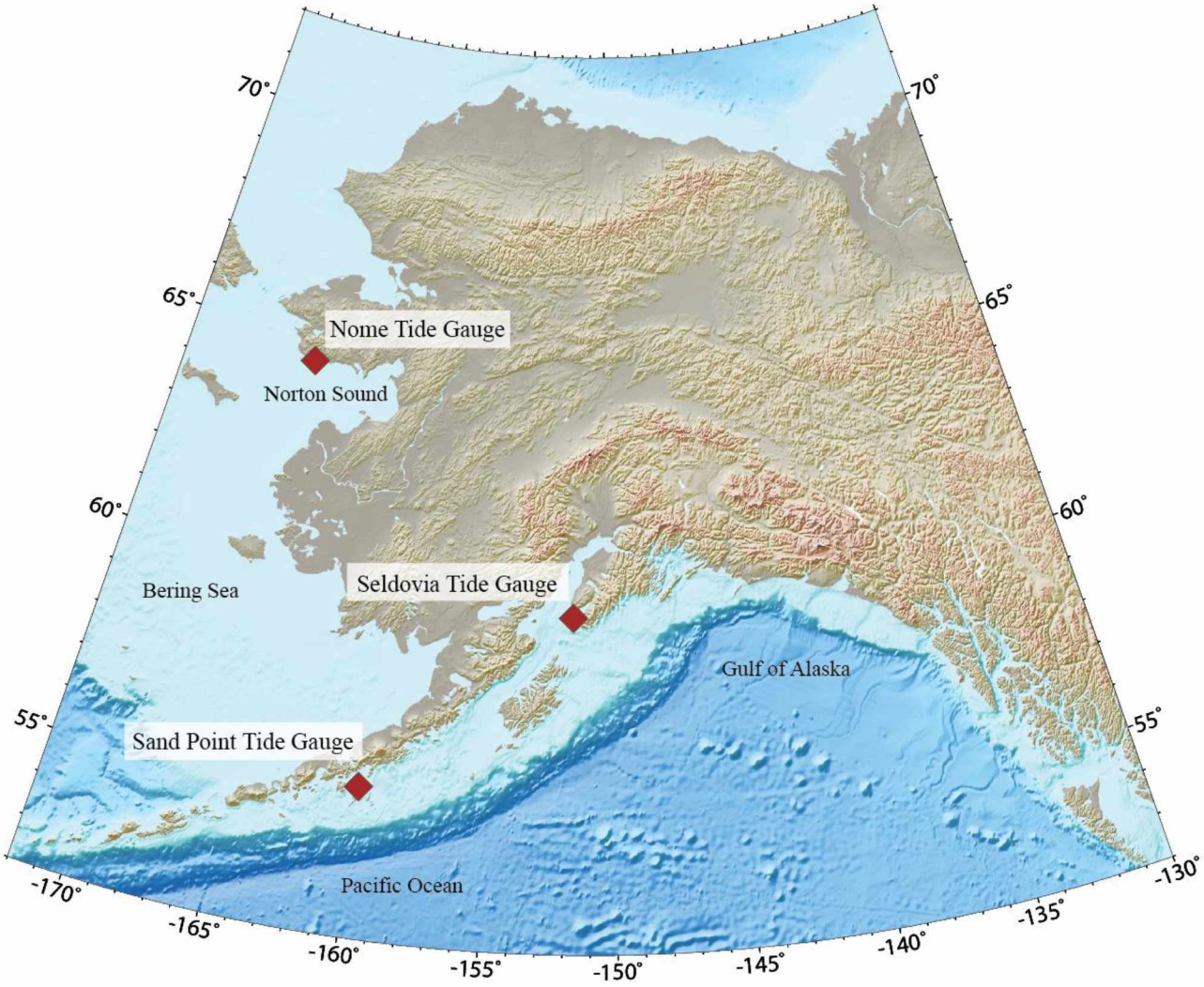

Figure A2.1. Location map of Alaska and the tide gauges used in this comparison

Introduction

Tide gauge data from two primary sources in Sand Point and Seldovia, Alaska (Figure A2.1) are compared in order to determine the most accurate selection of data for use in my master's thesis, *Relative Sea Level Change in Western Alaska as Constructed from Satellite Altimetry and Repeat GPS Measurements* (completed in the summer of 2015). Obtaining a published value for RSL trend or obtaining RSL trend data from the Nome tide gauge would be

ideal, but unfortunately NOAA has not done this at this time. Currently they require a 30 year data span before publishing a trend. Therefore, I need to determine a trend estimate and error bar that are as consistent as possible with the published results for Sand Point and Seldovia.

Nome has the only long-term tide gauge record in the defined study area and the record continuity is suboptimal, so satellite altimetry must be substituted to achieve greater coverage of the coastline for the calculation of RSL change in Western Alaska. The datum to be used in this thesis is a trend estimated from water level measurements relative to mean sea level (MSL) at a tide gauge surveyed to a fixed benchmark in Nome, Alaska. This estimate of relative sea level (RSL) change can be compared with satellite altimetry and GPS measurements in order to observe the accuracy of near shore satellite altimetry in Western Alaska.

A comparison of some of the available forms of data for the longer and more complete tide gauge records, located at Seldovia and Sand Point is presented here. The comparisons are also performed on the data from the Nome tide gauge in an effort to exhibit similar relationships as those seen between the more complete datasets of Sand Point and Seldovia.

Magnitudes of the RSL trend at each location differ greatly because each tide gauge is located in a different tectonic setting that affects the vertical motion of the ground surface, and the tide gauges are measuring water levels for three separate bodies of water subject to different oceanographic effects. The magnitudes of the trends between the three locations are not the focus of this report, that is concerned with the differences between available data for an individual tide gauge at one location.

DATA

All data were collected by the National Oceanic and Atmospheric Administration (NOAA) (Zervas et al., 2013; C.E. Zervas, personal communication, January 30, 2015) and obtained from the tide gauge at each location. Monthly MSL, monthly mean lower low water (MLLW), hourly MLLW, and monthly MSL signal processed data available as part of the NOAA online database of water level trends, and monthly MSL obtained from the online database of the Permanent Service for Mean Sea Level (PSMSL) were analyzed in order to obtain an average rate of RSL observed at each location.

These six datasets had differences based on the time interval of values, exclusion or inclusion of missing or removed data as NaN or -99999, water level datum or reference frame, and general formatting of date and time. All data were normalized about their individual means before use in any calculations or differences. All calculations and filtering were performed in MATLAB using the function "detrend" to find a linear least square fit to the data.

The difference between several datasets was calculated in order to observe the potential causes of variation in the trends. Often the datasets are of different lengths for a given time span because of the way a partial month of data was treated. If one set had more data than the other, the less complete record was augmented with NaN where a value was missing. Differences between datasets were taken over the time period of the shorter record and normalized water level measurements were differenced according to date, after automatically filtering measurements when possible by corresponding date. Automatic filters were occasionally ineffectual because of formatting or time interval differences; in these cases datasets were matched manually.

Permanent Service for Mean Sea Level (PSMSL)

http://www.psmsl.org/data/obtaining/

This source is considered because it is a commonly used global database for long-term sea level change information from tide gauges and bottom pressure recorders. Metric monthly mean water level data is provided by NOAA and maintained by PSMSL. PSMSL offers the raw metric data, but encourages use of their 'revised local reference' (RLR) for time series analysis. The RLR was established in order to reduce the monthly and annual means to a common datum defined as approximately 7000 mm below sea level (Holgate et al., 2012; Permanent Service PSMSL, 2015). This data is available for tide gauges at all three of the locations and diagrams of the specific RLR used at each tide gauge is included in the site specific sections that follow. A full explanation of PSMSL's data submission and processing requirements and procedures can be found at http://www.psmsl.org/data/obtaining/psmsl.hel.

NOAA Center for Operational Oceanographic Products and Services (CO-OPS)

http://co-ops.nos.noaa.gov/stations.html?type=Water+Levels

Five types of datasets derived or obtained from NOAA's website are used during this comparison. With raw data NOAA includes the following statement; "These raw data have not been subjected to the National Ocean Service's (NOS) quality control or quality assurance procedures and do not meet the criteria and standards of official NOS data. They are released for limited public use as preliminary data to be used only with appropriate caution." (Zervas et al., 2013). The data are collected in six minute intervals and NOS does perform preliminary processing and filtering that "consists of manually or automated checks of the data, making relevant comparisons with backup sensors, tide staffs, nearby stations, or predicted tides, and scanning any automated instrument and data acquisition reports. [...] NOS fills small gaps up to 3 to 4 hours using least-squares curve fits of the 6-minute data. Longer gaps in data up to 3-days are filled in a hierarchical sense depending on location and availability of source data. If data from backup sensors are not available, the gaps are inferred using data from nearby stations or predicted tides. Gaps are left in the data if source data to fill them is insufficient." (NOAA/NOS, 2003). The datum used for referencing the tide gauge measurements is an arbitrarily established zero point that is set when the tide gauge is installed and is referred to as station datum (T. Ehret, personal communication, April 14, 2015). To generate data for use with a different reference datum NOS uses a tabulation process described in NOAA/NOS (2003). The datum used to reference the data should not matter for trend calculations because it all originates with the same dataset and is just being shifted from that arbitrary zero point in order to reference it to a different datum. There is only one set of data for each tide gauge, but there are differences in what the data is in reference to. When MLLW and MSL are used in this study it is to identify the datum associated with a particular dataset, but they should both result in the same trend if the tabulation process is accurate. Once the data is tabulated it is verified both visually and numerically by a senior analyst at NOS (NOAA/NOS, 2003).

Hourly (MLLW) – Verified hourly data relative to MLLW are used to calculate the sea level trend, but additionally to calculate mean monthly sea level values independently from mean monthly sea level data provided by NOAA CO-OPS. Hourly data is determined by taking "every tenth 6-minute interval value" (NOAA/NOS, 2003). The observed water level data is then tabulated to reference it to the MLLW datum. There are values for "Hourly 1" and "Hourly 2", which differ only in temporal scale used. "Hourly 1" data are hourly values relative to MLLW

expressed in meters, as obtained from personal communication with L. Nathan Epps (personal communication, February 5, 2015) at the Alaska Division of Geological and Geophysical Survey (ADGGS). The trend for hourly MLLW is compared to the trend calculated using monthly MLLW values that were calculated from the hourly MLLW values and the trend calculated from the NOAA CO-OPS monthly MLLW values to illustrate the effects these differences in datasets have on the overall trend. These data are available for tide gauges at all three of the locations, but was only used for the tide gauge at Nome. Hourly mean data can only be downloaded one month at a time and both Seldovia and Sand Point could be analyzed further, but would require significant manual effort to download and filter the dataset over their much longer tidal records; this dataset was originally introduced because of its use by other agencies.

Monthly (Calculated) – Monthly values relative to MLLW were calculated by myself from the hourly MLLW data previously described. These are used to compare to monthly MSL and monthly MLLW values that are provided by NOAA CO-OPS, to check for any differences in calculating monthly means. These monthly means are calculated by averaging the hourly means over a month. No seasonal or interannual trends are removed. When a month is incomplete the mean for the available values is calculated, which is most likely the primary contributing source to differences between datasets, as no constraint for values per month is required, yet this is a factor considered in both NOAA and PSMSL means. These data are only calculated for the Nome tide gauge.

Monthly (MLLW) – Monthly values relative to MLLW are also downloaded directly from the NOAA CO-OPS water level website and have not had any interannual or seasonal signals removed. These data are available for tide gauges at all three of the locations, but are only used in the Nome trend comparisons.

Monthly (MSL) – Monthly values relative to MSL are downloaded directly from the NOAA CO-OPS water level website for each station and have not had any interannual or seasonal signals removed. These data are available for tide gauges at all three of the locations and are used in trend comparisons at each one.

Monthly (MSL Trend) – Monthly values relative to MSL that result from NOAA calculations of MSL trends are downloaded. These values have had interannual and seasonal signals removed simultaneously with calculation of the trend. The tidal harmonics predicted for each station can be found on the water level website and range from short temporal estimates of shallow water constituents to longer estimates of annual variation. Monthly MSL values are used to check that trends calculated here are similar to those calculated by NOAA. Personal communication with NOAA Oceanographer Dr. Chris E. Zervas (January 30, 2015) confirms that a linear least squares trend of these values should very closely approximate the trends published by NOAA. These data are available for tide gauges at Seldovia and Sand Point, but not for the Nome tide gauge. NOAA published RSL trends are also included for these two locations and an unpublished value for Nome was provided by Dr. Zervas (personal communication, January 30, 2015). Further details on the derivation of this value will be outlined later in the Nome site specific section following.

Summary

Each location is affected by different oceanic and tectonic processes, but the length of the record is the most significant factor in error and variability (C.E. Zervas, personal communication, January 30, 2015). For this reason the Nome tide gauge has the greatest amount of uncertainty. Some distinct differences between datasets can be observed (Table A2.1).

Table A2.1. Table of data and trend results from this study. Location of data indicates from which website the data was obtained, "calculated in this study" refers to monthly means that were calculated from the NOAA hourly values. Type of data defines the interval and datum to which the water level measurements are referenced. All trends are calculated here in this study, with the exception of the published trends that are calculated and provided by NOAA. Published error refers to the 95% confidence levels for the published data that NOAA provides.

Location of Data	Type of data	Trend (mm/yr)		
		Nome	Sand Point	Seldovia
PSMSL	MSL - Monthly	0.91	0.84	-9.65
NOAA	MSL - Monthly	0.5	0.56	-10.41
NOAA	MLLW - Monthly	1.32	0.44	-10.79
NOAA	MSL Trend - Monthly	NA	0.68	-10.36
NOAA	MLLW - Hourly 1	0.02	NA	NA
Calculated in this study	MLLW - Monthly 1	0.37	NA	NA
NOAA	MLLW - Hourly 2	0.65	NA	NA
Calculated in this study	MLLW - Monthly 2	0.52	NA	NA
NOAA	MSL - Published	-0.48*	0.38	-10.47
NOAA	MSL - Published Error	+/- 4.24*	+/- 0.97	+/- 0.85

* Values calculated using same method as published values by Dr. Zervas (personal communication, January 30, 2015) at NOAA, but were shared via personal communication because the error is too high for NOAA's publishing standards.

All three locations have large discrepancies between data downloaded from PSMSL and that from NOAA. The PSMSL dataset was submitted by NOAA, but is not updated when NOAA makes adjustments or corrects for discovered errors in the datasets available on their website (C.E. Zervas, personal communication, January 30, 2015). There is a known adjustment that was made by NOAA for the Seldovia tide gauge because of a stability issue with the benchmark that

the tide gauge was referenced to that in most likelihood did not get corrected in the data at PSMSL. Differences of these datasets are available for all three tide gauges in following sections. Seldovia and Sand Point do have longer more consistent records that show less variability between datasets as expected from their record length.

There will of course be a difference in trend between MSL and MLLW as the trend of MLLW could reflect longer temporal scale oscillations or more indicative of spatial variability such as local water storage and distribution. The difference between MSL and MLLW was minor but observable for Seldovia and Sand Point, but quite significant at the Nome tide gauge, potentially indicating a more dynamically changing environment. There are also small differences between the published MSL trend and the trend that I calculated. This must be because of numerical differences between my trend calculation and that of NOAA, as both trends are calculated from the same dataset.

The minimum difference between datasets for Seldovia and Sand Point are between the calculations I performed on the raw MSL and the published MSL trend data available on NOAA's website. The published trends in Table 2.1 and their associated errors are calculated by removing the seasonal and interannual signals and calculating the 95% confidence bounds. These products for Seldovia and Sand Point are publically available, but the Nome values were obtained through personal communication with Dr. Zervas (January 30, 2015) who recently executed the calculations. Because of the large error associated with this MSL trend at Nome these values will not be made publically available on the website until there is a longer record that can reduce the uncertainty.

Because of the sensitivity to gaps and potential errors in the Nome data I did a comparison of trends where I used the whole Nome raw hourly dataset ("Hourly 1" and "Calculated 1") and also a truncated set of the raw hourly dataset ("Hourly 2" and "Calculated 2") that removed the first 11 months and the last 11 months. These two versions of hourly calculations exhibit different trends, and the truncated dataset begins to more closely resemble that of the raw MSL trend. There is also better coherence between the hourly trend and the mean monthly trend that is calculated from the hourly trend, implying that the data that was removed in "Hourly 2" may have been incorrectly skewing the calculations when using "Hourly 1". The monthly MLLW data provided by NOAA has an extraordinarily high trend when compared to data of different time intervals and datums, so this is assumed to have tabulation or calculation errors.

These comparisons lead to the conclusion that for the purpose of use in the aforementioned thesis the raw MSL data will be used to calculate a trend, but mention of the NOAA calculated value will also be included to indicate the magnitude of variance and error involved with the water level data available at the Nome tide gauge.

--------- SELDOVIA – Gulf of Alaska

Seldovia is located on the Kenai Peninsula on the south shore of Kachemak Bay (Figure A2.2) opposite of Homer, Alaska. Kachemak Bay opens to Cook Inlet in the east which in turn flows into the Gulf of Alaska. The tide gauge is located at 59.440° N, -151.720° E and has recorded water levels from 1964 to 2012 with minimal gaps in the time series. The Seldovia tide gauge is identified under the identification number 1070 in the PSMSL database and 9455500 in the NOAA database (Holgate et al., 2013; Permanent Service for Mean Sea Level (PSMSL), 2015).

Tectonic vertical motion in Seldovia includes uplift from glacial isostatic adjustment as a result of ice loss from the little ice age, subduction effects of the Pacific Plate colliding with the North American Plate, and uplift due to post seismic deformation (Freymueller et al., 2000 and Suito and Freymueller, 2009). These processes result in considerable uplift in Seldovia of 7.47 +/- 0.30 mm/yr as measured by GPS and thus RSL change at the tide gauge is expected to reflect magnitudes akin to this tectonic motion (DeGrandpre et al., 2015).

Data downloaded from PSMSL defined referenced to RLR (1972) is 13.014 m below benchmark BM 19 1967 (Figure A2.3). The reference benchmark changed on "24 November 2011 using information from the NOAA website" Holgate et al., 2013; Permanent Service for Mean Sea Level (PSMSL), 2015. Former Primary benchmark BM 13 measured 10.458 m relative to the tide gauge originally is NO 13 1964 with a value of 10.438 m in the 1999 report and 10.432 m in the 2011 report. The Primary benchmark is now BM 19 1967 and is measured as 11.272 m relative to the tide gauge. Holgate et al., 2013; Permanent Service for Mean Sea Level (PSMSL), 2015.

Figure A2.2. Location map of the Seldovia tide gauge on the Kenai Peninsula.

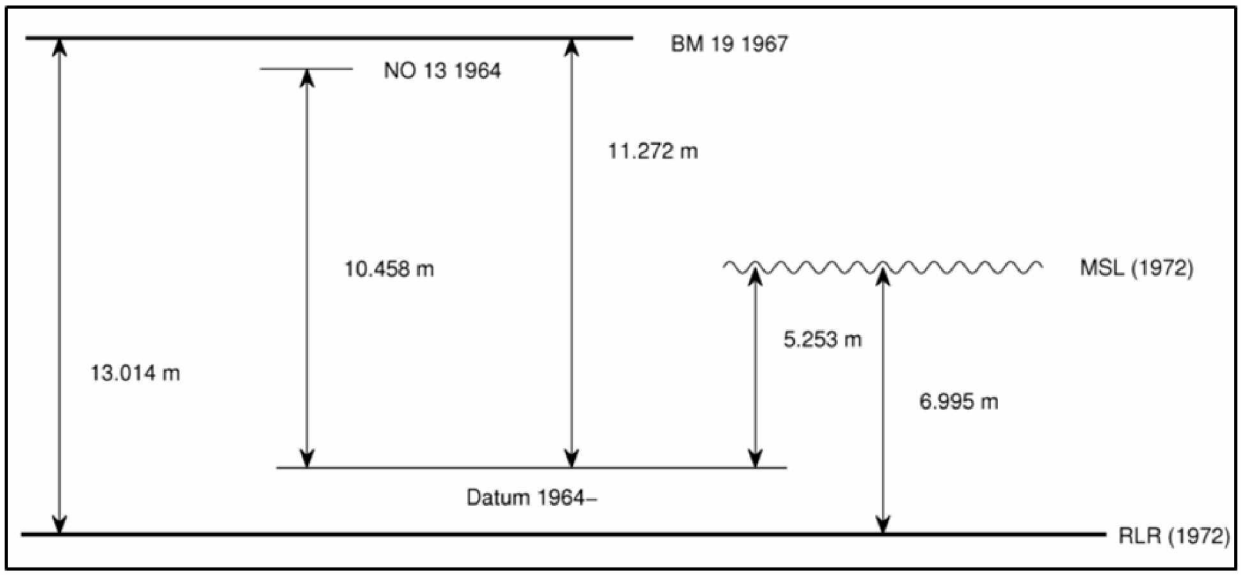

Figure A2.3. Diagram of the RLR defined for the tide gauge in Seldovia. Add 1.742m to data values to refer to RLR (1972). RLR (1972) is 13.014 m below BM 19 1967 (Holgate et al., 2013; Permanent Service for Mean Sea Level (PSMSL), 2015).

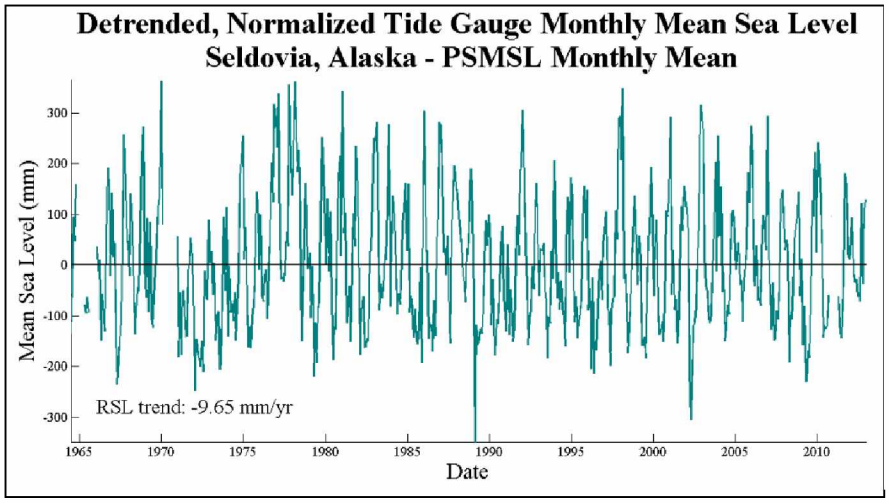

Figure A2.4. Plot of monthly MSL data from 1964 to 2012 exhibiting a trend of -9.65 mm/yr made available by PSMSL. This data is submitted by NOAA, so it should be consistent with NOAA values.

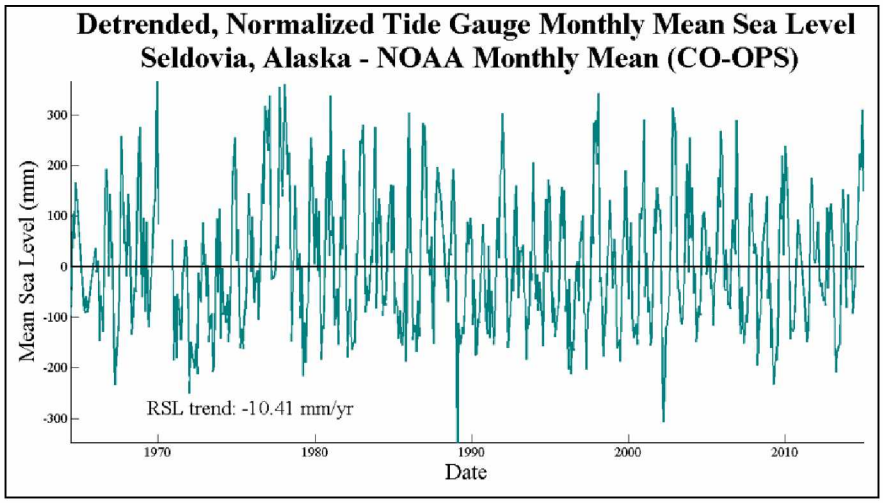

Figure A2.5. Plot of monthly MSL data from 1964 to 2013 exhibiting a trend of -10.41 mm/yr, made available by NOAA. This data is submitted to PSMSL, so it should be consistent with those values in Figure A2.3. There is a known adjustment that NOAA made to this data due to benchmark instability.

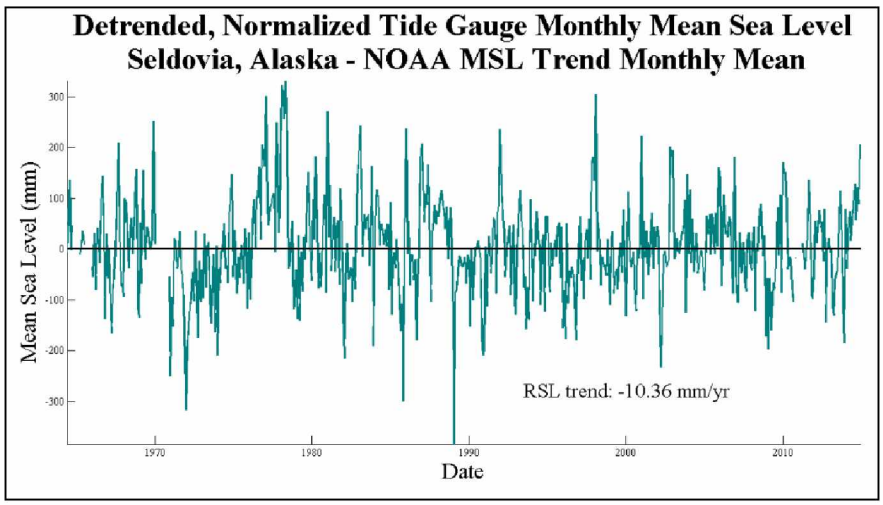

Figure A2.6. Plot of monthly MSL data from 1964 to 2013 exhibiting a trend of -10.36 mm/yr with seasonal and interannual signals removed by NOAA. This data is made available as sea level trend data. If the seasonal and interannual signals were to be added back in to this data it would be the same as Figure A2.4.

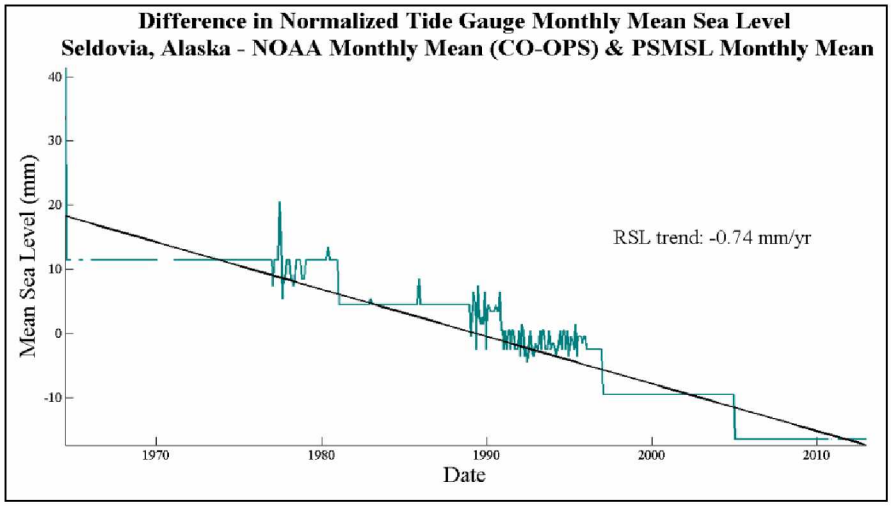

Figure A2.7. Plot of the difference between the NOAA and PSMSL monthly MSL datasets. These two sets should be identical as this is the data that NOAA submitted to PSMSL, but there are obvious differences that look like a combination of factors. The step like appearance is most likely the effect of the corrections to the benchmark error that was found and fixed in the NOAA dataset, but not the PSMSL one.

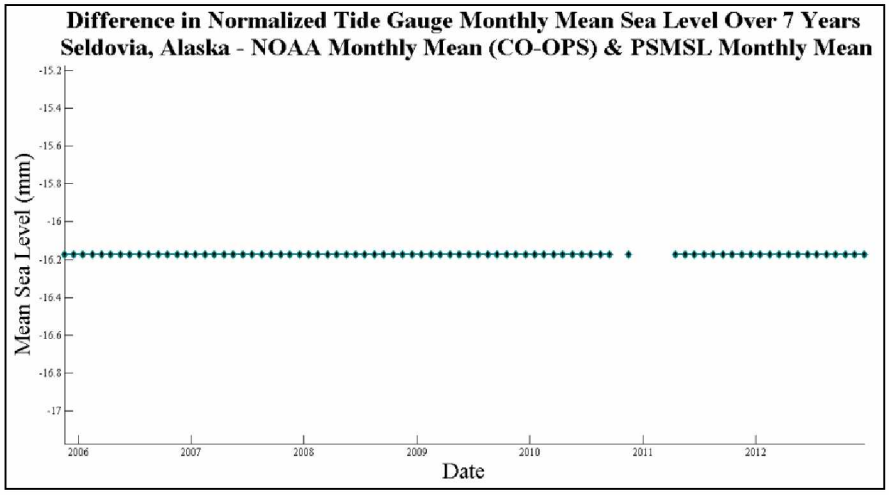

Figure A2.8. Plot of the difference between the NOAA and PSMSL monthly MSL datasets during the last 7 years. This shows the overall offset that had accumulated by the end of this time period that is likely due to the benchmark corrections that NOAA performed on their data, but that has not been corrected in the PSMSL dataset.

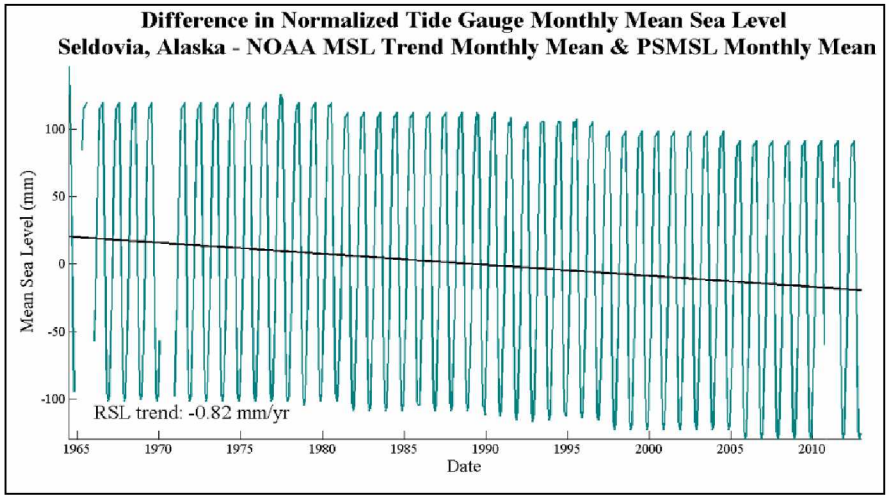

Figure A2.9. Plot of the difference between the NOAA published monthly MSL trend and PSMSL monthly MSL datasets. The NOAA data has had the seasonal and interannual signals removed while the PSMSL has not. This plot shows those signals that were removed from the NOAA unaltered data in order for NOAA to calculate the published MSL trend of -10.47 mm/yr.

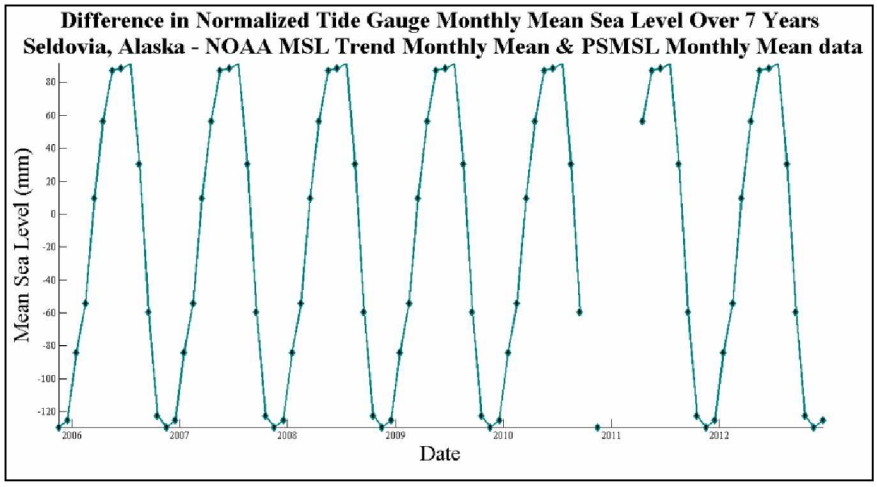

Figure A2.10. Plot of the difference between the NOAA published monthly MSL trend and PSMSL monthly MSL datasets during the last 7 years. A consistent signal is observed to have been removed from the NOAA published monthly MSL trend dataset.

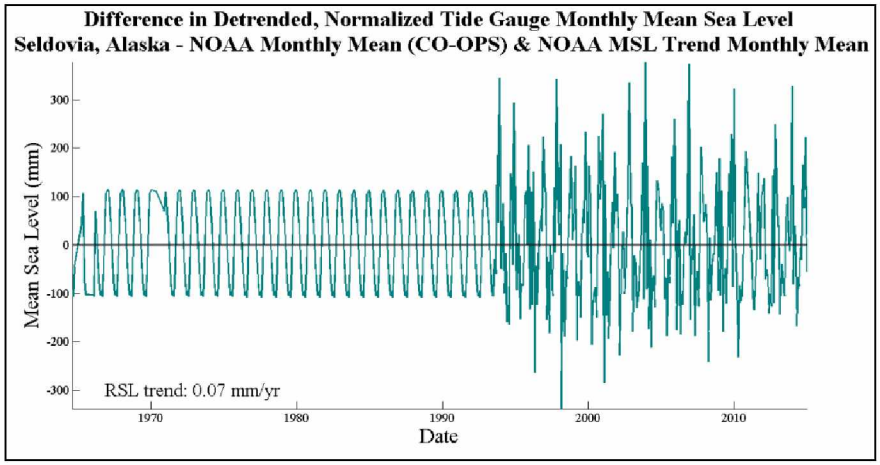

Figure A2.11. Plot of the difference between the NOAA published monthly MSL trend and unaltered NOAA monthly MSL datasets. The annual and seasonal signal that was removed is visible in the first half of the dataset, but there seems to be an error in the subtraction of these datasets for the second half. I have been unable to resolve the cause of this discrepancy.

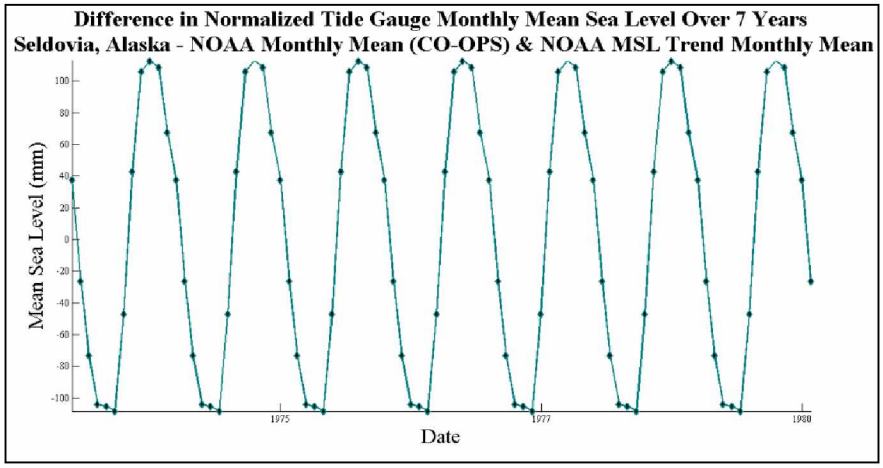

Figure A2.12. Plot of the difference between the NOAA monthly MSL trend and unaltered NOAA monthly MSL datasets during 1973 - 1980. A consistent signal is observed to have been removed from the NOAA published monthly MSL trend dataset.

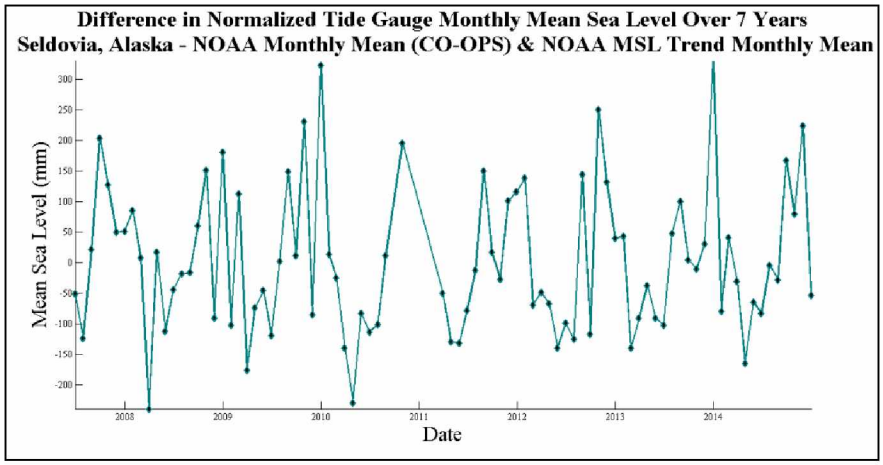

Figure A2.13. Plot of the difference between the NOAA monthly MSL trend and PSMSL monthly MSL datasets during the last 7 years. A consistent signal is observed to have been removed from the NOAA published monthly MSL trend dataset. Because this trend is not being compared to other, shorter datasets the full record from 1964 – 2014 was used.

--------- SAND POINT – Pacific Ocean

Sand Point is located on the northwest coast of Popof Island which is part of the Shumagin Islands offshore of the Alaska Peninsula (Figure A2.14) on the northern extent of the Pacific Ocean near the entrance to the Bering Sea. The tide gauge is located at 55.337° N, -160.502° E and has recorded water levels from 1985 to 2013 with minimal gaps in the time series. The Sand Point tide gauge is identified by the identification number 1634 in the PSMSL database and 9459450 in the NOAA database (Holgate et al., 2013; Permanent Service for Mean Sea Level (PSMSL), 2015).

Tectonic vertical motion in Sand Point is driven by complex subduction dynamics of the Pacific Plate colliding with the Bering Plate. The Shumagin Islands region is a complicated subduction setting described by Fournier and Freymueller (2007) as a transition zone (~ 30% locked) from an almost fully (~ 90%) locked subduction zone in the east to an unlocked subduction zone that is freely slipping in the west. GPS data shows vertical velocities of -1.09 +/- 0.30 mm/yr at Sand Point and the tide gauge is expected to be of similar magnitude (DeGrandpre et al., 2015).

RLR for data downloaded from PSMSL defined as RLR (1986) is 13.894 m below benchmark 9450 R 1991 (Figure A2.15). The reference benchmark changed on 20 December 2011 using information from the NOAA website. Former Primary benchmark 5 1953 is 14.886 m relative to tide gauge datum was found to not be in the 2001 and 2003 NOAA reports. The primary benchmark as of 20 December 2011 is 9450 R 1991 and is 13.894 m above tide gauge datum (Holgate et al., 2013; Permanent Service for Mean Sea Level (PSMSL), 2015).

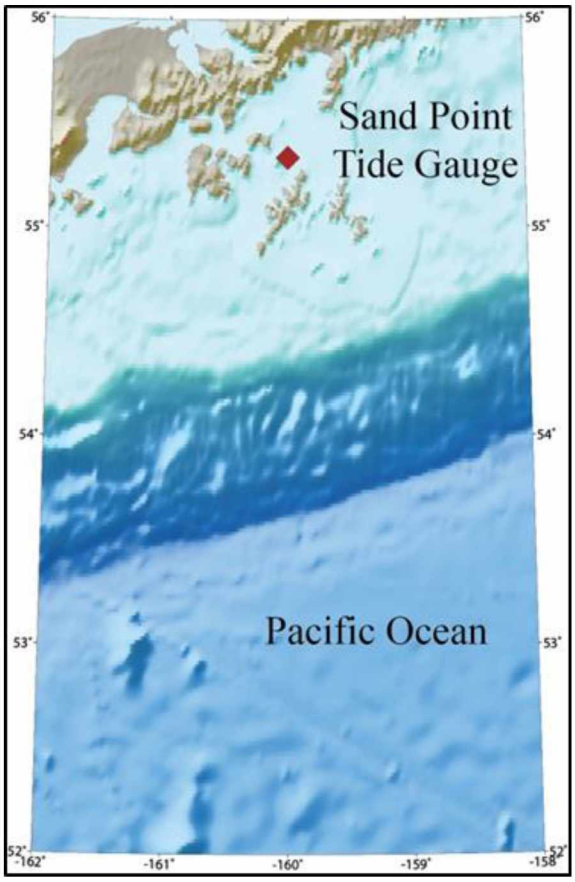

Figure A2.14. Map of Sand Point tide gauge. This tide gauge is located on Popof Island in the Shumagin Islands.

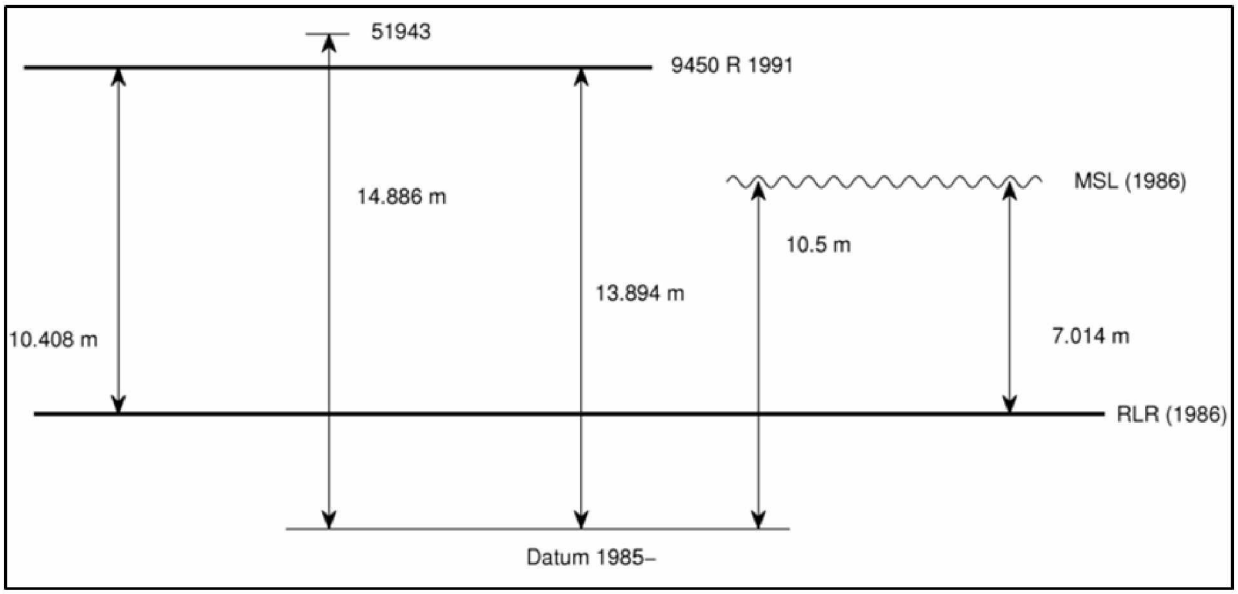

Figure A2.15. Diagram of the RLR defined for the tide gauge in Sand Point (Holgate et al., 2013; Permanent Service for Mean Sea Level (PSMSL), 2015).

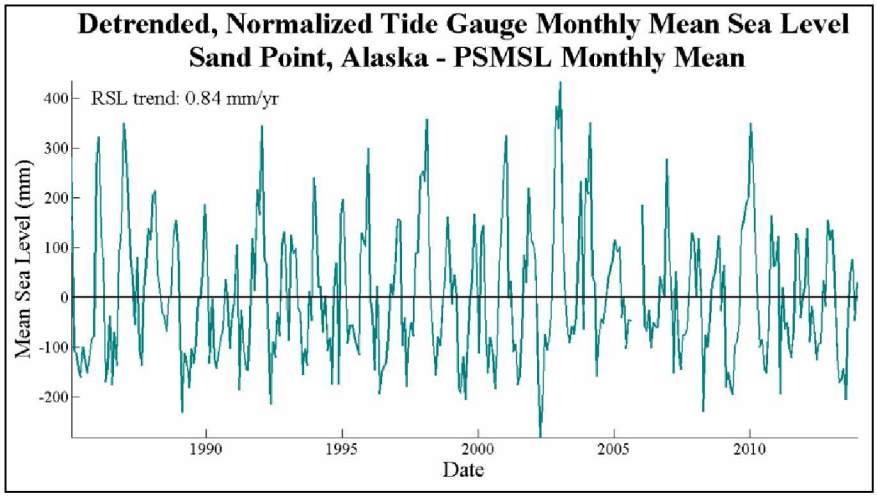

Figure A2.16. Plot of monthly MSL data from 1985 to 2013 exhibiting a trend of 0.84 mm/yr made available by PSMSL. This data is submitted by NOAA, so it should be consistent with NOAA values.

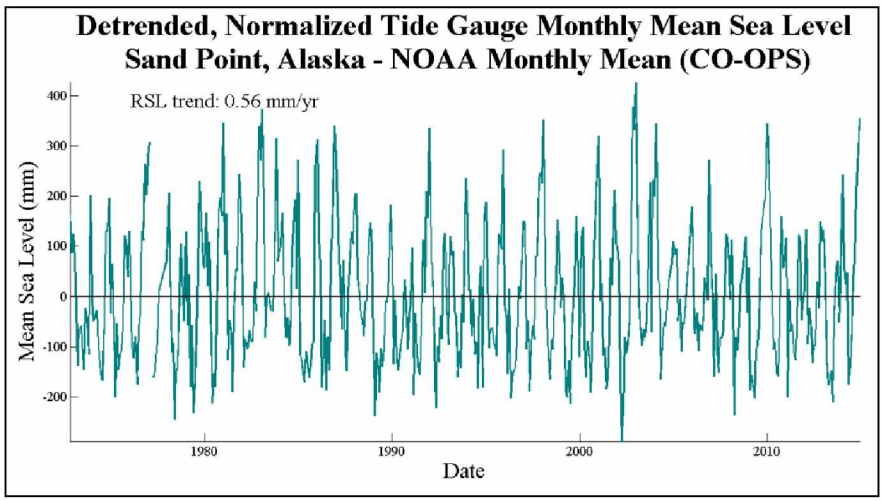

Figure A2.17. Plot of monthly MSL data from 1972 to 2014 exhibiting a trend of 0.56 mm/yr made available by NOAA. This data is submitted to PSMSL, so it should be consistent with those values in Figure A2.15.

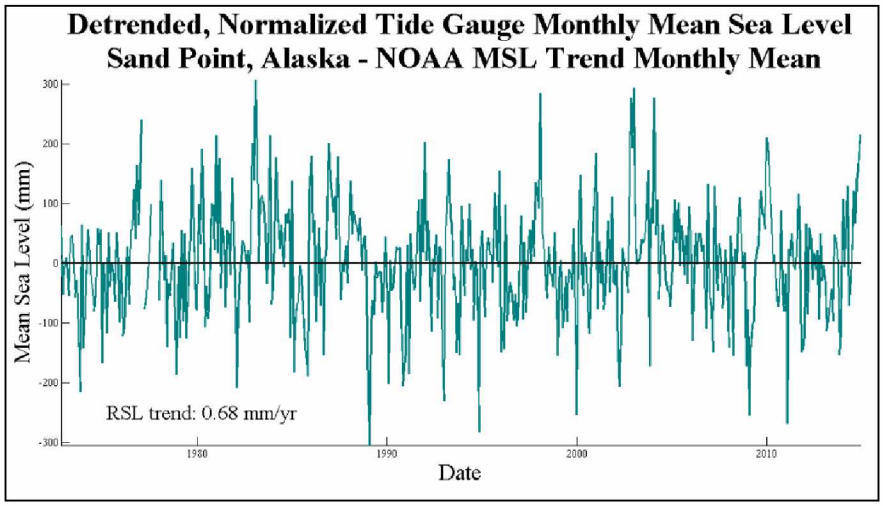

Figure A2.18. Plot of monthly MSL data from 1972 to 2014 exhibiting a trend of 0.68 mm/yr with seasonal and interannual signals removed by NOAA. This product is made available as sea level trend data. If the seasonal and interannual signals were to be added back in to this data it would be the same as Figure A2.16.

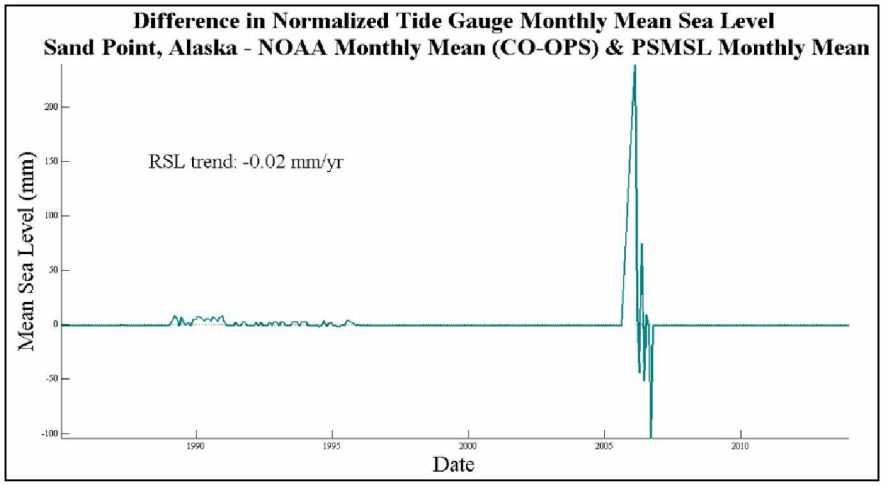

Figure A2.19. Plot of the difference between the NOAA and PSMSL monthly MSL datasets. These two sets should be identical as this is the data that NOAA submitted to PSMSL, but there are obvious differences that look like a combination of factors. The noise in the early 90s is very different from some sort of signal offset or error in 2005-2006.

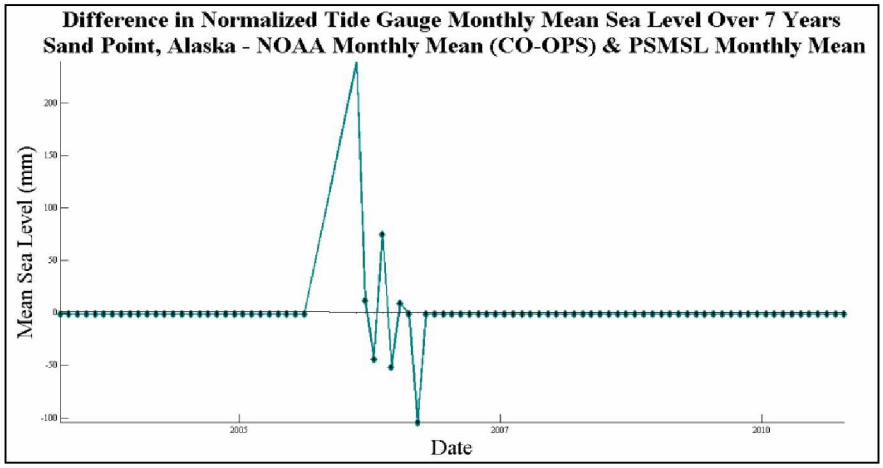

Figure A2.20. Plot of the difference between the NOAA and PSMSL monthly MSL datasets during the last 7 years. This shows the signal error that occurred in 2005 – 2006.

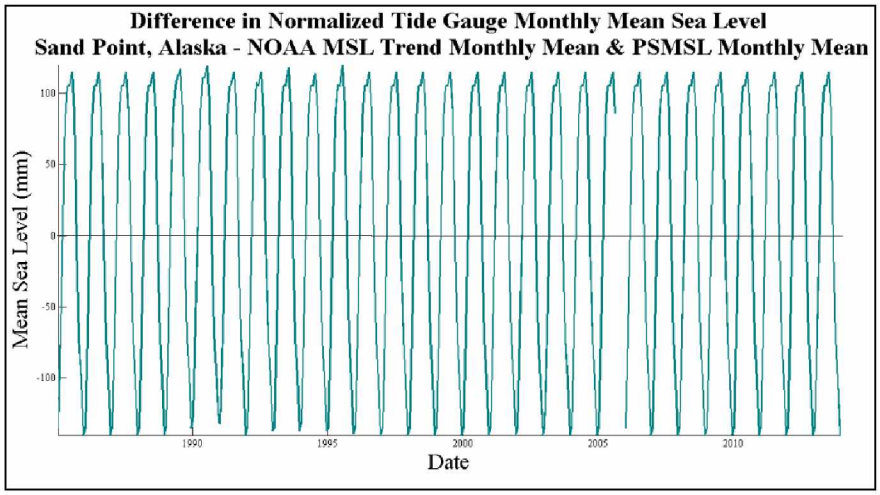

Figure A2.21. Plot of the difference between the NOAA published monthly MSL trend and PSMSL monthly MSL datasets. The NOAA data has had the seasonal and interannual signals removed while the PSMSL has not. This plot shows those signals that were removed from the NOAA unaltered data in order for NOAA to calculate the published MSL trend of 0.38 mm/yr

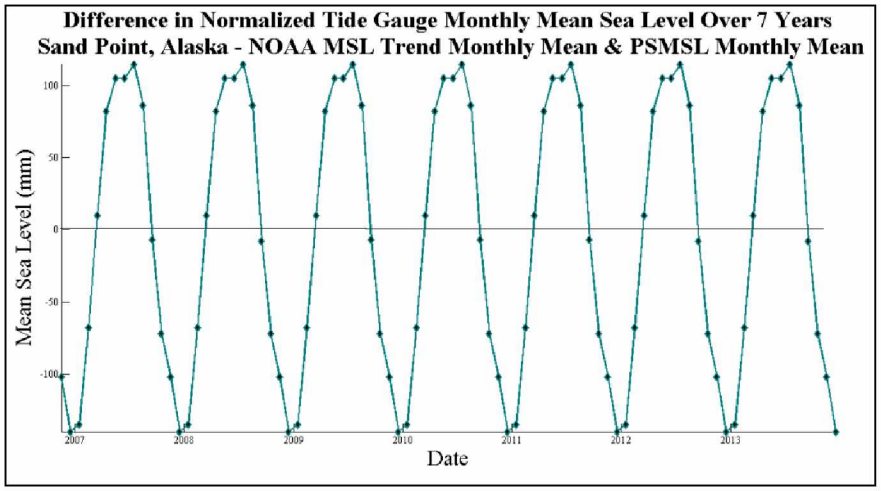

Figure A2.22. Plot of the difference between the NOAA published monthly MSL trend and PSMSL monthly MSL datasets during the last 7 years. A consistent signal is observed to have been removed from the NOAA published monthly MSL trend dataset.

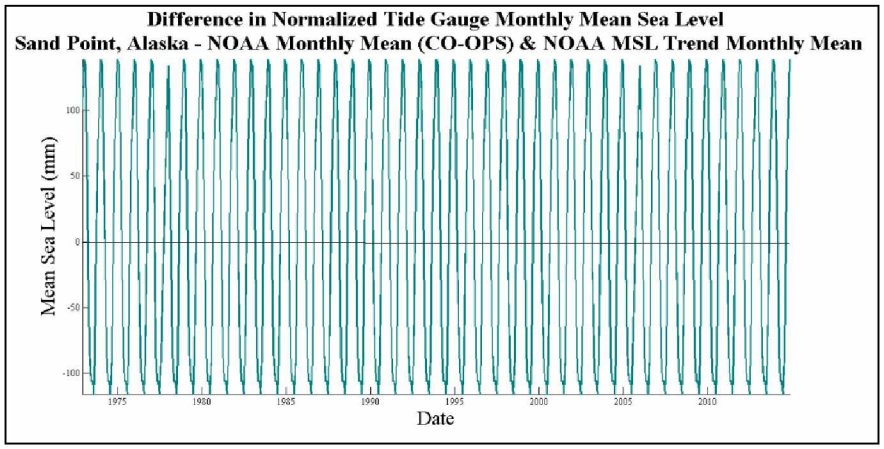

Figure A2.23. Plot of the difference between the NOAA published monthly MSL trend and unaltered NOAA monthly MSL datasets during 1973 - 1980. A consistent signal is observed to have been removed from the NOAA published monthly MSL trend dataset.

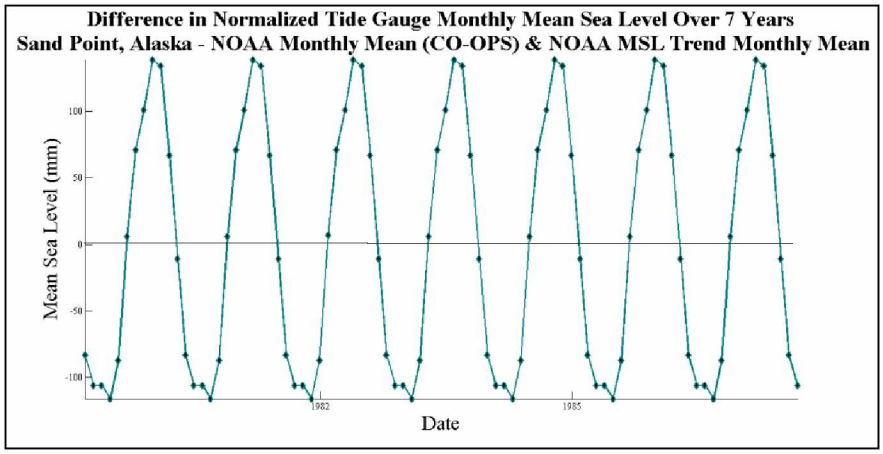

Figure A2.24. Plot of the difference between the NOAA published monthly MSL trend and unaltered NOAA monthly MSL datasets during 1980 - 1987. A consistent signal is observed to have been removed from the NOAA published monthly MSL trend dataset. This looks like the negative of Figure A2.21. because of the order of differencing.

--------- NOME – Norton Sound

Nome is located on the southern coast of the Seward Peninsula (Figure A2.25) in northwest Alaska. Nome is on the northern shore of Norton Sound which opens east into the Bering Sea. The tide gauge is located at 64.5° N, -165.43° E and has recorded water levels from 1992 to 2013 with multiple gaps in the time series. The Nome tide gauge is identified by the identification number 1800 in the PSMSL database and 9468756 in the NOAA database and is described as a pneumatic bubbler with a Paroscientific pressure system (Holgate et al., 2013; Permanent Service for Mean Sea Level (PSMSL), 2015).

Tectonic vertical motion in Nome and the Seward Peninsula is subsidence as a result of glacial isostatic adjustment of a forebulge produced by the Laurentide and Cordillran ice sheets during the last glacial maximum (DeGrandpre et al., 2015). GPS vertical velocities calculated for Nome are -1.73 +/- 0.23 mm/yr (DeGrandpre et al., 2015).

Data downloaded from PSMSL defined as RLR (1993) (Figure A2.26) is 11.2 m below the primary benchmark 946 8756 SHEET PILE C and 7.036 m below the tide gauge water level measurements. (Holgate et al., 2013; Permanent Service for Mean Sea Level (PSMSL), 2015; Zervas et al., 2013).

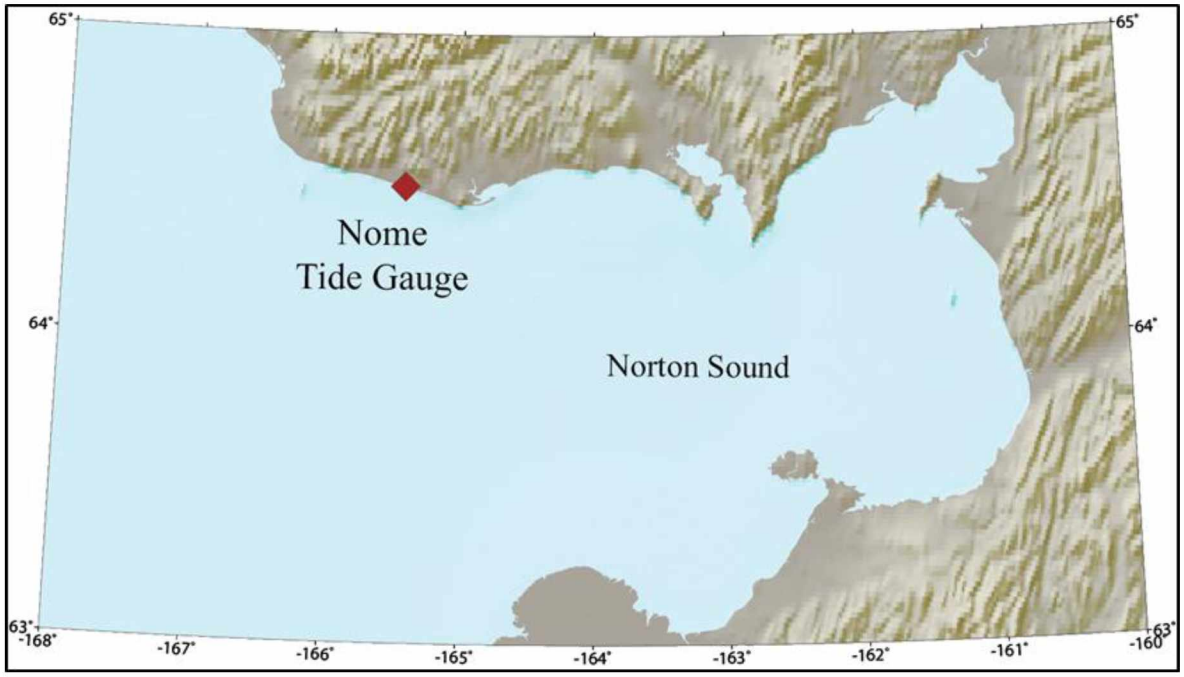

Figure A2.25. Location map of the Nome tide gauge on the southern shore of the Seward Peninsula.

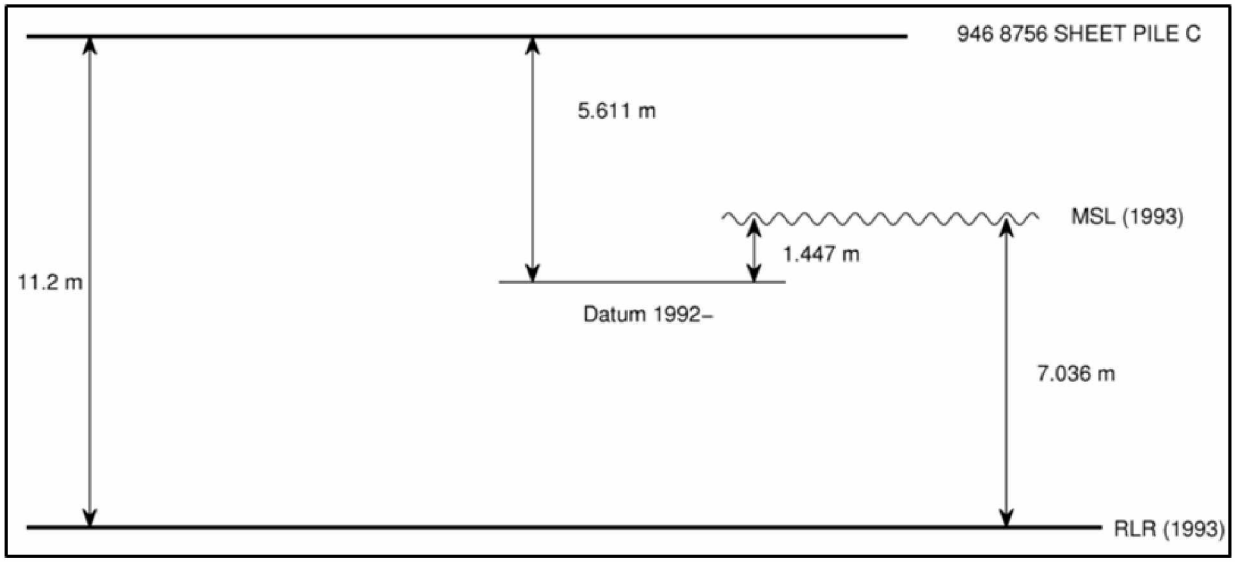

Figure A2.26. Diagram of the RLR defined for the tide gauge in Nome. Add 5.589 m to data values to refer to RLR (1993). RLR (1993) is 11.2 m below BM 946 8756 SHEET PILE C.

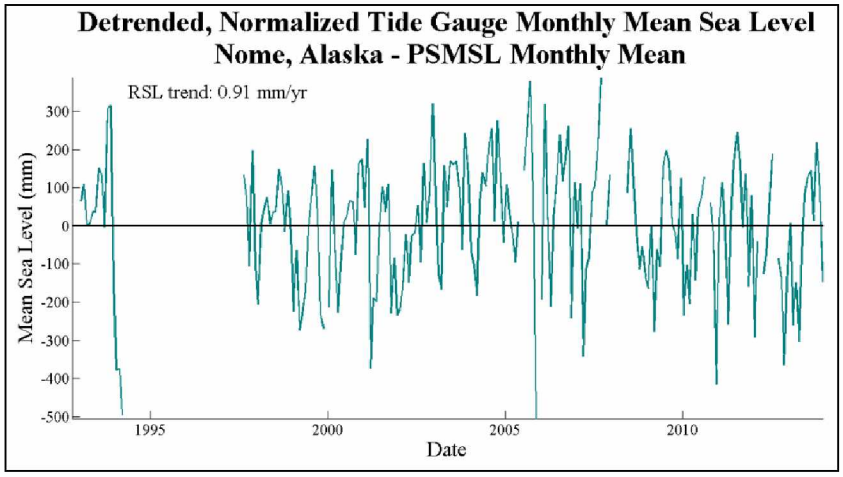

Figure A2.27. Plot of monthly MSL data from November 1992 to January 2014 exhibiting a trend of 0.91 mm/yr made available by PSMSL. These data are submitted by NOAA, so they should be consistent with NOAA values.

Figure A2.28. Plot of monthly MSL data from November 1992 to January 2014 exhibiting a trend of 0.50 mm/yr made available by NOAA. This data is submitted to PSMSL, so it should be consistent with those values in Figure A2.26.

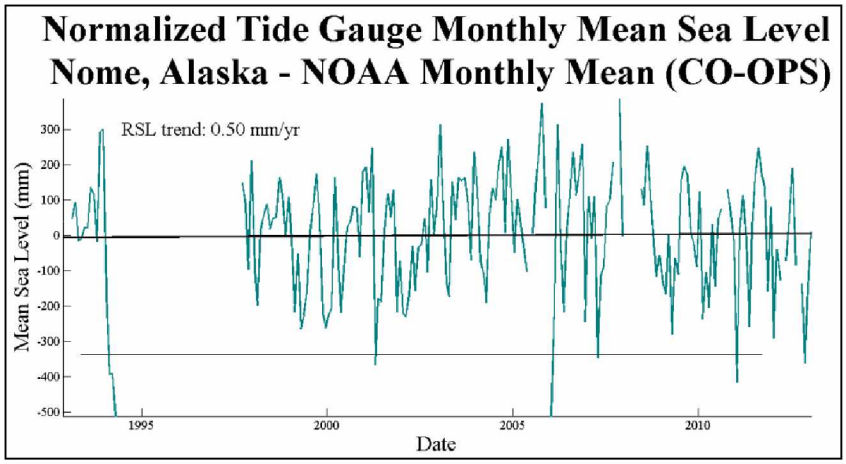

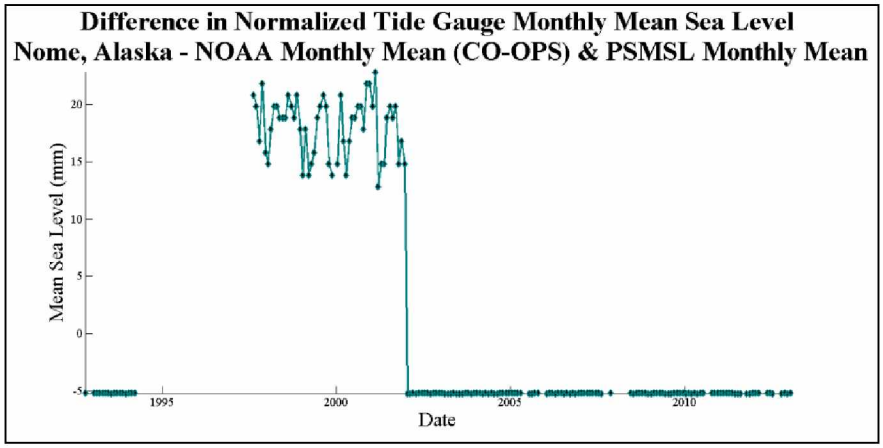

Figure A2.29. Plot of the difference between the NOAA and PSMSL monthly MSL datasets. These two sets should be identical as this is the data that NOAA submitted to PSMSL, but there are obvious difference that look like a combination of factors. There is a constant offset from zero and a difference in signals between 09/1997 and 01/2002, though the differences are quite small if scale is considered.

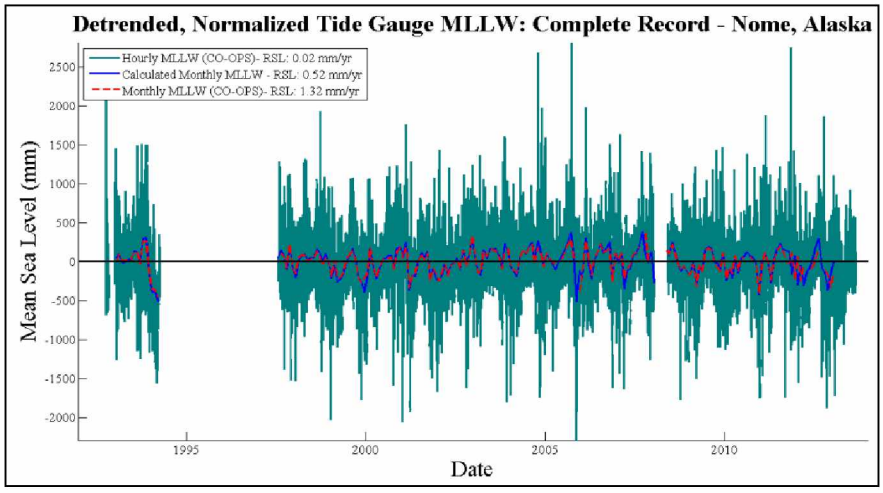

Figure A2.30. Plot of hourly MLLW data from 1992 to 2014 exhibiting a trend of 0.02 mm/yr made available by NOAA. Calculated monthly values are averages calculated from the hourly data and monthly MLLW that NOAA calculated is included as a comparison. These three have wildly different trends, with my calculated value most resembling the trend of MSL in Figure A2.27.

Figure A2.31. Plot of the monthly MLLW made available by NOAA compared with that calculated by taking the average of hourly values over each month. The trends are significantly different

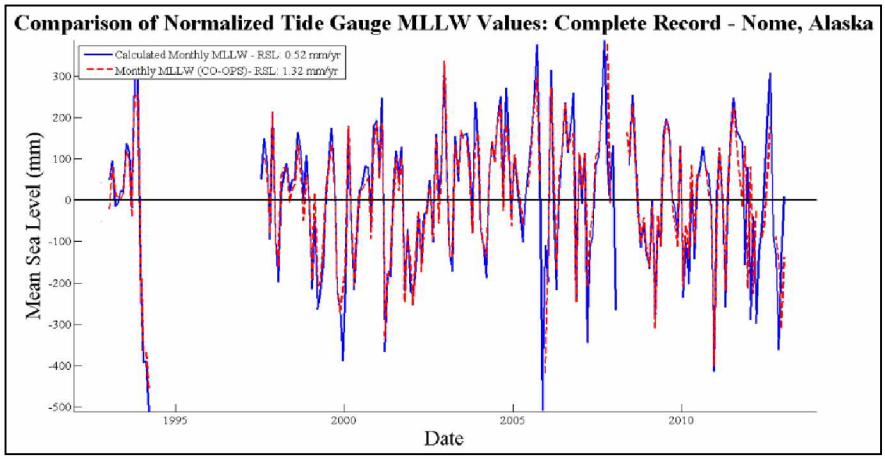

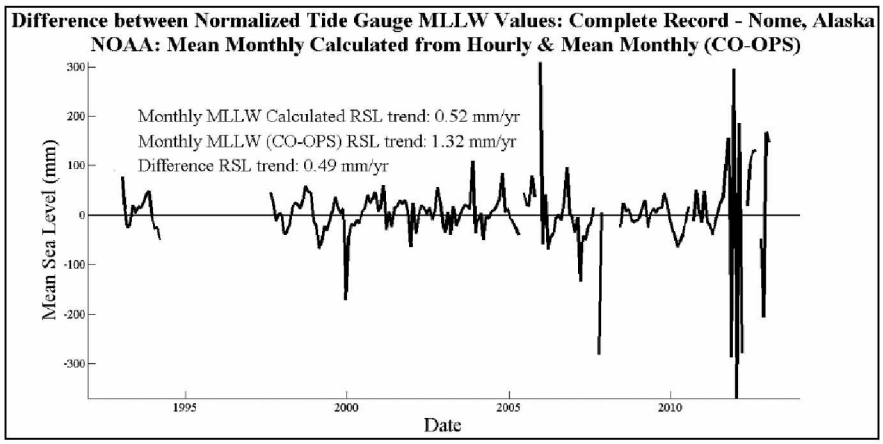

Figure A2.32. Plot of the difference between MLLW datasets made available by NOAA and the monthly average calculated from hourly data made available by NOAA. There appears to be almost a yearly cycle in this signal that could be due to the way the monthly average was calculated and the date it was assigned.

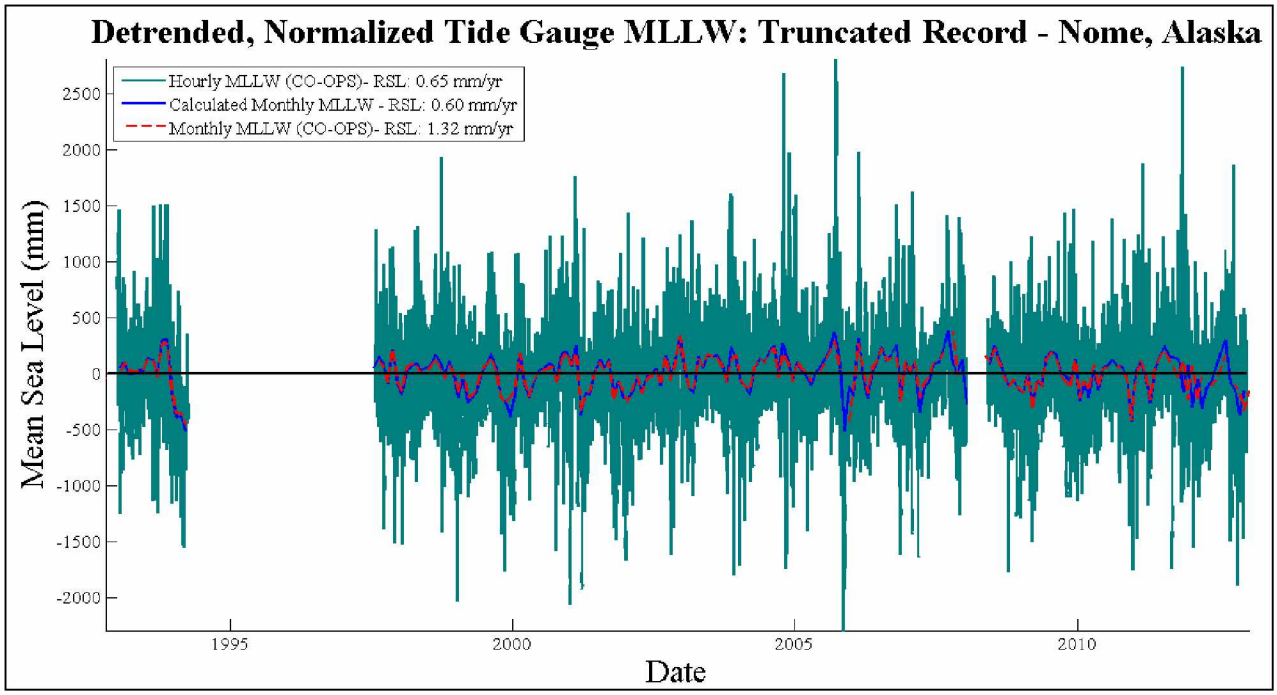

Figure A2.33. Plot of hourly MLLW data from November 1992 to November 2013 exhibiting a trend of 0.65 mm/yr made available by NOAA. Calculated monthly values are averages calculated from the hourly data and monthly MLLW that NOAA calculated is included as a comparison. The trends estimated from the hourly dataset and the monthly average calculated from the hourly data now are much more similar to both each other and that of the trend of monthly MSL provided by NOAA (Figure 24.). Truncating the full hourly dataset to remove the majority of the beginning of 1992 has had a significant impact on the trend, increasing it from 0.02 mm/yr to 0.65 mm/yr. The monthly MLLW provided by NOAA is still significantly different from any trends observed in the datasets analyzed in this report.

Appendix 3

GPS Field Work

Table A3.1. List of all benchmarks occupied during the summers of 2013 and 2014. Tidal benchmarks are reoccupations of NOS or NOAA established tidal benchmarks. Geodetic benchmarks are those used in the tectonic velocity model. Where possible all located benchmarks in a community were occupied, thus, to our knowledge some have not yet been used as a tidal or geodetic benchmark. NGS PID allows them to be located online; shared solutions are through NGS OPUS and are available both online at sites listed in Table 3.2.

Station ID	Community	Station Name	NGS PID	Tidal Benchmark	Geodetic Benchmark	Shared
3651	Golovin	GOLOVIN	BBDJ67		X	X
8756	Nome	8756 K NOME	DF3653	X	X	X
2BAD	Nome	2 BAD	DF3650		X	X
833E	Unalakleet	UNK TIDAL E	BBDH09	X		X
833G	Unalakleet	UNK TIDAL G	BBDH10	X		X
833H	Unalakleet	UNK TIDAL H	BBCK34	X		X
875B	Nome	8756 B NOME	BBDP98	X		X
875G	Nome	8756 NOME	BBBD24	X		
875H	Nome	8756 H		X		
875L	Nome	8756 L NOME		X		
886J	Elim	ELIM TIDAL J		X		
923B	Teller	TELLER TIDAL		X	X	
AKNA	King Salmon	AKN A 2001	DF3662		X	X
AKNB	King Salmon	AKN B 2001	DF3663		X	X
BETB	Bethel	BET B	DF3623		X	X
BETC	Bethel	BET C	DF3624		X	X
BM6_	Bethel	BM 6 1970	DF3625	X	X	X
CABN	Bethel	CABIN RESET	BBDP88		X	X
ELCR	Elim	ELIM AIR C RESET	BBDQ51		X	X
ELIB	Elim	ELIM AIR B	DF3655		X	X
ENMA	Emmonak	ENM A	DI8247		X	X
ENMB	Emmonak	ENM B	DJ2634		X	X
ENMC	Emmonak	ENM C	DJ2633		X	X
ESKI	King Salmon	ESKIMO	UW8054		X	
ETID	Elim	ELIM TIDAL GPS	DF3657	X	X	X
GAMB	Gambell	GAMBELL AIRPORT	UW3556		X	X
HEID	Port Heiden	PORT HEIDEN	UW1428		X	
HOOP	Hooper Bay	HOOPER BAY	UW8061		X	X
HPBB	Hooper Bay	HPB B	DF3630		X	X
JIMM	Port Heiden	JIMMY'S PLACE	UW1430		X	
KALS	Kalskag	KALSKAG	UW8066		X	X
KMJV	Nome	NOME PORT				
MELS	Council	MELSING (COUNCIL)	CA4540		X	X
MESH	Port Heiden	MESHIK	UW1432		X	X
MKAZ	Port Heiden	MESHIK AZ MK	UW1437		X	
MMKT	Serpentine	MIDNIGHT MTN	BBDH13		X	X
NOME	Nome	NOME	TT4629		X	X
OMEA	Nome	OME A	DF3651		X	X
OMEB	Nome	OME B	DF3652		X	X
SVAC	Savoonga	SAVOONGA AIRPT C	DJ2781		X	X

TLTA	Tuluksak	TLT A	DL3335		X	X
UNK1	Unalakleet	UNK NO. 1				
UNKA	Unalakleet	UNK A 2010	DM4448		X	X
UNKB	Unalakleet	UNK AIR B	DM4449		X	X

Table A3.2. The online locations for the NGS OPUS solution for each of the shared benchmarks listed in Table A3.1.

Station ID	Community	OPUS Solution Location
3651	Golovin	http://www.ngs.noaa.gov/OPUS/getDatasheet.jsp?PID=BBDJ67
8756	Nome	http://www.ngs.noaa.gov/OPUS/getDatasheet.jsp?PID=DF3653
2BAD	Nome	http://www.ngs.noaa.gov/OPUS/getDatasheet.jsp?PID=DF3650
833E	Unalakleet	http://www.ngs.noaa.gov/OPUS/getDatasheet.jsp?PID=BBDH09
833G	Unalakleet	http://www.ngs.noaa.gov/OPUS/getDatasheet.jsp?PID=BBDH10
833H	Unalakleet	http://www.ngs.noaa.gov/OPUS/getDatasheet.jsp?PID=BBCK34
875B	Nome	http://www.ngs.noaa.gov/OPUS/getDatasheet.jsp?PID=BBDP98
AKNA	King Salmon	http://www.ngs.noaa.gov/OPUS/getDatasheet.jsp?PID=DF3662
AKNB	King Salmon	http://www.ngs.noaa.gov/OPUS/getDatasheet.jsp?PID=DF3663
BETB	Bethel	http://www.ngs.noaa.gov/OPUS/getDatasheet.jsp?PID=DF3623
BETC	Bethel	http://www.ngs.noaa.gov/OPUS/getDatasheet.jsp?PID=DF3624
BM6_	Bethel	http://www.ngs.noaa.gov/OPUS/getDatasheet.jsp?PID=DF3625
CABN	Bethel	http://www.ngs.noaa.gov/OPUS/getDatasheet.jsp?PID=BBDP88
ELIB	Elim	http://www.ngs.noaa.gov/OPUS/getDatasheet.jsp?PID=DF3655
ENMA	Emmonak	http://www.ngs.noaa.gov/OPUS/getDatasheet.jsp?PID=DI8247
ENMB	Emmonak	http://www.ngs.noaa.gov/OPUS/getDatasheet.jsp?PID=DJ2634
ENMC	Emmonak	http://www.ngs.noaa.gov/OPUS/getDatasheet.jsp?PID=DJ2633
ETID	Elim	http://www.ngs.noaa.gov/OPUS/getDatasheet.jsp?PID=DF3657
GAMB	Gambell	http://www.ngs.noaa.gov/OPUS/getDatasheet.jsp?PID=UW3556
HOOP	Hooper Bay	http://www.ngs.noaa.gov/OPUS/getDatasheet.jsp?PID=UW8061
HPBB	Hooper Bay	http://www.ngs.noaa.gov/OPUS/getDatasheet.jsp?PID=UW8061
KALS	Kalskag	http://www.ngs.noaa.gov/OPUS/getDatasheet.jsp?PID=UW8066
MELS	Council	http://www.ngs.noaa.gov/OPUS/getDatasheet.jsp?PID=CA4540
MESH	Port Heiden	http://www.ngs.noaa.gov/OPUS/getDatasheet.jsp?PID=UW1432
MMKT	Serpentine	http://www.ngs.noaa.gov/OPUS/getDatasheet.jsp?PID=BBDH13
NOME	Nome	http://www.ngs.noaa.gov/OPUS/getDatasheet.jsp?PID=TT4629
OMEA	Nome	http://www.ngs.noaa.gov/OPUS/getDatasheet.jsp?PID=DF3651
OMEB	Nome	http://www.ngs.noaa.gov/OPUS/getDatasheet.jsp?PID=DF3652
SVAC	Savoonga	http://www.ngs.noaa.gov/OPUS/getDatasheet.jsp?PID=DJ2781
TLTA	Tuluksak	http://www.ngs.noaa.gov/OPUS/getDatasheet.jsp?PID=DL3335
UNKA	Unalakleet	http://www.ngs.noaa.gov/OPUS/getDatasheet.jsp?PID=DM4448
UNKB	Unalakleet	http://www.ngs.noaa.gov/OPUS/getDatasheet.jsp?PID=DM4449

Appendix 4

GPS Data

Table A4.1. GPS data produced from the Alaska vertical velocity model data from the UAF-GI geodetic database to construct a site velocity at each location. The velocity at each site is given referenced to both the ITRF 2008 reference frame and North American plate motion (NOAM). Locations that are in bold italics are later used in calculations of weighted means. Locations are ordered from western most at the top, to the farthest east at the bottom (longitudes are given in degrees east from 0 to 360).

Site ID	Longitude (degrees East)	Latitude (degrees)	ITRF GPS (cm/yr)	ITRF GPS Sigma (cm/yr)	NOAM GPS (cm/yr)	NOAM GPS Sigma (cm/yr)
BRNG	165.983586	55.193848	-0.257935	0.061122	-0.342707	0.064311
BKI	165.983626	55.192167	0.15434	0.044364	0.06957	0.048664
PEV2	170.251165	69.678394	0.347042	0.163175	0.249806	0.164397
PEVK	170.258207	69.700811	-0.079309	0.108911	-0.176561	0.110732
PEV1	170.273506	69.702815	-0.244205	0.145248	-0.34146	0.146619
MRKV	170.404221	64.682793	0.159831	0.077329	0.065943	0.079874
MRK1	170.428048	64.677136	0.076975	0.284979	-0.016912	0.28568
MURD	173.173341	52.804019	0.208107	0.031252	0.123773	0.037104
WALT	173.177954	52.870542	0.148304	0.096936	0.063905	0.098978
GEO1	173.180493	52.851031	0.502177	0.157854	0.417796	0.159116
ANDY	173.18179	52.880457	0.435213	0.193211	0.350803	0.194243
SIDE	173.192402	52.864626	0.319154	0.083328	0.234757	0.085694
AC60	174.076269	52.71462	0.183419	0.04863	0.098929	0.052583
BR2	174.099073	52.724031	0.388629	0.045269	0.304124	0.049491
ANAD	***177.497925***	***64.735541***	***-0.021465***	***0.065529***	***-0.116722***	***0.068513***
UGOL	***177.689148***	***64.731076***	***-0.226177***	***0.145687***	***-0.321466***	***0.147053***
BER2	179.101325	63.00924	0.426078	0.264174	0.331719	0.26493
CNNK	179.104021	51.470293	-0.15278	0.080169	-0.237437	0.082627
BERI	179.259324	63.06139	-0.110125	0.090564	-0.204552	0.092746
BER1	179.263205	63.063041	-0.933651	0.17085	-1.02808	0.172017
AC66	179.301326	51.37813	0.254404	0.036481	0.169782	0.041604
SHM1	180.566663	68.918984	-0.03748	0.190084	-0.135866	0.191134
SHMI	180.589095	68.892055	-1.252723	0.20743	-1.351098	0.208392
EGV1	180.881211	66.32532	-0.030182	0.125754	-0.127088	0.127334
EGVK	180.881598	66.32204	0.030225	0.097291	-0.066679	0.099326
MIDK	182.764664	51.761495	0.749897	0.052811	0.663974	0.056471

KICM	182.803986	51.918784	0.464394	0.507165	0.378314	0.507559
GATE	182.8485	51.85442	0.637761	0.132157	0.551729	0.133662
ROE2	182.87638	51.760473	0.711105	0.079465	0.625153	0.081944
KIRH	182.906818	51.899399	0.230785	0.161227	0.144696	0.162463
WHAL	183.293483	51.872418	0.554102	0.052912	0.467935	0.056565
WABM	183.294642	51.872429	0.486655	0.066638	0.400488	0.069575
BR6	183.326636	51.871267	0.538788	0.148501	0.452613	0.149842
AB21	183.337353	51.86415	0.362964	0.035548	0.276793	0.040788
J122	183.357718	51.877611	0.838186	0.748251	0.751997	0.748518
BED1	183.358101	51.877951	0.564994	0.04078	0.478805	0.045421
AT18	183.358849	51.861413	0.301494	0.086941	0.215319	0.089212
CLUB	183.359397	51.848257	0.7585	0.062159	0.672337	0.065297
BETT	183.364732	51.821815	0.503297	0.094814	0.417158	0.0969
FNGB	183.367038	51.831124	0.582614	0.06969	0.496465	0.072503
BUGS	183.369869	51.845198	0.545655	0.062489	0.459492	0.065612
LORA	183.384345	51.99305	0.424103	0.047015	0.3378	0.051093
ZETP	183.443875	51.930826	0.410808	0.062828	0.324547	0.065935
GSPA	183.930027	51.97899	0.513844	0.049319	0.42741	0.05322
WNDA	185.710998	52.161102	0.262728	0.125481	0.175659	0.127065
ACHU	185.752999	52.179118	0.242449	0.124375	0.155353	0.125973
PUPA	185.763942	52.199517	0.718386	0.130572	0.631268	0.132095
ATKA	185.793329	52.218456	0.012894	0.085204	-0.074249	0.08752
AB01	185.795244	52.209505	0.081889	0.040082	-0.005246	0.044795
2-Dec	185.830733	52.231346	0.581816	0.107671	0.494652	0.109513
PRVD	186.767029	64.421069	0.21185	0.103198	0.115081	0.105118
PRV1	186.776104	64.476595	-0.036553	0.208552	-0.133358	0.209508
GAMB	188.267994	63.774466	-0.07087	0.068932	-0.167508	0.071775
LAV1	188.897575	65.616687	-0.485883	0.112943	-0.583756	0.1147
AB04	***189.432557***	***63.656865***	***-0.13191***	***0.056025***	***-0.22869***	***0.059488***
SVAC	***189.503384***	***63.684693***	***-0.115997***	***0.160609***	***-0.212807***	***0.16185***
4212	189.714272	57.125675	0.340792	0.121522	0.24856	0.123157
SPSW	189.751512	57.152339	-0.09793	0.094116	-0.190192	0.096217
AC58	189.78218	57.156089	-0.106513	0.0463	-0.198785	0.050435
ROWD	191.145327	52.970665	0.519273	0.111662	0.430106	0.113439
AB02	191.14533	52.970606	0.025864	0.0406	-0.063302	0.045259
BLO1	191.596871	53.397625	-0.807486	0.554271	-0.897128	0.554632
AB09	191.937875	65.614982	-0.059252	0.04042	-0.157646	0.045098
BRCT	192.049941	53.34424	-0.080662	0.041524	-0.170369	0.04609
HUB1	192.069473	53.374807	-0.232801	0.085433	-0.322539	0.087743
FTGL	192.091861	53.384343	0.019748	0.083496	-0.070003	0.085858
SHIP	192.169548	53.373174	-0.3027	0.896459	-0.392461	0.896682

UNAL	192.245153	53.343807	0.109738	0.091299	0.019984	0.093464
MSWB	193.212118	53.914694	0.3113	0.091348	0.220836	0.093512
DHFA	193.451501	53.904646	0.205057	0.104356	0.114543	0.106255
AV09	193.458165	53.875635	0.232289	0.028252	0.141798	0.034615
DT19	193.467191	53.874457	0.349448	0.152514	0.258956	0.153819
DT16	193.468793	53.873984	0.36182	0.156421	0.271327	0.157694
DCH1	193.472397	53.888671	0.310842	0.023928	0.220337	0.031186
GUNN	193.483617	53.923853	0.223404	0.042811	0.132867	0.047253
SBS2	193.484728	53.897424	0.281419	0.063825	0.190903	0.066885
ILIU	193.515111	53.852434	0.258958	0.042561	0.168473	0.047026
AB08	193.799143	60.384832	0.039466	0.055474	-0.056014	0.058969
HOOP	193.859939	61.521162	0.507394	0.059425	0.411144	0.062701
REF2	193.902605	54.114351	0.265838	0.066748	0.175045	0.06968
FLOW	193.921524	54.169116	0.512979	0.131423	0.422137	0.132936
AKRB	193.928918	54.129228	0.239935	0.034068	0.149124	0.039505
AV07	193.961464	54.162938	0.322931	0.032523	0.232085	0.038181
AV08	193.971729	54.1363	0.296592	0.03258	0.205766	0.038229
LVA2	193.98386	54.163559	0.38736	0.340345	0.296508	0.340932
AKMO	193.987711	54.090259	0.310629	0.024378	0.219836	0.031533
AKGG	194.006329	54.198178	0.442278	0.036009	0.351392	0.041191
FTOP	194.00951	54.116029	0.409513	0.077927	0.318695	0.080452
AKLV	194.044177	54.162698	0.69434	0.03424	0.603474	0.039653
AV10	194.066236	54.09761	0.36415	0.031819	0.273333	0.037583
HSB	194.086193	54.186063	0.830216	0.065893	0.739322	0.068861
AV13	194.102185	54.153082	0.538138	0.034336	0.447266	0.039736
AV12	194.102454	54.2108	0.408037	0.03173	0.317119	0.037507
BROD	194.131111	54.110699	0.587507	0.31387	0.496663	0.314507
AKPS	194.150108	54.145325	0.57327	0.073685	0.482393	0.076351
AV14	194.158432	54.118895	0.317835	0.031686	0.226978	0.03747
WHL	194.173664	54.11865	0.643896	0.089539	0.553036	0.091746
AV06	194.23428	54.14718	0.237028	0.031554	0.146131	0.037359
AKU	194.2369	54.143082	0.357928	0.0772	0.267033	0.079749
AKHB	194.265977	54.104063	0.865096	0.274012	0.774227	0.274741
AV15	194.289888	54.100194	0.24305	0.031642	0.152178	0.037434
OMEA	***194.556196***	***64.509774***	***-0.010562***	***0.05444***	***-0.108776***	***0.057998***
2BAD	***194.564103***	***64.507243***	***-0.04104***	***0.052097***	***-0.139255***	***0.055804***
OMEB	***194.566355***	***64.51293***	***-0.083348***	***0.054406***	***-0.181566***	***0.057966***
8756	***194.569946***	***64.507257***	***-0.054382***	***0.075826***	***-0.152597***	***0.078419***
875G	***194.570808***	***64.505559***	***0.073431***	***0.265348***	***-0.024783***	***0.266101***
AB11	***194.626542***	***64.564497***	***-0.07849***	***0.036493***	***-0.176748***	***0.041614***
NOME	***194.628772***	***64.562701***	***-0.194123***	***0.055146***	***-0.29238***	***0.058661***

AC10	195.113272	54.522582	0.336059	0.046881	0.244652	0.050969
AV25	195.220503	54.530003	0.709269	0.04763	0.617832	0.051659
AV24	195.245197	54.589984	0.569695	0.047313	0.478203	0.051367
SCAP	195.25547	54.397899	1.14629	0.475456	1.05495	0.475877
AV27	195.276838	54.492351	1.075221	0.076439	0.983801	0.079012
AV29	195.41385	54.472354	0.976163	0.079634	0.884728	0.082107
AV26	195.419535	54.571654	0.744888	0.047706	0.653371	0.051729
AC50	195.433431	65.553849	-0.156992	0.040445	-0.255939	0.04512
ENMA	***195.507796***	***62.780471***	***-0.205022***	***0.094053***	***-0.302379***	***0.096156***
ENMC	***195.510124***	***62.791753***	***-0.043926***	***0.330745***	***-0.14129***	***0.331349***
ENMB	***195.511613***	***62.780277***	***-0.742558***	***0.242628***	***-0.839915***	***0.243451***
AV35	195.613084	54.846695	-0.045924	0.073742	-0.137705	0.076406
AV36	195.873197	54.771795	-0.056392	0.047657	-0.148173	0.051683
AV39	196.001534	54.811342	0.056968	0.048673	-0.034873	0.052622
AV37	196.002766	54.70938	-0.078058	0.071686	-0.169819	0.074424
AV38	196.219127	54.831469	0.089931	0.047873	-0.001976	0.051883
AV40	196.257033	54.644537	0.181752	0.068728	0.089985	0.071579
AV34	196.287081	54.724909	0.19484	0.047385	0.103003	0.051434
MELS	196.30774	64.922341	-0.10695	0.038712	-0.205698	0.043574
KATY	196.476182	55.044275	-0.22383	0.102835	-0.315963	0.104762
AB06	196.576546	54.885323	0.075313	0.032339	-0.016717	0.038024
TOMH	196.677169	54.741357	0.531115	0.270175	0.439176	0.270914
PANK	196.886796	54.679095	0.203863	0.13802	0.111925	0.139462
CROW	197.198985	54.490829	0.317007	0.057491	0.225148	0.06087
AC42	197.216349	54.471777	0.141188	0.056415	0.04934	0.059855
SATT	197.268025	55.173777	-0.317852	0.144016	-0.410264	0.145398
CDB7	197.281529	55.200336	0.074724	0.050083	-0.017712	0.053929
BAY5	197.292841	55.190271	-0.014805	0.040887	-0.107236	0.045517
BAY1	197.292842	55.190274	0.039745	0.026367	-0.052686	0.033094
BAY6	197.293235	55.190418	-0.027868	0.042265	-0.120299	0.046758
BAY2	197.293237	55.19042	0.058412	0.030847	-0.034019	0.036763
PETE	197.38103	54.383872	0.124098	0.024247	0.032282	0.031432
AB18	***197.386493***	***66.858364***	***-0.31648***	***0.038806***	***-0.416423***	***0.043657***
OTZ1	***197.388627***	***66.887333***	***-0.286217***	***0.044859***	***-0.386174***	***0.049116***
TELE	197.39532	54.984411	-0.191978	0.266986	-0.28427	0.267734
REEF	197.477017	54.857379	0.111956	0.382692	0.019745	0.383214
CHRN	197.630693	54.629043	-0.100167	0.279901	-0.192233	0.280615
FAWN	197.644807	54.824575	-0.061038	0.47438	-0.153261	0.474801
AC25	197.685948	55.088969	0.053036	0.041419	-0.039402	0.045995
ELIB	***197.728988***	***64.613977***	***-0.259416***	***0.09219***	***-0.358233***	***0.094335***
ETID	***197.747871***	***64.616514***	***-1.350457***	***0.520453***	***-1.449278***	***0.520837***

AC31	***197.760874***	***64.637977***	***-0.089581***	***0.036231***	***-0.188416***	***0.041385***
CABN	***198.15448***	***60.794506***	***0.53572***	***0.062076***	***0.439117***	***0.065219***
BETB	***198.157831***	***60.777609***	***0.763784***	***0.066779***	***0.667192***	***0.06971***
BET1	***198.158275***	***60.787917***	***-0.157441***	***0.044489***	***-0.25404***	***0.048778***
BETC	***198.16432***	***60.784197***	***0.158358***	***0.040288***	***0.061761***	***0.04498***
AB12	198.253739	58.950795	-0.077735	0.057386	-0.173127	0.060772
AC07	198.713384	65.961293	-0.10543	0.040155	-0.205127	0.04486
TLTA	199.078449	61.088489	2.099926	0.066618	2.002962	0.069555
AB17	199.305269	63.886359	-0.152583	0.049451	-0.251261	0.053343
LSD1	199.504719	55.302023	0.67816	0.157433	0.585156	0.158698
LSDP	199.504838	55.302049	-0.066739	0.043105	-0.159743	0.047519
AB07	***199.523243***	***55.349277***	***-0.086496***	***0.029489***	***-0.17954***	***0.035631***
SDP1	***199.524503***	***55.353013***	***0.101967***	***0.1172***	***0.00892***	***0.118894***
SNDP	***199.524511***	***55.352322***	***0.139413***	***0.05598***	***0.046367***	***0.059445***
AC41	199.592696	55.908669	0.000289	0.036084	-0.093193	0.041256
KALS	199.665465	61.537197	-0.429433	0.066049	-0.526787	0.069011
4168	199.882147	70.599855	-0.780849	0.185469	-0.882801	0.186544
AC28	199.95084	55.078491	-0.047016	0.044844	-0.139946	0.049102
AB15	200.121639	61.039753	-0.001088	0.035828	-0.098216	0.041032
AC12	200.410438	54.830963	-0.135822	0.045103	-0.228661	0.049339
SMNF	200.743763	54.914539	-0.188654	0.150324	-0.28163	0.151649
AC21	200.872278	55.92109	-0.062052	0.035668	-0.155816	0.040893
AB14	200.908469	59.108166	-0.041011	0.055781	-0.137035	0.059258
AC40	***201.38143***	***56.930353***	***0.184944***	***0.058714***	***0.090337***	***0.062027***
JIMM	***201.382555***	***56.916884***	***-0.023106***	***0.066905***	***-0.117704***	***0.06983***
HEID	***201.387657***	***56.963885***	***-0.00561***	***0.028134***	***-0.100243***	***0.034519***
ISLK	201.399682	56.113417	-0.786599	0.385846	-0.880616	0.386364
AB13	***201.496206***	***56.307326***	***0.009603***	***0.036891***	***-0.084575***	***0.041964***
DILL	***201.529185***	***59.061955***	***0.711447***	***0.210498***	***0.615333***	***0.211446***
AC52	202.425784	57.56725	0.085724	0.041137	-0.009545	0.045741
ATQK	202.592132	70.472033	-0.124411	0.035369	-0.226662	0.040632
AB27	203.095111	67.055887	-0.108985	0.04018	-0.209883	0.044882
BRW1	203.210076	71.282766	-0.017052	0.045143	-0.119669	0.049375
BASC	203.32209	71.324944	-0.041346	0.038957	-0.143992	0.043791
AKNA	***203.345538***	***58.671209***	***0.162473***	***0.069009***	***0.066271***	***0.071849***
AC24	***203.347245***	***58.681573***	***0.133313***	***0.035076***	***0.037104***	***0.040378***
AKNB	***203.349894***	***58.6782***	***0.469006***	***0.059768***	***0.372798***	***0.063025***
ESKI	***203.35306***	***58.674898***	***-1.115617***	***0.394815***	***-1.211823***	***0.395321***
SG27	203.389669	71.322896	-0.244924	0.023856	-0.347577	0.031131
TATB	203.971354	62.927338	-0.503186	0.546054	-0.602115	0.54642
AB25	203.976609	62.929311	-0.020022	0.069065	-0.118953	0.071903

TAAZ	203.976673	62.929304	0.214157	0.189456	0.115226	0.190509
CHIR	***204.271504***	***55.825882***	***-0.873025***	***0.111994***	***-0.967423***	***0.113765***
AC13	***204.3776***	***55.821896***	***-1.080615***	***0.047496***	***-1.175032***	***0.051535***
MGRA	204.396443	62.957707	0.509717	0.04813	0.410699	0.05212
NARM	204.409387	58.625881	0.382243	0.134844	0.285868	0.13632
LIME	204.555558	61.356532	0.714942	0.146969	0.616821	0.148324
BKDM	204.808548	58.281059	0.490581	0.042087	0.394361	0.046597
NOVR	204.839945	58.265252	-0.162531	0.040162	-0.258747	0.044866
UNAM	205.039048	58.428984	0.385255	0.098875	0.288892	0.100878
AB22	205.301741	59.899321	0.278368	0.034977	0.181006	0.040291
DAKA	205.31771	58.088	0.927641	0.288207	0.831453	0.2889
AC02	205.816956	56.950586	-0.042198	0.032522	-0.137704	0.03818
AC45	205.81904	56.564453	-0.389322	0.035161	-0.484558	0.040451
AHKI	205.825386	56.941082	0.486866	0.070947	0.391364	0.073713
AC27	205.83712	59.252508	0.237384	0.036679	0.140335	0.041777
AC26	205.849708	58.214556	0.432964	0.045951	0.336591	0.050115
SITK	205.864141	56.540276	0.145638	0.128969	0.050409	0.130511
KNUT	206.113503	59.8957	0.468685	0.053958	0.37118	0.057545
AC37	206.134617	60.439688	0.303425	0.04152	0.205581	0.046086
AC08	206.3553	58.928775	0.782951	0.041711	0.686016	0.046258
AC19	206.392667	62.519214	0.264518	0.045828	0.165414	0.050002
A18	206.412205	59.570065	0.498055	0.11677	0.4007	0.11847
AC59	206.4148	59.567199	0.474996	0.029063	0.377643	0.03528
AUGW	206.456655	59.384424	0.77485	0.225321	0.677604	0.226207
AV16	206.464955	59.385911	0.456395	0.036016	0.359146	0.041196
AUGS	206.476564	59.323207	0.2341	0.196128	0.136889	0.197146
A5	206.480772	59.378124	0.773071	0.054684	0.675824	0.058227
AV01	206.5392	59.358532	0.376525	0.03536	0.279281	0.040624
AV17	206.548555	59.403947	0.34376	0.036125	0.246485	0.041292
AV04	206.555328	59.362584	0.116864	0.049073	0.019614	0.052992
A1	206.562183	59.381559	0.767119	0.153445	0.669856	0.154742
A6	206.562673	59.371182	0.248585	0.151493	0.151328	0.152807
AV18	206.563165	59.380434	-0.212065	0.036127	-0.309328	0.041294
AUGK	206.563444	59.345662	0.715483	0.170667	0.618242	0.171835
AV02	206.571609	59.332975	0.490599	0.035188	0.393365	0.040475
AV20	206.571794	59.347382	0.244363	0.03658	0.14712	0.041691
A2	206.575494	59.366625	0.707177	0.092938	0.609921	0.095066
A4	206.576533	59.362372	0.157403	0.19382	0.06015	0.194849
AUGB	206.583579	59.411881	0.525754	0.055262	0.428468	0.05877
AV19	206.585672	59.354908	-0.128852	0.048162	-0.226102	0.05215
A9	206.586016	59.323005	0.862815	0.115758	0.765584	0.117473

A11	206.613232	59.348653	0.64285	0.10731	0.545599	0.109158
AUGM	206.64494	59.370692	0.912149	0.197847	0.814878	0.198855
AV11	206.645315	59.370628	0.539854	0.036105	0.442583	0.041274
AUGL	206.64609	59.3703	0.972301	0.060884	0.875029	0.064085
AC38	206.658129	57.753686	0.699694	0.031353	0.603477	0.037189
AC34	206.720823	57.220027	0.266428	0.03513	0.170562	0.040425
DRYB	206.826204	59.677256	0.611105	0.059416	0.513608	0.062692
CRSC	206.912447	60.434696	0.77591	0.142479	0.677932	0.143876
RDWB	207.156365	60.486806	1.06261	0.09382	0.964558	0.095928
AB28	207.185083	62.093816	0.456506	0.04691	0.35751	0.050996
RDJH	207.194759	60.590764	0.89166	0.06868	0.793539	0.071533
AC47	207.376055	60.081452	0.67333	0.059041	0.575486	0.062337
SKI	207.390602	57.80234	1.153211	0.075714	1.056824	0.078311
CLAM	207.493749	57.65219	1.374723	0.084756	1.278418	0.087084
KODK	207.498624	57.735107	1.038461	0.049655	0.942099	0.053532
KOD2	207.502698	57.73991	1.193664	0.043167	1.097298	0.047575
PASA	207.542219	57.436024	0.499557	0.085997	0.403389	0.088292
AC67	207.574568	57.790718	0.819322	0.035336	0.722909	0.040604
AC17	207.596154	60.663903	0.849806	0.036516	0.751571	0.041635
AC39	207.605927	58.60972	0.949993	0.034898	0.853036	0.040223
SPBG	207.627622	61.259152	0.409499	0.049995	0.310908	0.053847
NCAP	207.650606	57.422727	0.275502	0.182483	0.179322	0.183576
QRRY	207.69626	60.629876	0.968806	0.122172	0.870574	0.123798
HAR3	207.728774	60.39035	0.923629	0.148097	0.825535	0.149441
AC18	207.750469	58.925958	0.95214	0.047259	0.854953	0.051317
SPCR	207.790825	61.200311	0.850672	0.044639	0.752087	0.048915
MCGA	207.803846	57.614002	0.939556	0.123575	0.843219	0.125183
KOD6	207.806118	57.617592	0.555857	0.039881	0.459517	0.044615
KDK2	207.80612	57.617592	0.946897	0.095767	0.850557	0.097834
KOD5	207.80657	57.617692	0.628712	0.067392	0.532372	0.070297
KDK1	207.806573	57.617692	0.75957	0.026932	0.663229	0.033547
MCGB	207.810336	57.619214	1.106636	0.086083	1.010294	0.088376
CHIN	207.842134	57.618742	0.905637	0.097983	0.809289	0.100004
SPCP	207.844517	61.265528	0.832219	0.089105	0.733588	0.091322
SPCG	207.977594	61.291219	0.76416	0.047493	0.665492	0.051533
EAMA	208.006147	58.912763	0.900531	0.067879	0.803306	0.070764
EBAY	208.08725	59.360535	1.003515	0.080323	0.905993	0.082775
AC03	208.135467	59.770638	0.850429	0.042691	0.752642	0.047144
EKG3	208.161815	60.484633	1.177201	0.13731	1.078976	0.138759
AC51	208.164652	61.498084	0.590714	0.05744	0.491894	0.060822
AC80	208.234958	62.394078	0.52916	0.067695	0.429824	0.070588

W86	208.238048	59.90193	1.808485	0.279468	1.7106	0.280183
NINI	208.284241	60.008538	1.01953	0.046919	0.921572	0.051004
SELD	208.29333	59.445711	0.844409	0.021485	0.746796	0.029353
B86	208.323409	59.673735	1.108592	0.116325	1.010833	0.118032
Z82	208.38074	60.08081	0.982337	0.067366	0.884318	0.070272
HDPW	208.46881	59.641684	0.960618	0.072055	0.862853	0.074779
BTTA	208.470167	66.914178	-0.301543	0.604379	-0.403142	0.60471
AC46	208.475999	61.98627	0.409754	0.047086	0.310606	0.051157
HOMA	208.508452	59.638992	0.960399	0.044848	0.862629	0.049106
N82	208.570231	60.187684	1.029243	0.111235	0.931126	0.113018
NIK	208.600747	60.682957	1.044585	0.111755	0.946167	0.113531
NIK2	208.608505	60.685305	0.905958	0.119924	0.807537	0.12158
KEN5	208.649817	60.675078	0.88948	0.041631	0.791059	0.046186
KEN1	208.649818	60.675081	0.99527	0.028497	0.896848	0.034815
KEN6	208.649835	60.674804	0.884137	0.041839	0.785715	0.046374
KEN2	208.649836	60.674807	1.413001	0.092201	1.31458	0.094345
H81	208.680376	60.579563	1.032877	0.138558	0.934507	0.139994
PBAY	208.727762	59.572707	0.843095	0.08234	0.745327	0.084734
MCES	208.742168	59.746077	0.938573	0.075276	0.840697	0.077887
W81	208.756047	60.331733	0.781974	0.07268	0.683739	0.075382
KIRT	208.758715	60.578848	1.516627	0.151632	1.418244	0.152945
DIAN	208.772066	60.58787	1.775548	0.142575	1.677157	0.143971
BLGA	208.794327	61.682959	0.075365	0.115405	-0.023664	0.117126
SXQC	208.947854	60.47524	1.153453	0.053893	1.055099	0.057484
SXQD	208.958275	60.475939	0.781204	0.05772	0.682849	0.061087
D79	208.969989	60.49687	0.931063	0.224896	0.832693	0.225784
WIKR	209.077788	63.552728	0.16186	0.047027	0.061772	0.051103
AC06	209.109442	59.763638	0.871712	0.032433	0.773761	0.038104
AC23	209.122046	60.475093	0.764733	0.040082	0.66635	0.044795
BRAD	209.148113	59.755131	1.060573	0.055111	0.962621	0.058628
PTVL	209.183284	62.531743	0.628764	0.055592	0.5292	0.05908
AC35	209.206755	59.375811	1.049179	0.036869	0.951451	0.041945
AB36	209.256016	65.030399	0.229883	0.051907	0.129031	0.055627
AC32	209.263083	61.473121	0.358498	0.037266	0.259511	0.042293
MSUN	209.263119	61.473388	0.100642	0.433355	0.001655	0.433816
S79R	209.268578	60.529688	0.76977	0.123364	0.67133	0.124975
AC33	209.314927	62.671178	0.18301	0.041462	0.083351	0.046034
152T	209.326465	66.820757	-0.067265	0.049661	-0.168941	0.053537
W152	209.32964	66.818606	2.518448	0.064065	2.416772	0.067115
MENA	209.34641	60.088765	0.277995	0.206068	0.179806	0.207036
AC36	209.391652	60.955318	0.710844	0.043944	0.612133	0.048282

2201	209.448609	59.524905	0.792396	0.041749	0.694534	0.046292
FNGR	209.50757	66.375537	-0.072985	0.045043	-0.174492	0.049284
MPEN	209.517311	60.735176	0.704702	0.058566	0.606099	0.061887
SKLK	209.704209	60.35294	0.772972	0.066596	0.674564	0.069534
BEAR	209.752231	60.455423	0.76959	0.088049	0.671113	0.090292
M78	209.784085	60.524343	1.221265	0.182032	1.122741	0.183127
AB33	209.827456	67.251013	-0.071555	0.037043	-0.173482	0.042097
AC53	209.931048	61.768973	0.180037	0.036252	0.080774	0.041403
POPL	209.93595	60.486963	0.735769	0.06798	0.637242	0.070861
POPZ	209.944172	60.484993	1.400242	0.307579	1.301715	0.308228
UNF	209.967433	59.790092	0.767467	0.072005	0.669352	0.074731
D151	209.997034	67.466805	0.624992	0.070644	0.522954	0.07342
ANC1	210.003229	61.182381	0.310591	0.062553	0.211648	0.065673
ANC2	210.016558	61.175225	0.366425	0.059378	0.267484	0.062656
VDUS	210.047205	61.174501	0.540786	0.162528	0.441841	0.163754
NWP	210.100291	59.748447	0.776199	0.080781	0.678088	0.083221
TSEA	210.105027	61.187328	0.494137	0.02846	0.395174	0.034785
FSHL	210.117585	61.524736	0.470323	0.084557	0.371167	0.08689
S103	210.129378	61.644303	0.672128	0.249771	0.572903	0.25057
ACCU	210.136756	61.155738	0.340616	0.035437	0.241667	0.040692
CMJV	210.155084	61.165835	0.802057	0.066749	0.703099	0.069681
UAAG	210.175908	61.191072	0.627143	0.032222	0.528167	0.037924
V77	210.188126	60.490614	0.38476	0.405953	0.286189	0.406445
TBON	210.21486	61.179717	0.490386	0.03484	0.39141	0.040173
ZAN1	210.219753	61.229203	0.502044	0.026019	0.403039	0.032817
1000	210.222429	61.160065	0.633295	0.176203	0.534329	0.177335
ISLZ	210.254395	61.020664	0.741624	0.084725	0.642733	0.087054
CPR	210.25455	60.489444	0.939784	0.062824	0.841202	0.065931
AC15	210.275994	60.481333	0.809722	0.032899	0.711142	0.038501
CPLK	210.279062	60.382976	0.757068	0.061508	0.658546	0.064678
HILS	210.280725	61.106143	0.983171	0.156064	0.884226	0.157341
JANE	210.356446	60.18298	0.547113	0.091929	0.448696	0.09408
AC43	210.371265	59.521279	0.309872	0.040592	0.211853	0.045252
TOOL	210.402243	68.627534	-0.194767	0.028624	-0.297314	0.034919
GRAV	210.418476	60.564368	0.782908	0.121374	0.684256	0.123011
M155	210.418768	68.076555	-0.071319	0.103891	-0.173656	0.105799
AC44	210.432875	61.242173	0.705294	0.047185	0.606247	0.051249
P118	210.452928	60.534768	1.786519	0.363911	1.687879	0.36446
TURN	210.456696	60.930528	0.725434	0.078001	0.626562	0.080524
4A1A	210.457123	61.571227	0.455309	0.138512	0.356072	0.139949
INDI	210.465148	60.983086	1.430299	0.207098	1.331395	0.208061

EAGL	210.471309	61.257486	0.777833	0.070641	0.678771	0.073418
DAHL	210.512119	60.654023	0.859774	0.072795	0.761054	0.075492
PRSP	210.538538	61.888292	-0.236369	0.179759	-0.335794	0.180869
NWOD	210.54896	61.420854	1.701505	0.492942	1.602338	0.493348
UAMF	210.5576	60.098495	0.498046	0.052472	0.399646	0.056155
S1	210.558244	61.58049	1.037169	0.448904	0.93791	0.449349
T19	210.571389	60.119208	0.452553	0.117987	0.354138	0.11967
TRLK	210.579747	60.501508	0.700497	0.054658	0.601854	0.058203
RGGI	210.592816	59.86519	0.170702	0.059214	0.072436	0.062501
REED	210.604083	61.542433	1.00104	0.146089	0.901795	0.147451
WLKR	210.60982	59.986809	0.539211	0.112278	0.440869	0.114045
U76	210.629352	60.428586	0.129157	0.598264	0.030549	0.598599
AC20	210.647498	60.929208	0.592448	0.032382	0.493546	0.038061
CROS	210.656881	60.285808	0.581245	0.120877	0.482717	0.122521
K76	210.657127	60.285969	0.403785	0.127908	0.305257	0.129462
EKLU	210.658753	61.462777	0.412642	0.144863	0.313433	0.146237
GOVP	210.710265	61.728273	0.455149	0.105209	0.355784	0.107093
T20N	210.730444	61.772856	0.534394	0.267533	0.435001	0.268279
FSHK	210.764959	61.716819	1.04668	0.407086	0.947312	0.407577
C85G	210.815193	60.804316	0.562184	0.118656	0.463326	0.12033
ATW2	210.867712	61.597755	0.635792	0.027004	0.536475	0.033604
POOR	210.884077	61.028245	1.063966	0.314395	0.964968	0.315031
YUKO	210.907011	65.676178	-0.084474	0.064044	-0.185863	0.067095
ALAS	210.936133	60.893074	1.050464	0.118957	0.951535	0.120627
T18N	210.942454	61.657271	1.192012	0.347358	1.09265	0.347933
MOS2	210.943952	61.675579	0.527485	0.068821	0.428112	0.071668
BODE	210.947364	61.545906	1.659931	0.285944	1.560629	0.286642
INCK	210.952126	60.841553	0.942396	0.08499	0.843494	0.087311
MSB2	210.972957	61.629209	1.64669	0.300317	1.547338	0.300982
GRNX	211.021808	63.8355	0.368951	0.028781	0.268425	0.035048
ENDI	211.024291	60.818466	0.576176	0.340758	0.477275	0.341345
GRN2	211.024752	63.834201	-0.101544	0.090996	-0.202071	0.093168
CGLO	211.050374	63.388266	0.202499	0.125906	0.102195	0.127485
DVC1	211.082984	63.730807	0.219015	0.04672	0.118532	0.050821
MINT	211.099113	65.100632	0.710354	0.128668	0.609204	0.130213
AB45	211.128849	68.760495	-0.108105	0.03947	-0.210792	0.044248
PRTG	211.170411	60.771211	0.685929	0.111658	0.587032	0.113435
HIWC	211.192743	63.464358	0.355613	0.026709	0.255248	0.033367
S119	211.375075	64.710509	-0.575578	0.27238	-0.676584	0.273113
X147	211.426756	69.503677	-1.448415	0.851885	-1.551405	0.852119
CKLN	211.463219	61.764657	0.978075	0.118871	0.87857	0.120541

LUKY	211.484339	64.926743	0.362054	0.203901	0.26093	0.20488
DSL1	211.527253	70.333438	-0.563115	0.024958	-0.666395	0.031983
GAIN	211.608098	60.706672	0.529821	0.173695	0.43089	0.174842
MDPK	211.644665	64.952926	0.191097	0.131063	0.089938	0.132581
MDR1	211.645113	64.952956	-0.163088	0.168582	-0.264246	0.169764
PUO1	211.656745	70.253873	-0.325939	0.024915	-0.429208	0.03195
PBOC	211.665087	70.256404	-0.366613	0.023448	-0.469883	0.030819
EDOC	211.681518	70.310272	-0.631369	0.024828	-0.734659	0.031882
M120	211.799892	64.791424	0.84086	0.220077	0.739755	0.220984
AC16	211.906766	60.518204	0.060239	0.055396	-0.03863	0.058896
HAM	211.908645	61.005563	-0.258287	0.19345	-0.357437	0.194481
THIN	211.909808	60.362685	0.119396	0.109331	0.020616	0.111145
PURI	211.91064	61.804591	1.159513	0.077688	1.059917	0.080221
ENUN	211.917255	60.595882	0.267689	0.123732	0.168772	0.125338
WICK	211.933803	65.182698	0.209839	0.078536	0.108532	0.081042
EST1	211.94507	64.879309	0.121218	0.252365	0.020052	0.253156
CHNG	211.987085	60.068457	0.110155	0.08914	0.011536	0.091356
AC14	212.00042	60.848701	0.06669	0.057616	-0.032385	0.060989
EGG	212.037348	60.774036	0.132554	0.129858	0.033516	0.131389
COGH	212.052871	61.070379	0.386457	0.248143	0.287247	0.248948
ROC	212.067107	60.653739	-0.063546	0.143258	-0.16252	0.144648
MOTG	212.092221	59.824843	0.439158	0.165683	0.340667	0.166886
RIDG	212.135361	64.849577	0.436189	0.181748	0.335009	0.182845
CLGO	212.139514	64.873777	0.088734	0.031495	-0.012458	0.037309
IARC	212.14931	64.859279	0.11371	0.028421	0.012524	0.034753
IAR2	212.149407	64.859279	0.138973	0.054791	0.037786	0.058328
FAI1	212.15266	64.809631	0.106989	0.06518	0.005826	0.06818
SUAF	212.164202	64.858691	0.041483	0.043398	-0.059706	0.047785
AC30	212.260767	59.855818	-0.504841	0.142095	-0.603378	0.143496
LSG1	212.334235	62.053313	0.950034	0.182947	0.850237	0.184037
REFL	212.401161	64.986403	-0.11497	0.171867	-0.216251	0.173027
FAIR	212.500763	64.978002	0.099182	0.031607	-0.00211	0.037404
FAI2	212.501406	64.9779	-0.019999	0.49587	-0.12129	0.496273
FAIV	212.501483	64.978144	-0.047355	0.051386	-0.148647	0.055141
DIXI	212.553599	60.731484	0.04898	0.216842	-0.050116	0.217762
PEDR	212.585278	65.043419	-0.211083	0.163015	-0.312416	0.164237
AC79	212.596955	59.997868	-0.241458	0.067489	-0.340135	0.07039
GIAN	212.613136	60.5278	0.195022	0.152986	0.096033	0.154288
AC48	212.656984	60.645862	-0.030201	0.056202	-0.129265	0.059655
ANCR	212.745627	60.884078	-0.231982	0.163348	-0.331196	0.164568
EIL2	212.887033	64.68794	0.182333	0.04265	0.081123	0.047107

EIL1	212.887033	64.687941	0.56261	0.026037	0.4614	0.032832
SPIL	212.915632	65.226817	0.087741	0.094751	-0.013722	0.096838
GULL	213.29629	60.722959	-0.066949	0.107655	-0.166159	0.109497
POT6	213.302641	61.056308	0.716018	0.041145	0.616619	0.045748
POT4	213.302645	61.056307	0.846143	0.065411	0.746744	0.068401
POT5	213.303163	61.056261	0.681167	0.041351	0.581768	0.045934
POT3	213.303167	61.05626	0.967001	0.036286	0.867602	0.041433
MIST	213.322939	60.943376	0.286309	0.072637	0.18697	0.075341
CHI1	213.353017	60.237471	0.171218	0.14476	0.072279	0.146135
CHI5	213.353432	60.237513	0.140669	0.043395	0.04173	0.047782
CHI3	213.353436	60.237512	0.311085	0.036355	0.212146	0.041493
CHI6	213.353474	60.23774	-0.020961	0.041242	-0.1199	0.045836
CHI4	213.353478	60.237739	0.068678	0.043021	-0.030261	0.047442
4240	213.640395	61.127179	0.7771	0.219545	0.677609	0.220454
RUB2	213.642037	60.447817	0.074224	0.194031	-0.024883	0.195059
DH32	213.687307	63.083607	0.404467	0.035208	0.303927	0.040493
GRIS	213.707983	60.639636	-0.238213	0.174984	-0.33744	0.176123
FAIT	213.738998	65.347127	-0.096482	0.306797	-0.198112	0.307448
VDZW	213.748756	61.132778	0.967463	0.42239	0.867952	0.422863
NATI	213.92359	60.745	-0.049354	0.149158	-0.148674	0.150493
TWLV	214.015476	65.408981	0.09771	0.061414	-0.003984	0.064589
TRM2	214.078352	60.525966	0.162727	0.16964	0.063507	0.170815
EYAK	214.250034	60.548668	0.189155	0.200672	0.089895	0.201666
EYAC	214.250142	60.548704	0.074488	0.032036	-0.024772	0.037767
AC57	214.257297	61.138596	0.827102	0.035084	0.72751	0.040385
THMP	214.267735	61.127998	0.90139	0.141738	0.801802	0.143142
THM1	214.26783	61.128041	0.696667	0.127577	0.597079	0.129135
BLF2	214.321809	60.651787	0.095495	0.21576	-0.003834	0.216685
AB46	214.432099	68.120672	-0.405269	0.038714	-0.508122	0.043575
CODO	214.524553	60.493716	-0.108751	0.073289	-0.208022	0.075969
GKNC	214.546712	62.156189	0.401518	0.255491	0.301331	0.256273
PAX2	214.548125	62.967323	0.541442	0.03746	0.440836	0.042465
EGL2	214.612452	65.490888	-0.143738	0.051666	-0.245549	0.055402
AB39	214.787369	66.559346	-0.320229	0.046771	-0.422517	0.050868
SWB4	214.973382	65.562192	1.606501	0.61424	1.504611	0.614565
CENA	215.32237	65.498165	0.051805	0.018467	-0.050103	0.027222
RAG	215.322718	60.386434	0.361635	0.085804	0.262302	0.088104
AFGR	215.420094	61.076617	0.936859	0.142828	0.837125	0.144221
AC09	215.476153	59.868478	0.243151	0.041623	0.144092	0.046179
FAUS	215.93391	60.953892	1.256879	0.112539	1.157135	0.114303
MAC	215.937613	65.826195	-0.218036	0.27888	-0.320165	0.279596

BERG	216.299425	60.39395	0.393415	0.117859	0.293929	0.119544
FARO	216.585497	61.120915	1.108163	0.13767	1.008231	0.139115
DON	216.623225	60.057856	0.387111	0.202816	0.287767	0.2038
LARI	216.675516	60.861973	1.507843	0.118611	1.40804	0.120285
HANN	216.854834	60.260614	1.232384	0.225093	1.13289	0.22598
ANCX	217.403348	60.442201	1.608387	0.32753	1.50871	0.32814
YAKK	217.491045	60.081273	1.735703	0.145485	1.636216	0.146853
VYAK	217.513541	60.081467	1.847069	0.125527	1.747577	0.127111
YAKR	217.513551	60.081457	1.204767	0.169642	1.105276	0.170816
AB35	217.610129	60.079066	0.912942	0.0408	0.813439	0.045439
M175	217.621032	63.548815	-0.001194	0.05491	-0.102515	0.058439
ISLE	217.659075	60.601223	1.40608	0.109488	1.306277	0.1113
999	217.725233	63.665002	-0.563311	0.093466	-0.664701	0.095582
DENN	217.824322	63.95522	0.513883	0.387948	0.412343	0.388463
2999	217.923894	64.028732	-0.300151	0.26588	-0.401739	0.266631
AC61	217.924153	64.02926	-0.15838	0.048258	-0.259968	0.052238
299C	217.924222	64.028926	-0.005967	0.080846	-0.107555	0.083283
TNAC	217.973465	63.112614	0.603459	0.175819	0.502301	0.176953
CHIK	218.058235	64.074871	-0.31625	0.181051	-0.417877	0.182152
W176	218.367387	64.075656	-0.180892	0.252575	-0.282559	0.253365
AMBE	218.522716	60.006024	1.435419	0.170638	1.335822	0.171806
RIOU	218.563013	59.888634	0.278164	0.192474	0.178628	0.19351
444C	218.630321	60.026492	0.635455	0.193531	0.53583	0.194561
KICH	218.630497	60.026886	2.145326	0.202536	2.045702	0.203521
3444	218.631241	60.026554	1.628028	0.15796	1.528403	0.159221
3443	218.640146	59.927088	0.483399	0.143196	0.383829	0.144586
I177	218.822394	64.086121	-0.005963	0.0477	-0.107694	0.051723
EAAA	218.839903	64.77865	0.342836	0.145544	0.240791	0.146912
AB41	218.841934	64.777326	-0.320864	0.036234	-0.422909	0.041387
EAAB	218.852204	64.778326	-0.426933	0.901388	-0.52898	0.90161
RALF	218.861337	60.22049	1.394328	0.204764	1.294561	0.205738
EAAC	218.861644	64.777196	-1.872034	0.92925	-1.974081	0.929465
126G	218.998664	64.086482	-0.054266	0.03786	-0.156019	0.042819
BEA2	219.137462	62.407843	0.092821	0.038713	-0.008145	0.043574
MLSP	219.802289	59.724054	1.4078	0.071558	1.308177	0.0743
YKTT	220.351203	59.510738	1.258805	0.054643	1.159226	0.058189
Y565	220.555102	61.592672	0.28047	0.042616	0.179728	0.047076
SITU	220.598103	59.666393	2.201065	0.209839	2.101363	0.21079
NQ1	220.865107	59.87933	2.543046	0.132397	2.443186	0.133899
NQ4	220.968449	59.827278	2.533713	0.189233	2.433868	0.190287
MOSR	221.008727	59.567967	2.604369	0.121864	2.504665	0.123494

HIDD	221.054538	59.705473	2.956284	0.104712	2.856495	0.106605
AB42	221.101189	59.340375	1.971844	0.036478	1.872257	0.041601
FLAT	221.137392	59.669277	2.955369	0.064681	2.855589	0.067703
MID	221.13862	59.758902	2.158416	0.064981	2.058586	0.067989
DEST	221.27812	61.216918	0.588384	0.034135	0.487741	0.039563
8130	221.305556	63.9585	-4.245176	1.005049	-4.347162	1.005248
COMB	221.360689	59.669847	2.362241	0.194625	2.26243	0.19565
CANN	221.365573	59.155187	2.092534	0.200103	1.993016	0.2011
NOVA	221.44265	59.573525	3.290586	0.041339	3.190819	0.045923
NSLM	221.503547	60.99267	0.851966	0.041924	0.751411	0.04645
ALSE	221.677183	59.183104	1.592907	0.174058	1.493329	0.175204
ALSC	221.681651	59.186032	2.364457	0.079065	2.264876	0.081555
MOTD	221.959538	60.957736	0.632011	0.051665	0.531414	0.055401
TATC	222.262039	59.630448	2.233677	0.046125	2.133764	0.050275
TATS	222.262069	59.630441	2.916364	0.174499	2.816451	0.175641
STRT	222.322346	58.625264	1.483397	0.095415	1.384054	0.097489
FROK	222.368143	58.639933	1.870972	0.112752	1.771614	0.114512
2915	222.379543	58.615632	2.023214	0.094175	1.923869	0.096275
CENO	222.426778	58.639845	1.836008	0.084931	1.736642	0.087254
LITU	222.444208	58.658308	2.324074	0.116059	2.224694	0.117769
GILB	222.482561	58.663292	2.026724	0.183443	1.927336	0.18453
ICE4	222.511122	58.668878	2.085668	0.080959	1.986273	0.083393
ANIT	222.899728	58.86044	3.062158	0.152764	2.962597	0.154068
X7	222.937149	60.859181	0.537779	0.0493	0.437105	0.053203
DEZA	222.945786	60.376227	1.272028	0.051803	1.171611	0.055529
MARG	222.979753	59.017425	2.776407	0.163774	2.676745	0.164991
MDFT	223.041568	60.12179	1.517752	0.172559	1.417462	0.173714
MDFC	223.041671	60.121821	1.523504	0.039316	1.423214	0.044111
SARA	223.067938	58.918428	3.027126	0.09492	2.927509	0.097004
489F	223.181065	59.972701	1.688444	0.051863	1.588217	0.055586
OVAL	223.208428	58.292747	1.556793	0.154913	1.457523	0.156198
R205	223.21174	58.905403	2.805576	0.048842	2.705947	0.052778
PEEP	223.263784	58.286222	1.963553	0.136746	1.86428	0.138201
NORM	223.312795	58.273624	1.748051	0.165177	1.648778	0.166384
MART	223.334741	58.892774	3.24797	0.144374	3.148332	0.145753
CAPE	223.359016	58.197675	1.651607	0.108437	1.552374	0.110266
AB43	223.359192	58.198842	1.548359	0.039315	1.449125	0.04411
TRTH	223.365108	59.819523	2.050244	0.046268	1.950077	0.050406
QUIC	223.413181	58.908563	2.972245	0.039352	2.872587	0.044143
QICT	223.413973	58.908517	2.6614	0.487635	2.561742	0.488045
KAOS	223.500193	58.426486	2.144105	0.158424	2.044716	0.159682

CINC	223.507604	58.797816	3.037797	0.093868	2.938191	0.095975
DEPT	223.514191	58.299911	2.05338	0.178214	1.954064	0.179332
BMCP	223.520406	58.782892	2.69357	0.058544	2.59397	0.061866
BEUT	223.534632	59.581482	2.460456	0.048882	2.3604	0.052816
KNBG	223.542893	58.612532	2.561262	0.089827	2.461758	0.092027
DACE	223.563962	58.091344	1.535972	0.096338	1.436774	0.098392
BLUE	223.573379	57.852219	0.990381	0.094644	0.891325	0.096734
EX	223.594913	58.269772	1.699609	0.108649	1.6003	0.110475
ADZE	223.619099	58.21219	1.685266	0.048914	1.585988	0.052845
DELT	223.622141	58.360178	1.99755	0.064031	1.898184	0.067082
508F	223.637443	59.450386	1.617471	0.25012	1.517474	0.250918
MINE	223.661773	58.007816	1.549386	0.13387	1.450224	0.135356
2629	223.673394	58.26441	1.982813	0.094036	1.883496	0.096139
AID1	223.740312	58.317776	2.002035	0.07232	1.902678	0.075035
BAGO	223.820361	59.057989	3.333115	0.087708	3.233316	0.089959
TLGT	223.824011	58.749863	2.92183	0.059	2.822208	0.062298
ELSE	223.847148	58.593499	2.341187	0.051357	2.241653	0.055114
LAST	223.858096	58.978874	3.502046	0.105526	3.402288	0.107405
DAM	223.959098	58.319135	1.942816	0.146875	1.843429	0.148231
GOOS	223.964069	58.211218	2.539472	0.185958	2.440148	0.187031
DUKY	223.976623	59.423989	2.436703	0.089082	2.336676	0.091299
MQTO	223.984155	59.422925	1.575277	0.168309	1.47525	0.169494
BR39	223.985537	58.730502	2.769927	0.06539	2.670295	0.068381
DMP2	224.092801	58.24616	1.975282	0.088731	1.875919	0.090958
BCT5	224.113621	58.45407	1.848964	0.102611	1.749476	0.104542
GUS5	224.302657	58.417486	1.835561	0.067144	1.73607	0.070059
GUS1	224.302659	58.417488	2.025012	0.072527	1.925521	0.075234
GUS6	224.302949	58.417757	1.739273	0.066947	1.639781	0.069871
GUS2	224.302951	58.417758	1.881526	0.027345	1.782034	0.033879
2484	224.344298	57.957439	1.057858	0.084695	0.958634	0.087025
EA22	224.355027	58.231919	1.92368	0.122701	1.824291	0.124321
BIS6	224.460421	56.854315	-0.067532	0.067703	-0.166096	0.070596
BIS5	224.460703	56.854492	-0.07012	0.067116	-0.168684	0.070032
BIS1	224.460705	56.854493	0.205692	0.036761	0.107128	0.04185
HNSD	224.465797	59.248097	2.365351	0.050474	2.265359	0.054292
HNSA	224.473093	59.245067	1.513539	0.35478	1.413547	0.355344
2447	224.511621	58.496455	2.433642	0.087421	2.334076	0.08968
2437	224.555356	58.41744	1.950297	0.085138	1.850772	0.087455
SITA	224.635718	57.04818	-0.461178	0.108898	-0.559886	0.110719
UDIG	224.641316	58.289698	1.809049	0.086594	1.709587	0.088874
FS32	224.653042	59.148681	2.274736	0.054913	2.174776	0.058442

T187	224.674819	59.455988	2.336323	0.380854	2.236187	0.381379
2400	224.675827	59.452806	1.658356	0.551706	1.558222	0.552068
FLCN	224.707716	58.831044	2.409724	0.177903	2.309938	0.179024
WHB0	224.767	58.7326	2.125264	0.082354	2.025528	0.084748
AB44	224.771702	59.528039	1.621328	0.032043	1.52114	0.037772
TENA	224.771899	57.771153	1.012256	0.096257	0.913087	0.098313
ELD	224.777685	58.971967	2.568783	0.147515	2.468908	0.148865
ELDC	224.777803	58.971868	2.106676	0.037615	2.0068	0.042601
WHIT	224.77789	60.750513	0.196211	0.014005	0.095361	0.024417
STCK	224.839673	58.649065	2.19746	0.090778	2.097762	0.092956
LSTR	224.869993	58.509542	2.019103	0.078357	1.919482	0.080869
BRGT	225.089357	58.596183	1.889747	0.060112	1.790047	0.063352
AB48	225.353004	56.245063	0.083398	0.048912	-0.014902	0.052844
JNU1	225.414295	58.362576	1.337814	0.031462	1.238208	0.037281
EDDI	225.430739	58.356267	1.252394	0.034647	1.15279	0.040005
AB50	225.4547	58.416776	1.535368	0.041257	1.435725	0.045849
MENG	225.454745	58.416762	1.68276	0.050955	1.583117	0.05474
JNUT	225.580599	58.2991	1.568153	0.137393	1.468563	0.138841
2210	225.589119	58.299379	1.249673	0.365379	1.150082	0.365926
ANNX	225.899488	58.31598	1.674927	0.106764	1.575285	0.108621
TKHR	225.986998	58.067556	1.298436	0.103826	1.19893	0.105735
ATLI	226.28553	59.589483	0.819956	0.025149	0.719542	0.032133
INVK	***226.47304***	***68.306186***	***-0.107676***	***0.034042***	***-0.211888***	***0.039483***
LEV5	226.907218	56.46568	0.439598	0.056519	0.340951	0.059953
LEV1	226.90722	56.465681	0.828598	0.049628	0.729951	0.053506
LEV6	226.907613	56.46566	0.416821	0.056642	0.318174	0.060069
LEV2	226.907615	56.465661	0.668341	0.051352	0.569694	0.055109
AB49	226.931513	55.580102	0.129857	0.04544	0.031775	0.049647
TUKT	***227.005651***	***69.438235***	***-0.157011***	***0.032862***	***-0.261606***	***0.038469***
PSGA	227.066537	56.804664	0.476811	0.161884	0.377931	0.163115
AB51	227.08644	56.797623	0.943906	0.04174	0.845029	0.046284
BLKP	227.455907	56.593981	0.333441	0.232995	0.234643	0.233852
MMOR	227.913417	53.019616	0.190359	0.08385	0.093898	0.086202
ALIF	228.005011	53.186316	0.121675	0.22419	0.025083	0.22508
SACC	228.017045	53.216132	-0.124776	0.167748	-0.221392	0.168936
NCRS	228.040257	53.143669	0.094156	0.078187	-0.002411	0.080705
YAKN	228.163198	54.070683	0.143996	0.194412	0.046764	0.195439
SDPT	228.176445	53.259221	0.419193	0.302579	0.322526	0.303239
KTNR	228.288311	55.354789	0.339229	0.182946	0.241118	0.184036
AIS5	228.400464	55.069072	-0.221295	0.072673	-0.319232	0.075375
AIS1	228.400466	55.069073	-0.001783	0.025153	-0.099719	0.032136

AIS6	228.400789	55.068883	-0.11137	0.065711	-0.209307	0.068688
AIS2	228.400791	55.068884	-0.10571	0.03127	-0.203646	0.037119
DEAS	229.970772	58.436782	0.205853	0.049612	0.105648	0.053492
BCDL	229.974298	58.425644	0.084126	0.038506	-0.016073	0.04339
BCDL	229.974298	58.425644	0.133915	0.029729	0.033716	0.035831
SMTH	232.81313	54.823752	0.255695	0.042588	0.157395	0.04705
BLCL	233.410748	52.388265	0.461121	0.049376	0.364437	0.053273
CMBR	234.673598	50.053361	0.454991	0.04737	0.359919	0.051419
WVN3	236.748949	49.351721	0.166477	0.056901	0.07174	0.060314
SUR6	237.308096	49.074186	-0.153405	0.120947	-0.247975	0.12259
PRG6	237.659613	53.910309	0.282305	0.050734	0.184125	0.054534
FSRH	237.712328	49.13801	0.032973	0.05165	-0.061686	0.055387
WLLL	237.83219	52.236869	0.160139	0.014321	0.063113	0.024599
VRN4	240.68223	50.199989	0.20984	0.048567	0.114088	0.052524
VRN9	241.426114	50.214801	0.202925	0.119798	0.107103	0.121457
GDPR	241.461255	55.187118	0.330899	0.07767	0.231562	0.080204
HNTN	242.280329	53.319195	0.180683	0.041032	0.08253	0.045647
GRMS	242.331455	56.363798	0.325279	0.04201	0.225145	0.046528
GLDN	243.015742	51.300522	0.318721	0.067135	0.221963	0.070051
FXCR	243.224775	54.382932	0.150479	0.034218	0.051542	0.039635
FTVM	243.84868	58.515084	0.409199	0.043686	0.307721	0.048047
NRDG	243.877499	52.479827	0.064435	0.041534	-0.033238	0.046099
CRNB	244.330528	49.600239	0.11059	0.071735	0.015047	0.074471
FTRS	244.799693	50.82874	0.006131	0.066529	-0.090388	0.06947
YELL	245.519303	62.480895	0.627361	0.013175	0.523838	0.02395
SASK	253.601646	52.196255	-0.085651	0.025663	-0.183526	0.032536
YRKT	257.595693	51.219202	-0.016638	0.036086	-0.113822	0.041258

Appendix 5

Satellite Altimetry Analysis of Trends and Standard Deviations

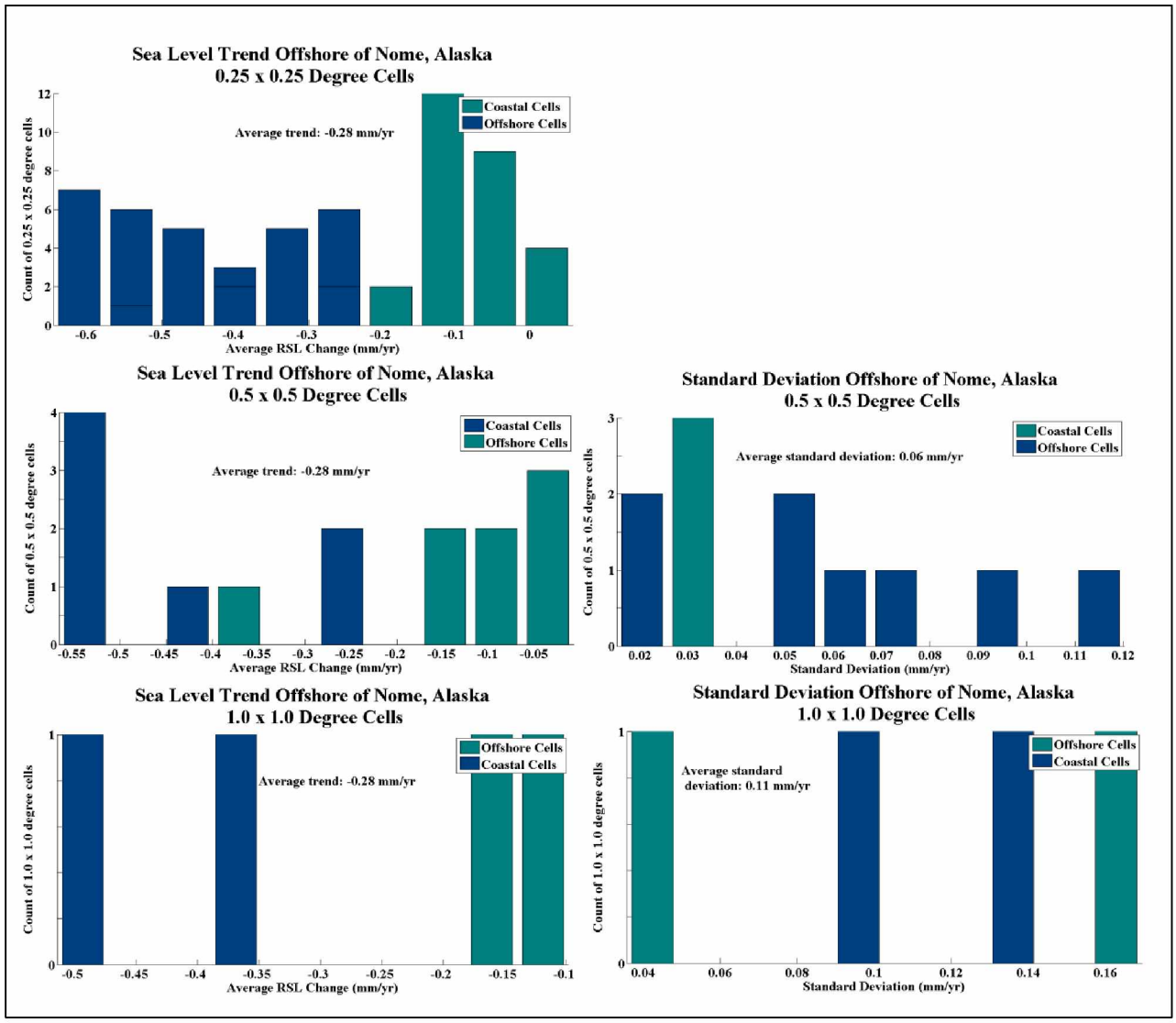

Figure A5.1. Histograms of MSL trends and standard deviations between AVISO satellite altimetry cells offshore of Nome, Alaska. AVISO cells are provided as 0.25° x 0.25° cells and were merged and averaged to 0.5° and 1.0° cells. Standard deviation of the 0.25° square cells is 0.21 mm/yr. MSL trend remains the same for each of these three sizes, but the standard deviation is lowest between the medium sized (0.5°) cells.

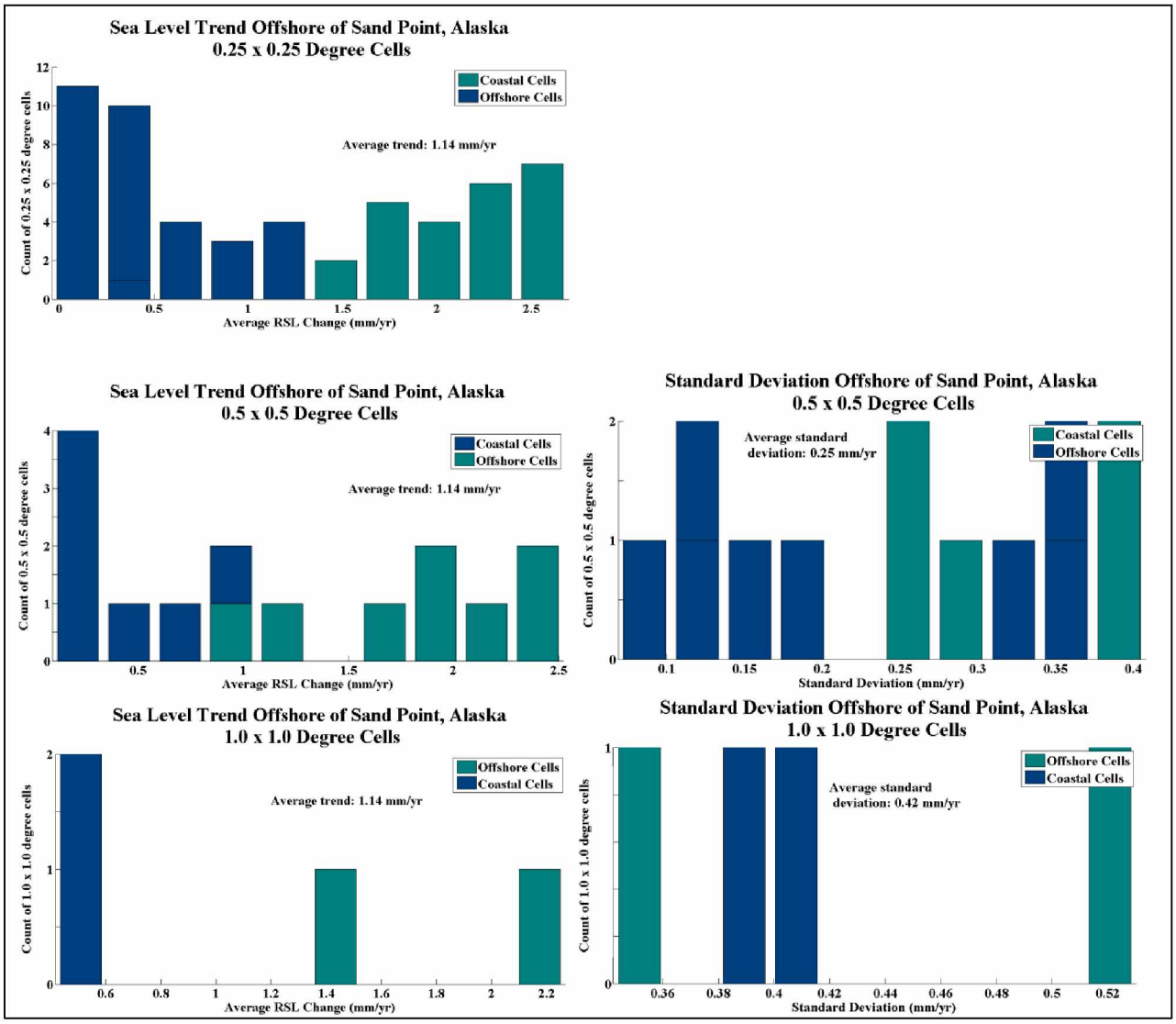

Figure A5.2. Histograms of MSL trends and standard deviations between AVISO satellite altimetry cells offshore of Sand Point, Alaska. AVISO cells are provided as 0.25° x 0.25° cells and were merged and averaged to 0.5° and 1.0° cells. Standard deviation of the 0.25° square cells is 0.87 mm/yr. MSL trend remains the same for each of these three sizes, but the standard deviation is lowest between the medium sized (0.5°) cells.

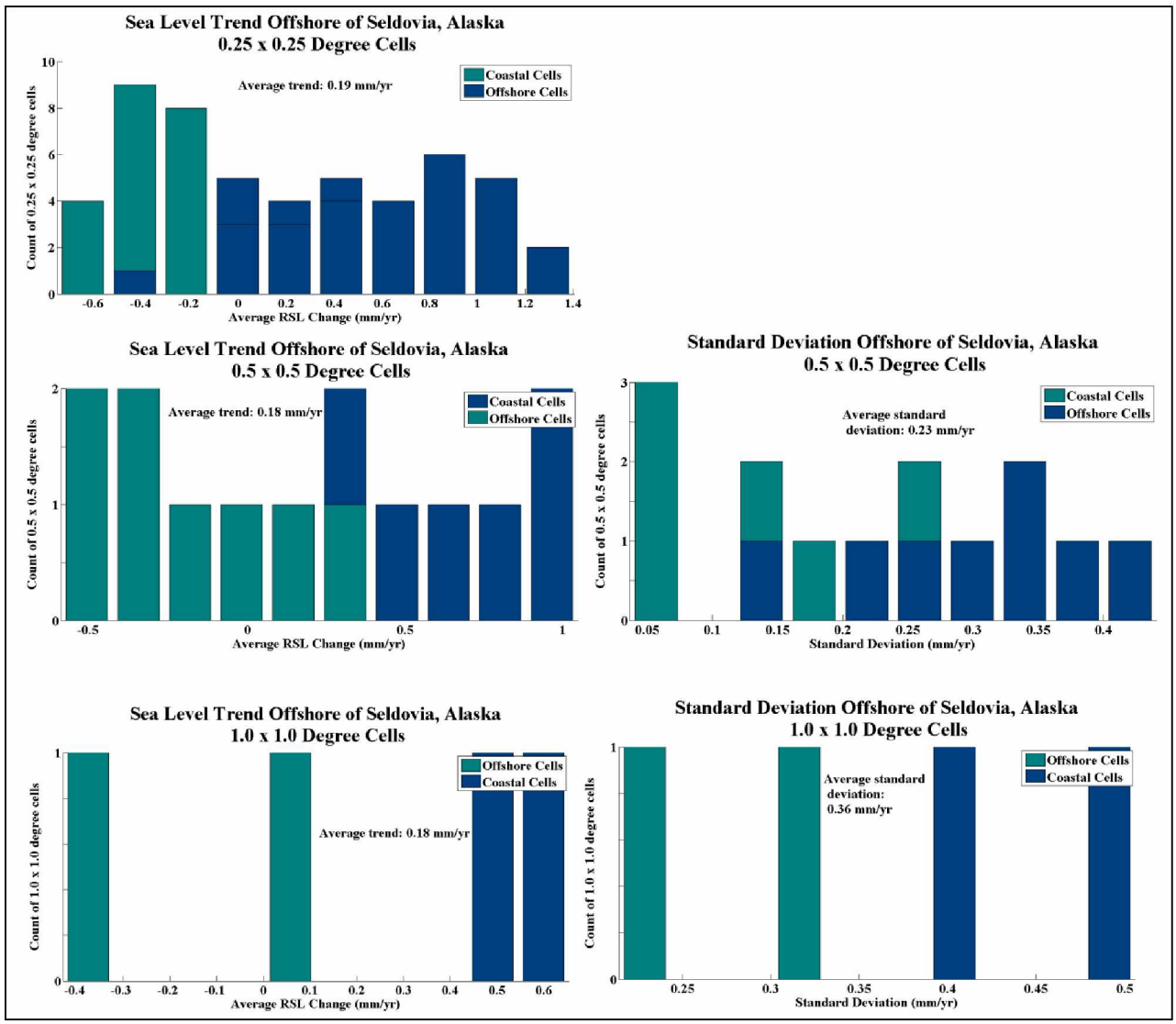

Figure A5.3. Histograms of MSL trends and standard deviations between AVISO satellite altimetry cells offshore of Seldovia, Alaska. AVISO cells are provided as 0.25° x 0.25° cells and were merged and averaged to 0.5° and 1.0° cells. Standard deviation of the 0.25° square cells is 0.56 mm/yr. MSL trend remains the same for each of these three sizes, but the standard deviation is lowest between the medium sized (0.5°) cells.

Appendix 6

Maps of Alaska GPS Horizontal Velocities

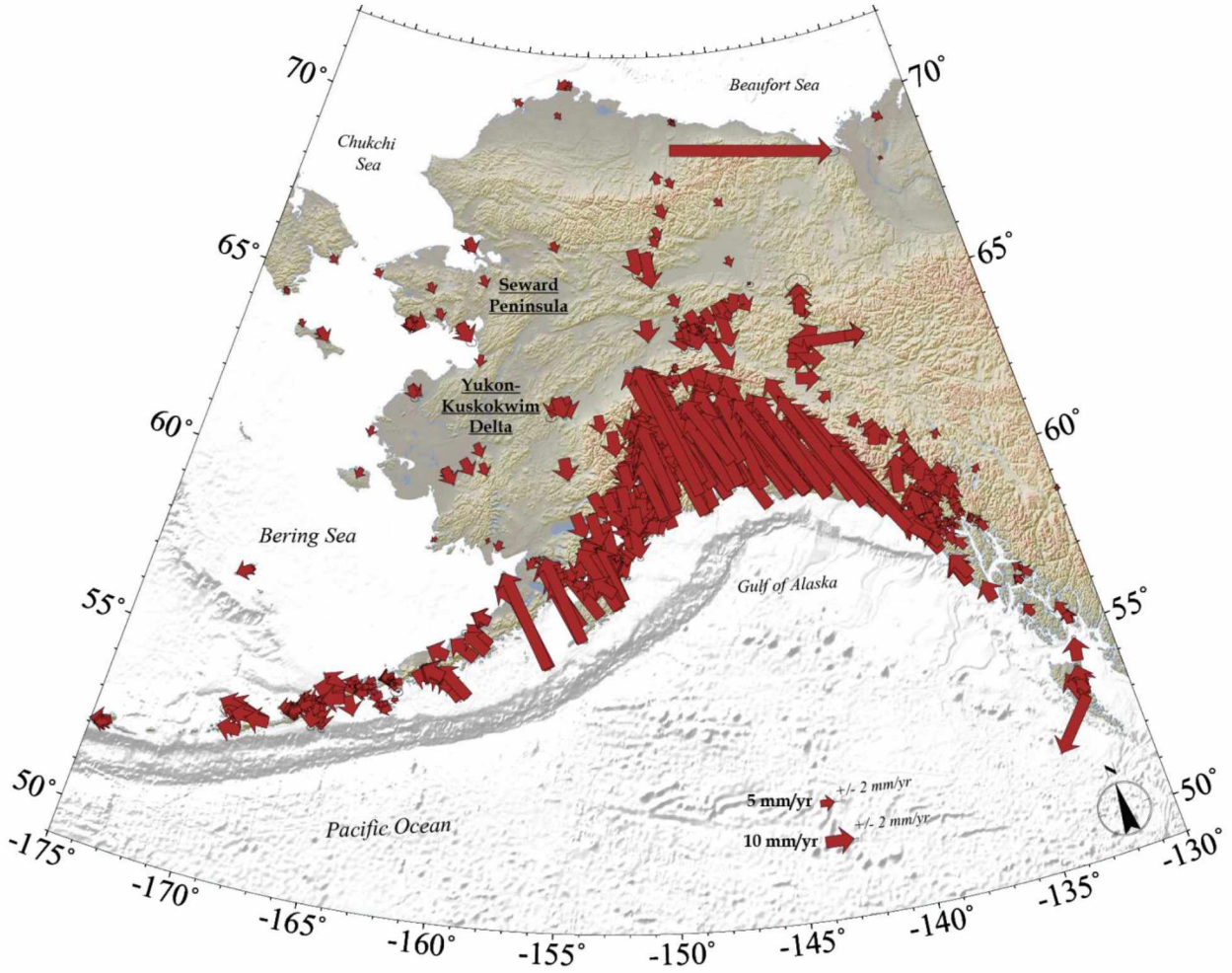

Figure A6.1. Horizontal velocity model of Alaska. Arrow bases show the locations of the GPS sites. Error ellipses are plotted at the point of the arrow (most are small). Horizontal values represent vectors calculated from northward and eastward measured velocities. The southern margin of Alaska is moving northwestward as the Pacific Plate collides with the North American plate. There is an apparent change in direction to the southeast in Northern and Western Alaska.

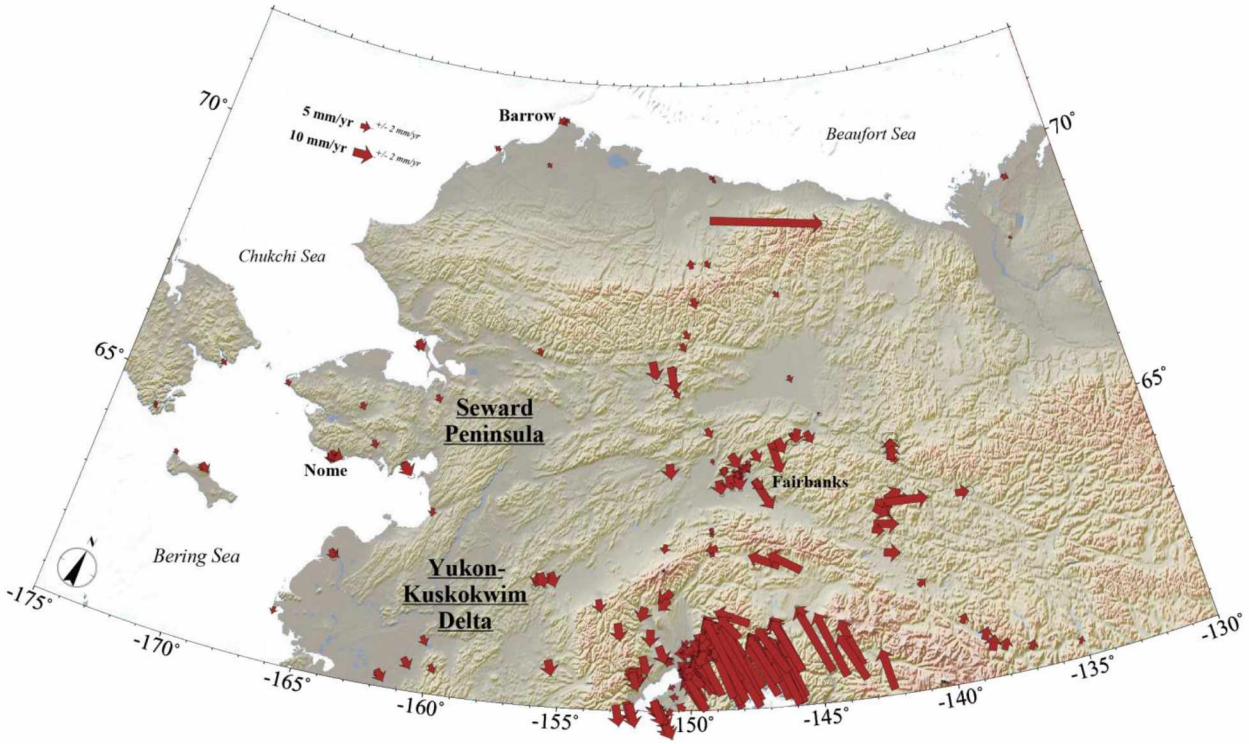

Figure A6.2. Horizontal velocity model of Northern Alaska. Arrow bases show the locations of the GPS sites. Error ellipses are plotted at the point of the arrow. Horizontal values represent vectors calculated from northward and eastward measured velocities. Here the counter-clockwise motion along the Denali Fault in the Alaska Range can be observed, with the shift in direction located approximately between Fairbanks and the Alaska Range. The eastern border of the Yukon-Kuskokwim Delta with the Alaska Range also appears to be the western extent of the counter-clockwise rotation.

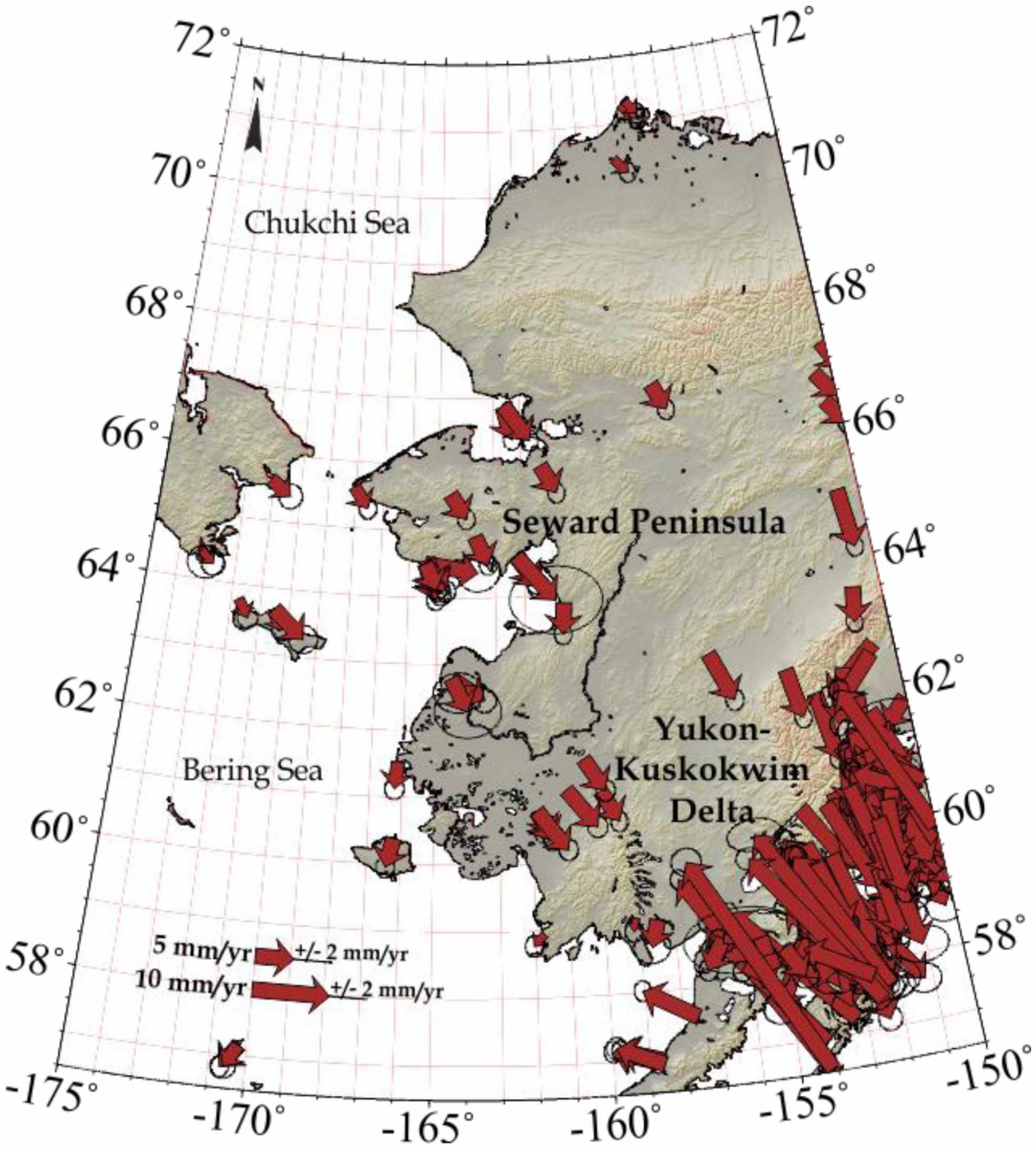

Figure A6.3. Horizontal velocity model of Western Alaska. Arrow bases show the locations of the GPS sites. Error ellipses are plotted at the point of the arrow. Horizontal values represent vectors calculated from northward and eastward measured velocities. Western Alaska is moving southeastward at velocities of 4-10 mm/yr, but there is a dramatic shift in direction on the eastern border of the Yukon-Kuskokwim Delta, where it comes into contact with the Alaska Range. Here the direction shifts to northwestward, with velocities that can exceed 20 mm/yr.

Appendix 7

GPS and GIA Velocities Used in RSL Change Calculations

Table A7.1. Locations where GIA and GPS were calculated. The GPS velocities and uncertainties referenced to ITRF 2008 are later used to analyze the best fit GIA model. The velocities of this best fit GIA model are shown here. Locations are ordered from eastern most at the top, to farthest west at the bottom.

Site ID	Longitude (degrees East)	Latitude (degrees)	GPS (mm/yr)	GPS Uncertainty (mm/yr)	GIA (mm/yr)	GIA (cm/yr)
MRKV	170.404221	64.682793	0.65943	0.79874	-1.10140	-0.11014
ANAD	177.497925	64.735541	-1.1672	0.68513	-0.71090	-0.07109
UGOL	177.689148	64.731076	-3.2147	1.47053	-0.68980	-0.06898
BERI	179.259324	63.061390	-2.0455	0.92746	-1.38240	-0.13824
EGVK	180.881598	66.322040	-0.6668	0.99326	-1.23160	-0.12316
GAMB	188.267994	63.774466	-1.6751	0.71775	-0.74487	-0.07449
LAV1	188.897575	65.616687	-5.8376	1.14700	-0.88705	-0.08871
Savoonga weighted mean	189.503384	63.684693	-2.268	0.55837	-0.63585	-0.06359
4212	189.714272	57.125675	2.4856	1.23157	-0.74024	-0.07402
SPSW	189.751512	57.152339	-1.9019	0.96217	-0.31687	-0.03169
AC58	189.782180	57.156089	-1.9239	0.52516	-0.31813	-0.03181
AB09	191.937875	65.614982	-1.5403	0.46625	-1.02580	-0.10258
AB08	193.799143	60.384832	-0.5617	0.62106	-0.89243	-0.08924
HOOP	193.859939	61.521162	4.11144	0.62701	-0.94857	-0.09486
Nome weighted mean	194.564103	64.507243	-1.751	0.22000	-1.13090	-0.11309
AC50	195.433431	65.553849	-2.6548	0.46636	-1.95700	-0.1957
Emmonak weighted mean	195.507796	62.780471	-3.591	0.86300	-0.96073	-0.09607
MELS	196.307740	64.922341	-2.057	0.43574	-1.90660	-0.19066
Kotzebue weighted mean	197.388627	66.887333	-4.031	0.32600	-2.10410	-0.21041
Elim weighted mean	197.747871	64.616514	-2.23	0.37800	-0.93611	-0.09361

Bethel weighted mean	198.164320	60.784197	1.212	0.27200	1.34070	0.13407
AB12	198.253739	58.950795	-1.7313	0.60772	-0.99707	-0.09971
AC07	198.713384	65.961293	-2.1173	0.46372	-2.03180	-0.20318
AB17	199.305269	63.886359	-2.5595	0.55731	-0.73465	-0.07347
KALS	199.665465	61.537197	-5.2679	0.69011	-0.66472	-0.06647
AB15	200.121639	61.039753	-0.9814	0.42196	-0.80340	-0.08034
Port Heiden weighted mean	201.387657	56.963885	-0.6501	0.276900	-0.74024	-0.07402
Dillingham weighted mean	201.529185	59.061955	-0.8225	0.570600	-0.67358	-0.06736
AC52	202.425784	57.567250	-0.049	0.473380	-0.31869	-0.03187
ATQK	202.592132	70.472033	-2.2898	0.417170	-1.46620	-0.14662
AB27	203.095111	67.055887	-2.144	0.463980	-1.15640	-0.11564
BRW1	203.210076	71.282766	-1.1686	0.512950	-1.48240	-0.14824
BASC	203.322090	71.324944	-1.4399	0.437910	-1.49320	-0.14932
King Salmon weighted mean	203.345538	58.671209	1.142	0.306000	-0.85296	-0.0853
AB25	203.976609	62.929311	-1.1894	0.719030	-0.83989	-0.08399
152T	209.326465	66.820757	-0.9715	0.678610	-2.24510	-0.22451
FNGR	209.507570	66.375537	-1.3969	0.596500	-0.64247	-0.06425
AB33	209.827456	67.251013	-1.9165	0.433170	-1.60790	-0.16079
YUKO	210.907011	65.676178	-1.6424	0.859590	-0.80840	-0.08084
AB45	211.128849	68.760495	-2.0865	0.456900	-2.40940	-0.24094
WICK	211.933803	65.182698	1.08532	0.810420	-1.92260	-0.19226
CLGO	212.139514	64.873777	-0.1512	0.381770	-1.90350	-0.19035
FAI1	212.152660	64.809631	0.0583	0.681800	-0.71015	-0.07102
SUAF	212.164202	64.858691	-0.7983	0.498060	-1.89450	-0.18945
FAIR	212.500763	64.978002	-0.0201	0.382800	-1.04100	-0.1041
FAIT	213.738998	65.347127	-1.9811	3.074480	-1.96410	-0.19641
CENA	215.322370	65.498165	-0.501	0.272220	-1.97720	-0.19772
I177	218.822394	64.086121	-1.161	0.965270	-1.14280	-0.11428
WHIT	224.777890	60.750513	0.95789	0.245320	-0.57140	-0.05714
INVK	226.473040	68.306186	-2.119	0.39483	-1.95870	-0.19587
Shishmaref	193.927800	66.255600	NA	NA	-0.96608	-0.09661
St. Michael/ Stebbins	197.946900	63.471100	NA	NA	-1.02460	-0.10246
Toksook Bay	194.857656	60.518576	NA	NA	-0.62001	-0.06200

Popokamute	197.497462	60.115970	NA	NA	-0.71326	-0.07133
Kivalina	195.460800	67.727200	NA	NA	-1.00310	-0.10031
Teller	193.642335	65.248106	NA	NA	-0.93722	-0.09372
Golovin	196.969580	64.544749	NA	NA	-1.05260	-0.10526
Shaktoolik	198.764226	64.379904	NA	NA	-1.14660	-0.11466
TUKT	227.005651	69.438235	-2.6161	0.38469	-2.41270	-0.24127

Appendix 8

Results From Additional GIA Modeling with a Higher Viscosity (5.01 x 10^{21} Pa s) Lower Mantle

An additional model to the one presented in the main thesis was tested using the post glacial rebound calculator TABOO (Spada et al., 2003). The viscosity of the lower mantle in the model presented in the main thesis is 3 x 10^{21} Pa s. The model run in this appendix was defined with the same Earth model and was tested over the same range of parameters as the thesis model. The only difference between these two models is the viscosity of the lower mantle which was increased to 5.01 x 10^{21} Pa s in this version. This model was tested so that a model for Northern and Western Alaska could be compared to the best fit model of Hu and Freymueller (2015) (in preparation), where they employed this higher viscosity lower mantle. The best fit model is for a 120 km thick lithosphere and a thinner 70 km thick asthenosphere. The asthenosphere and upper mantle viscosities were best fit at 1 x 10^{20} Pa s and 5 x 10^{20} Pa s. This model estimates approximately the same thicknesses for the lithosphere and asthenosphere as the lower viscosity model. The viscosity structure is not like either the lower viscosity model in the thesis of the same lower mantle viscosity model employed by Hu and Freymueller (2015) (in preparation) in the Southern Alaska model. The lower viscosity lower mantle model has a large range of viscosities from 2.5 x 10^{19} in the asthenosphere to 1.5 x 10^{21} in the upper mantle. This model shows a much more homogenous layer with perhaps a more gradual contact between asthenosphere and upper mantle. This model produces vertical velocities that suggest the subsiding forebulge is centered on north central Alaska, and the transition from uplift to subsidence is a north south trending boundary approximately following the -140° E longitude (Figure A8.1).

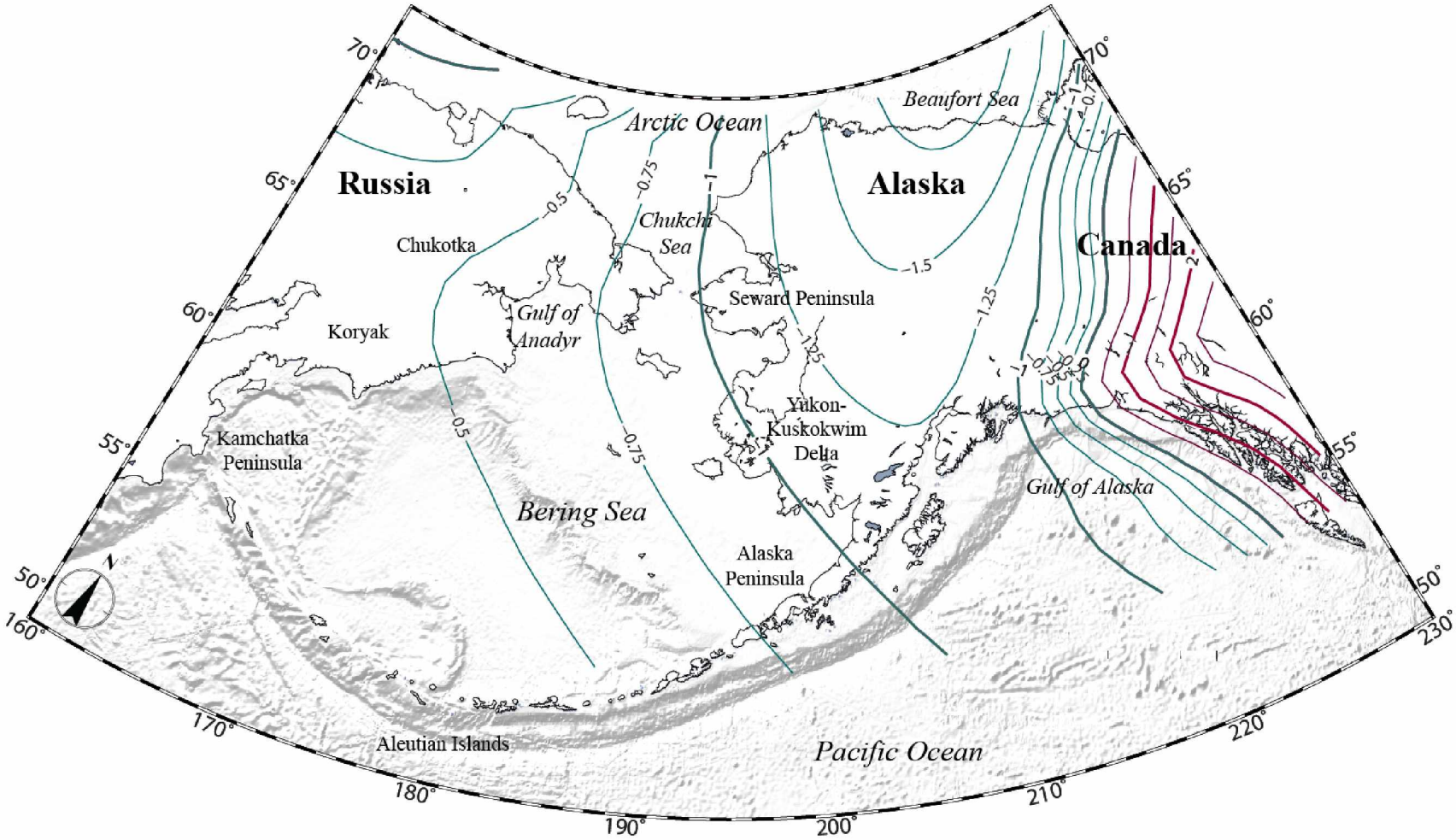

Figure A8.1. Contour map for vertical velocity resulting from the best fit GIA model with a lower mantle viscosity of 5 x 10^{21} Pa s. Countours are every 0.25 mm/yr, with 0, 1, and 2 in bold. Positive vertical velocities (uplift) are in red and negative vertical velocities (subsidence) are in green.

Appendix 9

Western Alaska GPS Suggested Benchmark Survey and Installation Priorities

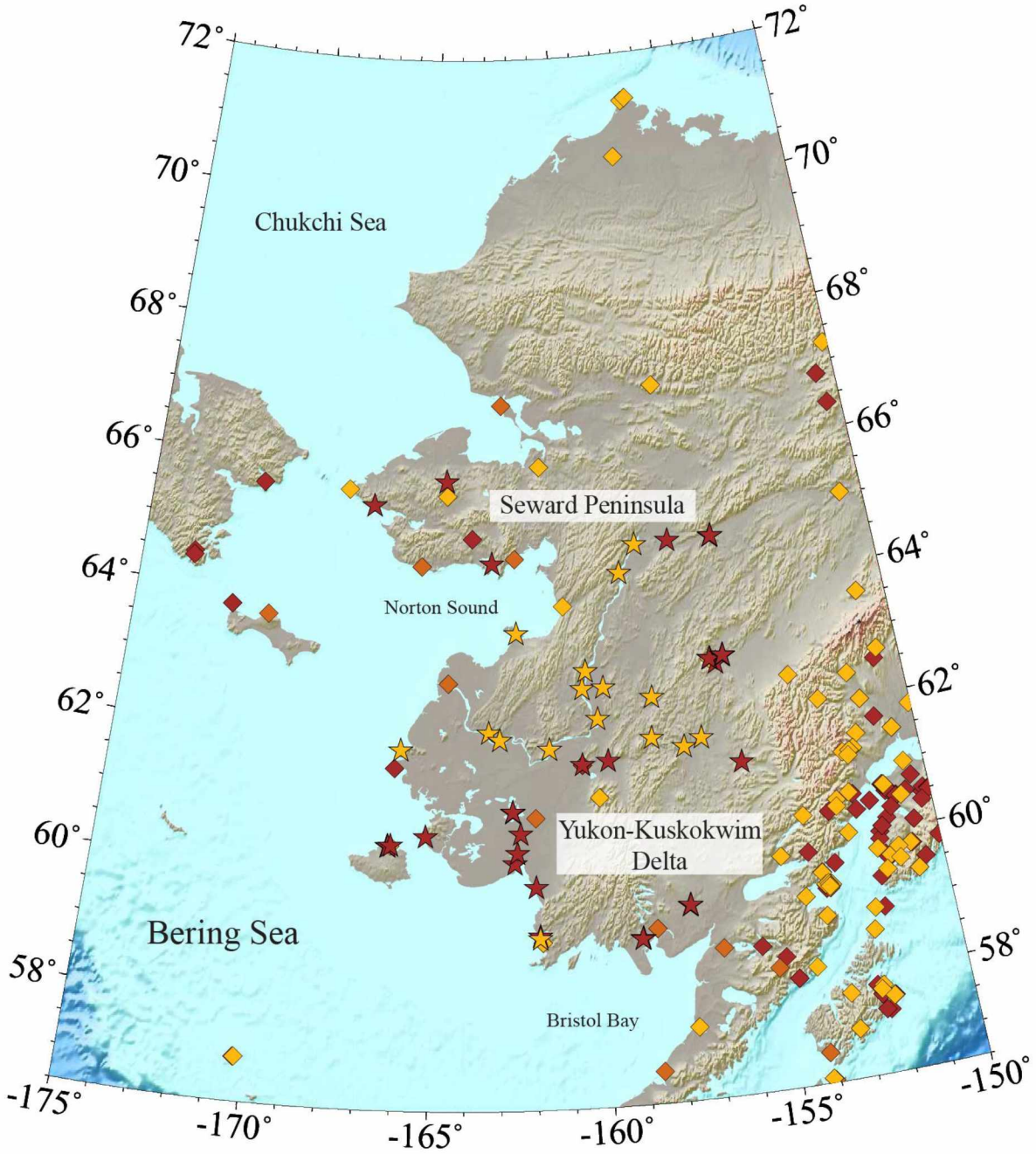

Figure A9.1. Map of current and suggested GPS sites. Red diamonds are current sites that UAF-GI can calculate velocities for. Red diamonds are campaign sites, yellow are continuous sites, orange are sites that have a weighted mean of both campaign and continuous. Stars are suggested sites that are listed later in this report in Tables 1. and 2. Red stars correspond to locations in Table 1. of sites to be reoccupied. Yellow stars can be found in Table 2. as sites that are not in the UAF-GI database but are potentially stable locations to install additional benchmarks to better constrain movement on the Y-K Delta in particular.

A list of priority benchmarks in Western Alaska to resurvey and potential locations for additional installations is presented here, in order to most efficiently augment the GPS database at the University of Alaska Fairbanks-Geophysical Institute (UAF-GI). The focus of this priority list is the Yukon-Kuskokwim Delta (Y-K Delta), but a few sites on the Seward Peninsula and inland of Western Alaska are also suggested to further constrain the eastern boundary of both the Seward Peninsula and the Y-K Delta (Figure A9.1).

Priority as it is used here is a very subjective suggestion based on a combination of personal experiences with communities in Western Alaska, geology and terrain in the area, and data availability in the UAF-GI database. Reoccupations (Table A9.1) are ordered according to several variables. Benchmarks that occupy the spatial gaps in the GPS network of Western Alaska are collected from the database and records that have only one occupation before 2000 were discarded due to reference frame and data quality issues in the 90s and the uncertainty associated with attempting to relocate a benchmark that has not been occupied for over 15 years. The exception to this is the site HAGA in Quinhagak, which was last occupied in 1991. It is listed as the lowest priority because the current data available is not very useful and the benchmark may not even exist anymore, but the community fills a large gap in the coastline of the Y-K Delta where it would be very valuable to make GPS measurements. Personal knowledge of locations with accessible outcropping bedrock and simple logistics were given the highest priority and are the reasoning behind the first four benchmarks. The remaining benchmarks are order based primarily on location.

Possible bedrock exposure was assessed via GoogleEarth, but unless otherwise noted is purely a function of "best guesswork". If no bedrock is observed the location is noted as "delta", "fluvial environment", or "island?". The term "delta" is used when there is a large percentage of standing surficial water features such as bogs, ponds, lakes, swamps, etc. The tundra, in these locations often saturates, becomes spongy and grows on potentially hundreds of feet of sands and gravels that often do not provide the most suitable environment for a stable benchmark. These locations are often prone to frost jacking and erosion. The eastern benchmarks are mostly located on bedrock, but "fluvial environment" is introduced to describe benchmarks that appear to be largely influenced by the local geomorphology from the Yukon and Kuskokwim river migrations. These sites are often a bit more stable than "delta" setting, but require some caution and the use of long rods driven deep to properly anchor the benchmark. The fourth category

"island?" is used for sites on Nunivak Island, which has a rocky and apparently volcanic interior but the shores appear to be more "deltaic" in setting with bogs, ponds, and swamps visible in GoogleEarth.

Some benchmarks are located near a continuous station, in which case they have a lower priority than communities that do not have a continuous station, but the campaign data often dates to earlier years than the continuous station, and the additional data could help extend the record back in time.

Table A9. 2 suggests locations for potential installation sites and communities where a GPS benchmark could be securely installed. These sites are again subjective and largely based on limited personal experience and GoogleEarth, but would greatly enhance the GPS spatial coverage in Western Alaska.

GPS measurements become good enough to be useful for studying the coastal uplift or subsidence when the uncertainties in the vertical rates are on the order of 1 mm per year or smaller. For sites with episodic campaign surveys, this requires at least three surveys over a several year period, usually close to a decade. For continuous GPS sites, this same level of precision can be obtained with 3-5 years of measurements, depending on the level of seasonal variations and noise. All of this assumes that the benchmark or continuous GPS monument is stably mounted so that it reflects the motion of the crust without frost jacking or seasonal freeze-thaw effects. These sites are from and related to the UAF-GI database, but a thorough search through OPUS and NGS datasheets will most likely result in additional benchmarks in communities not mentioned here as well as the ones that were included. Private companies such as JOA Surveys, LLC and R&M Consultants, Inc. have also been helpful and have an intimate knowledge of many of the benchmarks in this area.

Table A9.1. List of priority benchmarks to reoccupy in Western Alaska.

Community	Site ID	Latitude (N)	Longitude (E)	Last Occupied	Number of Occupations	Type of Benchmark
*Golovin	3651	64.54474931	-163.0304195	2013	2	bedrock
*Kalskag	KALS	61.5372008	-160.3345347	2014	3	bedrock
*Aniak (1)	ANI1	61.57484219	-159.5370461	2001	1	bedrock
*Midnight Mountain	MMKT	65.76469182	-164.5932945	2013	1	bedrock
Lime Village	LIME	61.35653198	-155.4444417	2004	2	boulder
Candle (2)	CNDL	62.85762315	-155.8482319	2003	1	bedrock
Takotna Mountain (3)	TA01	62.92924967	-156.0180027	2001	1	bedrock
Takotna Mountain (4)	TAAZ	62.9293034	-156.0233272	2004	3	bedrock
Takotna Mountain (4)	TATB	62.92733784	-156.0286464	2004	3	bedrock
Lost River	9338	65.39240376	-167.1530361	2005	1	bedrock?
Popokamute (5)	6057	60.11597012	-162.5025376	2010	1	delta
Helmick Point (5)	6153	60.27014285	-162.4096066	2010	1	delta
Toksook Bay (5)	6298	60.51857627	-165.1423443	2010	1	delta
Lomavik Slough (5)	6328	60.55420178	-162.2973885	2010	1	delta
Ruby	RBYA	64.73023521	-155.4631162	2005	1	fluvial
Ruby	RBYB	64.72415485	-155.4806725	2005	1	fluvial
Ruby	RBYC	64.729344	-155.4623942	2005	1	fluvial
Galena	STA8	64.73686234	-156.9562372	2010	1	fluvial
McGrath (6)	MGRA	62.95770584	-155.6035578	2012	2	fluvial
McGrath	MGRB	62.95155885	-155.6077825	2001	1	fluvial
McGrath	MGRC	62.94712341	-155.606963	2001	1	fluvial
McGrath	NWBS	62.95505869	-155.6026017	2001	1	fluvial
Kasigluk	Z09A	60.87033769	-162.5241727	2001	1	delta
Kasigluk	Z09B	60.87302845	-162.5232844	2001	1	delta
Kasigluk	Z09C	60.87588905	-162.5225646	2001	1	delta
Ekwok	KEKA	59.35197197	-157.4774613	2007	1	delta
Ekwok	KEKB	59.35487171	-157.4722266	2007	1	delta
Ekwok	KEKC	59.35846102	-157.4657634	2007	1	delta
Manokotak (7)	MBAA	58.93093943	-158.9008128	2009	1	delta
Manokotak	MBAB	58.93385375	-158.8960664	2009	1	delta
Manokotak	MBAC	58.92775998	-158.9067029	2009	1	delta
Platinum (8)	5396	59.0464919	-161.8182877	2007	1	delta
Mekoryuk	MYUA	60.37122294	-166.2807096	2007	1	island?
Mekoryuk	MYUB	60.37436386	-166.2702892	2007	1	island?
Mekoryuk	MYUC	60.37301917	-166.2615192	2007	1	island?
Mekoryuk (9)	6217	60.38355991	-166.1873447	2010	1	coast
Quinhagak	HAGA	59.75688689	-161.8846966	1991	1	delta

* Communities where bedrock has been personally observed - (1) Daily flights to ANC - (2) Questionable stability: "brass cap on rod" - (3) Near continuous: AB25 - (4) 3 occupations 2001, 2003, 2004 but only for less than a day each - (5) JOA has been here and might have records, or installed new benchmarks - (6) Questionable stability: 10' rod - (7) Near continuous: AB14 - (8) Near continuous: AB12 (9) Near continuous: AB08.

Table A9.2. List of potential new benchmarks to be installed in Western Alaska. Sites are ordered from top to bottom by estimated stability. Type of benchmark was assessed via Google Earth except for Saint Mary's and Anvik, where bedrock was personally witnessed.

Community	Latitude (N)	Longitude (E)	Type of Benchmark	Notes
Saint Mary's	62.045278	-163.218611	bedrock	Daily flights to Anchorage and the airport is on top of a cliff with lots of outcrop nearby
Cape Romanzof AFS	61.789722	-165.961944	bedrock	Refer to Craig Ely - Frequent Anchorage flights, bedrock, military (safe)
Platinum/Good News Bay	59.006944	-161.815278	bedrock	Bedrock nearby, mine means infrastructure and transportation to bedrock
Kaltag	64.325278	-158.726944	bedrock	These two would be good places, east of Unalakleet but have lots of bedrock
Nulato	64.73	-158.114167	bedrock	
Anvik	62.655556	-160.209167	bedrock	
Holy Cross	62.198056	-159.773333	bedrock	
Crooked Creek	61.859722	-158.128889	bedrock	
Grayling	62.910556	-160.067222	bedrock	
Pilot Station	61.936111	-162.883333	bedrock	
Russian Mission	61.785556	-161.334167	potential bedrock	
Stony River	61.7875	-156.591111	potential bedrock	
St. Michael's/Stebbins	63.511944	-162.274722	potential bedrock	These sites are all scouted on google earth with no prior knowledge for potential bedrock and are villages located where there are currently gaps in GPS coverage.
Flat	62.454167	-158.008333	potential bedrock	
Shageluk	62.656111	-159.531111	potential bedrock	
Sleetmute	61.683889	-157.151944	potential bedrock	